



PhD
ESciences
Environmental

UNIVERSITÀ DEGLI STUDI DI MILANO

PhD School in Environmental Sciences

XXX Cycle

**Assessing shallow landslide susceptibility of
vegetated hillslopes through a physically-based
spatially-distributed model**

PhD Thesis:

Alessio CISLAGHI

Student ID: R11030-R24

Disciplinary scientific sector: AGR/08

Supervisor: Prof. Gian Battista BISCHETTI

Academic Year 2016-2017

Dedicated to the memory of my beloved grandfathers Aldo and Bruno,
and my lovely family and friends

Abstract

Slope instabilities are a serious threat to human activities, settlements, and safety worldwide. Among the different types of slope movement, shallow landslides are the most common phenomena and are often associated to other soil instabilities and to various channel processes (i.e. sediment transport, woody debris). Vegetation and in particular forests is an effective and well-known tool in preventing and mitigating hydrogeological hazards, mainly through the effects of the reinforcement exerted by the root systems.

Root reinforcement, then, is a factor that should be included in hazard estimation and the resulting maps that represent a fundamental tool for planning and managing the hydrogeological hazards. Accordingly, in the last two decades, a wide number of different methods and approaches have been proposed to produce landslide hazard maps, with particular reference to Physically-Based Spatially-Distribute Models, PBSDM. However, including root reinforcement is still a challenge for the scientific community due to the huge spatial and temporal variability and the difficulties in incorporating into slope stability analysis.

The main gaps to be filled can be summarized as follows:

- the knowledge on the spatial distribution of the soil reinforcement due to the root systems have to be improved and linked to the stand forest characteristics;
- a 3-D probabilistic PBSDM of hillslope failure able to include in a comprehensive but simple manner the presence of the forest vegetation have to be developed;
- the use of information at coarse spatial resolution, which introduces an additional source of uncertainty has to be properly managed.

This study gives a brief review of the role of forests against natural hazards and on the state of the art concerning the implementation of root reinforcement into stability models. Thereafter, it attempts to fill such gaps

improving the knowledge about modelling and quantifying the effects of vegetation on slope stability.

The main outcome is the development of a 3-D probabilistic PBSDM of hillslope failure, based on geotechnical sound hypothesis and stochastic approach through the Monte Carlo Simulation (MCS) analysis. Such a model is able to manage the uncertainty of model parameters and is a reliable way to deal with the problem of a lack, or a poor knowledge of terrain characteristics over large study areas. In addition, it allows evaluating the effects of silvicultural operations, to estimate the woody material, recruitable from the hillslopes in small mountainous catchments, and to quantify the additional soil reinforcement provided by some cultivations such as the grapevine. Moreover, a series of field experiments on the rooted-soil under compression is presented in order to investigate the hydro-mechanical process that occurs during the triggering mechanisms of shallow landslides.

Finally, the proposed modelling framework will allow:

- to assess the probability of hillslopes failure considering the characteristic of the vegetation and to provide more reliable shallow landslide hazard maps at catchment scale;
- to improve the efficiency of prevention and protection due to vegetation, and particularly to the forests, against natural hazards evaluating different land management strategies;
- to support the planning of eventual forest interventions or soil-bio engineering works identifying the areas affected by high landslide susceptibility.

Sommario

Le frane sono una seria minaccia per la popolazione, gli edifici, le infrastrutture e le attività umane in tutto il mondo. Tra le diverse tipologie di instabilità di versante, le frane superficiali sono le più comuni e spesso sono associate ad altri processi idrogeomorfologici (trasporto di sedimenti e di materiale legnoso, colate detritiche, ecc.). Le piante sono uno strumento molto efficace, noto da tempo, per la prevenzione e la mitigazione dei rischi idrogeologici, in particolare attraverso l'effetto stabilizzante fornito dagli apparati radicali, noto come rinforzo radicale.

Il rinforzo radicale dovrebbe essere sempre incluso nella valutazione della pericolosità e considerato nelle mappe di rischio franamento che rappresentano il più grande supporto alla pianificazione e alla gestione del rischio. La consapevolezza di tale ruolo ha portato, negli ultimi vent'anni, a sviluppare un cospicuo numero di metodologie per la valutazione del rinforzo radicale e la mappatura del rischio franamento, tra cui i modelli fisicamente basati e spazialmente distribuiti (Physically-Based Spatially-Distribute Models, PBSDM). Tuttavia, includere il rinforzo radicale nel calcolo della stabilità di versante resta per la comunità scientifica una questione non ancora risolta compiutamente a causa della grande variabilità, sia spaziale che temporale, di tale fattore e della complessità di incorporare l'effetto stabilizzante delle radici nei metodi geotecnici comunemente usati.

Le principali lacune da colmare possono essere riassunte nei seguenti punti:

- la comprensione della distribuzione spaziale del rinforzo del suolo dovuto alla presenza delle radici deve essere approfondita e connessa alle caratteristiche della copertura vegetale;
- occorre implementare un modello tridimensionale e probabilistico in grado di incorporare in maniera semplice ma efficace la presenza della vegetazione;

- occorre sviluppare metodi che consentano di utilizzare informazioni a bassa risoluzione e/o parziali che introducono errori aggiuntivi.

Questo studio fornisce dapprima una breve rassegna bibliografica sul ruolo delle foreste nel contrastare i rischi idrogeologici e sullo stato dell'arte riguardante l'implementazione del rinforzo radicale all'interno dei modelli geotecnici. Successivamente, tratta del miglioramento delle conoscenze legate alla modellizzazione e alla quantificazione di tali effetti sulla stabilità di versante ai fini di uno sviluppo modellistico.

Il principale risultato è lo sviluppo di un modello tridimensionale, stocastico, fisicamente basato e spazialmente distribuito, basato su solide ipotesi geotecniche e un approccio stocastico mediante la simulazione Monte Carlo. Tale modello è in grado di gestire l'incertezza dei parametri di ingresso e di trattare le problematiche legate alla mancanza di dati affidabili su vaste aree. Inoltre, questa metodologia permette di valutare gli effetti degli interventi selvicolturali, di stimare il materiale legnoso proveniente dai versanti dei piccoli bacini montani e di quantificare il contributo alla stabilità fornito da coltivazioni come la vite.

Infine, si presentano i risultati di una serie di esperimenti condotti in campo su terreni forestali sotto compressione al fine di capire e quantificare il processo idrologico e meccanico che avviene durante l'attivazione di una frana superficiale.

In conclusione, lo schema di modellazione proposto permette di:

- valutare la probabilità di franamento di un versante tenendo in considerazione le caratteristiche della copertura vegetale e di produrre più accurate mappe di rischio franamento a scala di bacino;
- migliorare l'efficacia del ruolo di prevenzione e protezione da parte della vegetazione, ed in particolare dalle foreste, contro i rischi naturali, valutando differenti strategie di gestione del territorio;
- supportare la pianificazione di eventuali interventi selvicolturali o di ingegneria naturalistica, identificando le aree più suscettibili al rischio franamento.

List of contents

General Introduction	1
Rationale of the study.....	1
Background	2
Aims and structure of the thesis	4
1 Protection Forests.....	7
1.1 Introduction.....	9
1.2 Materials and methods.....	32
1.3 Results	58
1.4 Discussion.....	65
1.5 Conclusions.....	70
2 A Probabilistic 3-D Stability Model.....	71
2.1 Introduction.....	73
2.2 Materials and methods.....	77
2.3 Results	92
2.4 Discussion.....	101
2.5 Conclusions.....	110
3 Effects of Forest Management.....	112
3.1 Introduction.....	113
3.2 Materials and methods.....	114
3.3 Results and discussion	118
3.4 Conclusions.....	123
4 Large Wood recruitment from hillslope	125
4.1 Introduction.....	127

4.2	Materials and methods.....	131
4.3	Results	142
4.4	Discussion.....	153
4.5	Conclusions.....	162
5	Root Reinforcement in a Vineyard	165
5.1	Introduction.....	167
5.2	Materials and methods.....	170
5.3	Results	183
5.4	Discussion.....	193
5.5	Conclusions.....	206
6	Rooted-Soil under Compression	209
6.1	Introduction.....	211
6.2	Literature review of passive earth force	216
6.3	Materials and methods.....	220
6.4	Field measurements.....	223
6.5	Results	233
6.6	Discussion.....	248
6.7	Conclusions.....	259
	Notations.....	261
7	Conclusive Remarks.....	265
	Appendix A	269
	Appendix B	289
	Appendix C	293
	Appendix D.....	295
	Appendix E	297

References	299
------------------	-----

GENERAL INTRODUCTION

Rationale of the study

Landslides are a serious threat for human activities, settlements, and safety in mountainous and hilly region worldwide. In particular, in Europe, landslide hazard is equally important with an estimated cost of 23 \$ million per landslide (van Asch et al., 2007) and a remarkably high number of deaths and injuries (Haque et al., 2016). The European Commission published an overview of the actions undertaken and the future challenges for ensuring protection from the natural threats and for safeguarding the soil conservation, titled "The implementation of soil thematic strategy and ongoing activities" (European Commission, 2012), and in consequence of that it has been published a preliminary landslide susceptibility map of the EU, collecting data of over 100,000 landslides (Günther et al., 2014; Panagos et al., 2012). However, the EU member countries are still at the beginning of the awareness of the landslide risk management strategy.

The term landslide is widely used to describe a large range of slope instabilities, from the rockslides to the soil erosion. Several classifications have been proposed according to the type of movement, dimensions, velocity and source material (Highland and Bobrowsky, 2008; Hungr et al., 2014; Varnes, 1978). The most common phenomena are the shallow landslides that are generally translational and rapid soil mass movement occurring in almost the first two metres of depth (e.g. D'Amato Avanzi et al., 2013; Fuchu et al., 1999; Godt et al., 2008). They are often associated to other soil instabilities and to various channel processes, such as sediment transport, debris flow, and woody debris, and constitute the major landform shaping process in steep terrain environments (Beguería, 2006; Rickli and Graf, 2009).

Although natural factors influencing the trigger mechanisms of landslides are various (e.g. geological, geomorphic, hydrological, meteorological), a key factor, too often neglected, is the vegetation cover that affects several

hillslope processes and consequently the susceptibility to slope instability. Indeed, plants can modify the soil hydrology through interception, evapotranspiration and drainage capacity and can reinforce soil structure through the presence of roots, also called root reinforcement. This last contribution is the main positive effect on slope stability.

For this reason, vegetation effects should be always included in hazard maps that represent fundamental tools for planning and managing the prevention and the mitigation of hydrogeological hazards, especially at regional scale. However, this issue remains a challenging task for the international scientific community.

Background

In the last two decades, several methods have been proposed to produce landslide hazard maps. They vary from simple expert knowledge systems to sophisticated mathematical procedures and can be grouped into statistical-based correlation analyses and Physically-Based Spatially Distributed Models, PBSDMs (Guzzetti et al., 1999; Montgomery and Dietrich, 1994). PBSDMs, combine a slope stability analysis and a hydrological flow model in a spatially-distributed form (e.g. Borga et al., 1998; Montgomery and Dietrich, 1994; Wu and Sidle, 1995; Zizioli et al., 2013), providing a good representation of the triggering process and are suitable for designing appropriate measures for preventing and mitigating the instability phenomena and assessing their effectiveness. In addition, PBSSMs can take into account the spatial and temporal variability of the land coverage, which is a driver in shallow instability processes due to its effects on hydrological and mechanic reinforcement mechanisms (Sidle and Ochiai, 2006).

The most common approach adopted in PBSDMs is the infinite slope stability model, a simplified and well-known low-dimensional approach that is generally combined with more or less simplified methods for including the hydrological dynamics. The infinite slope approach has proven to be able to provide reliable results for shallow instabilities and when the topography has

a major influence on the trigger mechanisms (Gorsevski et al., 2006a) and has also been applied to forest areas (Dietrich et al., 2001; Pack et al., 1998). Several studies have evaluated the effects of vegetation on slope stability in terms of hydrological processes (Bathurst et al., 2010; Kim et al., 2013), and mechanical effects (e.g. Kuriakose et al., 2009). In particular, the water pore pressure reduction and the effect of roots crossing the shearing surface have been included in many PBSDMs (e.g. Borga et al., 2002; Wu and Sidle, 1995). However, the PBSDMs based on the infinite slope approach cannot fully consider the heterogeneity and variability of vegetation cover and their role in triggering landslides such as the additional shear reinforcement due to root crossing the lateral surfaces of a landslide. Some authors, as a consequence, attempted to include the lateral reinforcement into the infinite approach by introducing simplifying assumptions (Casadei et al., 2003a; Chiaradia et al., 2016), which however are not entirely correct. In fact, a real physically-based inclusion of the role of vegetation into shallow landslide modelling, ultimately, requires a shift from a 2-D to a 3-D approach.

Simplified 3-D solutions have been proposed in the past, starting from the pioneering work of Burroughs and Thomas (1977). This approach was the basis of simplified multidimensional shallow landslide models, which neglect the significant role of lateral earth pressure (Casadei et al., 2003a; Schmidt et al., 2001). Unfortunately, such assumption significantly affects the accuracy of the results (Dietrich et al., 2007; Terwilliger and Waldron, 1991), and recently, Milledge et al. (2014) developed a model that is robust and suitable to include in a more reliable manner the presence of roots in the soil. Considering the physical factors affecting landslides triggering, PBSDMs request a large number of parameters such as the geotechnical properties, geomorphological and hydrological variables, and the reinforcement exerted by the root system linked to the land cover characteristics. Such parameters are generally affected by a certain degree of uncertainty due to their spatial variability and measurements errors. To manage this uncertainty, several authors have been introduced Monte Carlo Simulation (MCS) analyses (e.g.

Hammond et al., 1992; Haneberg, 2004; Zhou et al., 2003). They assumed a probability distribution function (PDF) for each input parameter. Although PDFs of geotechnical soil properties have been the object of many studies and some reference functions can be identified, PDFs of the root reinforcement are still lacking because of the scarcity of data. Additionally, this term varies spatially in function of vegetation species, stand characteristics (density, age, etc.) and environmental conditions, and varies temporally due to natural and/or human disturbances.

Aims and structure of the thesis

This dissertation thesis focuses on extending the knowledge about the contribution of vegetation to slope stability, especially due to the root systems. The research work explores the quantification of root reinforcement taking into account both its spatial and the temporal variability and including it into a procedure for mapping the landslide susceptibility. In *Chapter 1*, a review summarizes the role of protection forests in contrasting natural risks in the European mountainous context, and the scientific background to evaluate this protective function analysing data collected in the field or from the literature. In *Chapter 2*, a new PBSDM, developed to obtain more accurate landslide hazard map, is presented and tested on a subalpine-forested catchment. It combines an accurate multidimensional slope stability analysis and a stochastic approach in order to overcome several limitations involved in the infinite slope theory, and due to the uncertainties of the input parameters, and to take into account all the mechanical processes due to the presence of roots in the soil. In *Chapters 3, 4 and 5*, three different applications of the developed model are illustrated. The first faces the evaluation of the effects of different silvicultural operations on slope stability, the second deals with the evaluation of the amount of woody material recruitable from the hillslopes into small mountainous catchments, and the last aims to quantify the contribution provided by the roots of grapevines in contrasting shallow landslide. In *Chapter 6*, a special attention was given to

the investigation of the role of the passive earth pressure into the slope stability analysis, designing and conducting experiments at local scale.

1 PROTECTION FORESTS

Keywords:

Protection forests;

Root reinforcement;

Tree roots;

Natural hazards;

Landslides.

1.1 Introduction

1.1.1 Historical background

The Alpine area is one of the widest natural space in Europe, yet is the home and workspace for 14 million people and a holiday destination for 120 million guests each year. The Alps are also the main source of water, hydropower, and natural products for populations of the surrounding plains. However, increasing population density and emerging tourism resulted in an increased demand for hydrological services and protection of settlements, activities, and infrastructures from natural hazards (Chatré et al., 2010). Although artificial structures, such as avalanches barriers, terraces, dams, and galleries can provide protection against natural hazards, another possible and attractive measure is certainly the forests (Schönenberger and Brang, 2004). Forests, in fact, provide many benefits, which consist of intrinsic services, including the reduction of natural risks with a lower environmental impact than the traditional engineering structures, and with a significant reduction of expenditure, because the relatively low maintenance cost of forests, which can make them an economically sustainable strategy in contrasting landslides, in synergy or substituting the investments required for more expansive works (Brang et al., 2001). In Switzerland, Zimmermann (2008) estimated that avalanches barriers cost about 1,000 times more than the silvicultural operations aimed to maintain the effectiveness of the protection functions of a forest. Thus, an appropriate identification and planned management of protection forests can, therefore, make mountainous settlements safer for people and infrastructures (Sakals et al., 2006).

This awareness of the role of forests in protecting people, settlements and resources from hydrogeological hazards including floods, debris floods, debris flows, snow avalanches, rockfalls and landslides, has been strongly present from immemorial time inside the mountain communities (Cheng et

al., 2002; Sakals et al., 2006; Sidle et al., 1985). The first allusions are even present in Greek, Hebrew and Roman literature (Hamilton, 1992).

The Alpine European countries have adopted regulations and laws concerning mountain protection forests since the Middle Age, in order to limit the exploitation of woods.

During the early ages of manufacturing developments, Alpine population exploited massive forest resources through huge clear cuts. As consequence, timber became a rare and therefore valuable good. In this context, the earliest orders, in the European continent, regulating timber harvest and controlling forest management was promoted by citizens of the Tyrolean sovereign in 1385 (Weiss, 1999). At the same time, the people of Andermatt (Canton of Uri) in Central Switzerland in 1397 banned any further cutting of remaining coniferous forests on the steep slopes above their houses and forbade to remove trees, branches, and cones (Brang et al., 2001). The protection forest currently maintains its fundamental function in contrasting natural hazards, in particular, snow avalanches (Figure 1.1)

Moreover, other local regulations of the Aosta Valley region (NW-Italy), predating the Tyrolean orders and dated back the XIII century, reveal that mountain people well know the function of forests in stabilizing slopes and limiting damages from extreme events. Additionally written evidence, relating to a period between 1333 and 1480, refer to protection forests above dwellings (Gerbone, 1997). Thereafter, the “Coutumier du Duché d’Aoste”, a written collection of Aosta Valley norms and customs, reiterated the ban on woodcutting in protective forests in 1587.

Similar rules limiting forest-clearing activities were found in documents and regulations of the Republic of Venice from as early XIII and XIV centuries (Bischetti et al., 2009).

These regulations were finally codified into laws in the mid of XIX century in most European Alpine countries.



Figure 1.1. The triangle of the forest above the town of Andermatt (Canton of Uri, Switzerland) provides a natural barrier against avalanches and rockslides since 1397. Photograph by swissinfo (<https://www.swissinfo.ch/>).

The earliest systematic recognition of the fundamental role of forest in contrasting natural hazards was obtained in the Bavarian forest law established in 1852 introducing the term “protection forest” (“Schutzwaldungen”) (Brang et al., 2001). In 1860, France promulgated a law concerning mountain restoration and reforestation after the extensive floods occurring 10 years before (Whited, 2005). In Austria, several local regulations already enacted in Tyrol region (S- Austria) in 1810, was codified into a forest

act, the Austrian Empire's forest act ("Reichsforstgesetz"), known also as liberal forest act, in 1852. This act removed forest from private and communal management and placed them under a rigorous supervision controlled by the State because of their importance in protecting the plains (Brotto, 2008; Whited, 2005). It was the first code promoting the idea of a "sustainable" forestry (Weiss, 1999).

In Switzerland, the federal institution codified a law of 1876 that approved the federal intervention on large-scale reforestation and extended its control on Alpine areas covered by forests in order to improve the safety of connections between highland and lowland (Whited, 2005). In Prussia, a series of laws, directives, and regulations governing the public use of forests were strengthened introducing a unique code, the Prussian forest protection act ("Preußisches Waldschutzgesetz") in 1875. In Italy, the awareness of the importance of mountain forests have been recognized and governed through the Royal Decree No 3267/1923 "Rearrangement and reform of legislation concerning woods and mountain land", so-called "forest law". This law imposed to regulate forest uses and silvicultural activities through hydrogeological constraints in those soils subjected to hydrogeological risk to guarantee the public interest (Agnoletti and Anderson, 2000).

Outside Europe, in the United States of America, the Organic Administration Act of 1897 introduced the national forest areas designated as forests for multiple use and sustained yield. Improving and protecting the forests, water flows and timber extraction were the primary concerns. Since the mid of the XIX century, Japanese planners decided to place snowdrift shelter-woods along railway lines in order to mitigate and prevent damages caused by snow avalanches (Shimamura and Togari, 2006). These solutions became the most indispensable and effective disaster prevention measure for all the XX century. An example was the Ganetsu Line, opened in 1914, and partially destroyed by a series of 75 avalanches in 3 years. To contrast these causalities, the railway authority designated slopes prone to avalanches and undertook necessary afforestation measures to create a shelter-wood.

Although this railway line was subjected to 250 avalanches in the first 20 years, once the wood reached the maturity, only seven events were experienced for the next 20 years. For more than one century, railways shelter-woods have been developed based on coniferous monocultures, which requested an ordinary forest management to cut the revenues, without an economic benefit from selling the timber. As a result, ecological, functional and aesthetic conditions of railway shelter-woods have deteriorated.

More recently, the Ministerial Conferences on the Protection of Forests in Europe (MCPFE) provided a specific definition for forests with protective functions as follows:

- (i) the management is clearly directed to protect soil and its properties or water quality and quantity or other forest ecosystem functions, or to protect infrastructure and managed natural resources against natural hazards;
- (ii) forests and other wooded lands are explicitly designated to fulfil protective functions in management plans or other legally authorized equivalents;
- (iii) Any operation negatively affecting soil or water or the ability to protect other ecosystem functions, or the ability to mitigate damages to infrastructure and natural resources from natural hazards.

This definition implies that two different typologies of protection coexist (Brang et al., 2006; Meloni et al., 2006): indirect and direct protection.

Forests with indirect protective function generally improve hillslope stability, reduce soil erosion and regulate yield and transport of sediments inside the watershed. They are usually located in the steeper areas and guarantee a mitigation of natural hazards, not primarily at the local scale, but at regional or catchment scale. The impact of the forest in contrasting catastrophic events depends on its dimension at the landscape scale, but not on its location inside the watershed. In this case, a relationship between protective effects and potential damages is impossible to evaluate.

Forests with direct protective function have the primary function to protect people, settlements or infrastructures against catastrophic natural events. The definition given by (Brang et al., 2001) implies that: (i) a natural hazard or a potentially adverse climate may cause the damage, (ii) people or assets may be damaged, and (iii) the forest has the potential to mitigate the damage (Figure 1.2).

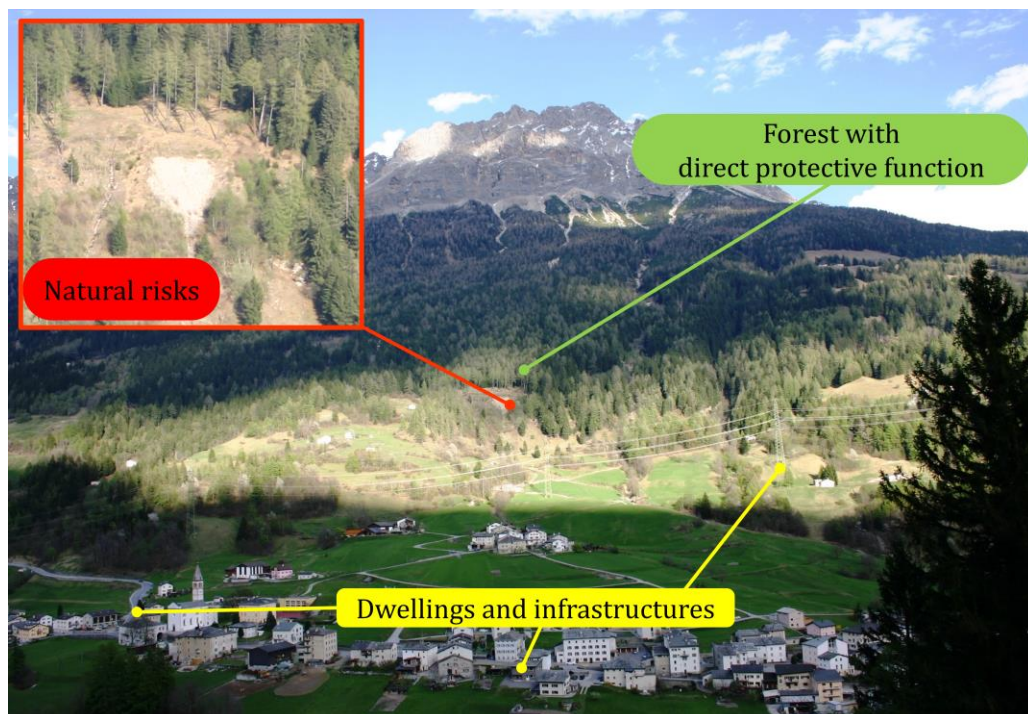


Figure 1.2. Common example of forest with direct protective function near the village of San Carlo in Poschiavo valley (Canton of Grisons, SE- Switzerland)

This central role in contrasting natural hazards is nowadays widely rediscovered by policy-makers in different countries, especially where the natural disasters are frequent. For example, Cheng et al. (2002) and Forbes and Broadhead (2011) showed a significant expansion of protection forests aimed to directly contrast extreme hydrogeological risk at watershed scale in the past century in Taiwan, and in the last 20 years in other Asian countries such as China, Republic of Korea, Myanmar, Thailand and Vietnam.

Although many governments adopted logging moratoria and financed reforestation projects, some of these decisions were proven to be not appropriate in relation to the soil instabilities occurred in those areas (Le et al., 2014). For this reason, a robust scientific and technical background is crucial to understand and evaluate the benefits or the disadvantages that a forest under specific conditions can provide in contrasting natural hazards, to address future forestry policies and to plan a sustainable forest management.

In European Alpine countries, such as Austria, Switzerland, France, Germany, and Slovenia, protection forests were mapped distinguishing direct or indirect functions considering gravitational hazards such as avalanches, landslides and rockfalls, or hydrological processes such as floods, water and wind erosion. A common restriction adopted by most of the European countries is the ban of indiscriminate harvesting; in fact, restrictions of forest operations exist and the owner of the forest must be authorised to plan adequate management in protective forests.

In particular, in Switzerland, the nationwide project SilvaProtect-CH defined uniform criteria for protection forest delimitation (Losey and Wehrli, 2013). As consequence, the Swiss Confederation pays service-based compensations to the cantons, which are responsible for carrying out silvicultural measures in forests that work as protection against natural hazards. Such measures aim to reach a defined target profile according to the criteria of Swiss guideline “Sustainability and success monitoring in protection forests” (Frehner et al., 2005).

In Italy, through an administrative decentralization process, the Regional Authorities adopted different rules and regulations both for the definition and for the determination of protection forests. In Aosta Valley region, protective forests mapping was the first step of a sustainable long-term silvicultural management. According to the procedure developed by Meloni et al. (2006), direct protection forests were identified taking into account the digital elevation model with a resolution of 10 x 10 m, aerial images and forest

coverage information. In Piedmont region (NW-Italy), the local authorities classified as protection forests those that directly protect settlement and infrastructure and the forests relevant for the protection of the streams from erosion. In addition, guidelines were proposed for a sustainable silvicultural approach in those areas. In Lombardy (N-Italy), the forests with protective function have to be identified in the plans of forest management defining a specific management of forestry interventions. In Liguria (NW-Italy) where the landscape is prone to erosion phenomena due to its geomorphology, protection forests are distinguished for their protective function against shallow landslides or soil erosion.

1.1.2 The management of protection forests

Effectiveness and reliability of the protective functions strongly depend on which natural hazard is considered, the frequency and intensity of damaging events and the condition of the forest itself (Brang et al., 2006). In many cases, protection forests cannot provide complete protection from all damages, because the residual risk is high. A typical example is a small-forested slope, located above a village, which cannot guarantee to stop rocks falling from a cliff (Brang et al., 2006).

Forest management is the key issue for an effective mitigation strategy affecting the forest dynamics in order to improve the contrast against a specific natural hazard. However, the common action regarding Alpine forests was to ban timber harvesting to impede an indiscriminate exploitation of forested areas (Motta and Haudemand, 2000). Nowadays, the lack of adequate economic benefits determines a progressive abandonment of forests and most of the protective forests are left unmanaged. This situation is acceptable if the potential damage is small and depends on forest conditions too (Brang et al., 2006). Indeed, an abandoned forest may not guarantee an adequate protective function over time because of natural or artificial disturbances such as disease, wind-throws or fire (Brang et al., 2006; Sakals and Sidle, 2004; Schönenberger et al., 2005). Thus, protection

forests request a complete evaluation in terms of resistance and resilience (Sakals et al., 2006). Resistant forests are less susceptible to reduce their protective functions after a disturbance, whereas resilient forests have the ability to recover rapidly direct-protection resistance characteristics following a natural hazard event. In general, healthy and mature forests have both these abilities, however, an active and continuous monitor of forest management is necessary to maintain or increase them. In particular, forestry based on the natural cycles of forests guarantees the stability of mountain protection forests (Berger and Rey, 2004). Motta and Haudemand (2000) suggest that an acceptable degree of stability ensuring that the functions of protective forests last over the following 20-50 years.

On this background, forest planners of European Alpine countries agree that guidelines are necessary. Swiss federal offices address the work of foresters through practical guidelines for the forest interventions developed by forest managers and scientists (Frehner et al., 2005). This collaboration emphasized the importance of combining the scientific knowledge, improved during the last decades, and the professional experiences in order to allow science-based decisions. Nevertheless, some aspects of the protective role of forest are still unknown. Moreover, quantifying every protective function is a crucial challenge in order to compare them with the engineering structures.

1.1.3 Effects of forests against landslides

Forests provide positive and negative effects on slope stability depending on their structure and condition. The effects of forests on shallow landslides can be distinguished into two groups: mechanical and hydrological. At the catchment scale, forests provide hydrological effects that influence quantity and velocity of runoff processes. At the local scale, mechanical effects are the most important contributions in contrasting slope instabilities (Vergani et al., 2017a). In the long term, forests may also have an indirect effect on the development of the soil under the influence of different tree species (Graham and Wood, 1991).

Hydrological effects

The main hydrological effect is to reduce the moisture content into the soil and to delay the onset of soil saturation levels at the soil depth where landslides are triggered (Forbes and Broadhead, 2011) through several processes (Figure 1.3):

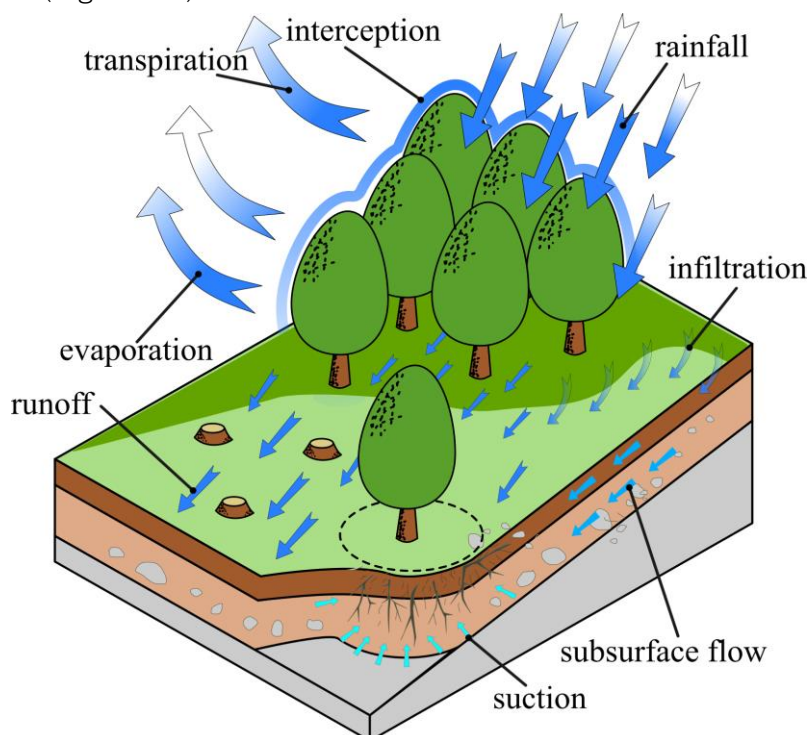


Figure 1.3. Effects of vegetation on hydrological processes.

(i) Interception and evaporation (+)

Vegetation modifies intensity and distribution of precipitation falling on through canopy and woody structures (Figure 1.4). Canopy with branches, shoots and leaves, and litter reduce the quantity of effective rainfall (i.e. throughfall, litterfall and stemflow) that reaches the soil surface and redistribute rainwater on the ground surface (Dhakal and Sullivan, 2014; Gerrits et al., 2010; Ghestem et al., 2011; Keim and Skaugset, 2003). This hydrological process is known as interception loss, I_C . The water, once retained by vegetation surfaces, later evaporates or is directly absorbed by plants. I_C strongly depends on different factors, such as species, age, and stand density, and varies from 2% to 67.5% of the annual precipitation, as verified through a review of the literature (Appendix A). Distinguishing the forest type, the range of the measured annual interception loss is generally similar (Figure 1.5). On average, however, conifers intercept more rainfall than the deciduous forests, 26.15% against 19.71%, accordingly to the structure of the forest canopy that is the greatest seasonal change in deciduous forests. (Link et al., 2004; Staelens et al., 2008). In fact, the intercepted rainfall is particularly larger in the growing season for small rainfall events, whereas throughfall is lower in the dormant season (Link et al., 2004; Staelens et al., 2008). Additionally, Liang et al. (2007) observed that the stemflow might concentrate the rainwater on the downslope side of tree trunk leading to an increase in pore water pressure. On the other hand, stemflow consists of a very small proportion of the rainfall (Liu, 1997). In literature, measured values of stemflow vary from 1.30 % to 4.10 % of the annual rainfall (Crockford and Richardson, 1998a, 1998b; Llorens, 1997; Singh, 1987; Sinun et al., 1992). Although canopy and litter layer have a constant moisture storage capacity, their contribution to intercept the effective rainfall usually play a minor role in modifying shallower soil water and pore pressure propagation, especially during prolonged wet periods (Dhakal and Sullivan, 2014; Sidle and Ziegler, 2017). Furthermore, the amount of stored water evaporates according to the weather factors. For

example, Gerrits et al. (2010) estimated the evaporation from litter layer of beech forest (*Fagus sylvatica* L.) in Luxemburg is around 20% of throughfall even during winter.

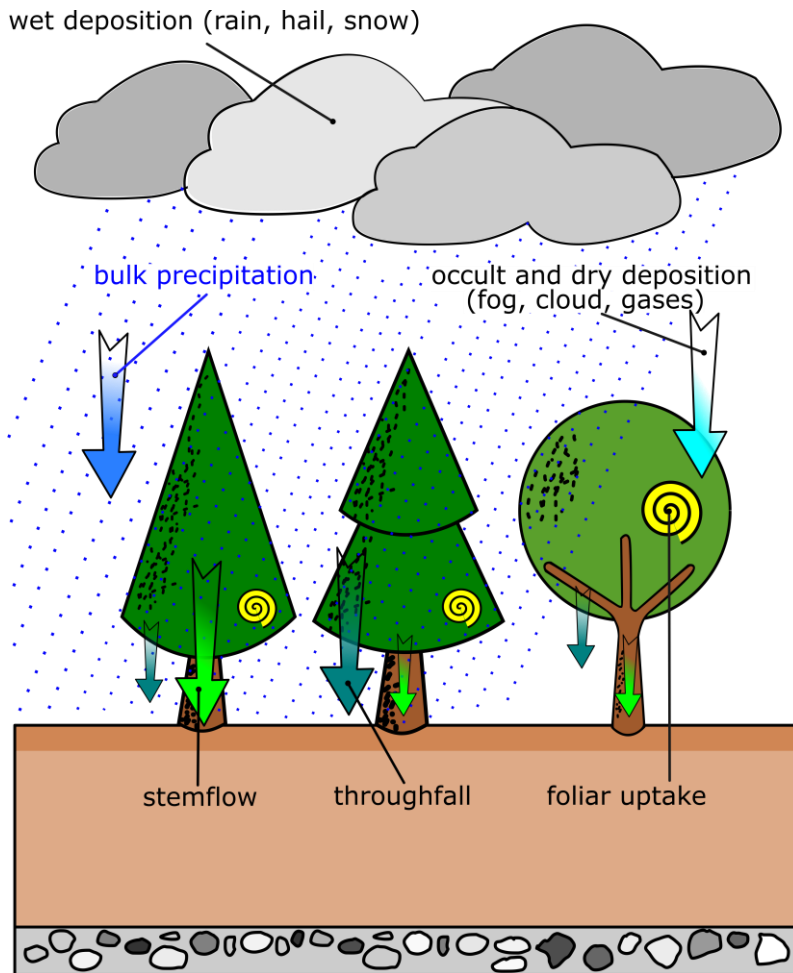


Figure 1.4. The generation of different hydrological processes causing interception loss and water moisture storage.

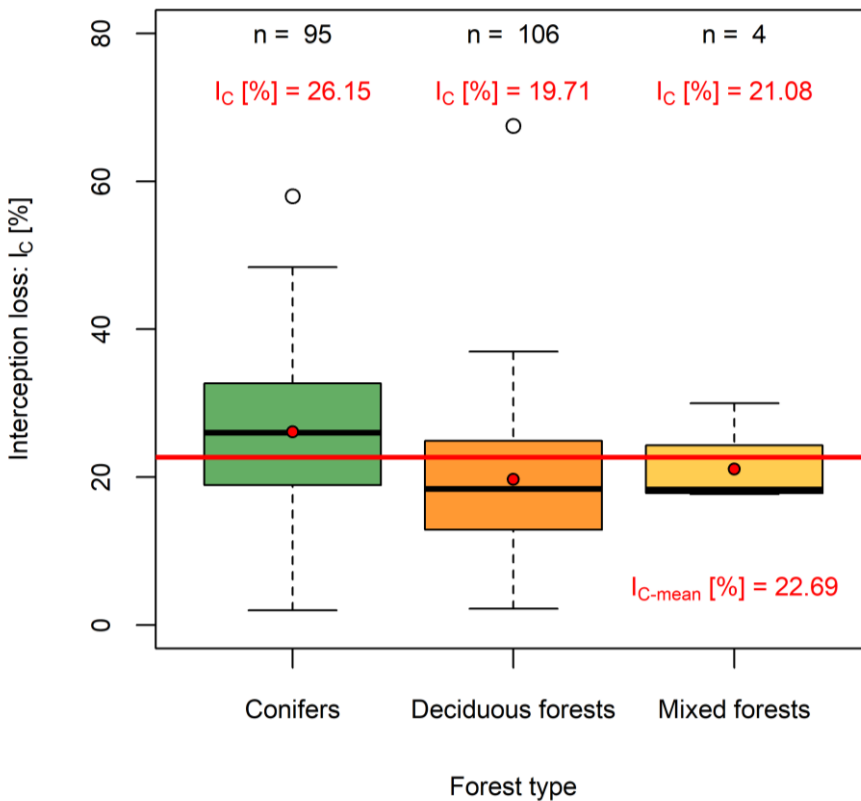


Figure 1.5 Statistical analysis on data of interception loss values in function of three forest types (conifers, deciduous and mixed forests) observed in several sites in Europe and North America, collected in the literature.

Finally, the characteristics of the rainfall such as intensity and duration affect the impact of I_C (Calheiros De Miranda and Butler, 1986; Llorens, 1997; Pypker et al., 2005). Sure enough, the interception storage capacity and, as consequence, I_C decreases with the rainfall duration, whereas tends to be highest for small storms on dry canopies (Reid and Lewis, 2009).

(ii) Suction and transpiration (+)

Trees have more extensive root systems that can extract moisture from the soil at considerable depth and then reduce moisture levels from distances of up to three times the radius of the crown (Gray and Sotir, 1996). However, the reduction of soil moisture is negligible in the case, common in cool temperature and subalpine regions, where the precipitation considerably exceeds potential evapotranspiration. Nevertheless, evapotranspiration may reduce soil moisture prior to a rainfall event and thus increase the amount of water that can be stored in the soil, although this may be effective only during dry periods (Sidle and Ochiai, 2006). For example, Dhakal and Sidle (2003) studied the triggering mechanisms of several landslides in a watershed in British Columbia (SW-Canada) covered by mature western hemlock showing how the reduction of evapotranspiration after logging causes the increase of the pore water pressure during moderate winter storms, but not for large storms.

(iii) Infiltration and subsurface flow (\pm)

Forests usually have high infiltration rates, but they may reduce soil moisture through subsurface flows pipes and channels formed by root decay and burrowing animals. Root system facilitates preferential flow in soils (Uchida et al., 2001). They, in fact, contribute to soil pore formation and to form networks or pathways that can help slopes to drain faster than if no channels were present (Vergani and Graf, 2015). It is also possible that the concentrated flow and the increase in pore water pressure in pockets cause the expansions of bedrock fractures (Ghestem et al., 2011).

(iv) Surface roughness (-)

Roots and stems increase the roughness of the ground surface and soil permeability, leading to an increase of infiltration capacity (Greenway, 1987). Very few studies have been paid particular attention to this topic, especially in forest environments (e.g. De Baets and Poesen, 2010; Gyssels et al., 2005; Vannoppen et al., 2015).

Mechanical effects

Mechanical effects of vegetation have been subject of research since the second half of the XX century (Endo and Tsuruta, 1969; O'Loughlin and Ziemer, 1982; Sidle and Ochiai, 2006). Such processes can provide stabilizing (Figure 1.6) or destabilizing effects (Figure 1.7).

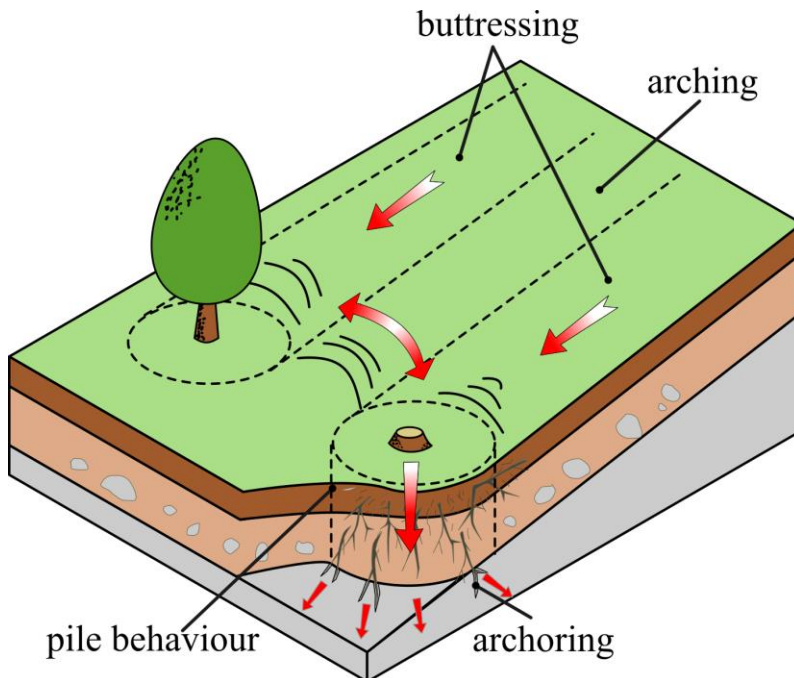


Figure 1.6. Positive mechanical effects on slope stability.

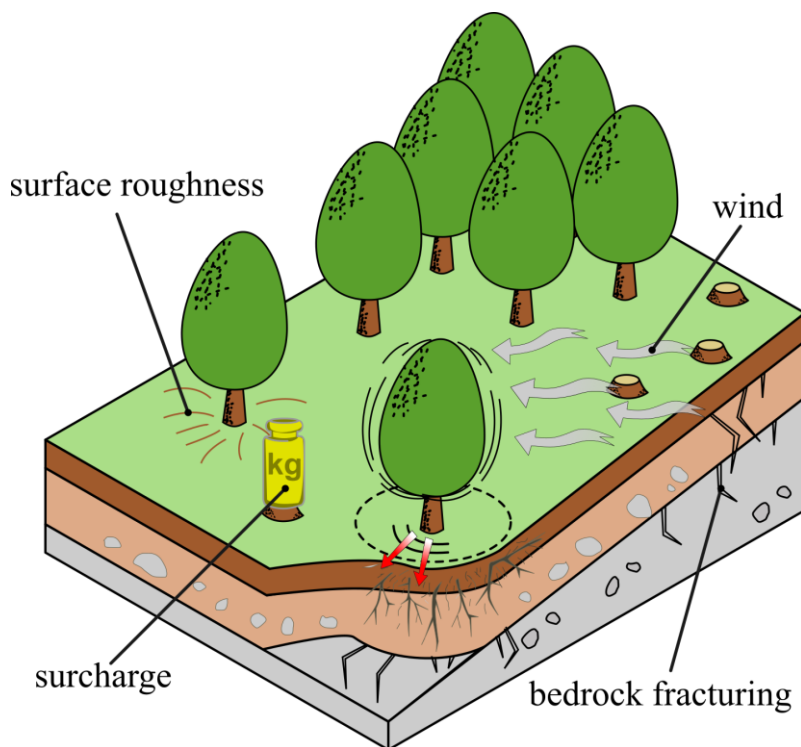


Figure 1.7. Negative mechanical effects on slope stability.

(v) Soil reinforcement by roots (+)

Soil reinforcement by roots is recognized as the main contribution of forests to slope stability especially playing a key role during the triggering of shallow landslides (Hubble et al., 2013; Roering et al., 2003; Schmidt et al., 2001; Sidle et al., 1985). Since the 1970s, a noticeable attention has been devoted to quantifying the reinforcing effect of tree roots (e.g. Burroughs and Thomas, 1977; O’Loughlin, 1974). Roots can stabilize the soil mantle through three different mechanisms (Schwarz et al., 2010b, 2015; Vergani et al., 2017a). The first is the basal root reinforcement and acts when roots reach the underlying stable layer crossing the slip failure surface. If roots do not expand until the failure surface, they mobilize their tensile strength along the lateral surface of the landslide. This mechanism is called lateral root reinforcement and is strictly affected by the dimensions of the potential shallow landslide (Schwarz et al., 2010a). The last is the compression resistance and is due to

the stiffness of the rooted-soil material. It occurs at the toe of the sliding soil mass and is relevant when there is a strong interaction between neighbouring root systems. Field experiments and modelling studies have extensively documented these mechanisms (Bischetti et al., 2005; Imaizumi et al., 2008; Waldron, 1977; Wu et al., 1988).

(vi) Surcharge (\pm)

Surcharge above the soil surface increases with increasing trees. Tree weight increases the normal force components as well as the tangential force components but in general plays a minimal role in the overall stability of a slope (Stokes et al., 2008). The local effects of loading due to wind and snow are not well known. However, it may be assumed that in general, these effects have no influence on the overall stability of a hillslope, whereas they can contribute to shallow landslide triggering only in extreme conditions. It even can provide benefits on slope stability when soil cohesion is low, groundwater table high or slope inclination low (Gray and Megahan, 1981).

(vii) Anchorage (+)

Roots anchor the soil mantle into a more stable substrate or firm strata (Gray and Megahan, 1981). Strong roots tie across planes of weakness and potential slip surfaces, thereby anchoring the soil, while small roots provide a membrane of reinforcement to the soil mantle, increasing soil shear strength. This mechanism is similar to the soil reinforcement, except that it occurs at a larger scale (Greenway, 1987). Although an apparent recognition that root anchorage provides a significant contribution to increase soil strength, few investigations have been carried out on the overall soil shear resistance (Riestenberg, 1994). Indeed, many authors have given little attention to the role of roots as single anchor focusing on the resultant buttressing effect (Gray and Leiser, 1982; Styczen and Morgan, 1995).

(viii) Buttressing and arching (+)

Roots and stems of woody vegetation can locally act as buttress piles to counteract downslope shear forces (Gray and Sotir, 1996; Roering et al., 2003; Schmidt et al., 2001; Sidle and Ochiai, 2006). In this way, trees help immobilize soil behind the tree extending upwards in particular at the bottom or toe of the slope (Gray and Sotir, 1996). The buttressing effect also extends laterally creating supporting arches to nearby trees (Forbes and Broadhead, 2011). Spacing, diameter of the soil-root cylinder, thickness of the yielding soil and soil properties affect the arching effects (Figure 1.8), which can be evaluated through a theory developed by Wang and Yen (1974) as follows:

$$P = \frac{1}{2} K_0 D_r \gamma z^2 + K_0 \gamma z - p B z \quad (1.1)$$

where P is the force acting on the soil and root system under each tree, K_0 is the coefficient of lateral earth pressure at rest, D_r is the diameter of the vertical soil-root cylinder, γ is the unit weight of the soil, z is the thickness of yielding soil layer, p is the average lateral pressure in the openings between soil-root cylinders, and B is the clear spacing between soil-root cylinders.

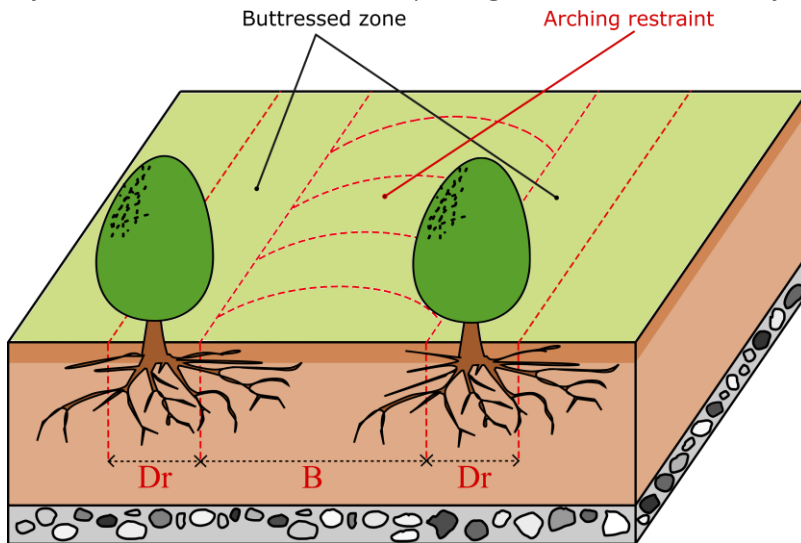


Figure 1.8. Schematic drawing of arching effects provided by two adjacent trees.

(ix) Wind loading (-)

Wind loading does not lead to landslide directly but the additional force has to be included in the force balance (Greenway, 1987). It can cause the pull-out of roots, soil cohesion reduction and decrease of shear stress. Additionally, wind uproots trees exposing mineral soil, allowing a large quantity of water to infiltrate and increase pore water pressure, as consequence. This negative effects increase with the tree height and are weaker for coppiced trees. Force of wind on trees can be significant during extreme meteorological events such as tropical storms or cyclones (Styczen and Morgan, 1995).

(x) Soil aggregation (+)

Soil aggregation expresses the ability of soil to retain its structure when exposed to different stresses. It is affected by plant growth and has been found to be directly related to the shear strength of soil (Frei et al., 2003). In addition, it is a critical factor when evaluating the effectiveness of the soil restoration methods as in case of soil bioengineering techniques. For this part, roots bind soil particles at the ground surface, thereby reducing susceptibility to erosion and shallower soil movement (Greenway, 1987).

Are the effects of vegetation more positive or negative?

Many studies were conducted regarding the effects of land use change on frequency and intensity of hydrogeological instabilities. Most of them observed the effects of substantial modifications of vegetation cover due, for example, to harvesting wood (Sidle and Terry, 1992; Steinacher et al., 2009; Ziemer and Swanston, 1977), grazing (Glade, 2003), expanding cultivated area (Chen and Huang, 2013), vineyards abandonment (Persichillo et al., 2017), building infrastructures (Larsen and Torres-Sánchez, 1998) or planting artificial forests in place of grassland (Phillips et al., 2017), or of natural forests (Genet et al., 2008).

On this background, most of the researchers showed that the positive effects are more relevant than the negative ones. In particular, natural forests with

their protective functions provide the greatest level of contrast to slope instabilities respect than other forms of land use (Forbes and Broadhead, 2011). Moreover, the investigations, conducted worldwide, on the consequences of the unlimited exploitation of the forests have demonstrated an increase in landslide frequency over the following 20 years (Guthrie, 2002; Jakob, 2000; Montgomery et al., 2000; O'Loughlin and Ziemer, 1982; Sidle et al., 2006). More specific works estimated the root decay in function of time after several disturbances that cause the decrease of root reinforcement and consequently the increase of slope instabilities, such as timber logging (Bischetti et al., 2016; Burroughs and Thomas, 1977; Schmidt et al., 2001; Vergani et al., 2014a; Ziemer, 1981), different forestry operations (Vergani et al., 2017a), bark beetle infestations (Ammann et al., 2009) and forest fire (Vergani et al., 2017b). Based on these studies, it has been possible to estimate a time window ranging from 3 to 20 years after forest clearing that coincides with an increase of the landslide susceptibility until 10 times more compared to undisturbed forest (Sidle and Bogaard, 2016). The loss of protective function persists until woody vegetation is re-established through the regrowth of regenerating vegetation.

1.1.4 Effects of forest on other natural hazards

Protective barrier

Trees and forests can provide a protective barrier against smaller avalanches or slides of rock, debris, and soil, as well as limit the run-out distances of material with respect to streams, roads and lines of infrastructure (Brang et al., 2001; Cattiau et al., 1995). Indeed, the effects of standing tree obstructing the downward movement of landslide material or rockfall may mitigate some or all of the potential damage (Dorren et al., 2005). For example, Guthrie et al. (2010) observed that debris flow deposited much of their load when hitting a forest boundary and stopped entirely within 50 m of that boundary in 72% of 1,700 examined cases in British Columbia (SW-Canada). The effect of tree buffers will depend on stand characteristics as width, spacing and tree diameter, and biological features (stiffness and elastic strength of woody materials) of tree species such as differences in protection against rock fall (Stokes et al., 2005).

Snow loading and avalanches

Snow loading and avalanches are other natural hazards that often cause damage in mountainous areas. The protective functions of forest are strictly influenced by its structure. Uneven and patchy structure of the forest, both horizontally and vertically, prevents extensive weak layers from developing across a hillslope, inhibiting avalanche initiation (McClung, 2001). Tree canopy contributes to getting the snowpack more heterogeneous through the interception. Moreover, forests shelter slopes exposed to snow loading by wind decreasing the wind transport (McClung, 2001). Indeed, several authors underlined that the ground roughness due to tree stems, woods, and stumps increases the stability of snowpack, and consequently increases the snow stability and limits the avalanche initiation (Frey and Thee, 2002; Kupferschmid Albisetti et al., 2003; McClung and Schaerer, 2006).

Floods

The forests also play a role in retaining material in channels even if it is not relevant as the effects on the hillslope (Sakals et al., 2006). At watershed scale, land cover strongly affects the flow paths and temporary storage capacity within a catchment. Afforestation can potentially mitigate flood risk through an increase in interception (Robinson et al., 2003), evaporation (Hewlett and Hibbert, 1967), infiltration (Bracken and Croke, 2007), temporary storage (Ghavasieh et al., 2006), slowing conveyance (Thomas and Nisbet, 2007), and attending runoff (Broadmeadow and Nisbet, 2010; Hundecha and Bárdossy, 2004). All these effects increase their effectiveness and reliability with increasing forest age (Harr, 1986). Schnorbus and Alila (2004) developed a numerical hydrologic simulation showing that the location of timber harvesting affects peaks of discharge caused by seasonal snowpack melting. Moreover, the forest structure is an additional factor for rate and timing of snowmelt influencing the energy balance within the forests (Winkler et al., 2005). At the channel and riparian scale, riparian forests strongly affect the hydraulic roughness of bed and bank of channels (Chow et al., 1988). In particular, many studies indicated the significant impact of roots in stabilizing streambanks and in limiting bank erosion (Abernethy and Rutherford, 2000, 2001; Adhikari et al., 2013; Docker and Hubble, 2008; Easson and Yarbrough, 2002; Hubble et al., 2010; Pollen, 2007; Pollen and Simon, 2005; Pollen-Bankhead et al., 2009; Pollen-Bankhead and Simon, 2009, 2010). Lisle (1995) emphasized that woody debris from forested slopes stabilizes bed and banks of channels reducing the transport of sediment during floods. Erskine and Webb (2003) observed that removal of vegetation and in-stream woody debris directly causes channel widening. In addition, it has been noticed that root systems and woody debris dissipate more energy than empty streambanks and to store sediments around the channels (Piégay et al., 1999; Wilford et al., 2005). Despite, this issue has been received great attention, there is no consensus on the general efficacy of forests in mitigating significantly flooding risk (Robinson et al., 2003), due to

the variability in climatic factors that have the same impacts than the land use changes (Andréassian, 2004) and due to the lack of evidence for large catchments over 10 km² (Archer et al., 1990). Finally, it is possible to synthesize that there is evidence on the effects of mitigation on moderate floods, but less or even not during extreme rainfall events (Anderson et al., 2006; Hess et al., 2010; Sholtes and Doyle, 2011).

1.2 Materials and methods

It has been found that the presence of forests on hillslopes significantly reduces the slopes susceptibility to rainfall triggered landslides. This is due largely to the reinforcement of the hillslope soil by plant roots, which increase the shear strength of the soil, and in some instances, anchor the soil mantle to the underlying bedrock by deeply penetrating roots. Quantifying such reinforcing contribution using mechanical and numerical models means providing accurate and reliable values of rooted-soil reinforcement to insert into slope stability analysis (Ekanayake and Phillips, 1999; Kitamura and Namba, 1981). Indeed, the key stabilizing factor is the root reinforcement, a mechanical effect that has been largely studied through different research areas including:

- theories of the reinforced earth (Schlosser and Long, 1974; Vidal, 1969);
- tests with low modulus fabrics and fibres (Gray and Ohashi, 1983; Shewbridge and Sitar, 1989);
- theoretical models of fibre-root reinforcement (Waldron, 1977; Wu et al., 1979);
- laboratory and field tests of root-reinforced soil (Endo and Tsuruta, 1969; Giadrossich et al., 2017; O'Loughlin, 1974; Wu et al., 1988; Zhou et al., 1998);
- studies on the interaction with landslide shear surfaces (Burroughs and Thomas, 1977; Riestenberg and Sovonick-Dunford, 1983; Terwilliger and Waldron, 1991).

Rooted-soil combines the strong resistance in compression provided by the soil, and in tension provided by the roots. The result is a mass that is stronger than either the soil or the roots. Roots transfer the shear stress on themselves and, then, distribute stresses through the soil, contrasting local and progressive failures. Despite the increase of studies focusing on this issue, the complex physical process of interaction remains an open issue and

continues to be widely investigated (Abe and Ziemer, 1991; Bischetti et al., 2005; Burylo et al., 2011; Chiaradia et al., 2016; Schmidt et al., 2001).

1.2.1 Theoretical models of fibre-root reinforcement

Basal root reinforcement

The contribution of roots crossing the basal failure surface, has been considered as an increase in apparent soil cohesion (c_r) varying in proportion to the root density within the soil, and not an increase of the frictional component of soil strength (Abe and Ziemer, 1991; Endo and Tsuruta, 1969; Waldron, 1977; Wu et al., 1979). This additional term, well known as basal root reinforcement is included into the Mohr-Coulomb criterion and, consequently into the infinite slope model (Taylor, 1948). This approach is the most common failure criterion encountered in geotechnical engineering. It analyses the equilibrium of stresses or forces acting on a soil slide of infinite extension and calculates the factor of safety, FS , defined as the ratio between the resistant (τ_R) and the driving stress (τ_M) acting on the sliding surface as follows:

$$FS = \frac{\tau_R}{\tau_M} \quad (1.2)$$

Where τ_M is strictly due to the weight of soil mass and τ_R is the rooted-soil resisting shear stress related through a linear relationship with the normal stress at failure, as follows:

$$\tau_R = c'_s + c_r + (\sigma - u) \tan \varphi' \quad (1.3)$$

where c'_s is the effective soil cohesion, σ is the normal stress due to the weight of the soil and water of sliding mass, u is the soil pore-water pressure and φ' is the effective internal friction angle of soil.

The modification of the Mohr-Coulomb criterion requested several assumptions:

- (i) roots extend vertically across a horizontal shearing zone of thickness y ;
- (ii) roots are flexible and linearly elastic according to their Young's modulus E ;
- (iii) tensile strain is not large, so that stressed length approximates the unstressed root length;
- (iv) soil loads the root in tension by tangential stress at the soil-root interface until a maximum value;
- (v) all longitudinal displacements of the soil relative to the root including elastic tensile strain and slippage, mobilize the maximum tangential stress.

Shear forces acting along the shallow slip surface lead to pull-out, breakage or buckling of roots, depending on the orientation of roots. In order to determine the maximum resistance, caused by any critical load (breakage, slippage or buckling), several pioneering models have been developed since the second half of the 1970s. Waldron (1977) and Wu et al. (1979) independently developed a simple model that describes the behaviour of a vertical root extending perpendicular to a potential sliding surface in a slope. They assumed that roots are elastic elements able to mobilize their tensile strength by means of root soil friction (Figure 1.9). Tensile strength can be divided into two components, one normal and one parallel to the shear surface. The tangential component opposed to shear resistance while the normal component increases the confining stress on the shear plane, as follows:

$$c_r = (\cos \theta \tan \varphi' + \sin \theta) \frac{A_R}{A_S} T_R = k' \frac{A_R}{A_S} T_R \quad (1.4)$$

$$\theta = \tan^{-1}(x/y) \quad (1.5)$$

where A_R/A_S is the fraction of soil area occupied by the roots, x is the shearing horizontal displacement, y is the depth of shear zone, T_R is mobilized tensile resistance per unit area of soil and θ is the root bending angle respect to the

vertical (equation 1.3). For simplicity, the generic formulation of the root inclination is indicated by the coefficient k' .

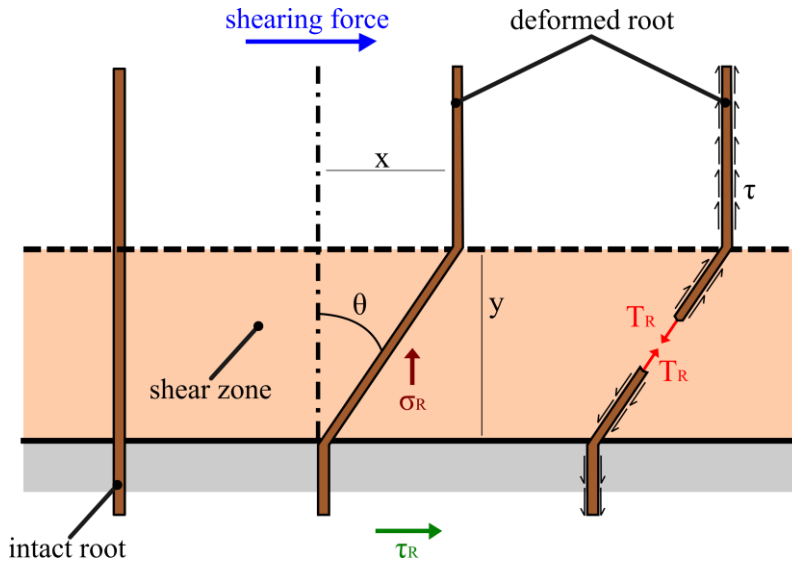


Figure 1.9. Schematic diagram of the perpendicular fibre-root reinforcement model (modified by Gray and Sotir, 1996).

Moreover, Waldron (1977) proposed to disassemble the mechanical response of the roots occurring during the loading. For the case of stretching, Waldron (1977) proposed to balance root-soil friction and tension in root during shearing of a soil layer. He assumed all roots had identical root diameter ϕ and mechanical properties such as Young's modulus E , and proposed the following model:

$$c_r^{stretching} = k' \frac{\pi [\tau' y (\sec \theta - 1)]^{0.5}}{2 A_s} E^{0.5} N \phi_m^{1.5} \quad (1.6)$$

where N is the number of roots, τ' is root-soil friction, A_s is the soil area and ϕ_m is the average root diameter.

Furthermore, Waldron and Dakessian (1981) extended the pioneering model including a spectrum of root diameters and developed a form of progressive failure of roots that can be described as:

$$c_r^{stretching} = k' \frac{\pi [\tau' y (\sec \theta - 1)]^{0.5}}{2 A_s} \sum_{i=1}^m E_i^{0.5} n_i \phi_i^{1.5} \quad (1.7)$$

where ϕ_i is the root diameter for the i -th diameter class, n_i is the number of roots of the i -th diameter class and m is the number of diameter classes. In addition, Waldron (1977) noted that when soil shearing causes roots to slip through the soil, they continue to contribute a reinforcing increment. Thus, for slipping roots, Waldron inserted the root length Λ in equation 1.6 in the following way:

$$c_r^{slipping} = k' \frac{\pi \tau' (\sec \theta - 1)^{0.5}}{2 A_s} N \Lambda \phi_m \quad (1.8)$$

This equation can be generalized for roots with different diameters as:

$$c_r^{slipping} = k' \frac{\pi \tau' (\sec \theta - 1)^{0.5}}{2 A_s} \sum_{i=1}^m n_i \Lambda_i \phi_i \quad (1.9)$$

where Λ_i is the root length of the i -th root diameter class.

For the breaking mode, Wu et al. (1979) proposed a simpler model excluding Young's modulus and assuming that the stresses in all roots crossing the failure surface are simultaneously at their ultimate tensile strength, as follows:

$$c_r^{Wu} = k' \frac{1}{A_s} \sum_{i=1}^m n_i T_i A_i \quad (1.10)$$

where A_i is the fraction of soil occupied by a root of i -th diameter class and T_i is the root tensile strength that is function of root diameter according to a power law form (Abe and Iwamoto, 1986; Bischetti et al., 2009; Burroughs

and Thomas, 1977; Genet et al., 2005; Gray and Sotir, 1996; Nilaweera and Nutalaya, 1999; Schwarz et al., 2016; Vergani et al., 2012), as follows:

$$T(\phi_i) = T_0 \phi_i^\zeta \quad (1.11)$$

where T_0 and ζ are two empirical coefficients.

Gray and Leiser (1982) further simplified the equation 1.4 considering an average root tensile strength for all roots, T_M :

$$c_r^{Gray\&Leiser} = k' \frac{A_R}{A_S} N T_M \quad (1.12)$$

Furthermore, many authors called the ratio of the cross-sectional area of roots cutting the shear plane over the area of shear plane considered is commonly called the root area ratio, RAR for simplicity. Such model has been widely adopted for its easy applicability although several assumptions are extremely restricting (Coppin and Richards, 1990; Wu and Sidle, 1995). For example, since not all roots are located perpendicular respect than the failure plane. Gray and Ohashi (1983) proposed a particular formulation for k' (equation 1.13) taking into account the inclination of roots ψ (Figure 1.10).

$$k' = \sin(90^\circ - \psi) + \cos(90^\circ - \psi) \tan \varphi' \quad (1.13)$$

$$\psi = \tan^{-1} \left(\frac{1}{k + (\tan^{-1} \varepsilon)^{-1}} \right) \quad (1.14)$$

where ε is the initial inclination of roots and k' is the distortion coefficient that corresponds to the ratio between the depth of the shear zone, y , and the displacement due to shearing, x .

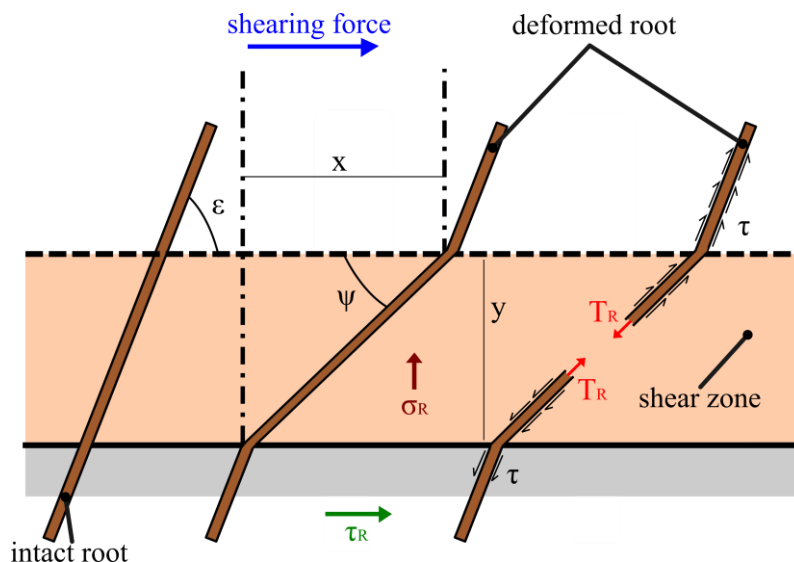


Figure 1.10. Schematic diagram of the inclined fibre-root reinforcement model (modified by Gray and Ohashi, 1983).

- Wu & Waldron model

Wu et al. (1979) carried out numerous direct shear tests showed that for soil with an internal friction angle ranging from 25° to 40° , θ varies between 40° and 90° . Thus the term k' , which indicates the component of root tensile strength according to the bending angle of roots respect to the shear plane, assumes values from 1.0 to 1.3. Therefore, average values have been set equal to 1.15 (Waldron, 1977), to 1.2 (Wu et al., 1979) or less to the unity for riparian vegetation in New Zealand (Docker and Hubble, 2008).

Moreover, another significant assumption is that all roots cross the shear surface and break at the same time. However, this fact is probably unreal because every root has a different tensile strength and breaks at a different time, as demonstrated by several pull-out experiments on branched roots (Norris, 2005; Riestenberg, 1994) and by direct shear tests (Docker and Hubble, 2008).

For this reason, several authors proposed to include a correction factor k'' in order to reduce the estimation of root reinforcement:

$$c_r^{W\&W} = k' k'' \frac{1}{A_s} \sum_{i=1}^m n_i T_i A_i \quad (1.15)$$

The value of k'' has been evaluated by many authors through back-analysis of occurred landslides, cumulative displacement-stress curve or direct shear tests and varied from 0.40 to 0.56 for several species trees (Bischetti et al., 2004; Hammond et al., 1992; Preti, 2006). In case of herbaceous plants, Greenwood et al. (2004) suggested a conservative value of 0.12. Such last version consists of the upgraded Wu & Waldron model, W&W hereafter.

- Fiber Bundle Model

In order to overcome the assumption of the non-simultaneous breaking of roots, Pollen and Simon (2005) introduced the Fiber Bundle Model, FBM, firstly developed by Daniels (1945) and used to study the properties of composite materials. FBM has been adapted to simulate the behaviour of roots bundle under tension and, in particular, the successive breakages of roots according to their individual tensile resistance. FBM takes into account simple rules:

- (i) an initial load is added and equally distributed between all the parallel fibres (roots) inside the bundle;
- (ii) the load is continuously increased until a root breaks (when the distributed load is greater than the single root tensile resistance) and then the load is redistributed to the remaining roots;
- (iii) if the redistribution causes a further rupture, the redistribution occurs once again;
- (iv) the process is repeated until all of the fibres, thus the entire bundle, have been broken.

The redistribution of the applied load from broken to unbroken roots can follow different approaches: according to the cross-section area of roots, the

root diameter or equally distributed by all unbroken roots (Mao et al., 2012). This last approach is the most common in FBM models because it showed to be more conservative in the estimation of soil shear strength reinforcement (Mao et al., 2012; Pollen and Simon, 2005; Thomas and Pollen-Bankhead, 2010). In addition, the simplest version of FBM considers the fibres in a static condition, time-independent, while a further extension includes a dynamic component that implies that time and the particular mode of stress affect the root strength (Gómez et al., 1998).

Many authors demonstrated how FBM provides more accurate estimates of soil shear strength reinforced by roots respect than W&W model (Bischetti et al., 2009; Loades et al., 2010; Mao et al., 2012; Pollen and Simon, 2005). For this reason, FBM is used to calibrate the correction factor k'' to calibrate the W&W model: Pollen and Simon (2005) estimated values between 0.60 and 0.82 for several riparian species in America, whereas Bischetti et al. (2009) found a range between 0.32 and 1.00.

Lateral root reinforcement

In case of deeper soil-bedrock interface, basal root reinforcement has less impact on the total resistance strength because few roots reach the depth of failure surface (Chiaradia et al., 2016; Schmidt et al., 2001; Schwarz et al., 2010b). At the same time, field evidence showed that shallow landslides commonly occur where the soil is deeper than the rooted zone (Casadei et al., 2003a; Schmidt et al., 2001). Thus, the presence of roots crossing the lateral areas of a landslide is significant in terms of contribution to slope stability (Reneau and Dietrich, 1987; Roering et al., 2003; Schmidt et al., 2001). To include such contribution, it is common to apply the limit equilibrium theory on a sliding volume of soil (Figure 1.11) as suggested by some authors (Casadei et al., 2003a; Chiaradia et al., 2016; Dietrich et al., 2007).

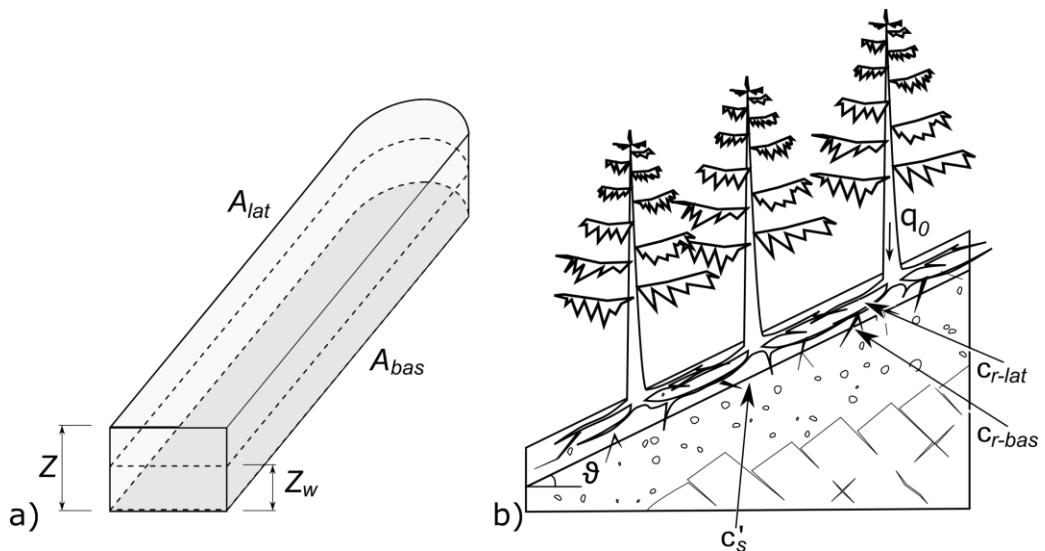


Figure 1.11. a) Schematic drawing of limit equilibrium theory on a sliding volume of soil proposed by Casadei et al. (2003a). The dark grey area represents the basal area of the potential landslide is coloured dark grey, while the light grey area is the lateral surface. b) Schematic representation of the transect of a forested slope (modified by Chiaradia et al. 2016)

Accordingly, it is possible to evaluate the FS as the ratio between the resistant forces F_R and the driving forces F_D , as follows:

$$F_R = A_{bas} (c'_s + c_{r-bas}) + A_{lat} (c'_s + c_{r-lat}) + [A_{bas} (Z \gamma_s - Z_w \gamma_w + q_0) \cos \mathcal{G}] \tan \varphi' \quad (1.16)$$

where A_{bas} is the basal surface of sliding volume, A_{lat} is the lateral surface of sliding volume, Z is the soil depth, Z_w is the water table depth, γ_s is the unit weight of dry soil, γ_w is the unit weight of water, q_0 is the tree surcharge per unit area, \mathcal{G} is the hillslope inclination, c_{r-bas} and c_{r-lat} are the contributions of plant roots to slope stability along the basal and the lateral surface of sliding volume, respectively.

$$F_D = A_{bas} (Z \gamma_s + Z_w \gamma_{sat} + q_0) \sin \mathcal{G} \quad (1.17)$$

where γ_{sat} is the unit weight of saturated soil.

In order to calculate the lateral contribution of roots, c_{r-lat} , Bischetti et al. (2009) proposed to adopt both the W&W model (equation 1.15) and the FBM model separating the root density into ranges of depth.

$$c_{r-lat}^{W\&W} = \sum_{j=1}^M \left[k' k'' \left(\sum_{i=1}^m n_{ij} T_i A_i \right) \frac{\Delta z_j}{Z} \right] \quad (1.18)$$

where M is the number of depths range and Δz is the thickness of depths range.

Later this modification, FBM was widely used because it is simple to implement, requires a small number of parameters and is currently considered a reference estimator of the basal and lateral root reinforcement (Hales et al., 2009; Ji et al., 2012; Mao et al., 2012; Mickovski et al., 2009).

Despite, several authors criticized the assumption that the peak tensile strength is mobilized at the same time of the maximum soil instability (Cohen et al., 2011; Pollen et al., 2004; Schwarz et al., 2010a). Pollen et al. (2004) performed laboratory and field tests on streambank material and roots of

riparian plants showing that root strength is typically mobilized at much larger displacement than soil strength. Moreover, Fannin et al. (2005) showed that the shear stress peaks are twice, one due to soil mobilize at its peak shear strength and one due to the tensile strength mobilization of roots. Overprediction of the increased soil shear strength may therefore occur, and therefore analysis of the stress-displacement characteristics of the roots are necessary to evaluate how significant is this overestimation (Docker and Hubble, 2008; Mickovski et al., 2009; Pollen, 2007). Consequently, both W&W and FBM do not permit calculation of root elongation for realistic root bundles.

- Root Bundle Model

Schwarz et al. (2010b) developed an extended version of FBM, called Root Bundle Model (RBM) implementing a strain step loading approach. The model imposes successive displacements to the bundle of roots, by which the calculation of pull-out forces takes into account single root strength, elastic modulus and length as functions of diameter. By the RBM, it is possible to calculate the complete force-displacement curve of a bundle of roots and derive the total pull-out work; furthermore, the model allows the evaluation of the progressive mobilization of root strength along the activation length during the pull-out process due to root soil friction for each root in the bundle. The characterization of the full force-displacement behaviour of root bundles under shear, as well as under tensile and compressive loading was demonstrated to be important for the understanding of the triggering mechanisms of shallow landslides. Cohen et al. (2011) implemented a simplified version of RBM taking into account only the root breakage. RBM considers the mechanical (elasticity and ultimate tensile resistance) and geometrical (root elongation) properties in addition to the root distribution and the maximum resisting force.

It is based on three power laws that relate the geometrical and mechanical properties in function of root diameter in the following way:

$$F_{\max}(\phi_i) = F_0 \left(\frac{\phi_i}{\phi_0} \right)^\xi \quad (1.19)$$

$$E(\phi_i) = r E_0 \left(\frac{\phi_i}{\phi_0} \right)^\beta \quad (1.20)$$

$$L(\phi_i) = L_0 \left(\frac{\phi_i}{\phi_0} \right)^\alpha \quad (1.21)$$

where F_{\max} is the ultimate root resistance force, E the average Young's modulus, L the average root length, F_0 , E_0 and L_0 are the multiplicative coefficients and ξ , β and α are the exponential coefficients, whereas the coefficient r represents the effect of root tortuosity on Young's modulus. These coefficients are estimated by the results of the tensile tests.

Considering the elasticity law, the root reinforcement of a bundle of roots F_{tot} is obtained by summing the force contributions F for each root as follows:

$$F_{\text{tot}}(\Delta x) = \sum_{i=1}^m F(\phi_i, \Delta x) \quad (1.22)$$

where F is the tensile force in function of the root diameter and the displacement Δx .

$$F(\phi_i, \Delta x) = \frac{\pi r E_0}{4 L_0} \phi_i^{2+\beta-\alpha} \quad F(\phi_i, \Delta x) < F_{\max}(\phi_i) \quad (1.23)$$

More recently, Schwarz et al. (2013) improved the RBM by implementing a survival function to include the variability of root mechanical properties and named it RBMw.

The root reinforcement of a bundle of roots F_{tot} is obtained multiplying equation 1.3 for the Weibull survival function S , as follows:

$$F_{tot}(\Delta x) = \sum_{i=1}^N F(\phi_i, \Delta x) S(\Delta x^*) \quad (1.24)$$

where S is a function of the normalized displacement Δx^* (equation 1.25), the ratio between the displacement measured by every single tensile test and the corresponding values of displacement obtained using the fitted values of tensile forces.

$$S(\Delta x^*) = \exp \left[- \left(\frac{\Delta x^*}{\lambda} \right)^\omega \right] \quad (1.25)$$

where λ is the scale Weibull parameter and ω is the shape Weibull parameter (dimensionless).

The application of RBMw requires the calibration of eight different parameters, six of which (F_0 , E_0 , L_0 , ξ , α and β) are obtained by fitting laboratory test or preferably by pull-out test data and field measurements using nonlinear least square regressions, as suggested by Giadrossich et al. (2016). In addition, RBMw needs the calibration of the two Weibull parameters (λ and ω) according to the procedure described in detail in Schwarz et al. (2013).

1.2.2 Measurements of root reinforcement

Early studies on root reinforcement focused on quantifying the mechanical behaviour of roots (Endo and Tsuruta, 1969; O'Loughlin, 1974). Giadrossich et al. (2017) reviewed the different approaches, developed over the following decades and classified them into tests on individual roots and on rooted-soil. These methods of measurements are:

- tensile tests on individual roots in the laboratory (e.g. Bischetti et al., 2005; Genet et al., 2008);
- pull-out tests on individual roots in the field (e.g. Abernethy and Rutherford, 2001; Anderson et al., 1989; Mickovski et al., 2007; Schwarz et al., 2010c);
- compression tests on individual roots in the field (Wu et al., 1988);
- laboratory shear tests on rooted-soil (e.g. Operstein and Frydman, 2000; Yildiz et al., 2015);
- field shear tests on rooted-soil (e.g. Abe and Iwamoto, 1986; Cammeraat et al., 2005; Docker and Hubble, 2008; Endo and Tsuruta, 1969; Wu and Watson, 1998; Wu et al., 1988);
- borehole shear tests on rooted-soil (Pollen-Bankhead et al., 2009; Simon and Collison, 2002);
- vane tests on rooted-soil (e.g. Abe and Iwamoto, 1986; Normaniza and Barakbah, 2006);
- triaxial tests on rooted-soil (Graf et al., 2009; Negadi et al., 2015; Zhang et al., 2010, 2006);
- laboratory compression tests on rooted-soil (Schwarz et al., 2015);

1.2.3 Effects of root growth on root reinforcement

As already underlined, investigating the root systems is greatly complex and extremely challenging due to the difficult to measure and to manipulate experimentally (Helliwell, 1986). The most common and ancient method of studying root systems was to excavate them, although it requires much time and energy. A typical form of excavation consists of cutting a trench, removing soil by hand, by shovel or through water or air jet and then mapping or counting roots on the profile of the trench (Giadrossich et al., 2017). The collected measurements of plant roots have reinforced the knowledge that many aspects of soil environment, such as physical impedance, soil biota, soil aeration, temperature, water availability, oxygen status and nutrient availability, modify their plasticity influencing their growth (BassiriRad, 2005). For this reason, the variability of soil conditions and presence of obstacles and barriers to root growth result in a variable and unpredictable distribution within the general overview (Dobson, 1995; Kozlowski, 1971). In fact, it is important not to forget that the root growth is opportunistic because roots proliferate wherever the conditions are favourable. Additionally, other remarkable factors are season change, water table depth, ecological interactions and mechanical stresses (Dupuy et al., 2005; Fitter, 1987; Khuder et al., 2007; Moore, 2000). Finally, forest stand characteristics such as species mix, tree height and weight, tree density, size of gaps, rooting depth, root architecture, have an impact on the network of root systems and consequently on slope stability (Forbes and Broadhead, 2011; Wu, 1995).

Root systems morphology

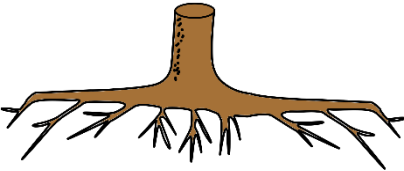
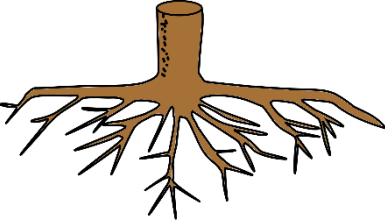
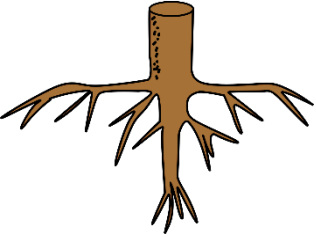
In case of shallow landslides, the shape of the root systems partly affects the tree stability and, therefore, the falling of trees. According to the classification of the tree root systems provided by Büsgen et al. (1929), the root systems are categorized into three basic three-dimensional shapes:

- *heart root system*: where both large and smaller roots descend diagonally from the base of the tree;

- *plate or surface root system*: where large, horizontal, lateral roots extend just below the soil surface whereas the small roots branch down vertically;
- *taproot system*: where a large main root that directly anchors the tree descending vertically from the underside of the trunk whereas the horizontal and lateral roots act as guy ropes (Ennos, 1993).

Table 1.1 reports an indicative and qualitative list of tree species with different types of the root system in the European continent.

Table 1.1. Classification of root system morphology including the main Alpine tree species. Black Locust is normally a shallow-rooted species that does not produce a taproot.

Plate	Heart		Tap
 <p>Silver birch European ash Norway spruce Sitka spruce Swiss pine Monterey pine White pine Poplars Common aspen Black locust European mountain ash</p>	 <p>Field maple Norway maple Sycamore Common alder Grey alder White birch European hornbeam Common hawthorn Sweet chestnut European beech European larch</p>	 <p>Poplars Sweet cherry Douglas fir Sessile oak English oak Northern red oak English yew Small-leaved lime Large-leaved lime European white elm Scots elm</p>	<p>Silver fir Common juniper Oaks Lodgepole pine Corsican pine Maritime pine Scots pine Wild pear Black locust Checker tree</p>

Root depth

Roots play a significant role in slope stability, in particular, where they are able to penetrate potential deep shear surface or the soil mantle into fractures or the fissures in the underlying bedrock (Cammeraat et al., 2005; van Beek et al., 2005). Typically, trees have relatively shallow but widespread root systems. Indeed, roots generally extend close to the soil surface where the soil is loosest and water, oxygen and nutrients are most readily available. With increasing soil depth, soil bulk density increases and aeration decreases and, consequently, root density and size decline (Dobson, 1995). Several studies showed that approximately 80-90% of tree roots are concentrated in the upper 0.90 m of soil (Di Iorio et al., 2005; Gray and Sotir, 1996; Tron et al., 2014; Tsukamoto, 1990). Moreover, Jackson et al. (1996) proposed an analysis of root extent at a global scale and showed that overall temperate broadleaves and conifers have 82% and 70% of their roots in the upper 0.50 m, respectively.

Although genetic characteristics have a significant role in rooting depth, RD hereafter, external factors such as excessive stoniness, compact soil layers, bedrock and high or perched water tables intensely halt downward penetration of tree roots (Dobson, 1995). An example of the effects of obstructions was reported in the study of Cutler et al. (1990). They surveyed the root plates of wind-thrown trees in Southern England after the storms of 1987 and 1990 showing that 44% of root plates were shallower than 1.00 m and 95% were shallower than 2.00 m.

Neglecting the physical and physiological limits, we proposed an indicative and qualitative classification of European and North American trees and shrub species according to their general behaviour and their genotypic rooting features (Table 1.2). Such classification is based on the pioneering categorizations proposed by Polomski and Kuhn (2001) and later by Glenz (2005), and it has been enlarged collecting a large amount of data from the literature (Breuer et al., 2003; Canadell et al., 1996; Gale and Grigal, 1987; Jackson et al., 1996; Köstler et al., 1968; Stone and Kalisz, 1991).

Table 1.2. Classification of typical rooting depth including the main Alpine tree species [* 0-1 m; ** 0.5-2.0 m; *** 1.0-2.0 m].

Shallow	Intermediate			Deep
< 0.50 m	0.50 – 1.00 m	0.50 – 1.50 m	1.00 – 1.50 m	> 1.50 m
Common hawthorn	Common hazel	Grand fir	Field maple	Field elm
Honey locust	Norway spruce	Sycamore	Norway maple	Common alder
Yews (<i>Taxus</i> spp.)	Corsican pine	Horse chestnut	White alder	Scots pine
Green alder	English holly*	Silver birch	Sweet chestnut	Silver poplar
Alder buckthorn		European hornbeam	Sitka spruce	Black poplar
Common buckthorn		European beech	Lodgepole pine***	Rowans (<i>Sorbus</i> spp.)
		European ash	Common aspen***	
		European larch**	Prunus spp.	
		Oaks (<i>Quercus</i> spp.)	Black locust	
		Limes (<i>Tilia</i> spp.)	Willows (<i>Salix</i> spp.)***	
		Wych elm		
		White aspen		
		Common juniper		
		Silver fir**		

In this classification, most of tree and shrub species have been included in the intermediate class characterized by roots able to penetrate soil mantle between 0.50 and 1.50 m. The extreme classes that incorporate shallower or deeper root systems include both six species. In agreement with the observations of Gale and Grigal (1987), willows and poplars show a very deep extension of their roots, whereas hawthorns and buckthorns reach superficial rooting zones.

Root spread

Root studies in forests and orchards involving excavations and soil coring showed that the lateral growth of several trees species (oak, hickory and maple) expand well beyond the canopy perimeter (Hodgkins and Nichols, 1977; Stout, 1956). Further studies proposed empirical rules for estimating the root spread in function of tree height, trunk diameter or canopy diameter (Day et al., 2010). Despite, the accuracy largely varies according to several factors such as species or cultivars (Gilman, 1988), tree condition (Balasubramanyan and Manivannan, 2008) and rooting environment (Gerhold and Johnson, 2003). First, Smith (1964) measured approximately 140 root systems of open-grown Douglas fir blown down during a typhoon in British Columbia (Canada) and found that less than 50% of the variation of root spread has been explained by tree height demonstrating that there is not an accurate relationship. Moreover, he developed an appropriate regression to evaluate the root spread using the crown width as an indicator. Notwithstanding, several authors criticized such relationship because it is highly species-dependent (Gilman, 1988; Tubbs, 1977). In particular, Gilman (1988) observed the maximum root spread ranged from 1.68 times the crown diameter for the green ash to 3.77 times for the Southern magnolia and live oak, on a plantation in New Jersey (U.S.A.). For this reason, he showed strong regression between maximum root system radius and trunk diameter considering site- and species-specific data.

Root density

Root density mostly influences the quantification of root reinforcement (Bischetti et al., 2005; Genet et al., 2008; Naghdi et al., 2013). The most common measure of root density is the root area ratio, *RAR*, computed as the total cross-sectional area of all roots divided by the total soil area. *RAR* shows a large spatial variability, both in the vertical and the horizontal planes. This is due to many factors, such as local soil and climate characteristics, land use management and associated vegetation communities and randomness (Sidle and Ochiai, 2006). In general, *RAR* decreases with depth below the soil surface and with distance from tree trunk as shown by many authors (Abernethy and Rutherford, 2001; Greenway, 1987; Schmidt et al., 2001; Zhou et al., 1998).

1.2.4 Effects of mechanical properties of roots on root reinforcement

Mechanical properties of roots directly influence the quantification of root reinforcement (see section 1.2.1). Several studies investigated which environmental factors mainly control the root mechanical characteristics (e.g. Genet et al., 2005; Hales et al., 2013; Zhang et al., 2014). Hathaway and Penny (1975) showed a strong dependence between the tensile resistance of each singular root and the amount of vascular tissue such as the xylem that increases with increasing root diameter. Other authors identified that cellulose content mainly contributes to the root strength (Genet et al., 2005; Hales et al., 2009; Zhang et al., 2014). Yang et al. (2016) found that root moisture content significantly influenced tensile strength. Moreover, tensile resistance can be expressed in term of stress, T , (Bischetti et al., 2009; Pollen and Simon, 2005; Zhang et al., 2014) or, force, F (Schmidt et al., 2001; Schwarz et al., 2013; Vergani et al., 2012), both in function of the root diameter (equations 1.11 and 1.19). The use of tensile force is probably preferable because tensile stress is calculated as the ratio between breaking force and root area, which is affected by the uncertainties of the measurements of root diameter. Additionally, there is not a unique relationship, in particular between force and root diameter. Hathaway and Penny (1975) suggested a linear regression, Schmidt et al. (2001) and Hales et al. (2009) a second order polynomial relationship, however, in most cases, researchers fitted data using a power law (e.g. Riestenberg and Sovonick-Dunford, 1983; Vergani et al., 2012). Additionally, root tensile resistance significantly differs among species, although there is also a certain variability inside the species and, sometimes, a reasonable similarity among different species in the same environmental context (Vergani et al., 2012). Considering the relationship described in equation 1.19, it has been possible to perform a statistical analysis in order to determine the effects of forest type on the empirical coefficients (F_0 and ξ) of the power law. For coniferous species, F_0 and ξ fall in a range between 3.25 and 53.70 N mm⁻² and 0.632-2.414,

respectively. For deciduous species, the variability is 8.66-51.18 N mm^{-2} for F_0 and 0.834-2.052 for ξ (Figure 1.12). Although Figure 1.12 showed that F_0 assumes smaller values for coniferous than deciduous species and conversely for ξ , t-test indicates a statistical similarity among the two forest types for both the coefficients (F_0 : $t=-2.620$, $p\text{-value}=0.012$, whereas ξ : $t=0.915$, $p\text{-value}=0.366$).

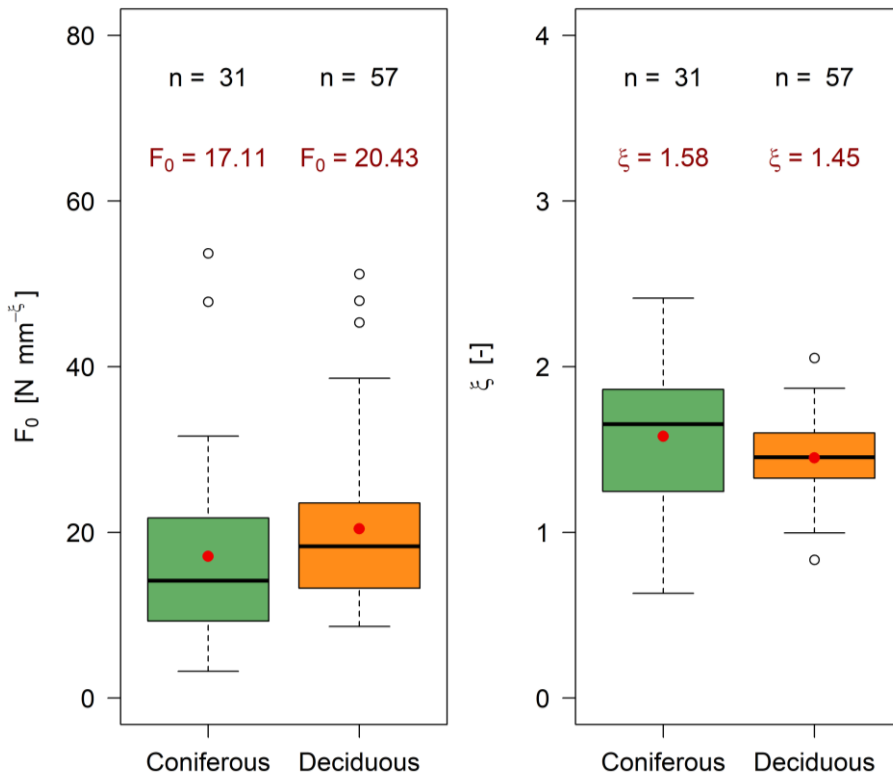


Figure 1.12. Boxplot of (a) F_0 and (b) ξ in different forest types. Dots are mean values. Outliers are points outside the boxplots and are plotted with circles.

1.2.5 Study cases

Since 2007, a series of large experiments have been carried out to quantify the contributions of root systems of different tree species on slope stability. The study sites are located in different spots of Lombardy and Piedmont regions, in North Italy as shown in Figure 1.13. A huge variability of ecological and climatic features distinguishes each site, which belongs to fluvial, hill and mountainous areas (Appendix B).

The main factors characterizing the morphology of study sites are quite various. The average altitude ranges between 67 and 1562 m a.s.l. and the average steep slope varies from 0° to 52°. In addition, the territorial differences in terms of orientation and exposure are pronounced, whereas the values of topographic wetness indices, *twi*, is quite similar and range from 7 to 12.

The local stand forest characteristics are analysed in different features such as tree species, tree density, tree age, and average tree diameter (from 0.06 m to 0.55 m). The selected species are typical of Alpine zone such as European silver fir (Aa, *Abies alba* Mill.), sweet chestnut (Cs, *Castanea sativa* Mill.), European beech (Fs, *Fagus sylvatica* L.), European ash (Fe, *Fraxinus excelsior* L.), European larch (Ld, *Larix decidua* Mill.), Norway spruce (Pa, *Picea abies* L.) and black locust (Rp, *Robinia pseudoacacia* L.). High forest management is the predominant silvicultural system for the conifers, whereas the coppice for the broadleaves.

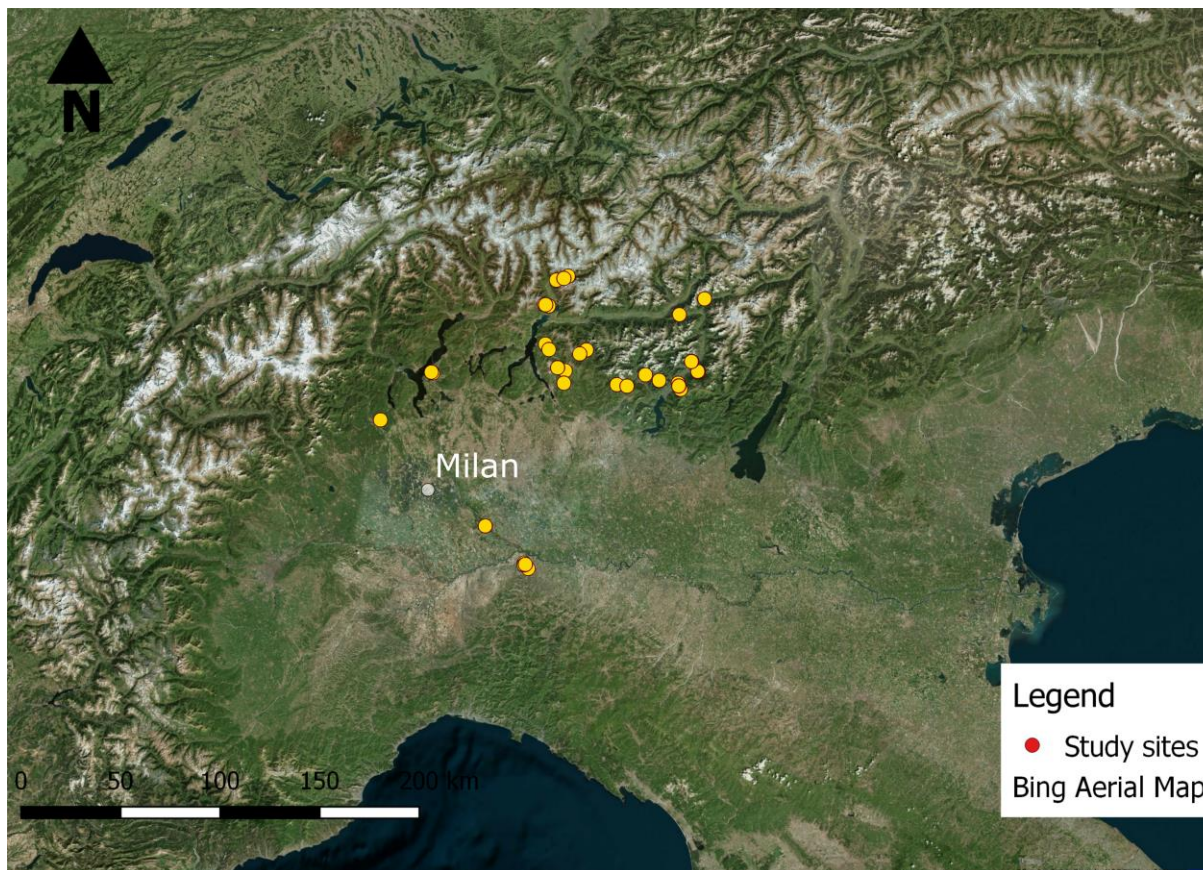


Figure 1.13. Location of study sites.

1.3 Results

1.3.1 Rainfall interception by selected Alpine species

Among the hydrological processes occurring inside the soil-vegetation-atmosphere system, the scientific community focuses on the interception loss, and a large collection of data is available, especially regarding the native Alpine tree species. As already demonstrated in section 1.1.3, conifers intercept more annual rainfall reaching average values of I_C around 27% (Figure 1.14). The measurements conducted in Norway spruce forest showed a slight difference in terms of variability, which is wider and falls into a range between 4% and 48%. Among the deciduous species, the highest average value has been observed in *Fagus sylvatica* forests ($21.62 \pm 8.03\%$), whereas the lowest in *Castanea sativa* forests ($15.56 \pm 7.73\%$).

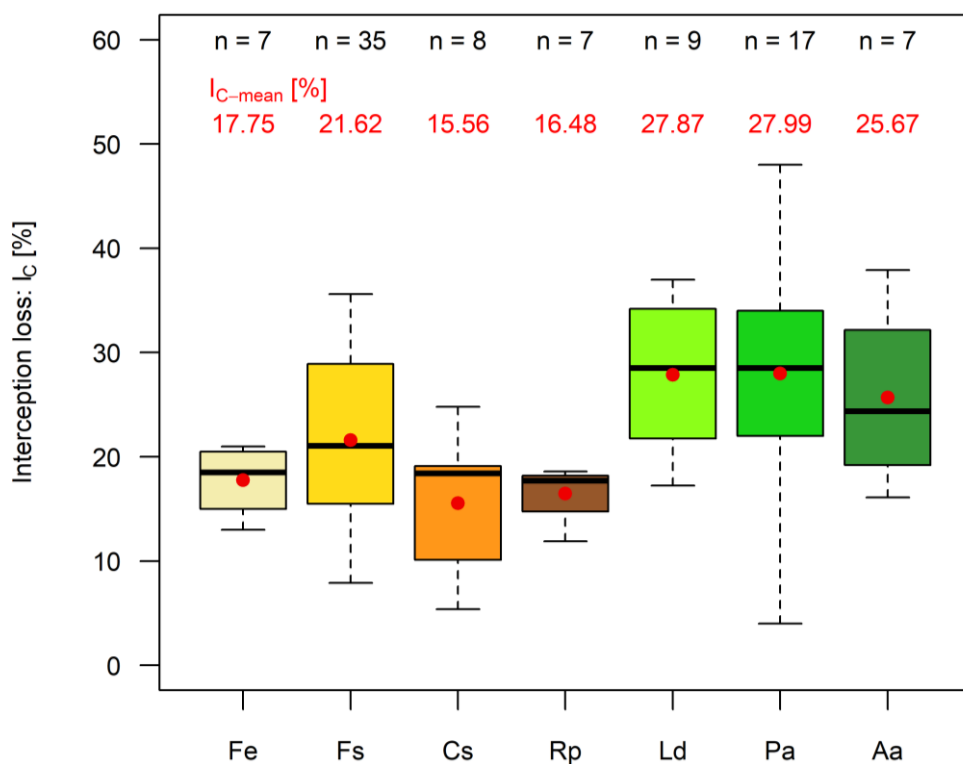


Figure 1.14. Boxplots describing the observed annual interception loss values of the selected Alpine tree species.

1.3.2 Characteristics of root growth of selected Alpine species

Many field measurements of RD have been conducted in mature stands of Alpine forest. The observations vary from 0.40 m to 2.23 m (Figure 1.15). On average, roots of *Abies alba* and *Larix decidua* extend until approximately 0.72 ± 0.10 m and 0.88 ± 0.20 m, respectively. Roots of *Fraxinus excelsior*, *Fagus sylvatica* and *Robinia pseudoacacia* reach deeper RD: 1.35 ± 0.10 m, 1.29 ± 0.35 m and 1.24 ± 0.20 m, respectively. On the other hand, a wide range of RD as observed for *Picea abies* from 0.40 to 2.23 m and for *Castanea sativa* from 0.42 to 2.00 m. Concerning the root density, most available data belongs to the range between 0.089% and 0.273% (Figure 1.16). Exceptions are the values measured in *Robinia pseudoacacia* and in *Abies alba* forests. In the first case, *RAR* is higher with an average value of $0.292 \pm 0.168\%$, whereas in the second case the average value is significantly lower and equal to $0.073 \pm 0.044\%$.

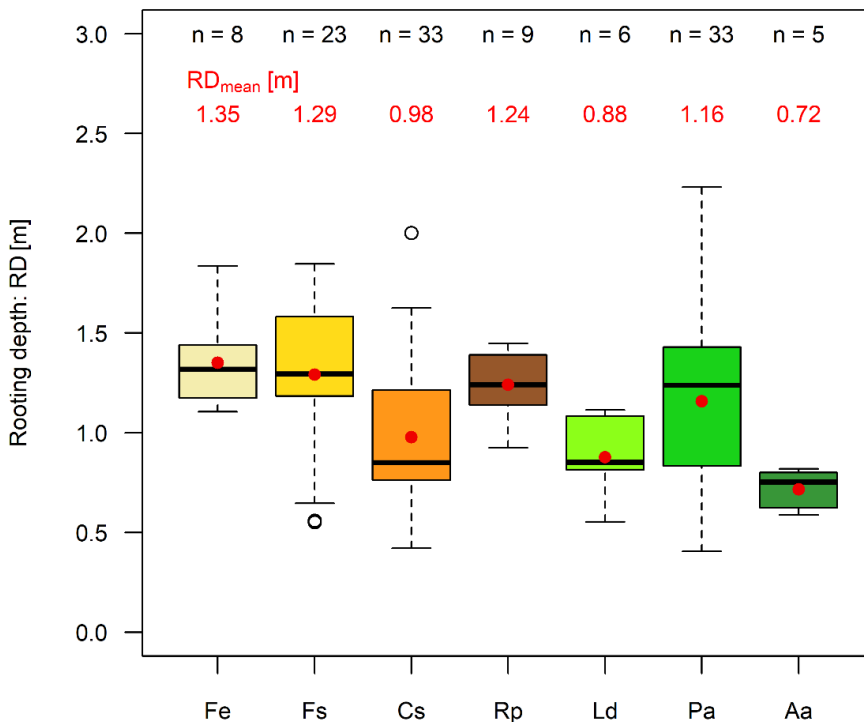


Figure 1.15. Boxplots describing the observed rooting depth of the selected Alpine tree species.

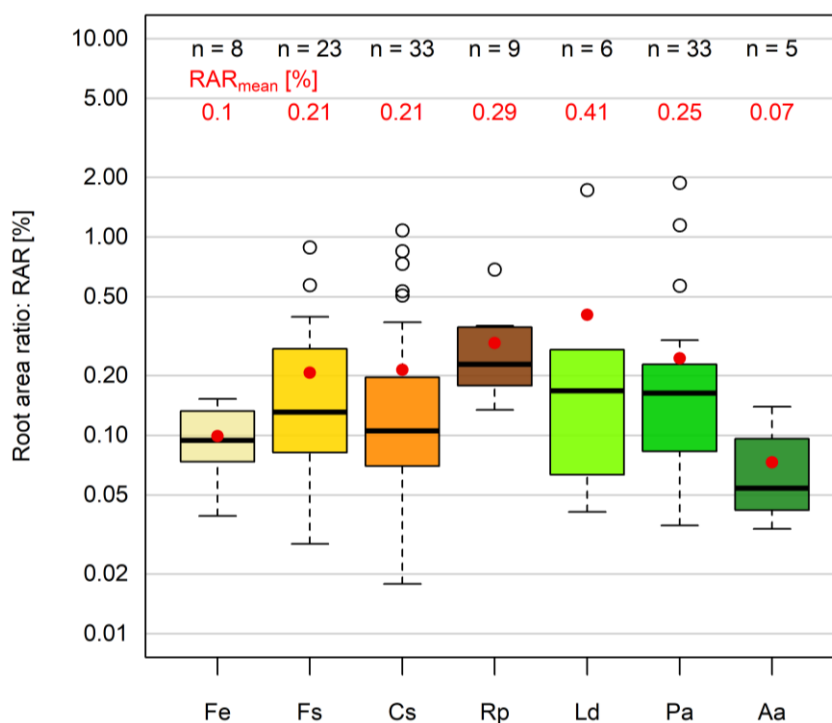


Figure 1.16. Boxplots describing the observed root area ratio of the selected Alpine tree species.

1.3.3 Input parameters of root reinforcement models

Root reinforcement models require a calibration of several parameters that describe the mechanical and geometrical characteristics of roots. First, both W&W, FBM and RBMw include the relationship between ultimate tensile force and root diameter, described by a power law (equation 1.19). Moreover, RBMw requests additional input parameters, which are the coefficients of non-linear regressions for the Young's modulus (equation 1.20), the root elongation (equation 1.21) and the Survival Weibull function (equation 1.25). To evaluate these non-linear regressions, laboratory tensile tests have been conducted on almost 30 alive roots with a diameter generally ranged from 0.25 mm to 6.00 mm. Results obtained by a large series of tensile tests confirmed the strong correlations between the mechanical and geometrical characteristics of roots with the root diameter through power laws. In

particular, a good fitting was determined for the ultimate resistant force and for the Young's modulus in terms of coefficient of determination, R^2 (Table 1.3). Low values of R^2 are obtained for the curves between L and ϕ . This fact is strictly affected by the natural tortuosity of the roots and by the initial pre-tensioning when the laboratory tensile test starts, too. For the calibration of survival function, results always emphasize an accurate fitting performance. All the fitted parameters of the root reinforcement models are reported in Figure 1.17. A wide variability is clearly visible for the ultimate tensile force, the elastic properties and the length of roots and even within the same tree species. On the other hand, the Weibull parameters can assume a small interval of values: λ is approximately 1.095 ± 0.034 , whereas ω is 3.059 ± 0.904 .

Table 1.3. Performance of fitting for equations 1.19, 1.20, 1.21 and 1.25 that represent the input parameter of root reinforcement models.

Equation	min (R^2)	median (R^2)	mean (R^2)	max (R^2)
equation 1.19	0.453	0.796	0.797	0.982
equation 1.20	0.382	0.733	0.711	0.841
equation 1.21	0.043	0.515	0.448	0.838
equation 1.25	0.968	0.988	0.987	0.997

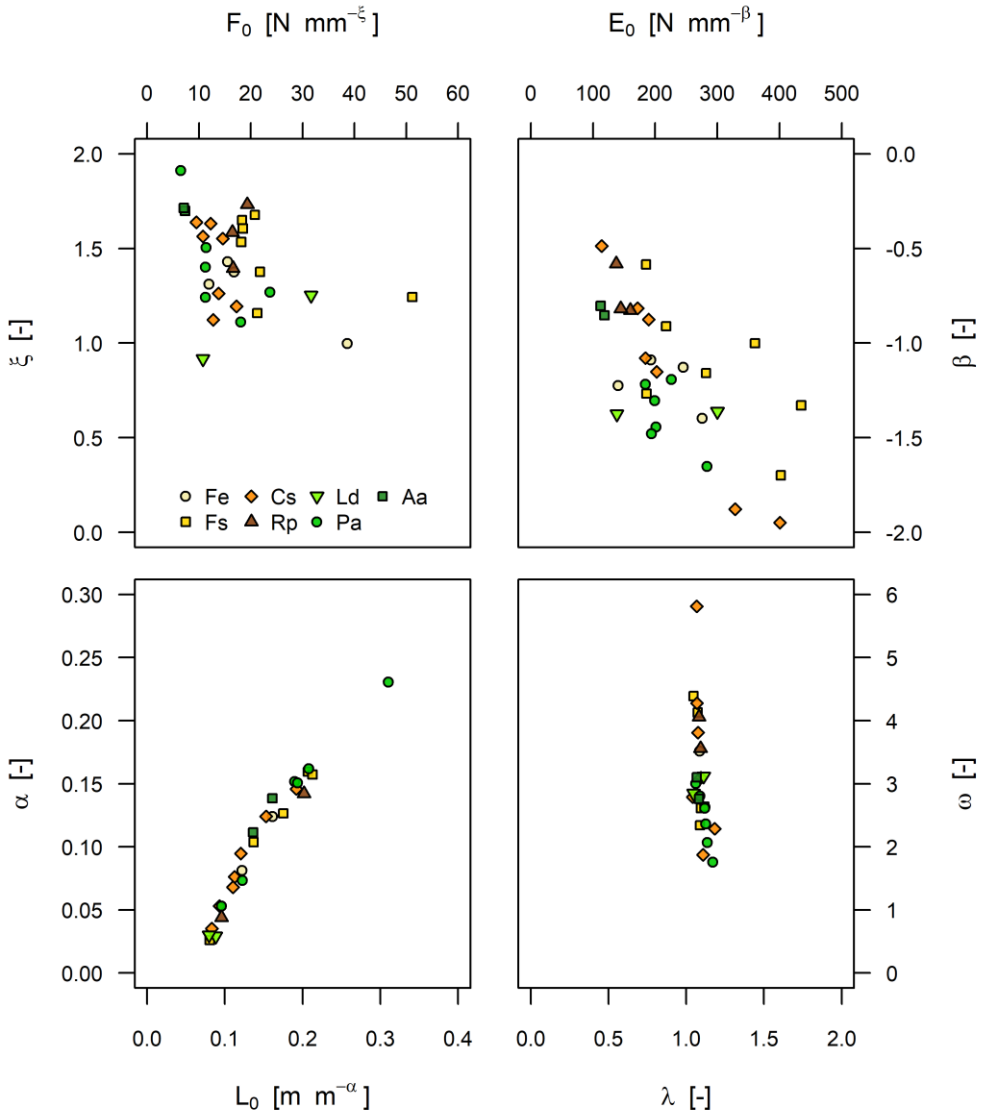


Figure 1.17. Calibrated input parameters of the root reinforcement models.

1.3.4 Comparison between the evaluated root reinforcement provided by the Alpine species

Once the root reinforcement models were calibrated, it is possible to insert data about root density: RAR for W&W (equations 1.4 with $k'=1.2$ and $k''=0.5$), whereas the number of roots with their diameter for FBM and RBMw. Their combinations led to estimates of the lateral root reinforcement provided by the root systems. The results of all models provided values between 0.46 kPa to 26.61 kPa: in particular, 1.59-26.61 kPa for W&W, 0.83-22.09 kPa for FBM and 0.46-22.77 kPa for RBMw. Among the Alpine species, c_{rl} assumes the highest values for *Robinia pseudoacacia* (16.5 ± 6.86 for W&W, 10.44 ± 4.39 for FBM and 12.09 ± 5.63 for RBMw, on average), whereas the lowest values for *Abies alba* (3.60 ± 1.63 for W&W, 1.89 ± 0.69 for FBM and 2.38 ± 1.35 for RBMw, on average). Moreover, results showed high average lateral root reinforcement for *Fagus sylvatica*, approximately 14.64 kPa for W&W and 8.90 kPa for the other models. Similar values of average c_{rl} were obtained for *Picea abies* (10.48 kPa for W&W and 4.60 for the other models), for *Castanea sativa* (7.69 kPa for W&W and 4.54 kPa for the other models) and for *Fraxinus excelsior* (9.28 kPa for W&W and 4.54 kPa for the other models). Contrasting results were obtained for *Larix decidua*: W&W and FBM estimated a similar average value of 7.00 kPa, whereas RBMw a lower value of 2.71 kPa. Figure 1.18 showed the results in function of the Alpine tree species.

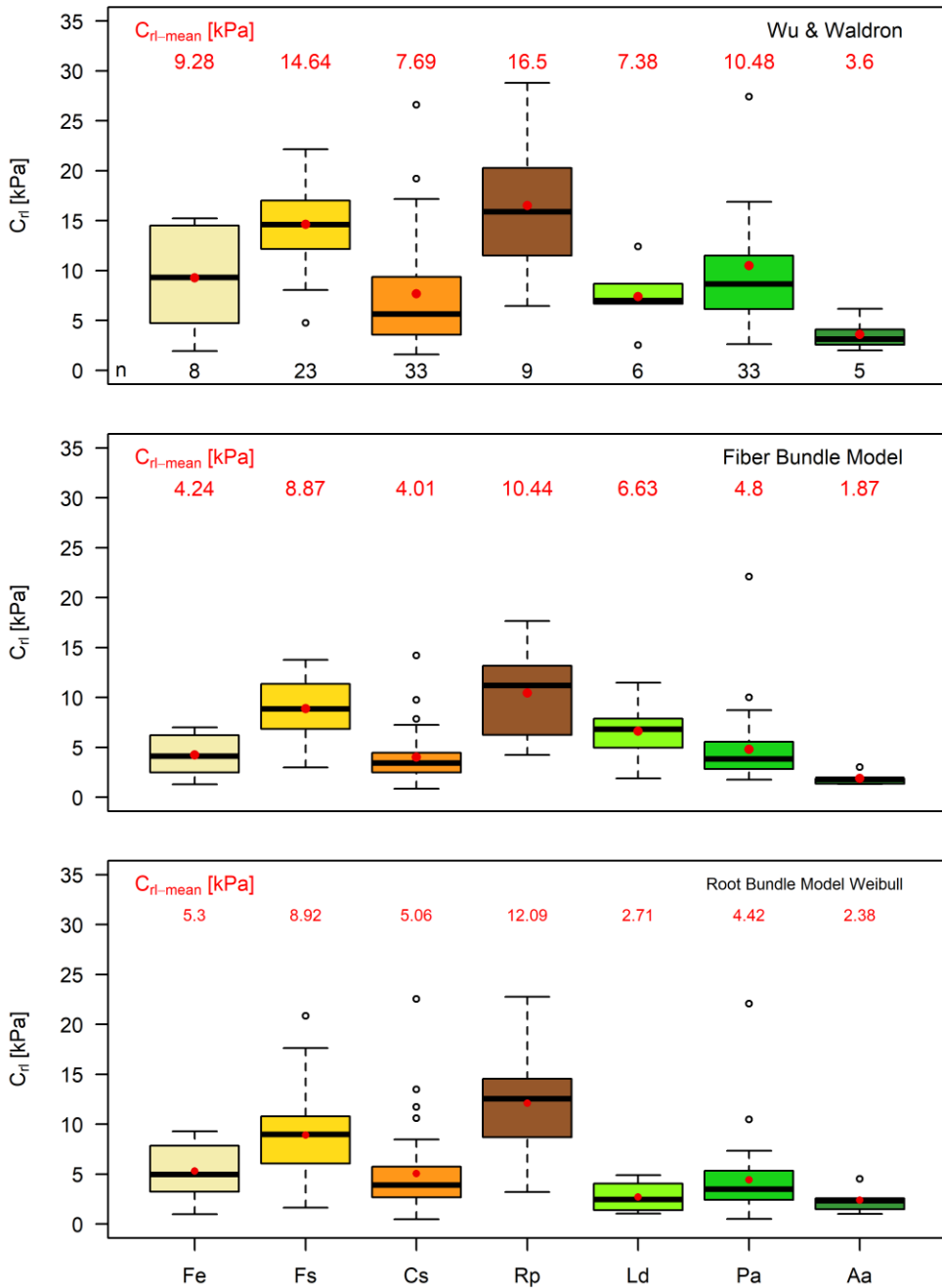


Figure 1.18. Results provided by the root reinforcement models using the available data of root density and of root mechanical properties for the selected Alpine tree species.

1.4 Discussion

1.4.1 Differences in root density and root depth

Field measurements of RD for the considered data are generally comparable with those observed by other researchers. According to the classification proposed in par. 5.3.2, most of root systems of the selected Alpine tree species belong to the intermediate class and are located in the first 1.5 m of the soil. In particular, the average RD ranges between 1.00 m and 1.50 m for *Fraxinus excelsior*, *Fagus sylvatica* and *Robinia pseudoacacia*, and between 0.75 m and 1.25 m for *Castanea sativa* and *Larix decidua*. A larger range of values is observed for *Picea abies*, the observations of RD on *Abies alba* (0.50-1.00 m) show a shallow root system in disagreement with the proposed classification. Additionally, these observations indicated that the maximum depth explored by roots considerably vary between site and species, in particular in the case of *Picea abies*. Exceptions are the observations on *Abies alba* roots; however, those analysed sites are geographically close and with a shallow soil layer. Despite, these surveys are in agreement with findings of previous studies on temperate forests that measured a range between 1.00-1.20 m of depth (Finér et al., 2011; Schenk and Jackson, 2002). Other studies investigating slope prone to shallow landslides and covered by forests measured lower RD. For example, Preti (2013) found an average RD equal to 0.83 ± 0.80 m in a forest of *Castanea sativa*. Tron et al. (2014) measured different RD from 0.40 m to 0.88 m: 0.57 ± 0.18 m for *Castanea sativa*, 0.88 m for *Picea abies* and 0.59 ± 0.12 m for *Robinia pseudoacacia*. Studying the most important characteristics governing the mechanical resistance to rockfall and wind loading in a mixed forest stand, Stokes et al. (2007) found average RD of 1.59 ± 0.20 m for *Abies alba*, 0.81 ± 0.03 m for *Fagus sylvatica* and 0.95 ± 0.15 m for *Picea abies*. Additionally, Tatarinov et al. (2008) measured mean RD in mature floodplain forests with *Fraxinus excelsior* as dominant tree species in Southern Moravia (Czech Republic), ranging between 1.20-2.00 m.

1.4.2 Differences in quantification of root reinforcement

The mean c_{r-lat} for *Robinia pseudoacacia* and *Fagus sylvatica* is higher than the other selected Alpine tree species (*Fraxinus excelsior*, *Castanea sativa*, *Larix decidua*, *Picea abies* and *Abies alba*) as shown in Figure 1.18. This difference can be ascribed to mechanical resistance and root distributions, which are characteristics of each dug trench. Comparing with other studies, our results were similar to those obtained for different forest mountainous stands worldwide. For example, Hales et al. (2009) applied FBM on data collected in different pits and trenches dug in a mixed deciduous stand inside Coweeta hydrologic laboratory (North Carolina, U.S.A.) quantifying a value of c_{r-lat} of 3.36 ± 2.43 kPa. Concerning studies that include measurements of root diameter and root tensile properties, several authors quantified c_{r-lat} ranging between 5.90 kPa and 17.50 kPa for several tree species in North America as sugar maple, Alaskan cedar, Western hemlock, Sitka spruce and Douglas fir (Burroughs and Thomas, 1977; Riestenberg and Sovonick-Dunford, 1983; Wu et al., 1979). Moreover, Vergani et al. (2016) and Vergani et al. (2017b) investigated the root distribution and the pull-out resistance of roots in a subalpine spruce protection forest in Canton Schwyz (Switzerland) and in a Scots pine protection forest in Canton of Valais (Switzerland) finding a range of lateral root reinforcement of 1.00-4.00 kPa and 0.20-7.40 kPa, respectively. Conversely, our results are more conservative with respect to those estimated by other authors. Schwarz et al. (2010a) estimated a variability of c_{r-lat} between 0-100 kPa in a chestnut stand in Tuscany (Central Italy), whereas Schwarz et al. (2012a) between 0-150 kPa in a subalpine spruce forest in Canton of Schaffhausen (Switzerland). In a mature mixed native forest in Oregon coast range (U.S.A.), Schmidt et al. (2001) calculated through back-analysis a value of c_{r-lat} ranging between 20 and 150 kPa.

1.4.3 Differences of root reinforcement models

Results of our study show a low difference between the root reinforcement provided by FBM and RBMw calibrated with the same input parameters (Figure 1.18). This discrepancy in terms of absolute difference is approximately $24.3 \pm 21.6\%$. On the other hand, the differences with the results calculated with W&W model using values of coefficients k' and k'' as suggested by literature ($k'=1.2$ and $k''=0.5$) are huge. Although the coefficient k' strongly depends on the root bending angle and the effective internal friction angle of soil, several studies demonstrated that the estimate of that value is generally around the unity for most soils with $\phi' > 25^\circ$ (Abe and Ziemer, 1991; Danjon et al., 2007; Wu, 1995). Moreover, values less than unity are obtained only for bending angle greater than 40° . Concerning the other W&W's coefficient k'' , most researchers quantified its values much lower than 0.6 (Docker and Hubble, 2008; Operstein and Frydman, 2000; Waldron and Dakessian, 1981). In particular, Bischetti et al. (2009) compared results estimating using W&W and FBM defined that k'' is strongly associated with the number of roots. It can assume a value greater 0.5 for a density smaller than 400 roots m^{-2} . In the cases of this study, we proposed to apply a different combination of the two multiplicative coefficients k' and k'' and evaluating the differences with FBM and RBMw as shown in Figure 1.19. Similar results are provided considering the product of k' and k'' equal to 0.3. Notwithstanding, both three models have strengths and weaknesses in their application. W&W is the simplest model among them and request a smaller amount of data (i.e. a quantification of RAR and $T-\phi$ curves). However, to provide more accurate estimates of c , avoiding an overestimation of the FS , a comparison and further a calibration of the correction factors (i.e. k' and k'') should be necessary. On the other hand, FBM improves the pioneering models to quantify the contribution of roots to slope stability overcoming the simultaneous root-breaking hypothesis. As suggested by several authors, FBM provided encouraging estimates using a reasonable number of available data. Finally, a reliable and accurate application of RBMw needs to an

extended number of input parameters describing the mechanical and geometrical characteristics of the roots systems. Despite, RBMw describes the breaking process of roots bundle with fewer simplifications considering a progressive failure of roots due to the heterogeneous distributions of them. In addition, the main output is the overall quantification of the force behaviour in function of the displacement, which remains unknown for the other models (Schwarz et al., 2013).

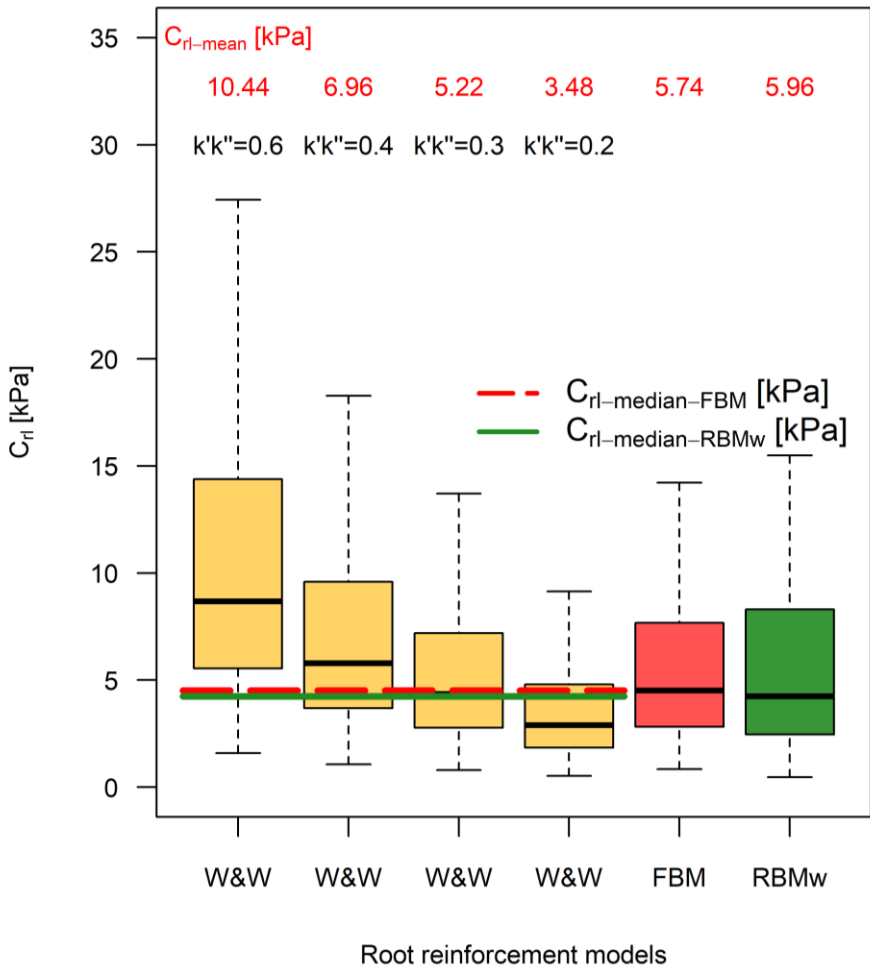


Figure 1.19. Comparison of results provided by the models on all the sites of the study: W&W is applied with a combination of four different multiplicative factors ($k'' = 0.2, 0.3, 0.4$ and 0.6).

1.5 Conclusions

This study provides a complete background on the protective functions provided by the forests in order to contrast the natural hazards. Such functions vary their effectiveness according to the typology of hydro-geological hazard. In particular, concerning the soil mass movement and the shallow landslides, the scientific community has developed remarkable knowledge on quantifying the contribution of protection forests in order to reduce frequency and intensity of catastrophic events and to improve the forecasting. Moreover, this study shows the implementation of pioneering and more recent models able to evaluate the impact of root systems on the stabilization of soil. Such models provide accurate and reliable results at stand scale that can be updated to wider scales (i.e. catchment scale). In addition, they can be very useful tools for the management of protection forests in order to maintain and, if possible, to increase the effectiveness of protective functions through specific operations/silvicultural measures. Increasingly, both scientific researchers and forestry planners can generate long-term views on different sensations of protection forests developments (Dorren and Schwarz, 2016). However, many issues remain open. Serious difficulties persist in quantifying the impact of protection forests in preventing several natural hazards such as snow avalanche release

While it is increasingly necessary to concentrate scientific efforts in understanding the impact of forest dynamics on their protective functions both to fill the lack of knowledge and to improve the practical necessity. Thus, future perspectives will focus on examining and handling forest renewal, stand growth, natural and human disturbances, silvicultural treatments or combinations of them, in order to maximize the reduction of natural hazards and of the financial costs of the traditional engineering structures and to improve ecological conservation.

2 A PROBABILISTIC 3-D STABILITY MODEL

Keywords:

Shallow landslides;

Forest structure;

Root reinforcement;

Physical-based models;

3-D slope stability model

2.1 Introduction

Shallow landslides are widespread geomorphological phenomena that can cause potentially catastrophic events, especially in steep landscape. Predicting such events is an arduous task for the international scientific community because has serious implications on civil society helping to save lives and to protect individual properties and collective resources.

For this reason, many researchers have developed models for providing landslide hazard maps and consequently for identifying the possibility of landslide occurrence at the regional scale. Such approaches can be divided into two categories (Luo et al., 2015): empirical approaches and physically-based models. The first class consists of statistical techniques that search for functional relationships between factors, characterizing sites where slope instability has been observed and past-present landslide distributions from inventory maps. Bivariate or multivariate analysis (e.g., Baeza and Corominas, 2001; Carrara et al., 1991; Naranjo et al., 1994; Pradhan, 2010; Santacana et al., 2003), discriminant analysis (Guzzetti et al., 1999) and artificial neural networks (e.g., Ermini et al., 2005; Gómez and Kavzoglu, 2005; Lee et al., 2004) are the most common methods. The result is a mathematical expression that represents a quantitative metric of landslide hazards, with variables based on terrain properties, including vegetation that explains slope instability. These types of models lack an explicit relationship between vegetation properties and landslide hazards, making them unsuitable for driving forest management strategies.

The second category includes approaches that combine, within a conceptual framework, topographically driven hydrological models and slope stability analyses to predict hazard areas (Okimura and Ichikawa, 1985). The infinite slope model is commonly adopted as the stability model. It is a simplified and well-known low-dimensional approach that assumes the plane of failure is parallel to the slope (Taylor, 1948). The hydrological framework, in terms of soil moisture dynamics, is generally based on a modified version of the

steady-state wetness index (Arnone et al., 2011; Borga et al., 2002; Montgomery and Dietrich, 1994; Pack et al., 1998) or an approximation of the Richards equation (Baum et al., 2002; Iverson, 2000; Simoni et al., 2008). Such models provide deterministic slope stability evaluations based on the Factor of Safety (FS), which is the ratio between resisting and driving forces (e.g., Baum et al., 2002; Pack et al., 1998), or as a function of the seepage flow (transmissivity) and rainfall rate (e.g., Borga et al., 2002; Montgomery and Dietrich, 1994).

Although such methods have been used with success to define shallow landslide occurrences when the topography has a major influence on the trigger mechanisms (Dietrich et al., 2001; Gorsevski et al., 2006b), some weaknesses exist in these methods (e.g., Casadei et al., 2003a; Crosta and Frattini, 2003; Milledge et al., 2012; Wu and Sidle, 1995). Moreover, under the infinite slope assumptions, it is difficult to include the effects of the presence of vegetation and root systems adequately. For example, during shallow movements, a prominent effect is exerted by the roots that cross the lateral shearing surface (Roering et al., 2003; Schwarz et al., 2010b), whereas those crossing the basal sliding surface are generally scarce (e.g., Riestenberg and Sovonick-Dunford, 1983; Schmidt et al., 2001). This contradicts the infinite slope stability assumptions, which are based on the absence of inter-slice interactions (Duncan et al., 2014). In addition, lateral earth pressure is commonly ignored (Casadei et al., 2003a; Schmidt et al., 2001), although it is not clear whether the lateral stress terms can be ignored in shallow landslides without significantly affecting the model results (Dietrich et al., 2007).

To circumvent these limitations, Burroughs (1985) proposed a simplified 3-D limit equilibrium force balance on a slope block with translation. This approach was the basis for a more recent multidimensional shallow landslide model, MD-STAB (Milledge et al., 2014), which has effectively included the presence of roots in the soil, providing a significant improvement in hillslope stability modelling (Bathurst et al., 2010).

Finally, physically-based models involve a certain degree of uncertainty in the parameters as a consequence of spatial variability and measurement errors (generally hydrological and geotechnical, but in our case, they also concern root reinforcement); therefore, their application can benefit from the adoption of Monte Carlo simulation (MCS; e.g., Hammond et al., 1992; Haneberg, 2004; Haneberg et al., 2009; Zhou et al., 2003). From this perspective, the probability distributions of input parameters are fundamental. Indeed, the probability distributions of geotechnical soil properties have been the focus of many studies, and some reference distributions can be identified (Hammond et al., 1992; Haneberg, 2004; Haneberg et al., 2009; Zhou et al., 2003). Conversely, although the literature provides values for root reinforcement, which are common in terms of additional cohesion (e.g., Bischetti et al., 2009; Genet et al., 2008; Roering et al., 2003), its variability is still unclear and, consequently, its probability distribution function is still difficult to evaluate. Some authors have adopted functions based on arbitrary considerations, including lognormal (Hammond et al., 1992), uniform (Pack et al., 1998) and normal (Haneberg, 2004; Milledge et al., 2014) probability distributions.

These models provide a way to account for the uncertainty and the probability distribution of root reinforcement by estimating the root resistance from root density and root tensile resistance (Bischetti et al., 2005; Hales et al., 2009; Schwarz et al., 2012a). Many studies have provided values of root tensile resistance in terms of force or strength for a number of species (Cazzuffi et al., 2014; De Baets et al., 2008; Mao et al., 2012). However, the data concerning root density with particular reference to the spatial distribution are less common. Jackson et al. (1996) provided general information regarding vertical root density for many of the world's environments, and several studies have shown that the root density declines with depth exponentially (Benda and Dunne, 1997; Dunne, 1991; Roering, 2008), or with different distributions according to the tree species (Bischetti

et al., 2005). The available data, however, exhibit considerable variability among species and sites, but this variability has not been quantified.

In addition, a large planar variability has been observed with respect to the horizontal distance from trees, tree size, and the presence of gaps in stands (Mao et al., 2014; Moos et al., 2016).

Roering et al. (2003) and Sakals and Sidle (2004) explored how local vegetation may affect landslide occurrence on forested slopes, emphasizing the large spatial variability of root cohesion. Moos et al. (2016) showed that forest structure strongly affects the stabilizing effects of trees. Roering et al. (2003) and Sakals and Sidle (2004) proposed computational models to simulate the spatial variability at the scale of individual trees, utilizing field data on root size distribution. Recently, Schwarz et al. (2010a) developed a similar model based on pipe theory and a static fractal branching model (Tobin et al., 2007) and applied it in forested areas (Schwarz et al., 2012a, 2012b).

Based on this background, this chapter develops a modular approach to evaluate slope stability, accounting for the horizontal spatial variability of root reinforcement and the related characteristics of forest stands, called the PRobabilistic MUltidimensional shallow Landslide Analysis, PRIMULA. The approach is based on a multidimensional slope stability model and incorporates several different sub-modules for defining the PDFs of the input parameters. In particular, a specific sub-model composed of an MCS for forest stand characteristic simulation, a root distribution model for root density assessment according to root diameter, and a root cohesion calculation is implemented to evaluate the distribution of the root reinforcement and introduced in PRIMULA to assess the hillslope stability.

2.2 Materials and methods

PRIMULA consists of the combination between a 3-D limit equilibrium model and MCS. In addition, other sub-models interact with PRIMULA and provide the PDF of each input parameter as shown in the flowchart in Figure 2.1.

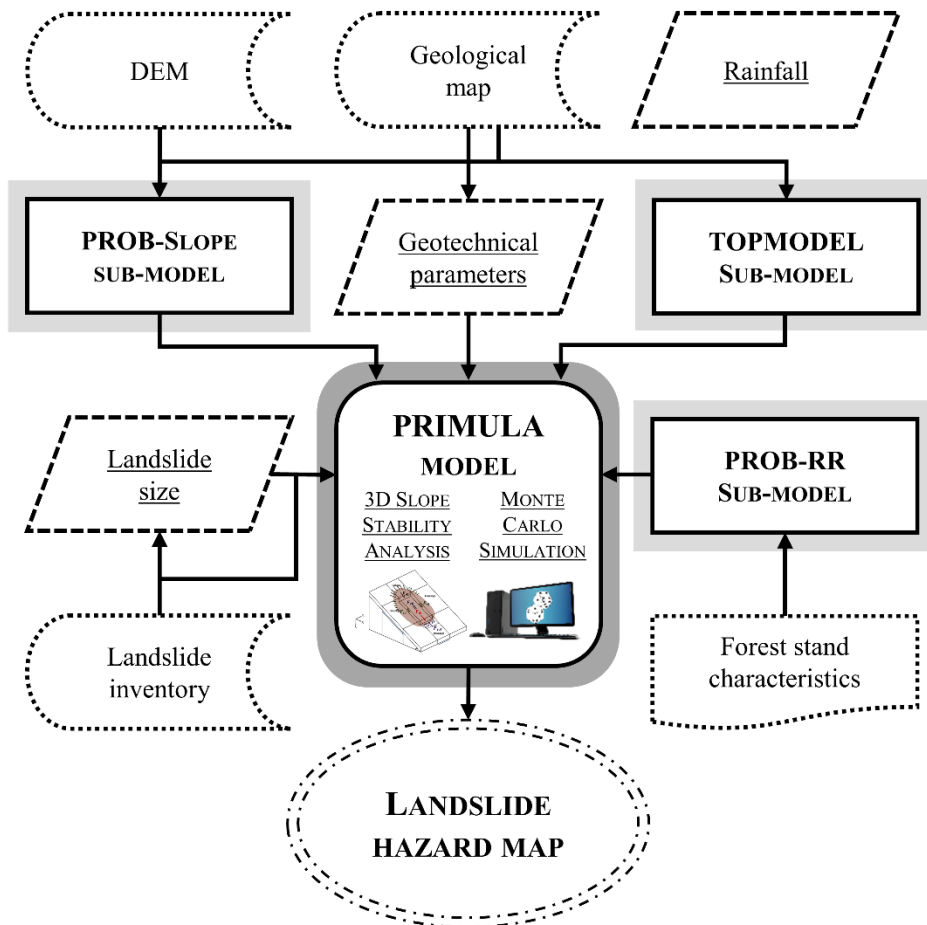


Figure 2.1. Flowchart describing the PRIMULA model and other sub-models to provide a landslide hazard map.

2.2.1 Multidimensional stability model

A 3-D approach to hillslope stability modelling was selected to overcome the limitations of infinite slope analysis and to adequately incorporate the effect of root reinforcement. The model is MD-STAB, which was recently developed by Milledge et al. (2014) and applied in a raster-based GIS by Bellugi et al. (2015a, 2015b). It is based on the horizontal and vertical force equilibrium principles and is capable of representing both the lateral forces acting on potential landslides and the effects of cohesion on the upslope and downslope surfaces. The force balance is calculated on the central block, whereas the momentum equilibrium can be considered negligible because the potential failure mechanism of shallow landslides is mainly translational. The main assumptions of MD-STAB are as follows: (i) the force balance is applied to the central block; (ii) the groundwater level is steady and parallel to the slope surface; (iii) the model ignores infiltration, suction and capillary rise effects in the unsaturated zone; and (iv) the single block is partitioned into saturated and unsaturated regions.

The FS of each block can be evaluated as the ratio between the resisting and driving forces:

$$FS = \frac{F_{rb} + 2 F_{rl} + F_{rd} - F_{du}}{F_{dc}} \quad (2.1)$$

where the driving forces consist of the downslope component of the central block mass, F_{dc} , and the force acting on the central block from the upslope wedge, F_{du} , assuming active earth conditions. The resisting forces acting on all boundaries of the block are due to the passive earth pressure from the downslope wedge, F_{rd} , the basal resistance force, F_{rb} , and the shear resistance on the two parallel slope sides of the element, F_{rl} (Figure 2.2). A comprehensive description of the equations used in the model is reported in Appendix C.

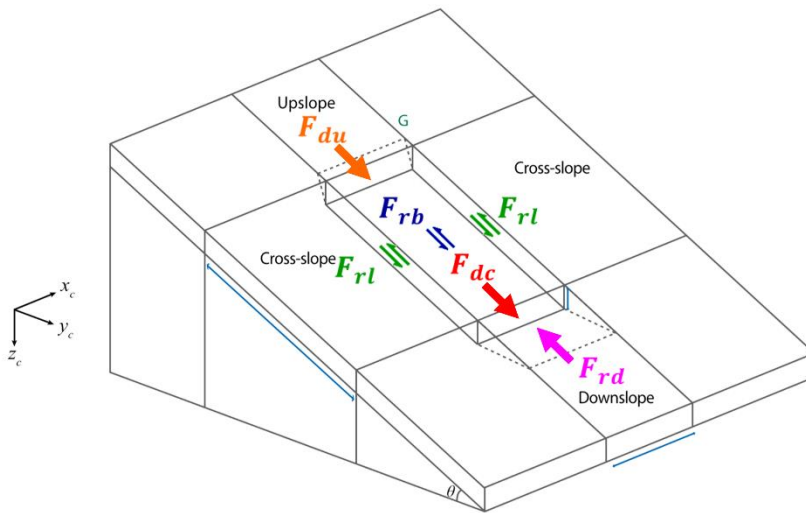


Figure 2.2. Forces and shear resistances applied to a 3-D slope stability case. The continuous lines represent the forces, and the double lines represent the shear stresses along the slides of the 3-D element.

The parameters of MD-STAB are the same as those used in infinite slope methods: (i) the geometry of the block, including the width (w), length (l), and surface slope (θ); (ii) the soil properties, including unit weight of the soil (γ_s), effective soil friction angle (ϕ'), failure depth (z), and saturation ratio (m); and (iii) the root reinforcement in terms of additional root cohesion (C'_{rb} and C'_{rl}).

The parameters w and l describe the failure surface as a rectangular shape, assuming that the soil mass behaves as a rigid block (Burroughs, 1985; Dietrich et al., 2007) or that the dimension of grid cells when the resolution of the grid is sufficiently fine represents a potential landslide as a collection of grid cells (Bellugi et al., 2015a). In both cases, the potential size of a landslide must be defined, and this is a challenging task at the watershed scale. Although an exhaustive search algorithm able to test all possible shapes of potential landslides is effectively unfeasible (Dietrich et al., 2007), many authors have examined this topic. Casadei et al. (2003b) and Gabet and Dunne (2002) assumed that a landslide has a rectangular shape with a

fixed length to width ratio to investigate the effect of lateral root reinforcement on landslide size. Okimura (1994) created an infinite slope stability model and explored a fixed number of potential rectangular slide masses, rejecting the hypothesis of a single length to width ratio. Qiu et al. (2007) developed a three-dimensional model for testing ellipsoidal slip surfaces in a landslide-prone area. Recently, Bellugi et al. (2015a, 2015b) proposed a spectral clustering search algorithm for applications at the catchment scale to identify clusters of adjacent cells. This search algorithm requests an optimal grid resolution (1-2 m) that is not commonly available and may introduce other sources of uncertainty (Penna et al., 2014).

To avoid such drawbacks, the slope stability model is applied cell by cell as a soil mass block, assuming a rectangular shape, with width and length randomly extracted from a probabilistic distribution obtained from the sub-model PROB-SLOPE. Thus, a parallelepiped block with vertical sides approximates each potential landslide and is consistent with field observations (Milledge et al., 2014).

2.2.2 Monte Carlo Simulation (MCS)

MCS is an effective solution for calculating the distribution of the FS using a mathematical function (Zhou et al., 2003) by generating independent and random sets of possible values of the input parameter to calculate a corresponding FS value for each pass. Each input parameter is then described by a probability distribution, and the MCS is repeated at least 1000 times (Hammond et al., 1992) for each grid cell to test all combinations of input parameters.

Following this procedure, samples of FS in each cell have been calculated to represent a probability density function of FS . On this basis, it is subsequently possible to calculate the probability of failure of any cell as the area under the distribution curve in which FS is less than unity, i.e., $Pr[FS < 1]$. MCS has also been adopted to produce sets of different forest configurations with the same characteristics, including tree density, average diameter at

breast height (DBH), and the minimum distance between trees, to evaluate the root density.

2.2.3 Landslide sizes

The sub-model PROB-SLOPE performs a statistical analysis of the landslide inventory generating a PDF of simplified rectangular failure surfaces, which are comparable with field observations (Dietrich et al., 2007; Milledge et al., 2014).

2.2.4 Geotechnical properties

The geotechnical parameters such as the effective soil friction angle and the unit weight of soil are spatially heterogeneous, affected by measurement errors, and subject to variable qualities of geotechnical analysis on which the estimation is based (van Westen et al., 2006). For these reasons, many authors have adopted geostatistical methods to predict the spatial distributions of soil properties; however, this requires extensive field observation (e.g., Aşkın et al., 2012; Davidovic et al., 2010; Griffiths et al., 2009; Kerry and Oliver, 2004; Raspa et al., 2008). Under the probabilistic approach, the probability distributions of geotechnical parameters are generally considered normal (e.g., Melchiorre and Frattini, 2012; Pathak and Nilsen, 2004; Refice and Capolongo, 2002; van Westen and Terlien, 1996; Zhou et al., 2003), uniform (Hammond et al., 1992) or empirically achieved by direct measurements (Park et al., 2013).

The failure depth in landslide-prone areas is rarely available (Ho et al., 2012). Many authors, however, have considered the soil depth a single value (e.g., Kim et al., 2015; Liao et al., 2011; Pack et al., 1998; Park et al., 2013) based on field observations, whereas under the probabilistic approach, it is based on a normal (Haneberg, 2004) or triangular distribution (Hammond et al., 1992).

2.2.5 Hydrological sub-model

A hydrological model is essential for estimating the relative soil moisture or saturation ratio (m). Although several detailed hydrologic methods have been developed to describe transient vertical infiltration and water movement within hillslopes (e.g., Baum et al., 2005, 2002; Iverson, 2000; Lu and Godt, 2008), the most common hydrological concept adopted for slope stability is the steady state shallow subsurface flow described in several TOPMODEL applications (Beven and Freer, 2001; Beven and Kirkby, 1979; O’Loughlin, 1986). This approach assumes that the flow infiltrates toward a low-conductivity layer that is invariant with depth and follows paths determined by the topography of the study site. TOPMODEL is based on Darcy’s law (equation 2.2) and the maximum lateral flux when the soil reaches saturation (equation 2.3):

$$R \frac{a}{b} = K_s h_w \cos \theta \sin \theta \quad (2.2)$$

where R is the steady-state recharge (in m/hr), a is the contribution area (in m^2), b is the contour length of the lower bound in each contributing area (in m), K_s is the saturated hydraulic conductivity (in m/hr), h_w is the groundwater level (in m) and θ is the terrain inclination.

$$T \sin \theta = K_s z \cos \theta \sin \theta \quad (2.3)$$

In equation 2.3, T is the soil transmissivity (in m^2/hr).

Combining the two previous equations, the level of groundwater corresponding to m is as follows.

$$m = \frac{h_w}{z} = \min \left(\frac{R}{T} \frac{a}{b \sin \theta}, 1 \right) \quad (2.4)$$

Moreover, we incorporated a stochastic factor that considers the compound parameters of steady-state recharge and transmissivity, R/T (in m^{-1}) as

uniformly distributed variables over the range of 10^{-4} to 10^{-1} based on Huang et al. (2006). Despite many reported values, we preferred to consider a probability distribution of the saturation ratio, which is independent of the topographic context. For example, Hammond et al. (1992) and Haneberg (2004) adopted triangular distributions for m , with the lowest boundary set to 0.3, the highest boundary to 0.8 and the peak to 0.5.

2.2.6 Root reinforcement (Prob-RR)

Root reinforcement represents the contribution to the shear strength of hillslope stability exerted by roots crossing the lateral and basal sliding surfaces. Root reinforcement is highly dependent on the spatial distribution of root systems in terms of number of roots of different diameters (Burroughs and Thomas, 1977) or root biomass (Ziemer, 1981) and on the ultimate resisting force before rupture. Although several models have been proposed, few studies have included detailed information regarding forest stand characteristics (Moos et al., 2016; Nandi and Shakoor, 2010; Neuhäuser et al., 2012; Piacentini et al., 2012).

Regardless of the physically-based model considered, determining the spatial distribution of root reinforcement as a function of the forest characteristics remains an open matter, and its measure is challenging, especially in mountain areas where root excavation is difficult or limited, e.g., at high altitudes or in naturally regenerated forests (Mao et al., 2014).

To overcome such limitations, a specific multi-step method, called PROB-RR, has been developed.

1. Starting from real stand features (e.g., the density of trees, DBH, the minimal distance between trees), a set of random forest configurations can be achieved by MCS in each cell. The procedure generated random locations of trees (a couple of coordinates) according to the minimal distance and tree density obtained via local measurements or the literature. Thus, the spatial variability of stand characteristics can be reproduced.

2. To better analyse the local scale variability of root reinforcement, the resolution of each cell was reduced to a finer grid of 0.1 m.
3. A Root Distribution Model, called RDM for simplicity, was adopted to evaluate the spatial distribution of root diameter using the generated forest configuration in each cell as an input. RDM was originally developed by Schwarz et al. (2010b) and is based on the strong correlation between DBH and the root zone around the tree (Roering et al., 2003). Appendix D describes the model and summarizes the main equations in detail. To apply RDM, it is necessary to calibrate the two main parameters, the pipe coefficient μ and the maximal lateral rooting distance a_0 , which can be performed by minimizing the discrepancies between field measurements and the simulated root densities. According to Schwarz et al. (2012a), the measurements were performed by digging three soil profiles three distances from the stem (0.5 m, 1.5 m and 2.5 m) and counting the number of roots per root diameter class using image analysis (Bischetti et al., 2009; Hales et al., 2009). To evaluate the differences between observations and simulations, two different indices were estimated: the mean percentage error, *MPE* (equation 2.5), and the root mean square error, *RMSE* (equation 2.6):

$$MPE = \frac{100\%}{n} \sum_{i=1}^n \frac{y_i - x_i}{x_i} \quad (2.5)$$

$$RMSE = \sqrt{\sum_{i=1}^n \frac{(x_i - y_i)^2}{n}} \quad (2.6)$$

where n is the number of observations, x_i is the observed root density and y_i is the simulated root density. The minimization of both indices was performed through the application of a standard gradient-based automatic optimization algorithm implemented in the MATLAB/Simulink software package (MATLAB R2015b, The MathWorks, Inc., Natick, Massachusetts, United States).

4. Once the distribution of root diameters has been obtained, a root reinforcement model, which combines the density of roots of different diameters within the soil and the mechanical characteristics of roots, can be run. In this case, the Fiber Bundle Model, FBM, proposed by Pollen and Simon (2005) was adopted according to the literature (Cohen et al., 2009; De Baets et al., 2008; Docker and Hubble, 2008; Hales et al., 2009; Schwarz et al., 2010a; Thomas and Pollen-Bankhead, 2010). FBM, in addition to the root density and diameter distributions, requires only root strength values at different root diameters based on force-diameter relationships obtained from laboratory or field tensile tests (Bischetti et al., 2009; De Baets et al., 2008; Mao et al., 2012). The result of FBM implementation is a root reinforcement map composed of 10,000 values and an empirical probability distribution function for each cell.
5. According to equation 2.1, additional lateral and basal cohesions were considered, although basal root reinforcement is generally negligible (Schmidt et al., 2001).

In summary, the procedure can be synthesized in the following steps (Figure 2.3): (i) generation of maps with tree locations based on MCS, taking into account real forest features; (ii) calibration of RDM based on field-collected data and its application using the generated forest features maps; (iii) application of FBM, incorporating the force-diameter relationships; and (iv) evaluation of the probability distribution of root cohesion from the root reinforcement map. It is possible to skip the first step if the actual spatially distributed tree stand data are available, for example, from detailed field surveys or LiDAR applications (Eysn et al., 2015; Hudak et al., 2008).

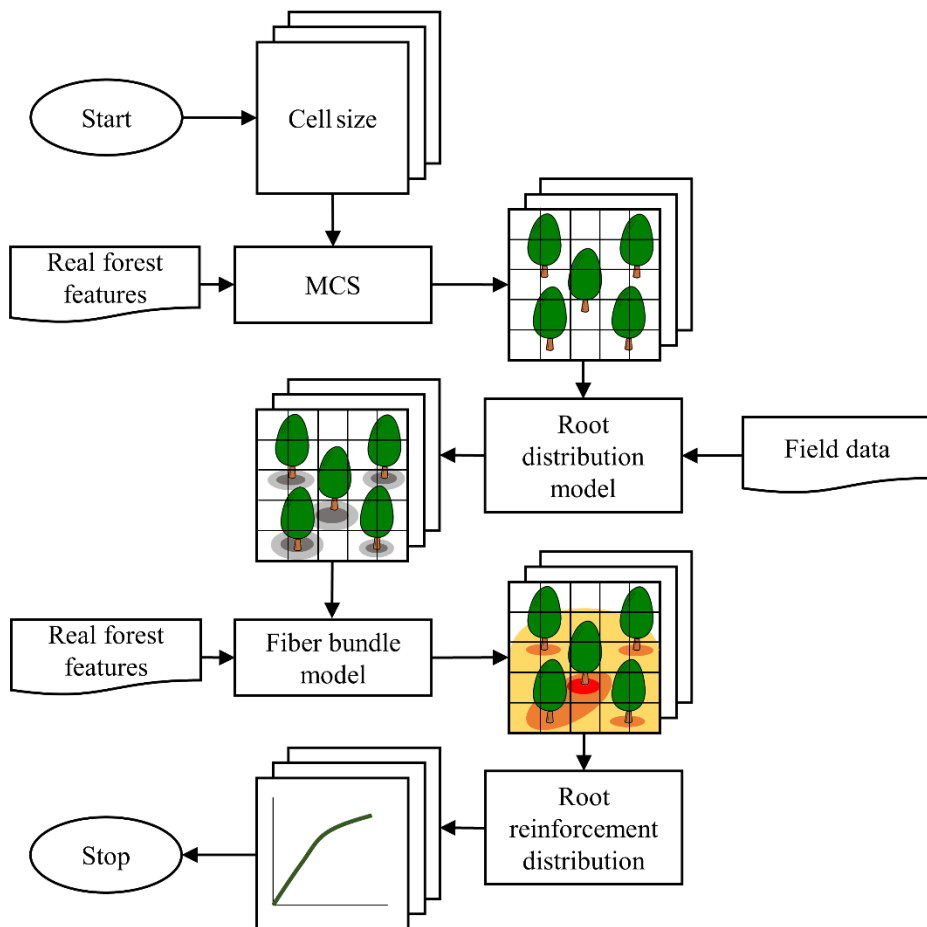


Figure 2.3. Flowchart for the evaluation of the distribution of root reinforcement through PROB-RR. The main steps are as follows: (i) generation of diameter at breast height (DBH) maps through Monte Carlo Simulation (MCS), (ii) root distribution mapping (density according to root diameter size) using Root Distribution Model (RDM), (iii) evaluation of root reinforcement by applying the Fibre Bundle Model (FBM) and (iv) calculation of root reinforcement distribution as a probability distribution function in each cell.

2.2.7 Stability model performance

The assessment of landslide susceptibility model performance consists of analysing the agreement between the model results and the observed data (Frattini et al., 2010). A simple method for evaluating the reliability of the model calculates a series of performance indices based on the binary classification between stable and unstable cells. The most common index is the Success Rate, SR , which is the ratio of successfully predicted landslides over the number of landslides that occurred (Duan and Grant, 2000; Huang et al., 2006). However, it ignores the component of stable cell prediction and many authors have proposed improved accuracy statistics by combining both correctly and incorrectly classified forecasts. Table 2.1 lists the model performance indexes based on the binary classification between stable and unstable cells. The value U_R represents correctly simulated unstable cells, U_0 represents observed unstable cells, U_C represents simulated unstable cells, S_R represents correctly simulated stable cells, S_0 represents observed stable cells, and S_C represents simulated stable cells.

In addition, the Receiver Operating Characteristic (ROC) curve has been considered, as suggested by many authors (e.g., Beguería, 2006; Nefeslioglu et al., 2008; Yesilnacar and Topal, 2005). Developed during the Second World War to assess the performance of radar receivers in detecting targets, ROC curve has been adopted in different scientific fields. In short, this curve is a plot of the probability of having a true positive (correctly predicted event response) versus the probability of a false positive (falsely predicted event response; Gorsevski et al., 2006b). The Area Under the ROC Curve, AUC, is used as a metric for evaluating the overall quality of a model. If AUC is close to 1, it indicates a perfect fit, whereas a value close to 0.5 indicates an inaccurate model, 0.7 an acceptable model and greater than 0.8 an excellent model (Moos et al., 2016).

Table 2.1. List of model performance indices based on binary classification between stable and unstable cells widely used in the literature (Bischetti and Chiaradia, 2010; Borga et al., 2002; Duan and Grant, 2000; Huang et al., 2006; Montgomery and Dietrich, 1994; Rosso et al., 2006).

Model performance indices	Equation
True positive or Success Rate or Sensitivity	$tp = U_R - U_0$
True Negative	$tn = S_R - S_0$
Modified Success Rate	$MSR = 0.5 \left(\frac{U_R}{U_0} + \frac{S_R}{S_0} \right)$
Performance Total Index	$I_{TOT} = average \left(\frac{U_R}{U_0}, \frac{U_R}{U_C}, \frac{S_R}{S_0}, \frac{S_R}{S_C} \right)$
Weighted Modified Success Rate	$WMSR = \frac{2}{3} \frac{U_R}{U_0} + \frac{1}{3} \frac{S_R}{S_0}$

2.2.8 Case study and model application

The proposed method was tested in the East D’Ornica catchment, a subalpine tributary of the Brembo River, which is located in the Upper Brembana Valley (Central Alps, Lombardy, North Italy; Figure 2.4). The study area is 2.29 km², the elevation ranges from 1,050 to 2,250 m a.s.l. and the steepness reaches 48° (Figure 2.5a and Figure 2.5b). The basin is equally divided into permanent pastures/grassland and coniferous forest (Figure 2.5c). The area is nearly completely natural, and the portion of the landscape marked by buildings and mountain paths is minimal (approximately 1.3% of the territory). The watershed is highly vulnerable to landslides, as reported by the Italian Landslide Inventory (ISPRA, 2006). The landslides cover approximately 8% of the area, and the inventory reported that shallow mass movements (i.e., rotational and translational shallow landslides and debris flows) compose the largest portion, as shown in Figure 2.5a. The catchment is characterized by rainy weather, with mean annual precipitation equal to 1,900 mm. Precipitation is mainly concentrated in autumn, as recorded over the last 10 years at a meteorological station installed by ARPA Lombardy

(Regional Agency for the Protection of the Environment) and located in Gerola Alta-Pescegallo (a few kilometres from the study area). The temperature is generally cold, and the mean annual temperature is approximately 7° C. Shallow landslides generally occur during the wettest period (the last documented events occurred during autumn 2012). The forest in the case study is located in the Mesalpic Forest Region and is a mixed forest of European silver fir (*Abies alba* Mill.) and Norway spruce (*Picea abies* (L.) Karst), which are the predominant species (60-70% and 20-30%, respectively). Del Favero (2002) classified the forest type as a typical silver fir forest. The forest stand is at least 80 years old. The basal area of the living stand was 30.36 m²/ha, and the density of trees is approximately 400 trees/ha. The mean height and DBH are 31 m and 0.31 m, respectively (Bischetti et al., 2016). From a geological point of view, the watershed can be divided into two different areas with different soils (Figure 2.5d). The upper part of the watershed is covered by Umbrisols on conglomerates and sandstone, whereas the soils of the remaining part are classified as Cambisols-Podzols on sandstone, siltstone and mudstone, according to the WRB soil classification (Food and Agriculture Organization, 2014). The textural composition is classified as fine gravel (FGR; according to the soil classification reported in Schoeneberger, 2002), with an average depth of 60 cm, and as clean sand or silt grains (SKF), with a depth of up to 150 cm, in the upper and lower parts, respectively.

The digital elevation model, DEM, used as input in the study had a resolution of 10 m x 10 m and was obtained from the Istituto Superiore per la Protezione e la Ricerca Ambientale (ISPRA) website:

<http://www.sinanet.isprambiente.it/it/sia-ispra/download-mais/dem20/view>).

The input probability distributions of geotechnical properties were set as uniform distributions, as performed by Hammond et al. (1992) and assigned different boundary values. The value of the effective internal angle of friction ϕ' varied from 24° to 28° in the lower area and from 37° to 39° in the upper area. The unit weight of soil γ_s was similar in the two geologic zones, ranging from 16 to 18 kN/m³ and 18 to 19 kN/m³, respectively. The failure depth was assumed to follow a triangular distribution, with the upper limit according to the lithological characteristic. In the upper part of the watershed, these values were 0.1 and 0.5 m, with an apex equal to 0.3 m. In the lower part, field data revealed an average depth of 1 m. Concerning the hydrological conditions, we assumed a uniform probability distribution for the ratio between steady-state recharge and transmissivity, R/T , with a range from 10^{-4} to 10^{-1} according to Huang et al. (2006).

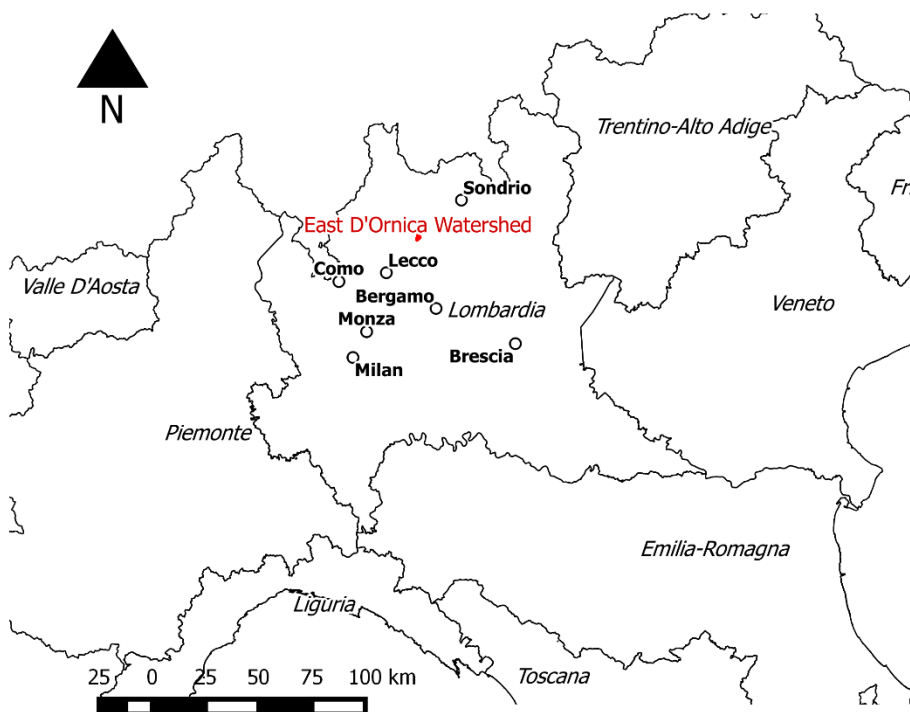


Figure 2.4. Location of the case study.

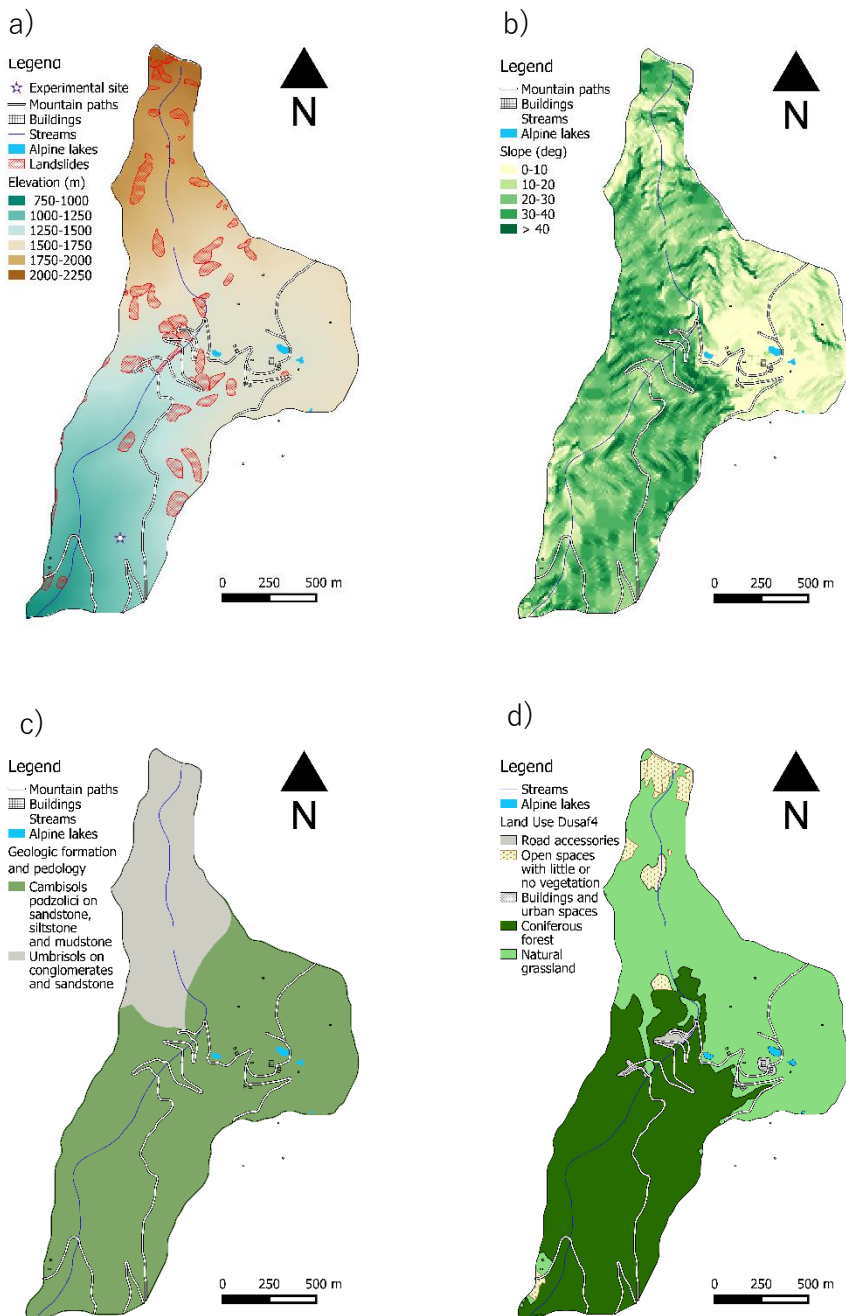


Figure 2.5. (a) Digital elevation model and landslide inventory of the East D'Ornica catchment, (b) topographic slope map, (c) land-use map, and (d) geological map.

2.3 Results

2.3.1 Landslide size

The size of shallow landslides strongly affects both hazard potential and geomorphic consequences (Benda and Cundy, 1990; Fannin and Wise, 2001). Therefore, a statistical analysis of landslide frequency is required to avoid the implementation of a search algorithm and consider the size of potential landslides as a stochastic factor in the probabilistic model based on the landslide inventory. Fifty-eight registered landslides were recorded in the study area and almost all were shallow landslides or debris flows; however, some located in the upper part of the catchment were classified as rockfalls. The landslide area ranged from 40 m² to 10,000 m², with a median value of 2,300 m². Only one mass movement exceeded this range, as shown in Figure 2.6. Approximating the landslides as rectangles, the width ranged from the 2.4 m to 71.2 m, whereas the length varied from 13 m to 261 m. The median values were 28.5 m and 78.4 m for the width and length, respectively. The probability distribution function that best fits the data of geometric parameters w and l is the two-parameter Weibull function. The fitting exhibited good reliability, with a coefficient of determination, R^2 , values equal to 0.992 and 0.987 for w and l , respectively, as shown in Figure 2.7.

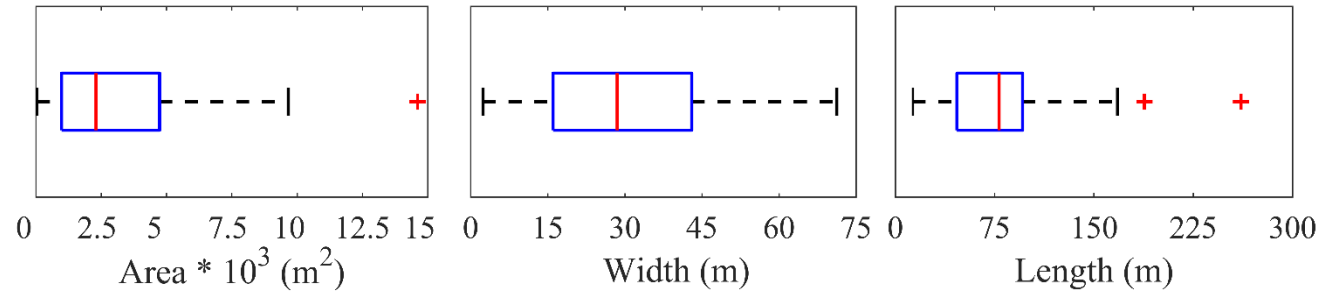


Figure 2.6. Distribution of landslide geometric size in three boxplots of the landslide area, the approximated width and the width/length ratio.

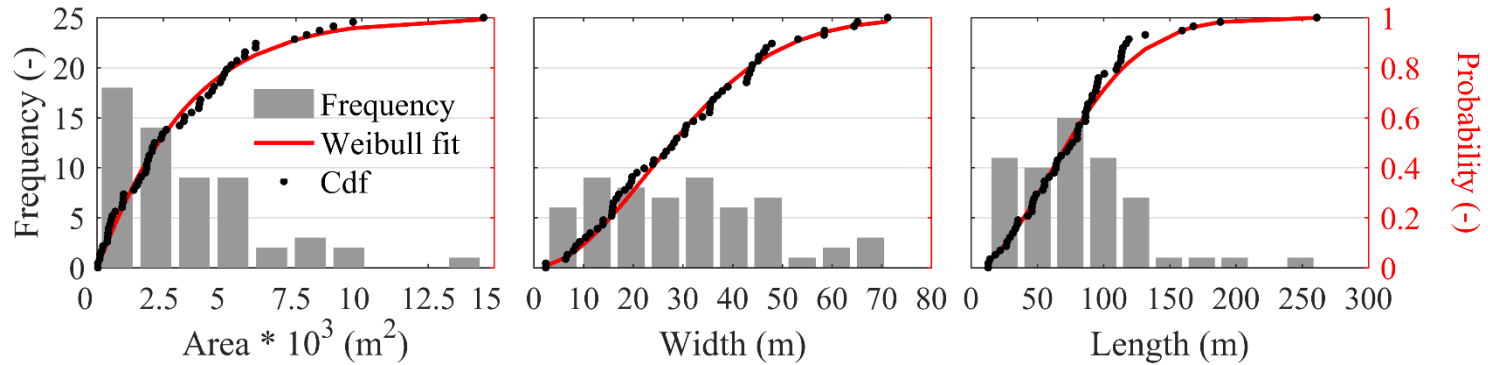


Figure 2.7. Histograms and Weibull fitting curves of geometric parameters width (w) and length (l).

2.3.2 Root reinforcement

As previously noted, the proposed methodology requires calibration with field data to obtain the root density-diameter distributions. Furthermore, nine trenches were dug at sites in undisturbed conditions, and the DBH values of trees around the trenches were measured (values ranged between 0.15 and 0.60 m). All roots intersecting the soil wall profile were counted, and their diameters were measured. The root distribution was estimated based on the diameter class according to the literature (e.g., Bischetti et al., 2016; Genet et al., 2008; Ji et al., 2012; Silva and Rego, 2003): 0-1 mm, 1-2 mm, 2-5 mm, 5-10 mm and >10 mm. The root density of each diameter class decreased as the distance from the tree increased. For example, the distribution of fine roots, which is an important input parameter for the calculation of the frequency of coarse roots (Schwarz et al., 2012b), ranged from 56 to 100 roots/m², as shown in Table 2.2.

Table 2.2. Root distribution measurements: minimum, mean and maximum root numbers for specific diameter ranges in the 9 soil profile walls.

Root (#/m²)	0-1 mm	1-2 mm	2-5 mm	5-10 mm	>10 mm	Total
Min	56	32	36	10	2	178
Mean	80	51	50	12	3	195
Max	100	82	64	16	4	214

The calibration phase aimed to minimize the differences between the simulated and observed root densities at specific distances at the experimental site (Figure 2.5a). The results are satisfactory. The fine root distribution ranges from null values in cells that are too far from trees to a maximum value of 180 roots/m², as shown in Figure 2.8a. The error ranges from -13% to 23.2% in terms of *MPE*. The average absolute *MPE* is 17%, whereas the *RMSE* is approximately 10.7. Values of 5524 roots/m² and 21.9 were assumed for μ and a_0 , respectively, in the RDM model.

The relationship between the maximum force value (F) and the root diameter (ϕ) necessary to evaluate root reinforcement was obtained from laboratory tensile tests performed using fresh root traits.

$$F = 4.78 \phi^{2.04} \quad (2.7)$$

The regression model was highly significant (F-test: p-value < 0.001) and explained the variability in the collected data ($R^2 = 0.90$ and $SE = 0.27$). The power regression is in agreement with most of the literature results (Abdi et al., 2009; Bischetti et al., 2009; De Baets et al., 2008; Mao et al., 2012; Vergani et al., 2012).

The FBM was applied based on the root distribution raster generated by the RDM, and the result consisted of a root reinforcement map, as shown in Figure 2.8. The values of root reinforcement at the experimental site vary from 0 to 35 kPa at a depth of 1 m. The map shows that there is an area of high root reinforcement (darker colour) and a gap in root reinforcement where the root density is minimal (clearer colour). The median value of root reinforcement is 11.62 kPa. After RDM parameters are calibrated and the accuracy of the models verified, the steps presented in Figure 2.3 are implemented.

Using MCS, 1000 virtual forest stand configurations in each cell covered by forest were generated according to the sampled stand characteristics (400 trees/ha, average basal area of 30 m²/ha, minimum distance between trees of 4 m). Then, additional root reinforcement maps were obtained through the application of the RDM and FBM. Therefore, 1,000 different probability distributions of root reinforcement were available in each cell. For the stand forest characteristics of the case study, the average root reinforcement is approximately 6.5 kPa, as shown in Figure 2.9. On average, 8% of each will likely exhibit negligible root reinforcement (less than 1 kPa), whereas approximately 40% will exhibit root reinforcement ranging from 5 to 10 kPa.

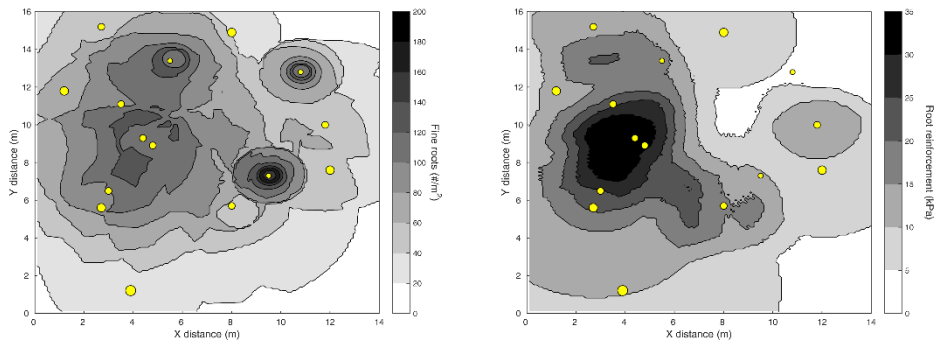


Figure 2.8. Maps describing the study site, including the positions of trees (circles), in terms of the (a) fine root distribution ($\#/m^2$) and (b) root reinforcement (kPa) at a depth of 1m.

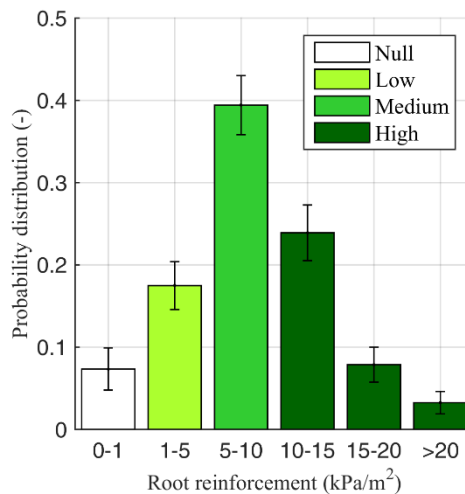


Figure 2.9. Average distribution of 1,000 root reinforcement maps.

In addition, we tested whether the probability density of root reinforcement in a single cell can be assumed normal or lognormal. By applying the statistical test of Jarque and Bera (1980), the hypotheses of both normal and lognormal distributions were rejected (p -value < 0.001).

In the cells covered by coniferous forest, the values of lateral root reinforcement vary from 0 kPa to 30 kPa, following an empirical distribution function, whereas the basal root reinforcement is considered negligible. Both basal and lateral root cohesion are null for meadow/grassland and areas with poor vegetation.

2.3.3 Stability model performance

The stability model was run in a probabilistic context using MCS and the input parameters summarized in Table 2.3.

The PRIMULA model, which was described in the previous section, provided a landslide susceptibility map in terms of the probability of failure $Pr[FS < 1]$, as shown in Figure 2.10. The areas with high probability of failure are located in the central part of the study watershed, particularly along the hairpins in the mountain roads that cross the coniferous forest. Such results are in accordance with shallow landslides recorded in the inventory. Moreover, the eastern part of the catchment, which is characterized by low slopes, was almost entirely simulated as stable. Concerning the lowest part of the catchment, the model showed that the stabilization effect of the coniferous forest, which almost entirely covers the area, is verified. In general, around 23% of the whole watershed has a probability of failure greater than 0.5, whereas 9% has a probability of failure greater than 0.75.

In addition, the model performance indices confirmed the visual analysis, ensuring accurate results. In fact, an optimal equilibrium exists between the successful and true negative rates, where t_p is 0.665 and t_n is 0.730. Additionally, the excellent performance of the model was confirmed by the other indices: $MSR=0.697$, $WMSR=0.686$ and $I_{tot}=0.633$. In addition, the AUC reflected the optimal performance of the model, with a value of 0.824, as shown in Figure 2.11.

Table 2.3. Range, units and probability distribution functions of input parameters used in PRIMULA.

Variable	Min	Max	Apex	Units	PDF
Upper East D'Ornica basin					
ϕ'	37	39	-	degrees	uniform
γ_s	18	19	-	kN/m ³	uniform
z	0.1	0.5	0.3	m	triangular
Lower East D'Ornica basin					
ϕ'	24	28	-	degrees	uniform
γ_s	16	18	-	kN/m ³	uniform
z	0.8	1.1	1	m	triangular
Coniferous forest					
C'_{rl}	0	30	-	kPa	empirical
Whole basin					
w	2	80	-	m	Weibull
l	10	300	-	m	Weibull
R/T	10 ⁻⁴	10 ⁻¹	-	m ⁻¹	uniform

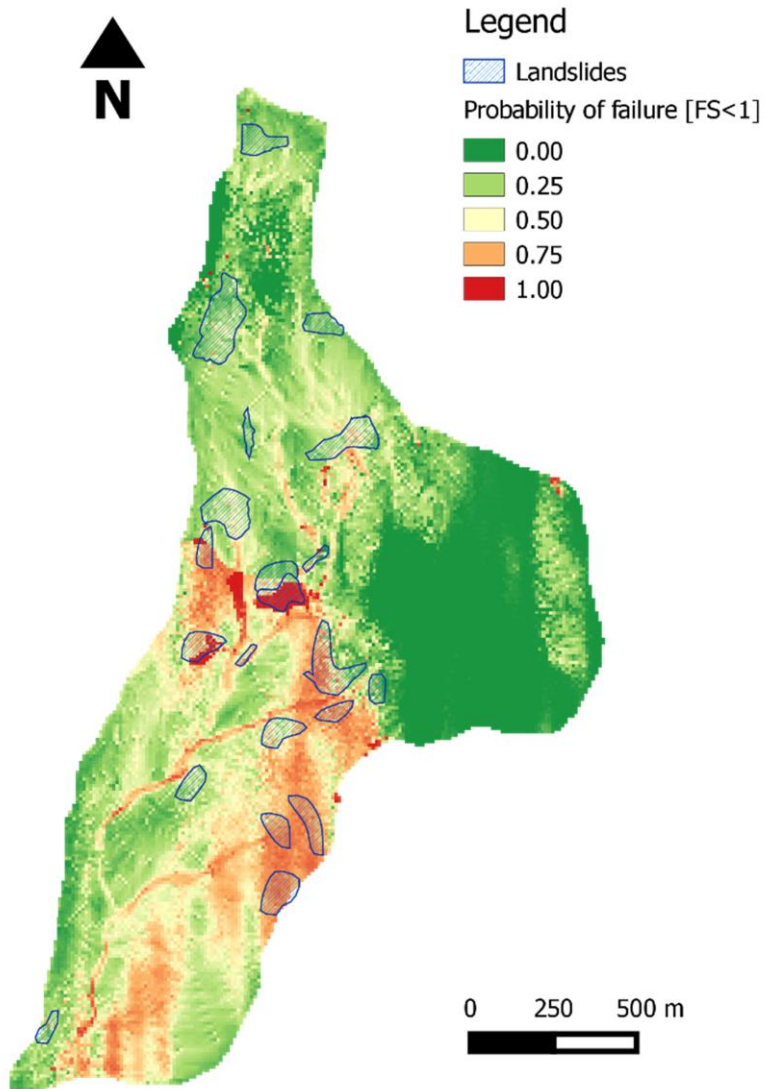


Figure 2.10. PRIMULA probabilistic landslide hazard map. The model suggests that 16% of the watershed area has a probability of failure greater than 0.5, and 9% has a probability of failure greater than 0.75.

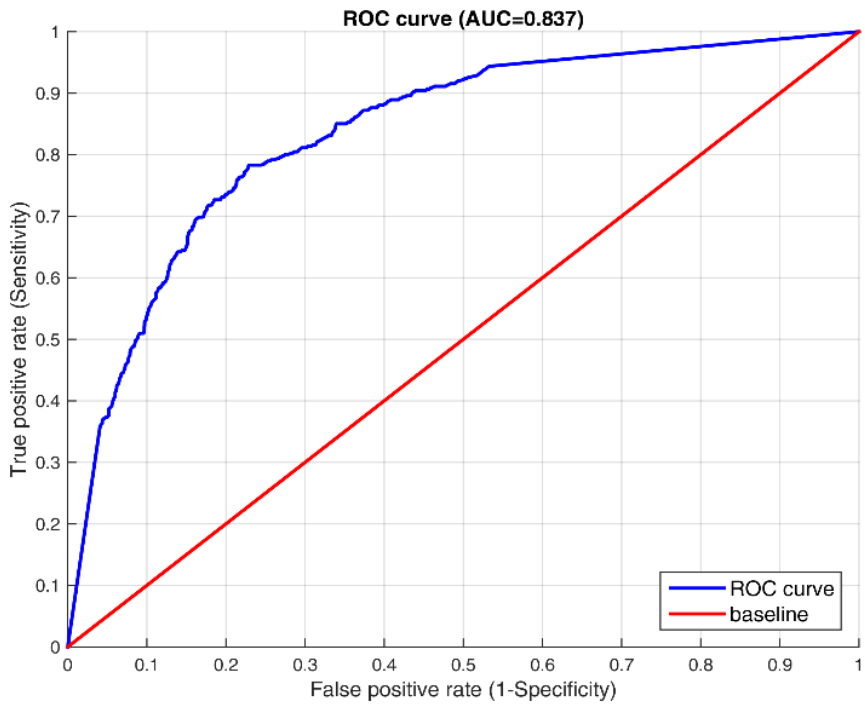


Figure 2.11. Receiver operating characteristic (ROC) curve of the probabilistic PRIMULA, including the variability in root reinforcement. The area under the ROC curve (AUC) is a quantitative measure of model performance.

2.4 Discussion

2.4.1 *Landslide size*

Statistical analysis of the landslide inventory provided important information for determining landslide hazards (Guzzetti et al., 2005) and the triggering mechanisms associated with slope failures. In our study area, most of the 58 landslides were classified as shallow landslides and debris flows. Such mass movements are rigid translational and rotational slides that can be correctly modelled by PRIMULA, which considers a potential landslide as a rigid block (Milledge et al., 2014). Concerning the size of landslides, the area varies from 40 m² to 10,000 m². The range of landslide areas is large, but it agrees with landslide inventories published in the literature (Table 2.4). Furthermore, the average width and the length are larger. The mean width and the mean lengths are 28.5 m and 78.4 m, respectively. Common values of mean width and mean length range from 5 m to 15 m and from 10 m to 40 m, respectively, as observed by Paudel et al. (2003) in Japan, Warburton et al. (2008) in the United Kingdom, Rice et al. (1969) in California, USA, Rickli and Graf (2009) in Switzerland and Montgomery (2001) in Oregon, USA. However, Parise and Jibson (2000) in the Santa Susana Mountains (California, USA) and Dewitte and Demoulin (2005) in the Flemish Ardennes (Belgium) observed landslide sizes similar to those obtained in our work. In addition, by approximating the landslides as rectangular areas, it was observed that the length exceeded the width, as commonly demonstrated in the literature (Gabet and Dunne, 2002; Marchesini et al., 2009).

Table 2.4. Landside area range reported in the literature.

Min area (m²)	Max area (m²)	Location	References
2	10,000	Appalachian Mountains, Virginia, U.S.A.	Morgan et al. (1997)
0.5	900	Hakoishi, Japan	Paudel et al. (2003)
7	500	San Gabriel Mountains, California, U.S.A.	Rice et al. (1969)
7	1,000	Santa Barbara County, California, U.S.A.	Gabet and Dunne (2002)
2	4,000	Cumbria, England	Warburton et al. (2008)
0.75	3,500	Oregon Coast Range, Oregon, U.S.A.	Montgomery (2001)
40	1,000	Pre-Alps and Alps of central and eastern Switzerland, Switzerland	Rickli and Graf (2009)

2.4.2 Root reinforcement

Estimating the spatial distribution of the root reinforcement at the stand scale is currently an arduous challenge for scientists because many physical and biological factors have to be taken into consideration. However, root systems are the “hidden half” of most terrestrial landscapes (Waisel et al., 1991). Root contributions to hillslope stability can dramatically change according to plant species (Bischetti et al., 2009, 2005; Tosi, 2007), topography (Hales et al., 2009), forest management (Bassanelli et al., 2013; Bischetti et al., 2016; Vergani et al., 2014a), local climatic conditions, soil water retention properties (Chirico et al., 2013; Preti et al., 2010), and stand characteristics (Moos et al., 2016; Schwarz et al., 2010a).

In this work, we used the forest stand properties, such as species type, tree density, mean DBH and the minimum distance between trees, to produce spatially distributed root density maps using the RDM. Combining such maps

with the mechanical properties of roots in a root cohesion model (in this case FBM), a reliable probability distribution of root reinforcement for a forest stand was obtained. As forest stand properties show considerable spatial heterogeneity, the MCS approach was adopted to generate reliable stand property maps and their associated probability distributions from averaged values obtained from forest survey samples. This type of approach, in addition to being practical at the operational level, is also useful for predicting the effects of different forest management scenarios, which can only be simulated using average target properties (del Rio et al., 2016). However, such steps could be replaced by the application of new techniques in forestry. In particular, airborne laser scanning (ASL) and light detection and ranging (LiDAR) are robust methods for detecting forest attributes, such as canopy characteristics, tree height and single tree positions (Eysn et al., 2015), even if these technologies are expensive and require highly specialized personnel. Moreover, a fine representation of the terrain should be maintained in slope stability modelling, and this requires further refinement of 3-D stability models. Estimating the probability distribution of root reinforcement in this manner is simple and inexpensive because stand forest characteristic data provided by regional forestry or forest management plans can be used. A possible further improvement could be the introduction of allometric models to better link root systems and the aboveground characteristics of forests (Anfodillo et al., 2013). Concerning root cohesion, the range of lateral root reinforcement values obtained is comparable with those obtained for the same species in several studies conducted at the stand scale (e.g., those obtained by Schwarz et al. (2012b) for a spruce and fir mixed forest in Switzerland), ranging from 0 kPa to 30 kPa, with an average value of 6.5 kPa. Such a range is more conservative with respect to the root reinforcement values estimated in Alpine stands of spruce forest (0-150 kPa in Schwarz et al., 2012a) and Apennine sweet chestnut forest (0-100 kPa in Schwarz et al., 2010a). However, the maximum value of lateral root reinforcement is underestimated with respect to that obtained in a 79-year-

old Douglas fir forest with a density of 400 stem/ha in Southern Coastal British Columbia, Canada (0-10 kPa in Sakals and Sidle, 2004). In addition, numerous studies have provided average values of total root cohesion (both basal and lateral). To provide a comparison, we reported a brief summary of root reinforcement values in Table 2.5, providing information concerning the methodologies used for the evaluation of plant species and sites.

The probability distribution of root reinforcement is rarely available in the literature but fundamental for slope stability modelling. We obtained an empirical distribution that represents a measure of the horizontal spatial variability of root reinforcement according to the distance from trees, tree density and DBH. The reinforcement is nearly negligible (0-1 kPa) in approximately 7% of the cases, low (1-5 kPa) in 18%, medium (5-10 kPa) in approximately 40%, and high (>10 kPa) in 35% (Figure 2.9). This is in agreement with the results of Moos et al. (2016), who, based on a multivariate analysis, including a proxy variable to account for root reinforcement, found that the ratio between root reinforcement at stable and unstable sites varied between 2.5 and 4.0. In approximately 75% of the cases, the root reinforcement values can be considered medium and high. This can be associated with the small distance between trees (4 m), which is shorter than the critical distance (i.e., the distance above which landslides are more frequent) of approximately 6 m found by Moos et al. (2016) and Mao et al. (2014).

In addition, note that “low” values can be observed in areas that are at least 2 meters from each tree stem, whereas the “negligible” class represents areas with poor presence of root systems, which are similar to clear-cut forest areas after 60 months, as reported in Bischetti et al. (2016). In terms of the PDF, the empirical distribution (Figure 2.9) was proven to be different than the uniform, normal and lognormal distributions adopted by other authors (Hammond et al., 1992; Milledge et al., 2014; Pack et al., 1998).

Table 2.5. Values of root reinforcement for different species and sites available from the literature and evaluated through different procedures ([#]in situ direct shear test, ^{*}laboratory shear test, [§]backward analysis, [@]vertical root model equation, ^{\$}FBM)

Root reinf. (kPa)	Vegetation type	Location	References
6.5 [§] -8.93 [@]	European beech (<i>Fagus sylvatica</i> L.)	Pre-Alps, Lombardy, Italy	Bischetti et al. (2004)
5.9±7.5 [*]	Aleppo pine (<i>Pinus halepensis</i> Miller)	Southeast Spain	Cammeraat et al. (2005)
2.0-12.0 [#]	Alder (<i>Alnus japonica</i> Steud.) in nursery	Japan	Endo and Tsuruta (1969)
4.4±3.5 [@] ^{\$}	Hardwood forest: sugar maple (<i>Acer saccharum</i>), eastern hemlock (<i>Tsuga canadensis</i>), rosebay rhododendron (<i>Rhododendron maximum</i>), northern red oak (<i>Quercus rubra</i>), black birch (<i>Betula lenta</i>), tulip poplar (<i>Liriodendron tulipifera</i>), hickory (<i>Carya</i> sp.), red maple (<i>Acer rubrum</i>), chestnut oak (<i>Quercus prinus</i>), and black oak (<i>Quercus velutina</i>)	Southern Appalachian Mountains, North Carolina, U.S.A.	Hales et al. (2009)
3.5±1.6 [@]	Mixed broad leaves woods	Apuane Alps, Tuscany, Italy	Preti (2013)
6.6 [#]	Beech (<i>Fagus</i> sp.)	New Zealand	O'Loughlin and Ziemer (1982)

A probabilistic 3-D stability model

6.2-7.0 [§]	Sugar maple (<i>Acer saccharum</i>)	Cincinnati area, Ohio, U.S.A.	Riestedberg and Sovonick-Dunford (1983)
6.8-23.2 [@]	Industrial forests: Douglas fir (<i>Pseudotsuga menziesii</i>), western hemlock (<i>Tsuga heterophylla</i>), orange maple (<i>Acer macrophyllum</i>) and red alder (<i>Alnus rubra</i>)	Oregon Coast Range, Oregon, U.S.A.	Schmidt et al. (2001)
3.4-4.4 [§]	Hemlock (<i>Tsuga martensiana</i>) and spruce (<i>Picea sitchensis</i>)	Alaska, U.S.A.	Swanston (1970)
1.0-3.0 [§]	Douglas fir (<i>Pseudotsuga menziesii</i>)	British Columbia, Canada	O'Loughlin (1974)
3.5-6.0*	Sitka spruce (<i>Picea sitchensis</i>) and western hemlock (<i>Tsuga heterophylla</i>)	Alaska, USA	Ziemer and Swanston (1977)
3.0-17.5 [§]	Douglas fir (<i>Pseudotsuga menziesii</i>)	Western Oregon and Idaho, USA	Burroughs and Thomas (1977)
5.9 [@]	Cedar (<i>Thuja plicata</i>), hemlock (<i>Tsuga mertensiana</i>) and Sitka spruce (<i>Picea sitchensis</i>)	Alaska, USA	Wu et al. (1979)
3.0-21.0 [#]	Lodgepole pine (<i>Pinus contorta</i>)	California, USA	Ziemer (1981)
5.0 [§]	Yellow pine (<i>Pinus ponderosa</i>)	California, USA	Waldron and Dakessian (1981)
10.3*	Ponderosa pine (<i>Pinus ponderosa</i>), Douglas-fir (<i>Pseudotsuga menziesii</i>) and Engelmann spruce (<i>Picea engelmannii</i>)	Idaho, USA	Gray and Megahan (1981)

3.3 [#]	Radiata pine (<i>Pinus radiata</i> D. Don)	New Zealand	O'Loughlin and Watson (1979)
3.7-6.4 [#]	Yellow pine (<i>Pinus ponderosa</i>) in laboratory		Waldron et al. (1983)
5.6-12.6 [*]	Hemlock (<i>Tsuga</i> sp.), Sitka spruce (<i>Picea sitchensis</i>) and yellow cedar (<i>Thuja occidentalis</i>)	Alaska, USA	Wu (1984)
1.0-5.0 [#]	Japanese cedar (<i>Cryptomeria japonica</i>)	Ibaraki Prefecture, Japan	Abe and Iwamoto (1986)
2.5-3.0 [§]	Alder (<i>Alnus</i> sp.), hemlock (<i>Tsuga</i> sp.), Douglas fir (<i>Pseudotsuga menziesii</i>) and cedar (<i>Thuja</i> sp.)	Washington, USA	Buchanan and Savigny (1990)
25.6-94.3 [*]	Natural forests: Douglas fir (<i>Pseudotsuga menziesii</i>), western hemlock (<i>Tsuga heterophylla</i>), vine maple (<i>Acer circinatum</i>), and sword fern (<i>Polystichum munitum</i>)	Oregon Coast Range, Oregon, USA	Schmidt et al. (2001)
0.6-18.2 [#]	Aleppo pine (<i>Pinus halepensis</i>)	Almudaina, Spain	van Beek et al. (2005)
5.7 [§]	River birch (<i>Betula nigra</i>)	Mississippi, USA	Pollen and Simon (2005)
5.0 [§]	Black willow (<i>Salix nigra</i>)	Mississippi, USA	Pollen and Simon (2005)
5.9 [§]	Eastern sycamore (<i>Plantanus occidentalis</i>)	Mississippi, USA	Pollen and Simon (2005)
2.8 [§]	Cottonwood (<i>Populus fremontii</i>)	Oregon and Kansas, USA	Pollen and Simon (2005)
6.1 [§]	Switchgrass (<i>Panicum virgatum</i>)	Mississippi, USA	Pollen and Simon (2005)
4.0 [§]	Longleaf pine (<i>Pinus palustris</i> Miller)	Mississippi, USA	Pollen and Simon (2005)

14.4-86.0 [®]	European beech (<i>Fagus sylvatica</i> L.)	Pre-Alps, Lombardy, Italy	Bischetti et al. (2009)
13.8-35.4 [®]	Norway spruce (<i>Picea abies</i> (L.) Karst.)	Pre-Alps, Lombardy, Italy	Bischetti et al. (2009)
17.4-38.3 [®]	European larch (<i>Larix decidua</i> Mill.)	Pre-Alps, Lombardy, Italy	Bischetti et al. (2009)
15.0 [®]	Sweet chestnut (<i>Castanea sativa</i> Mill.)	Pre-Alps, Lombardy, Italy	Bischetti et al. (2009)
14.6 [®]	European hop hornbeam (<i>Ostrya carpinifolia</i> Scop.)	Pre-Alps, Lombardy, Italy	Bischetti et al. (2009)

2.4.3 Stability model performance

The use of the probability function of root reinforcement obtained by the proposed procedure in the physically-based 3-D slope stability model led to satisfactory and reliable results. The predictive capabilities of the whole procedure are illustrated by the performance indices presented in section 2.4, which have values similar to those calculated by several authors (e.g., Bischetti and Chiaradia, 2010; Huang et al., 2006; Rosso et al., 2006). Moreover, the ROC plot, which represents one of the most commonly used tools and is threshold independent, suggests that our methodology exhibited very good performance. The global accuracy statistic related to the ROC curve, AUC, has a value of 0.824, which is greater than what is generally considered a reasonable prediction (Pradhan, 2013). Zizioli et al. (2013) compared four different physically-based models and obtained AUC values of approximately 0.80. Cervi et al. (2010) assessed the predictive capabilities of statistical and deterministic methods, obtaining AUC values under 0.80. Günther et al. (2013) assessed landslide susceptibility at a national scale and

achieved values of approximately 0.7. Mergili et al. (2014a) performed GIS-based slope stability modelling over a large area and obtained AUC values less than 0.7.

Finally, note that the presented results were only obtained by calibrating the RDM and without calibrating the stability model. The AUC value is almost the same as those obtained by Moos et al. (2016) by introducing the characteristics of forest stands in a multivariate model (AUC=0.82) and using a random forest model after validation (AUC=0.84). Beyond the positive performance of the methodology, the results show its clear advantages and great potential. For example, the probabilistic approach minimizes the uncertainty and errors due to the poor quality and quantity of several input parameters. Although probability density functions of soil properties could be improved through additional field measurements and observations in principle, geotechnical analyses are often affected by errors and are of variable quality (van Westen et al., 2006). Additionally, in the case of forest characteristics, the probabilistic approach maximizes the use of standard forest information and is suitable for use in a scenarios perspective.

A potentially critical issue is the DEM resolution. Slope morphology and hydrological patterns are theoretically better represented by DEMs with high resolutions (e.g., Bathurst et al., 2010; Claessens et al., 2005) obtained by airborne LiDAR, which can provide a vertical resolution of a few centimeters and a horizontal resolution of a few decimeters to meters (e.g., McKean and Roering, 2004). However, Tarolli and Tarboton (2006) noted that an excessively fine grid resolution leads to unrepresentative values of terrain slopes, and Freer et al. (2002) and Lanni et al. (2012) suggested that a smoother topography better represents hydrological processes and approximates a more realistic water distribution than do detailed DEMs. In terms of landslide prediction performance, some authors compared the results of physically-based models using DEMs with multiple resolutions and obtained worse outcomes at resolutions finer than 10 m (Keijsers et al., 2011; Penna et al., 2014; Tarolli and Tarboton, 2006).

Finally, in modelling slope stability using physically-based models, high-resolution DEMs must be combined with a “search algorithm” to find all unstable collections of grid cells, as proposed by Bellugi et al. (2015a). This approach demands massive computational power, such large core count and high memory density, and elevated capability of implementation without providing clear benefits. The advantages of using high-resolution DEMs are not clear, especially at large scales of investigation and/or in areas with poor data or scarce availability of information. Thus, we suggest that a 10 m-resolution DEM represents a good balance.

2.5 Conclusions

The procedure described in this paper combines recent advances in the field of soil reinforcement exerted by roots and of slope stability modelling to incorporate forest stand characteristics into a 3-D stability model from a probability perspective. In particular, the procedure evaluates the occurrence probability of values of $FS < 1$, accounting for the spatial heterogeneity of vegetation, according to the stand characteristics of forests through repeated randomization of the forest configuration.

The proposed methodology was validated in a subalpine catchment partially covered by coniferous forest and with associated landslide risks. A comparison between modelled unstable areas and the distribution of observed landslides was quantitatively performed in terms of a ROC curve analysis and many other performance indices. The performances of the approach are comparable or even better than other physically-based models and multivariate analyses.

Note that good performance was obtained without calibration of the stability model using data provided by landside inventories. One of the reasons for such performance was to overcome the difficulties to estimate the root reinforcement, which is recognized as one of the limits of physically-based slope stability models. Indeed, better results were provided using a more

sophisticated procedure as compared with the use of a uniform additional cohesion term.

The robustness and accuracy of the method in computing failure probabilities while accounting for forest stand properties suggest its application in sustainable forest management and bioengineering studies. Additionally, potential improvements to future research include assessing the model performance in different geographic locations and conditions (i.e., forest management and plant species) and taking into account local discontinuities such as roads, bioengineering structures, forestry practices, clear-cuts of trees, etc.

3 EFFECTS OF FOREST MANAGEMENT

Keywords:

Shallow landslides;

Forest structure;

Root reinforcement;

3-D slope stability model;

Forest management

3.1 Introduction

Forests have a stabilizing effect on slope stability, especially in mountainous terrains (Bischetti et al., 2009). Indeed, vegetation influences both hydrological processes, which affect the water content of the soil and consequently the pore pressure, and the mechanical mechanisms of soil reinforcement. In recent decades, several scientific works studied and quantified the beneficial effect of the root systems on the soil strength, commonly defined root reinforcement. It is now well-known that the intensity of such reinforcement mainly depends on root distribution and on root tensile strength (Bischetti et al., 2005; Genet et al., 2008; Schwarz et al., 2013). Root density is related to forest stand characteristics such as the trees density, the diameter at breast height of the trunk DBH, the trees age, etc. (Mao et al., 2014; Moos et al., 2016; Roering et al., 2003).

Root reinforcement is an input parameter of the physically-based slope stability models used to analyse and predict slope instabilities in forested landscapes. However, measures and evaluations of such factor incorporate a certain degree of uncertainties and variability. For these reasons, the quantification of the root reinforcement taking into account its spatial and temporal variability remains an open issue for the scientific community (Haneberg, 2004; Hammond et al., 1992).

Moreover, such variability can be associated with the forest dynamics, which are strongly influenced by the forest management practices. Indeed, sustainable forest management requires establishing decisions on the regeneration method, species composition, forest structure (e.g. growth, development, and spacing) through the thinning interventions (Kerr and Haufe, 2011). Forestry operations, in fact, generally aim to maximise the economic returns, to provide better conditions in order to produce quality timber. At the same time, however, they should guarantee a canopy cover able to prevent soil erosion and landslides on steep slopes.

Against this background, this study applies a modular approach, based on a 3 D stability model coupled with MCS and root reinforcement models for estimating slope stability after different forestry interventions.

Because the types and the intensity of such operations are numerous, this study considers only the most common thinning and cutting strategies for the study case that is a small subalpine catchment covered by a coniferous forest.

3.2 Materials and methods

3.2.1 A probabilistic 3-D slope stability model

In this study, the selected slope stability model is PRobabilistic MUltidimensional shallow Landslide Analysis, PRIMULA, recently developed by Cislighi et al. (2017). Based on the combination between a simplified 3-D physically-based model and a Monte Carlo technique, it provides a probability distribution of Factor of Safety values for each cell of a digital elevation model. The sections 2.2.1 and 2.2.2 show additional details.

Among the input parameters requested by the model, root reinforcement is the more complex to evaluate. This stabilizing factor is highly dependent on the forest stand characteristics, such as the spatial distribution of root systems (Burroughs and Thomas, 1977; Moos et al., 2016; Neuhäuser et al., 2012) In addition, it is a function of the root density of different diameter classes and of the ultimate resisting force before the rupture (Bischetti et al., 2009; Schwarz et al., 2013). On these premises, PRIMULA incorporates a specific multi-step method that estimates a probability distribution function starting from the real stand features (e.g., the density of trees, average DBH, the minimal distance between trees). This sub-model is called Prob-RR and is already described in section 2.2.6.

3.2.2 Scenarios of forest management

Thinning is the main method for influencing the growth and the development of the trees. According to Piussi (1994) and Kerr and Haufe (2011), any thinning or cutting can be described in terms of thinning type, thinning intensity and distribution of remaining trees. There are two main types of thinning: the low thinning (L) or “thinning from below” and the crown thinning (C) or “thinning from above”. The first aims to remove the lower canopy (i.e. suppressed, sub-dominant trees, trees with smaller DBH) and to concentrate potential for growth on the larger diameter trees, whereas the other aims to remove trees from the dominant crown classes in order to favour the best trees of the same crown size. In addition, a common approach is the intermediate thinning (I) that combines the other two. In addition, the thinning intensity is strongly influenced by the characteristic of regrowth of the forest and it is difficult to quantify for a generic coniferous forest. Concerning the distribution of trees, uniform stands are clearly the best solution from a timber perspective, but not in terms of habitat diversity and resilience after disturbances. Basing on this description, three scenarios are set (Figure 3.1 and Table 3.1) and, in addition, an additional scenario is a clear-cut (woF) in order to quantify the beneficial role of the forests on slope stability and to identify which areas are less prone to the instabilities. Such areas are suitable for the gap-cutting approach that is common in monocultures of conifers, improving the natural regeneration, diversifying the tree species and guaranteeing economic sustainability for forest companies. The application of Prob-RR (described in section 2.2.6) also allows to evaluate the effects of different forestry interventions on the root reinforcement, and consequently on the slope stability. Indeed, such thinnings modify the values of two fundamental input parameters of Prob-RR as the tree density and the DBH. However, in order to obtain realistic maps of root reinforcement, two additional assumptions are necessary:

- the impact of forest management is evaluated for a period of ten years after cutting condition, because such time is necessary for a complete

decay of the root systems, as demonstrated by several studies (Bischetti et al., 2016; Burroughs and Thomas, 1977; Sidle and Bogaard, 2016; Vergani et al., 2014a; 2016);

- the growth of DBH of the remaining standing trees that can be evaluated through a power law observed by Bertogliati and Conedera (2012) for a Norway spruce forest near the village of Sobrio, Canton of Ticino (Switzerland).

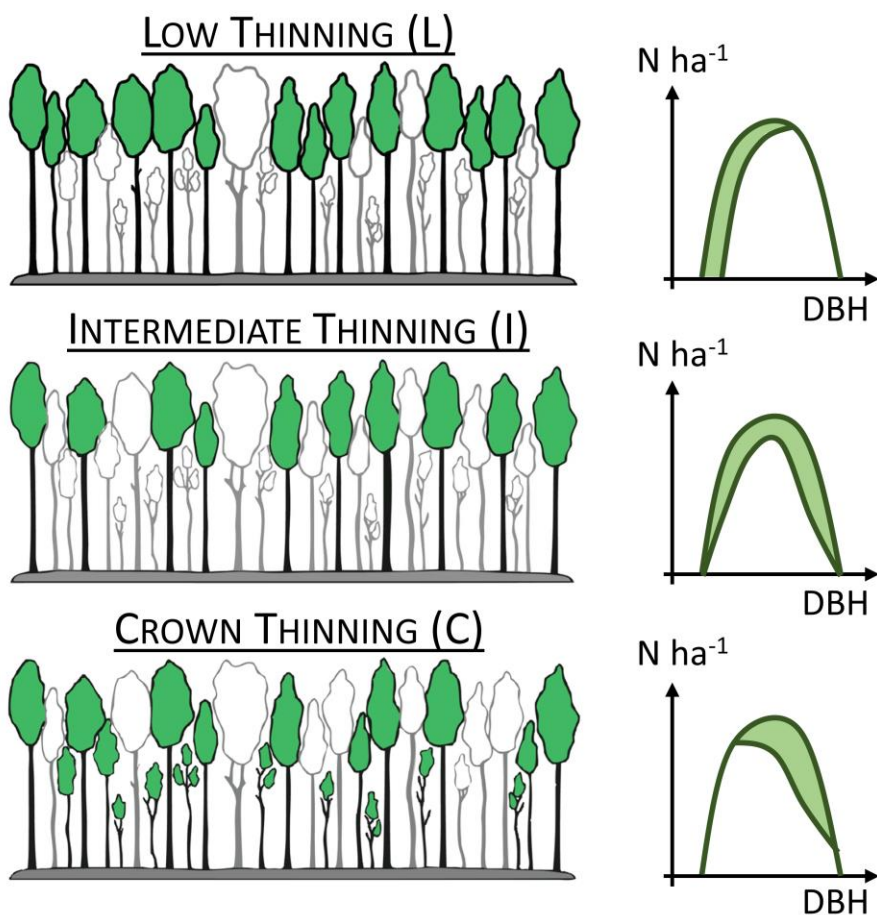


Figure 3.1. Examples of trees to remove and how this would affect the diameter distribution (modified from Kerr and Haufe, 2011).

Table 3.1. Different scenarios combining thinning type and thinning intensity after 10 years from the cutting.

Thinning type	Thinning intensity		
	Light thinning	Moderate thinning	Severe thinning
Low thinning	L10	L20	L30
Intermediate thinning	I10	I20	I30
Crown thinning	C10	C20	C30

3.2.3 Study area

The proposed method was tested in the East D'Ornica catchment, a subalpine tributary of the Brembo River (Central Alps, Lombardy, North Italy). Information about geomorphology, climate, land use and forest characteristics and the input parameter for the PRIMULA model are reported in section 2.2.8.

3.3 Results and discussion

3.3.1 Root reinforcement

For the proposed procedure, the Prob-RR sub-model needs to be calibrated with field observations of root density at different distances from the tree trunk. The parameters of Prob-RR have been evaluated minimizing the differences between the simulated and observed root density at the experimental site and fitting the relationship between the ultimate tensile force (F) provided by tensile test and the root diameter.

Then, Prob-RR generated 1,000 virtual for-est stand configurations for each cell, making available 1,000 different probability distributions of root reinforcement. The base scenario (A), characterized by the actual forest coverage, provided an average value of root reinforcement equal to $18.23 \text{ kPa} \pm 5.59 \text{ kPa}$, ranging from 1.50 to 34.95 kPa. Considering the post-intervention scenarios, the values of root reinforcement for the same thinning type with different intensity produced rather similar results, whereas greater differences were obtained as a function of the type of thinning (Figure 3.2).

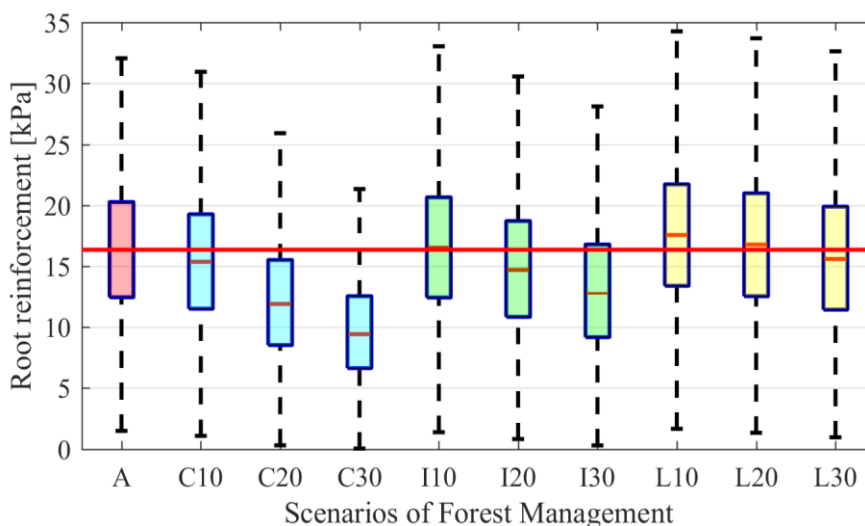


Figure 3.2. Values of root reinforcement according to the different scenarios combining type and intensity: actual forest coverage (A), post-crown thinning (C), post-intermediate thinning (I) and post-low thinning (L),

In particular, a light intensity of thinning does not cause significant differences in quantifying the root reinforcement: the average values are 17.48 kPa, 18.59 kPa and 19.35 kPa, respectively for C10, I10 and L10.

On the other hand, crown thinning seems to cause an intense decrease of root reinforcement for moderate and severe thinning intensities: the mean values of root reinforcement are 14.67 kPa and 12.56 kPa for C20 and C30 respectively. On the contrary, low thinning generates an increase of root reinforcement with time: the average values increase up to 18.77 kPa and 18.09 kPa for L20 and for L30. Such results can be ascribed to a spreading of the root systems of the surrounding, more robust trees, which colonize the soil left free by the felled trees, which root systems decay.

In the case of intermediate thinning, which maintains the same distribution of DBH, there is a significant decrease of root reinforcement, only for the severe intensity (I30), approximately of 14.0%, whereas a slight decrease of 5.5% for the moderate thinning with respect to the condition before the cutting.

3.3.2 Slope stability

PRIMULA model has been applied to provide a landslide hazard map and to evaluate the probability of failure $Pr[FS < 1]$ for the different scenarios of forest management. The areas with a high probability of failure are located on the Eastern side of the catchment and, in particular, along with the hairpins in the mountain roads (Figure 3.3a). The results are in agreement with the shallow landslides recorded in the inventory. In general, approximately 25% of the study area has a probability of failure greater than 0.5, and 10% has a probability of failure greater than 0.75. This is mainly due to the great steepness of the hillslopes and the results of the clear-cut scenario (woF) showed a significant increase of the probability of failure, highlighting the beneficial role of forest (Figure 3.3b). Such hazard increases up to 30% in the eastern part of the catchment.

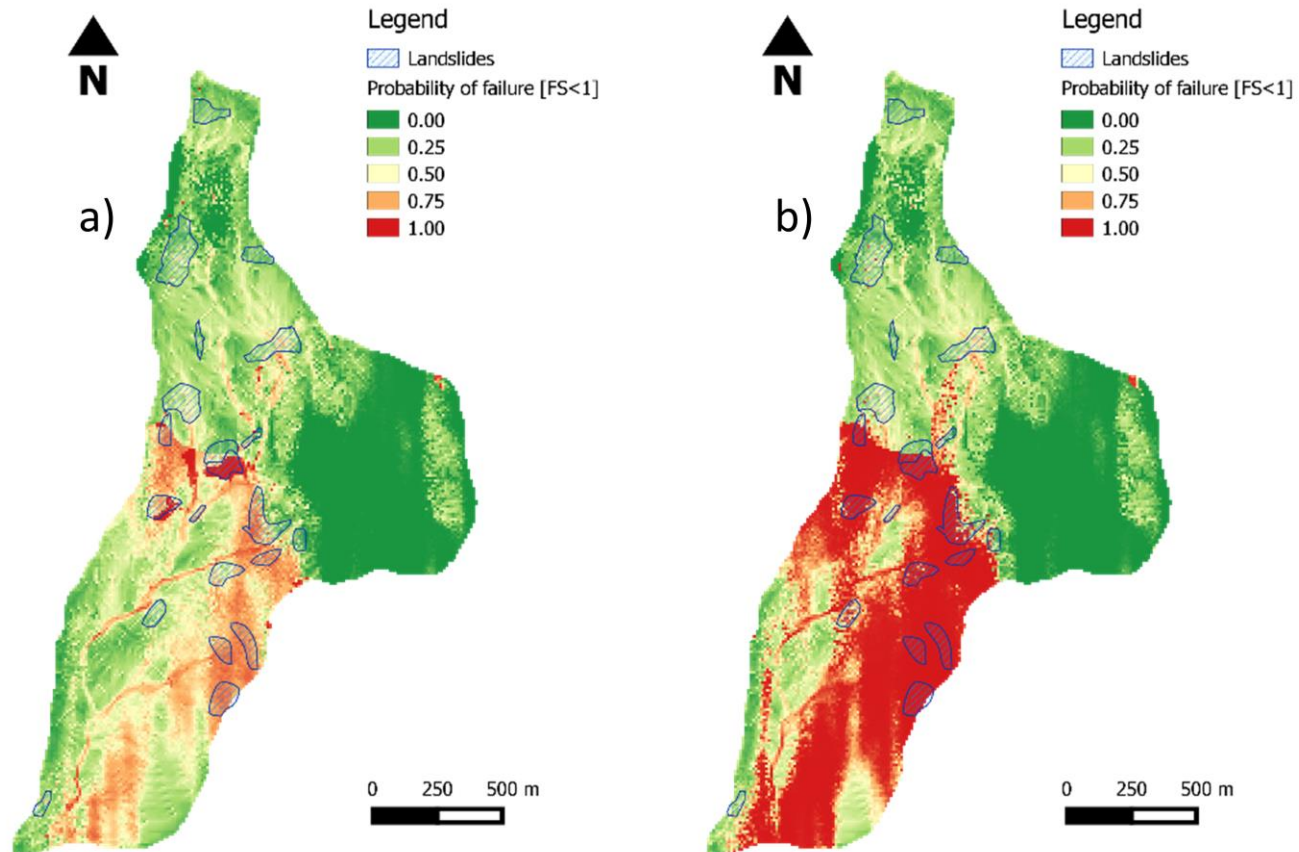


Figure 3.3. Shallow landslide hazard maps provided by PRIMULA model: a) for the base scenario (A) and b) for the clear-cutting scenario (woF).

The influence of the thinning types and intensities is significant in terms of the average value of root reinforcement and consequently on the slope stability in terms of probability of slope failure with respect to the actual situation.

Crown thinning resulted to be less suitable for the steep slopes in the Eastern part of the study area. Cutting trees with larger diameter causes a significant reduction of root reinforcement and as a consequence of the slope stability. Indeed, the shallow landslide hazard map based on such scenario with severe intensity (C30) shows an increase of the instability up to 36% in several cells of the catchment. The intermediate scenario with severe intensity (I30) is more conservative causing a maximum increase of 19% in few parts of the study area. On the other hand, low thinning or single tree selection should be suggested for the critical hillslopes, because do not cause a significant decrease of stability. These three cases are illustrated in Figure 3.4.

In addition, light and moderate thinning intensities also have a slight effect on the probability of failure and do not significantly modify the landslides risk of the catchment, respect than severe thinning intensity.

Although the root reinforcement is generally important for the entire area, the stability of the western part bordered by the mountain path appeared less affected by such reinforcement, and thus suitable for gap-cutting approaches and in general for clear-cutting.

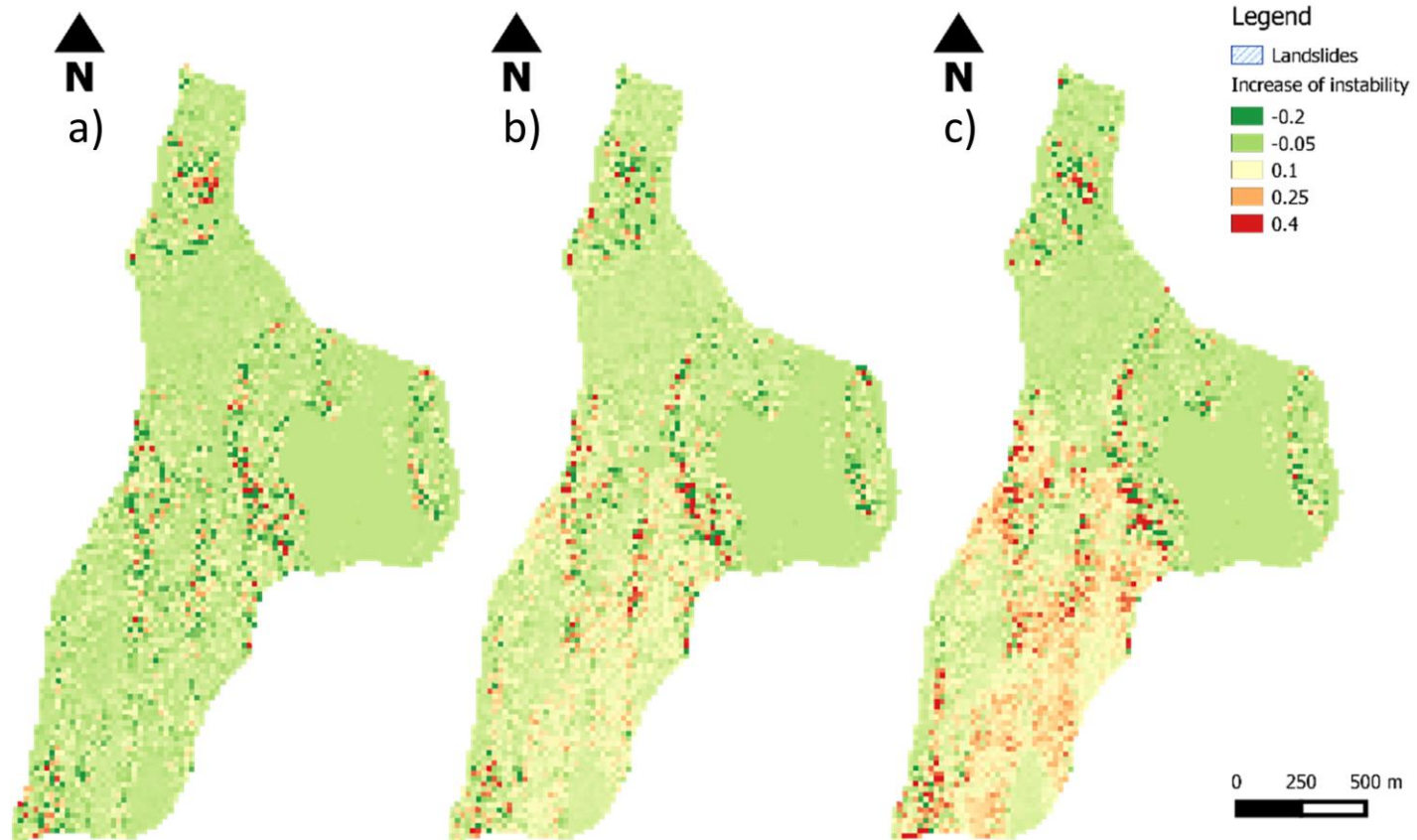


Figure 3.4. Differences in terms of increase of instability after thinning interventions with severe intensity respect the actual condition: a) low thinning, b) intermediate thinning, and c) crown thinning.

3.4 Conclusions

The PRIMULA model described in this study incorporates the more recent advances in the field of soil reinforcement due to the vegetation and combines a 3-D stability model with a probabilistic procedure through the MCS. The method has been applied in a subalpine study area covered by a coniferous forest. Its performance is comparable, or even better than other physically-based models and multivariate analyses. The robustness and the accuracy of the method suggest its application for a sustainable forest management in order to evaluate the effects on slope stability of different scenarios of forest interventions in terms of typology and intensity. A quantitative analysis of the consequence of forest management strategies, in fact, is a necessary step to carry out good thinning practice. The application of the method to the study case shows that low and intermediate thinning, independently of the thinning intensity cause a small decrease of root reinforcement, and then a negligible increase of probability of slope failure. On the contrary, crown thinning causes a significant reduction of root reinforcement and then of slope stability.

These results suggest carrying out specific analyses to define the location and the intensity of the forest cutting, especially where slopes are steep.

In conclusion, a sustainable forest management, which must not lead to an abrupt reduction of slope stability, should be supported by a robust procedure in order to evaluate the suitable location, type and intensity of the thinning strategies. The presented method is an example of such a procedure.

4 LARGE WOOD RECRUITMENT FROM HILLSLOPE

Keywords:

Large wood;

LW mobilization;

Forest structure;

Hillslope instabilities;

3-D slope stability model.

4.1 Introduction

Large wood (LW) is a key factor in a woodland fluvial ecosystem as in-channel LW elements directly influence physical, environmental, chemical and biological aspects of aquatic life (Abbe and Montgomery, 1996; Anderson et al., 1978; Beckman and Wohl, 2014; Gregory et al., 2003; Montgomery and Piégay, 2003; Seo et al., 2008; Tockner et al., 2003; Wohl, 2017). However, floating and deposited LW also affects river morphology and sediment dynamics (Montgomery et al., 2003; Wohl and Scott, 2016), causing obstructions of narrow channel cross-sections, especially bridges and hydraulic structures, with hazardous clogging phenomena (Gippel et al., 1996; Mazzorana et al., 2011a; Wohl, 2017). Such phenomena usually occur during low-frequency and high-magnitude flood events (Mao et al., 2013) and induce a significant potential hazard for human populations and infrastructure (Badoux et al., 2015; Comiti et al., 2016; Lucía et al., 2015b). Although the removal of LW storage is common practice in hydraulic management of watercourses (Wohl, 2014), recent restoration projects have included a reintroduction of woody material into fluvial systems in order to recover pristine conditions by improving their hydrological, morphological and ecological status (Abbe and Brooks, 2011; Antón et al., 2011; Kail et al., 2007).

In recent years, several authors have studied LW dynamics and budget, making a major effort especially in the understanding of LW recruitment mechanisms and transport (see Wohl, 2017). LW recruitment processes vary widely in terms of space and time within watersheds (Benda and Sias, 2003; Gurnell et al., 2002; Piégay et al., 1999). The processes can be divided into the following categories:

- (i) geomorphological (e.g. landslides, debris flows) (Ruiz-Villanueva et al., 2014);
- (ii) episodic disasters (e.g. wildfire, snowstorms and windstorms) (Benda et al., 2002, 2003b; Keller and Swanson, 1979; Miller et al., 2003);

- (iii) hydraulic (e.g. bank erosion, channel migration, bank cutting and fluvial transport) (Kaplan and Garrick, 1981);
- (iv) biological (e.g. tree growth, senescence and mortality, insects, fungal diseases) (Bragg, 2000; Harmon et al., 1986);
- (v) human-induced (e.g. harvesting, arson) (Bragg, 2000).

Bank erosion is the main source of LW recruitment in high-order lowland rivers, whereas colluvial processes such as landslides and debris flows are the dominant mechanisms for delivering woody material from hillslopes and small headwater channels to valley-bottom streams in low-order mountain streams (Cadol et al., 2009; Comiti et al., 2008a; Iroumé et al., 2010; Keller and Swanson, 1979; Nakamura and Swanson, 1993; Rigon et al., 2012).

In this context, investigating the LW dynamics in a reach of a watercourse requires a quantification of the LW budget, accounting for inputs, storage and inputs (e.g. Comiti et al., 2016):

$$\Delta S = \left(L_i - L_d + \frac{Q_i}{\Delta x} - \frac{Q_o}{\Delta x} - D \right) \Delta t \quad (4.1)$$

where ΔS is the change in LW storage, L_i is lateral recruitment per unit of channel length and unit of time, L_d is lateral deposition on the floodplain, Q_i and Q_o are the fluvial transport into and out of the stretch, D is LW decay due to degradation processes, Δx is channel length and Δt the time interval considered.

Lateral input is, in turn, the result of several different processes (Wohl, 2017), although most LW volume recruitment can be assumed to originate from the fluvial corridor, due to bank and floodplain erosion, and from the hillslopes, due to landslides and debris flow processes (Comiti et al., 2016).

In the scientific literature, a variety of models have been proposed to evaluate LW recruitment, including stochastic (Lancaster et al., 2003; Marcus and Fonstad, 2008), physical (Braudrick and Grant, 2000; Wallerstein et al., 1997) and theoretical models (Braudrick et al., 1997). Detailed models have also been proposed for large-scale analyses to identify the potential source area

of LW. Czarnomski et al. (2008) developed a statistical and simple mass balance analysis to assess the impact of natural processes and forest management on the wood input to streams. Mazzorana et al. (2009) introduced a series of empirical indicators to determine the relative propensity of mountain streams to recruit woody material. Rigon et al. (2012) presented a GIS-based model focusing on LW recruitment from hillslope instabilities combining a bivariate geo-statistical analysis (WofE) for slope stability and a slope decay function for connectivity. Eaton and Hassan (2013) proposed a stochastic model in order to investigate the geomorphic function of wood changes as a consequence of tree mortality at the watershed scale. Recently, Ruiz-Villanueva et al. (2014) developed a procedure based on multi-criteria and multi-objective assessment analysis using fuzzy logic principles in a spatially distributed way. Detailed reviews on this subject are given in Gregory et al. (2003) and Ruiz-Villanueva et al. (2016).

Despite all this, the assessment of LW recruitment volumes is still challenging and subject to great uncertainty, especially in cases where hillslope instability is a concern (Comiti et al., 2016) and a spatially distributed numerical simulation of LW recruitment is considered a gap that needs to be filled (Wohl, 2017).

Indeed, the extreme complexity and spatial and temporal variability of LW recruitment processes from hillslopes is a considerable challenge for most conceptual models and needs a spatially distributed implementation. In addition, forest characteristics (e.g. tree sizes and density) strongly affect both slope stability (e.g. Cislighi et al., 2017) and the potential LW quantity and size (e.g. Comiti et al., 2016). The identification of potential LW sources and the quantification of LW amount from hillslopes would, therefore, require the use of physically-based spatially-distributed models able to relate forest characteristics to slope stability.

Given this background, this study aims to investigate the relationship between low-order forested mountain catchments prone to soil instabilities

and potential LW volume, providing a new method to evaluate LW recruitment from forested hillslopes. The proposed approach is able to produce a more precise estimation of LW input from different sectors of the catchment and to evaluate the effects of different forest management strategies.

To reach this goal, a probabilistic multidimensional approach has been adopted to model shallow landslides susceptibility and the related recruitable LW.

4.2 Materials and methods

4.2.1 Slope stability analysis and potential LW recruitment

A reliable method to evaluate the potential LW recruitment volume from a hillslope starts from the prediction of potentially unstable areas over the entire catchment with particular reference to forested ones. To achieve this, we adopted a two-step procedure. The first step involves a slope stability analysis to identify the potential source areas of LW recruitment and the second estimates the related potential LW volume based on forest maps.

Slope stability model

Evaluating the potential areas of slope instability and as a consequence, the sources of LW recruitment requires the temporal and spatial variability of each input parameter. The adopted method is the Probabilistic Multidimensional shallow Landslide Analysis, PRIMULA, recently developed by Cislighi et al. (2017) and described in detail in Chapter 2. The output of PRIMULA model is the susceptibility map in which each cell indicates the probability of shallow landslide occurrence. Once obtained the susceptibility maps, it is possible to filter them by a set of threshold values of failure probability, obtaining the unstable areas within the catchment for fixed probability values. Elaborating forest maps, in which all silvicultural and forest stand features (i.e. tree density, average DBH, average height, etc.) are reported, a map of tree volume values can be obtained. By overlaying the two maps, the LW volume that can potentially be produced by unstable areas (in m^3ha^{-1}) can be easily obtained. The additional elements of the original are illustrated in a flowchart in Figure 4.1. PRIMULA and the related sub-models were developed using MATLAB/Simulink software (MATLAB R2015b, The MathWorks, Inc., Natick, Massachusetts, United States).

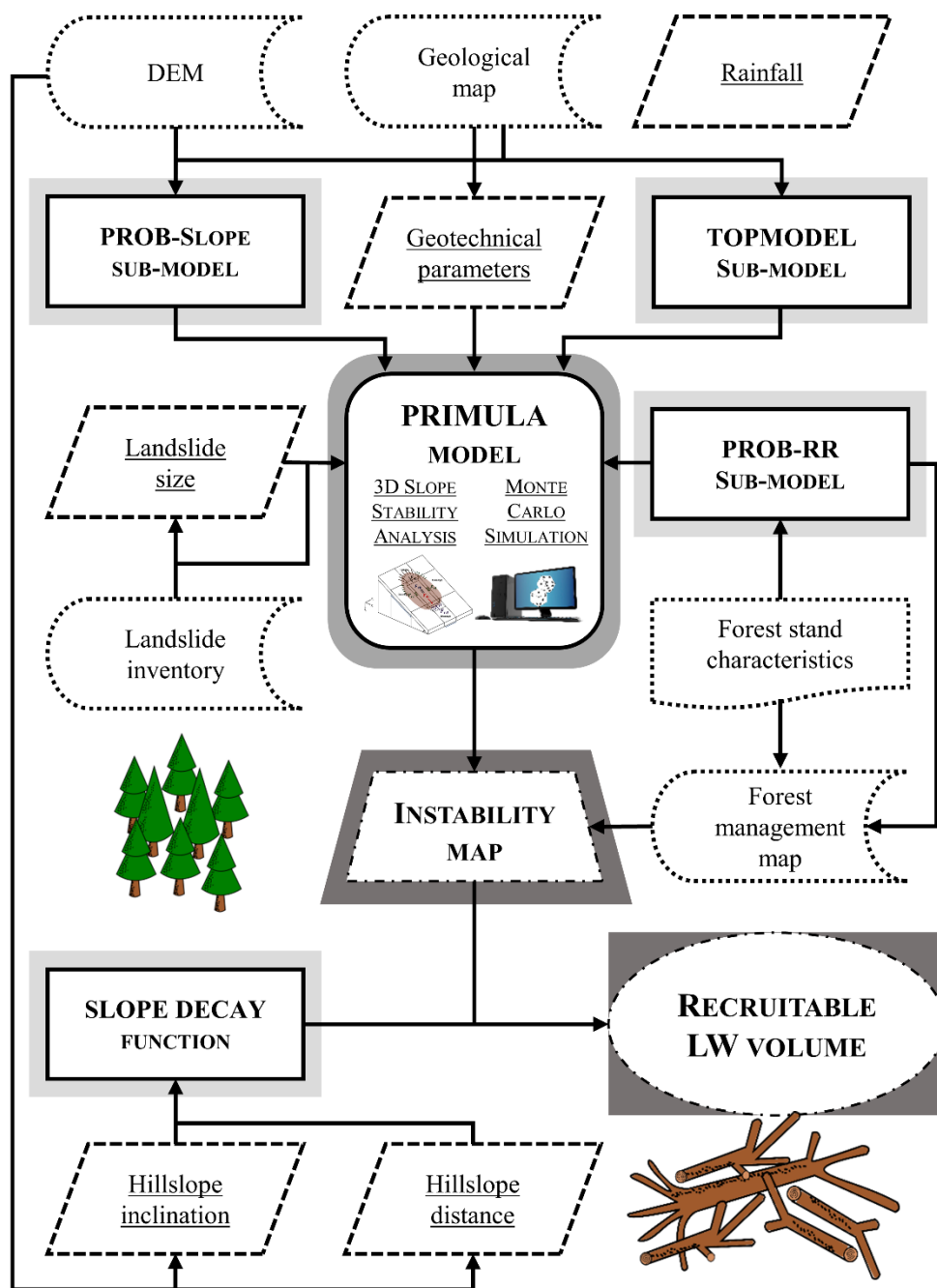


Figure 4.1. Flowchart describing the procedure to evaluate the recruitable LW volume combining a probabilistic multidimensional stability model PRIMULA and the hillslope-channel transfer model based on the slope decay function.

Potential LW volume estimation

To quantify the LW recruitment from hillslopes, it is common to sum the tree volume that covers unstable areas, by applying forest stand volumes from forest inventories (Comiti et al., 2016; Hassan et al., 2016; Lucía et al., 2015b). Once a reliable landslide hazard map has been obtained by PRIMULA, the LW volumes potentially produced by unstable hillslopes have been estimated by considering information from the forest map (forest function, stand age, dominant and secondary tree species, tree density, average tree DBH and height) and elaborating the hazard map in a probabilistic perspective.

This map provides the probability of slope failure, $Pr[FS < 1]$, thus by fixing a threshold level, P^* , it is possible to identify all areas in which the landslide hazard is greater than the threshold. Summing the volume of trees standing on all areas selected for P^* , we can obtain the potential maximum released LW volume at hillslope scale.

However, the potential maximum released LW volume by hillslopes does not have a probability of P^* because the threshold refers to every single unstable area, whereas the total volume refers to all unstable areas, i.e. those with a $Pr[FS < 1] > P^*$. This means that to reach the potential maximum LW mobilised volume, all unstable areas have to fail together.

Therefore, if each unstable area indicates a single potential landslide, which can be considered as a separate and independent event from other potential landslides, a compound probability, $cP(P^*)$, has to be calculated for each P^* in the following way:

$$\begin{aligned} cP(P^*) &= (\Pr[FS < 1] \geq P^*)_1 \cap \dots \cap (\Pr[FS < 1] \geq P^*)_n = \\ &= \prod_{i=1}^n (\Pr[FS < 1] \geq P^*)_i \end{aligned} \quad (4.2)$$

where $Pr[FS < 1] \geq P^*$ is the value of the probability that $FS < 1$ in the i -th area. Thus, it is possible to calculate the volume of trees mobilised by the unstable areas for different P^* and the corresponding $cP(P^*)$ in order to obtain a curve

that relates the potential LW released by the hillslope and its probability of occurrence (and consequently the recurrence time).

LW recruitment estimation

In LW studies, several authors assume that all trees mobilised by landslides and/or debris flows, reach the channel network (e.g. Hassan et al., 2016). However, the LW ability to reach a stream strongly depends on the connectivity between LW source and channel network (Lucía et al., 2015b). Moreover, a significant part of LW volume can be stored both on the hillslopes and in unchanneled valleys. For example, Comiti et al. (2016) reported that Amorfini et al. (2002), investigating a flood in Alta Garfagnana (Tuscany, Central Italy), estimated that less than half of the LW volume mobilised by landslides arrived in the channel network.

Except in the case of headwater catchments where channels are highly confined, hillslope instabilities are expected to be strictly connected to the channels, so the actual connectivity between LW sources and channels should be considered. Generally, when a landslide occurs, the woody material included in it moves to the nearest channel as a debris flow. Iverson (1997) and George and Iverson (2011) evaluated this process through a simplified model that describes debris flow runout with mixture theory and depth-averaged conservation of mass and momentum in two dimensions. Mazzorana et al. (2009) identified preferential recruitment paths through geomorphic analysis of either a digital terrain model or a dataset of surface watercourses. These routes hydrologically connect LW sources with the in-channel deposition areas. In addition, Lancaster et al. (2001) hypothesised that wood deposits by mass movements form dams that lead to persistent storage and inhibit the correct propagation of sediment. Lucía et al. (2015b) extended the connectivity index developed by Cavalli et al. (2013) for sediment to LW.

In the present study, according to Rigon et al. (2012), we adopted a procedure describing the hillslope-channel transfer through a “slope decay” function,

which includes permanent or temporary LW storage on hillslopes. The “slope decay” takes the unstable LW volume as input, moves with the flow and is subject to a first-order decay in moving from cell to cell to the channel network. Such a process depends on many factors, and the slope decay function is expressed as a function of the flow distance and upslope area. Indeed, the potential recruited LW mass is subject to a progressive decrease depending on the distance along the flow path from unstable area to channel. Summing up the LW volume reaching the channel network, it is possible to estimate the in-channel LW recruitment. This function was featured in the software TauDEM (Terrain Analysis Using Digital Elevation Models; Tarboton, 2003), which is a set of Digital Elevation Model (DEM) tools for the extraction and analysis of hydrologic information available both for ESRI ArcGIS software (<https://www.arcgis.com/>) and for Quantum GIS (<https://www.qgis.org/>).

4.2.2 Accuracy analysis

Assessing the accuracy of the slope stability model is a necessary step to verify its applicability in practice. A simple way to evaluate model performance is to analyse the agreement between simulated unstable areas and observed data (Frattini et al., 2010). The most common performance index is the Success Rate, S_{pr} which corresponds to the ratio of successfully predicted landslides over the number of observed landslides (Duan and Grant, 2000; Huang et al., 2006). However, it does not take into account the correct/uncorrected prediction of stable cells. Because of this limit, a large number of performance indices were proposed to validate the landslide susceptibility models (Frattini et al., 2010; Rosso et al., 2006), as shown in the section 2.2.7. The selected model performance indices are tp , tn , MSR , I_{tot} and $WMSR$ (see Table 2.1). Moreover, the Area Under the ROC Curve, AUC, is used as an additional metric.

4.2.3 Study area

The area considered in this study is the Rio Davedino catchment, a tributary of the Cordevole River in the Southeastern Italian Alps, within the administrative boundaries of the Province of Belluno, Italy (Figure 4.2). The area is 8.69 km² with a range of elevation between 1,194 m and 2,512 m a.s.l. (Figure 4.3a). The hillslope inclination varies from 0 to 56 degrees (Figure 4.3).

Rio Davedino catchment is located in the Endalpic climatic district that belongs to the continental temperate and wet climatic zone, common to most Southern Alpine regions. Mean annual rainfall is 1,100 mm. February is the least rainy month, whereas June and November are the rainiest. Heavy snowfalls are not rare and generally occur from late November to early April. The mean annual temperature is 5 ° C.

The land cover is completely natural with pastures, shrubs and forests (Figure 4.3c). Coniferous and deciduous forests cover most of the western part of the catchment. Del Favero et al. (2000) classified the coniferous forest as spruce forest, in which Norway spruce (*Picea abies* (L.) Kast.) and European larch (*Larix decidua* Mill.) are the predominant species, whereas European beech (*Fagus sylvatica* L.), stone pine (*Pinus cembra* L.) and silver fir (*Abies alba* Mill.) are secondary. At higher altitudes in the southern part, the predominant plant is green alder (*Alnus viridis* (Chaix.) D.C.).

Although the geology of the area is very complex, the watershed can be divided into four zones with different bedrock and soil characteristics (Figure 4.3d). According to the WRB soil classification (Food and Agriculture Organization, 2014), most of the watershed is covered by Follic Entic Podzols on silicate, sandstone and siltite with a loamy sand texture and approximate depth of 1.0 m. The northeastern part is covered by Cutanic Luvisols on calcareous and marls bedrock to a depth of up to 1.5 m and fine loam texture. In the northwestern part, Haplic Umbrisols and Haplic Phaeozems are present on silicate, sandstone and siltite; soil depth strongly depends on the elevation and the texture is loamy sand. The southwestern part is

characterised by Haplic Cambisols on silicate, sandstone and siltite, constituted of loamy sand to a depth ranging from 0.5 and 1.0 m.

The input probability distribution of geotechnical parameters and soil properties have been set as uniform distributions as suggested by Hammond et al. (1992), except for the failure depth. Indeed, the failure surface was assumed to be located at the interface between soil and bedrock and to follow a triangular distribution with the upper limit according to the lithological characteristics (Zhou et al., 2003). Table 4.1 summarises these input parameters.

Concerning hydrological conditions, we assumed a uniform probability distribution for the steady-state recharge with a range between 1 and 30 mm/hr.

The digital elevation model, DEM, used to evaluate the topographic parameters has a resolution of 5 x 5 m and is freely downloadable from the website of ARPA VENETO (Regional Agency for Environmental Protection and Prevention of the Veneto Region).

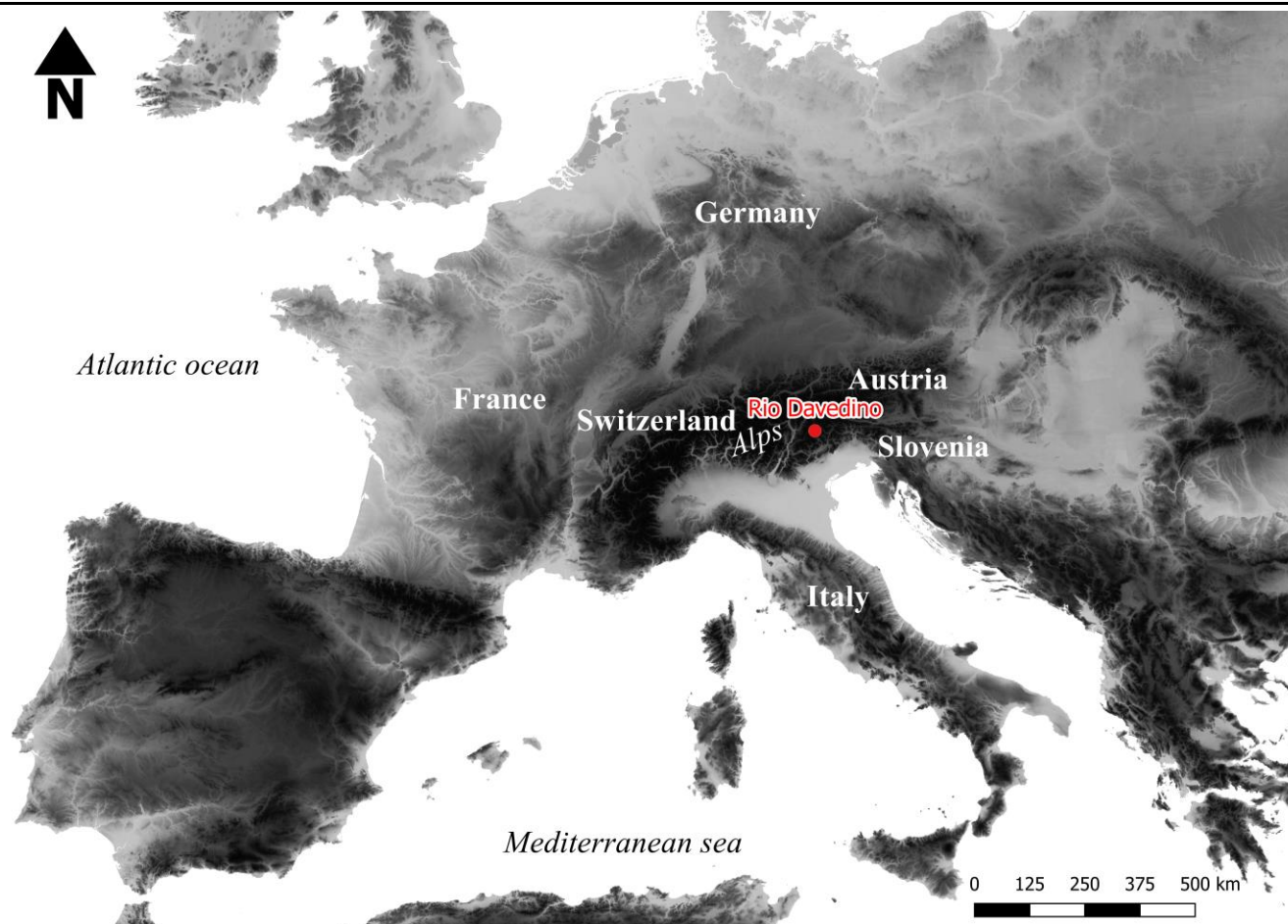


Figure 4.2. Geographic position of Rio Davedino catchment on the European continent.

Table 4.1. Range and units of the geotechnical characteristics of the different soils: WRB classification, texture, elevation range (in m), effective soil friction angle range (ϕ' in degrees), soil unit weight range (γ_s in KN m^{-3}), failure depth (z in m), soil cohesion range (c' in KPa), saturated hydraulic conductivity (K_s in m hr^{-1}) and degree of saturation range (S_R in percentage).

WRB	Texture	Elevation	ϕ'	γ_s	z	c'	K_s	S_R
Haplic Umbrisols	Loamy sand	> 1900	30-36	17-18	0.25-0.50	0	0.001-1.00	35-50
Haplic Phaeozems	Loamy sand	< 1900	30-36	17-18	1.00-1.50	0	0.001-1.00	50-60
Folic Entic Podzols	Loamy sand	< 2300	30-36	17-18	0.50-1.00	0	0.001-1.00	50-60
Haplic Cambisols	Loamy sand	< 2000	30-36	17-18	0.50-1.50	0	0.001-1.00	35-60
Cutanic Luvisols	Fine loam	< 2000	28-32	18-19	1.00-1.50	0-5	0.01-1.00	35-50

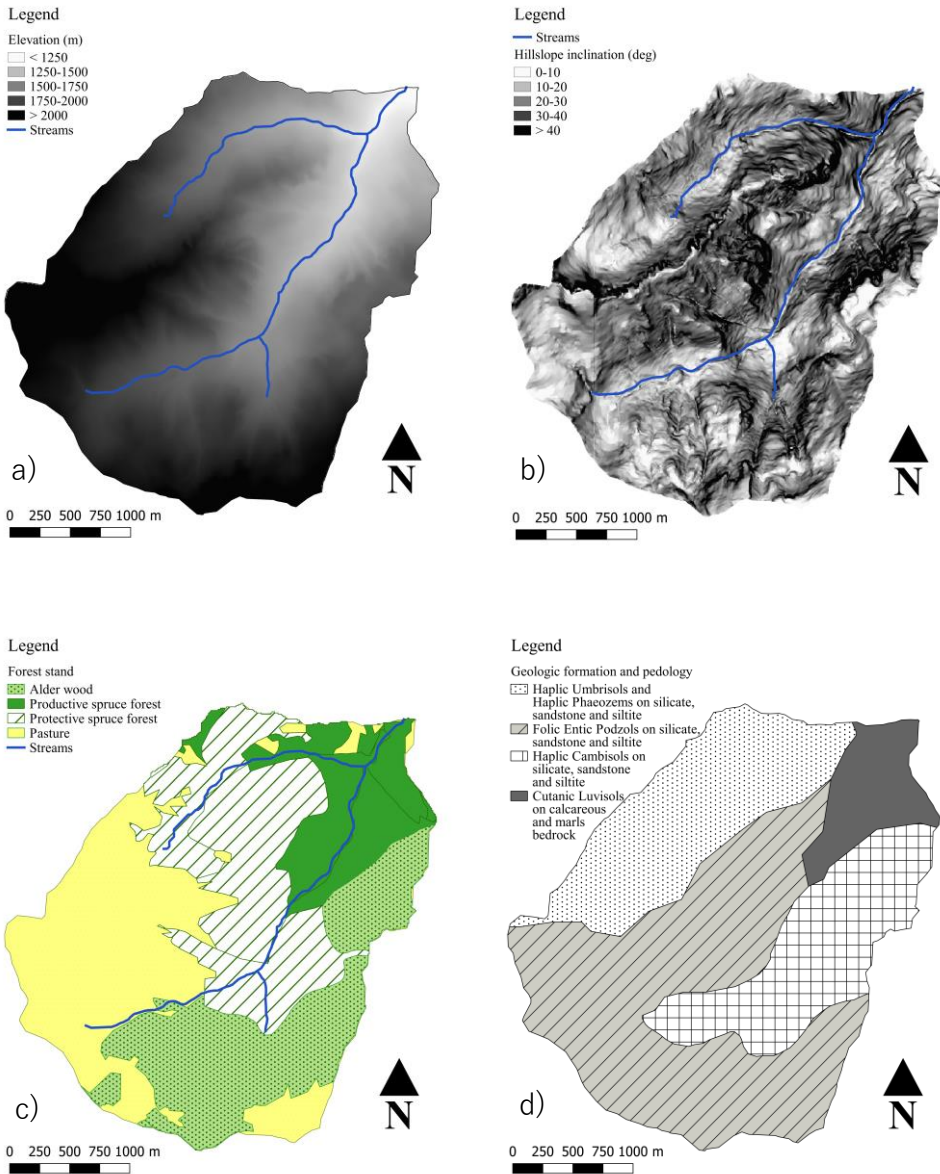


Figure 4.3. Thematic maps of Rio Davedino catchment: a) digital elevation model with 5 x 5 m resolution; b) hillslope inclination; c) land use map; and d) geological map.

4.2.4 Landslide inventory

The study area is prone to shallow landslides and debris flows especially during late spring and autumn. Since 2006, the Italian National Institute for Environmental Protection and Research (ISPRA) has been registering all landslide events in the Italian Landslide Inventory (IFFI). In the study area, almost 90% of landslides are classified as debris flows, which begin as rigid or translational shallow landslides that liquefy (Iverson et al., 1997). The inventory registered all landslide bodies as polygons, which bound the whole landslide perimeter through the analysis of post-event aerial photographs and field surveys. The collected GIS information does not represent the source areas of the landslides, which are subsequently extracted through a post-processing procedure. The procedure is a semi-automatic method proposed and used by some authors (e.g. Galve et al., 2015; Persichillo et al., 2016). The source areas automatically extracted were compared with those obtained by a visual interpretation of orthophotos, aerial and satellite images. In addition, landslide size was measured for all registered events following the method proposed by Orris and Williams (1984). The method consists of measuring reproducible short and long axes drawing a rectangle tangent to the landslide polygons.

4.3 Results

4.3.1 Statistical analysis of landslide inventory

A statistical analysis of landslide sizes was performed to determine the typical topographic characteristics and dimensions. 132 landslides were registered in the considered catchment and classified as shallow translational and rotational landslides, and debris flows. Although they were uniformly located within the entire catchment, the hillslopes facing northwest, east and southeast are more prone to soil movements, as shown in **Figure 4.4a**. Average hillslope inclination values range from 8.5 to 56 degrees with a median value of 39 (**Figure 4.4b**). The landslide area varied from 12 to 25,000 m² with a median of 6,437 m². Only 10 large landslides, around 7.5%, exceeded 25,000 m². Moreover, the width ranged from 2.5 to 151.9 m, while length varied from 16 to 405.4 m. The median values were 35.4 and 110.8 m for width and length, respectively. Boxplots in **Figure 4.5** show the distribution of landslide areas, widths and lengths. To consider the size of landslides as stochastic input parameters for the probabilistic model, we fitted the data with a probabilistic distribution function (**Figure 4.6**). The best fitting was obtained with the two-parameter Weibull function:

$$f(x|a,b) = \frac{b}{a} \left(\frac{x}{a}\right)^{b-1} \exp\left[-\left(\frac{x}{a}\right)^b\right] \quad x \geq 0 \quad (4.3)$$

where a is the scale parameter ($a > 0$) and b is the shape parameter ($b > 0$). The coefficients a - b assumed the values of 54.06 - 1.72 and 183.24 - 2.05 respectively for w and l . The performance was evaluated with the coefficient of determination R^2 equal to 0.985 and 0.990 respectively for w and l .

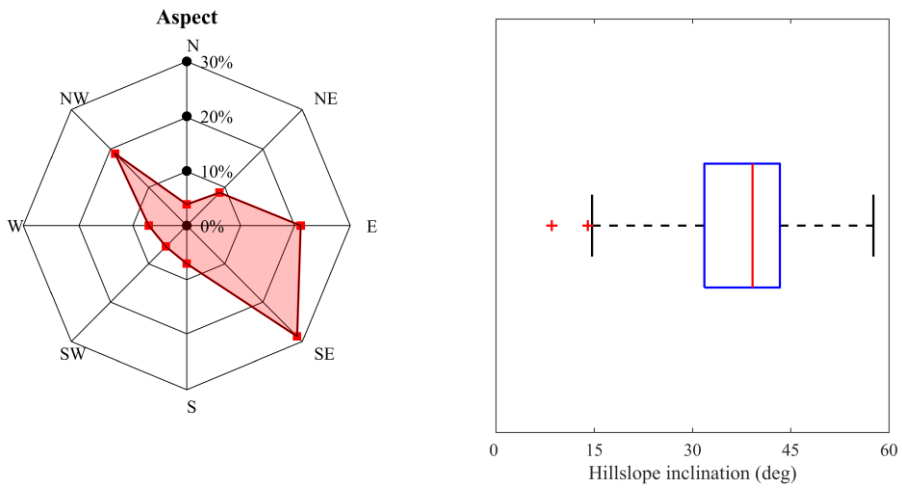


Figure 4.4. Distribution of (a) average topographic aspect and (b) average hillslope inclination analysing the landslide inventory.

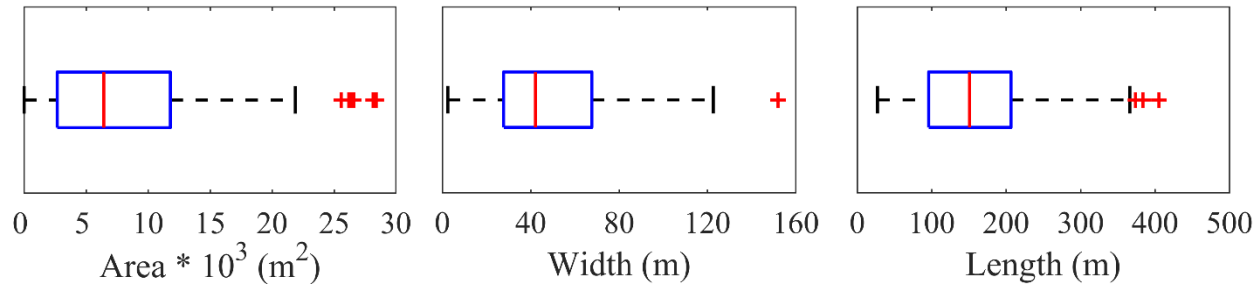


Figure 4.5. Distribution of landslide geometric sizes in three boxplots, for landslide area, approximated width and length.

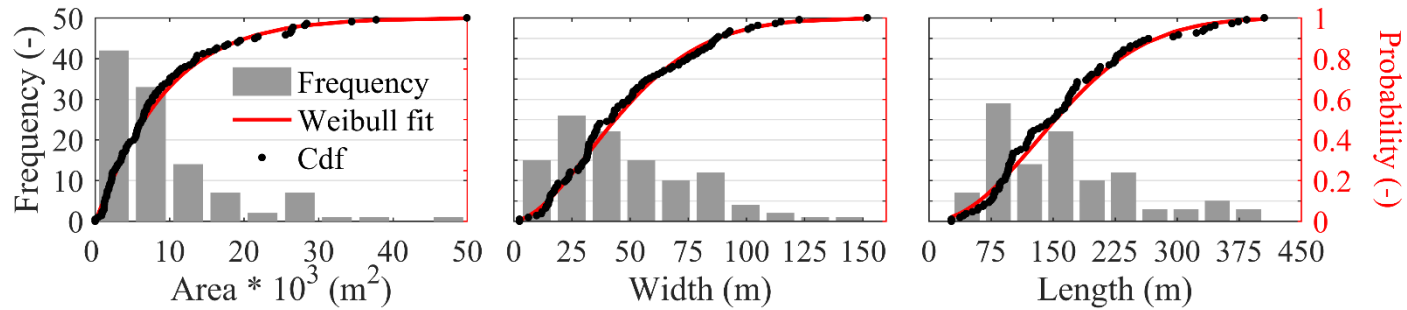


Figure 4.6. Histograms and Weibull fitting curves of geometric parameters w and l .

4.3.2 Application and performance of the slope stability model

As mentioned in section 4.2.1, PRIMULA interacts with the sub-model PROB-RR that simulates the spatial distribution of roots and then quantifies the root reinforcement at a spatially distributed scale according to the forest characteristics. In order to obtain reliable values of this parameter, Prob-RR (described in section 2.2.6) was calibrated using literature data of root distributions observed in a subalpine spruce forest (Schwarz et al., 2012a) and the tensile resistance of Norway spruce and European larch roots in the Alpine region studied by many authors (e.g. Chiaradia et al., 2016; Vergani et al., 2012, 2014b). In addition, forest stand characteristics were collected for the entire catchment from forest management plans and field surveys. Rio Davedino catchment was divided into three areas according to the forest function and dominant species, as shown in Figure 4.3c and Table 4.2.

PRIMULA was run 1,000 times using the probability distribution function of each input parameter. The result is a landslide hazard map in terms of probability of failure $Pr[FS < 1]$, as shown in Figure 4.7. It is clearly possible to identify two areas with higher probability of failure. The largest is located between the streams where the hillslope inclination ranges from 30 and 40 degrees. The second is in the eastern part of the catchment and is in accordance with the landslide inventory that registered eight large landslides covering approximately 6,000 m² each. In general, the model classified about 35% of the study area with a probability of failure greater than 0.75 and about 16% greater than 0.90. These results showed the areas covered by woodland and forest that have a significant landslide hazard.

In terms of performance, the model showed a robust accuracy. There was a slight overestimation of the probability of failure highlighted by the true positive and true negative rate values (0.839 and 0.479, respectively), but the other indexes confirmed a good accuracy ($MSR = 0.659$, $WMSR = 0.719$ and $I_{tot} = 0.609$). In addition, the ROC curve showed a very good model

performance, as shown in Figure 4.8 (AUC=0.832), especially given that no calibration on the landslide inventory was performed.

Table 4.2. Forest stand characteristics reported in the forest management map (Figure 4.4c) including area (in ha), forest function, forest management, density (in tree ha⁻¹), tree diameter at breast height (in m), tree height (in m), stand age (in years), dominant and secondary species.

Code	Pa	Pa*	Av
Area (ha)	1.25	2.46	2.18
Forest function	Productive	Protective	Protective
Forest management	High forest	High forest	No management
Density (tree/ha)	200-400	50-200	50
DBH (m)	0.34	0.32	0.10
Tree height (m)	29.57	25.00	5.00
Age (years)	140	165	40
Dominant species	Norway spruce	Norway spruce	Green alder
Secondary species	European larch	European larch	Large-leaved willow

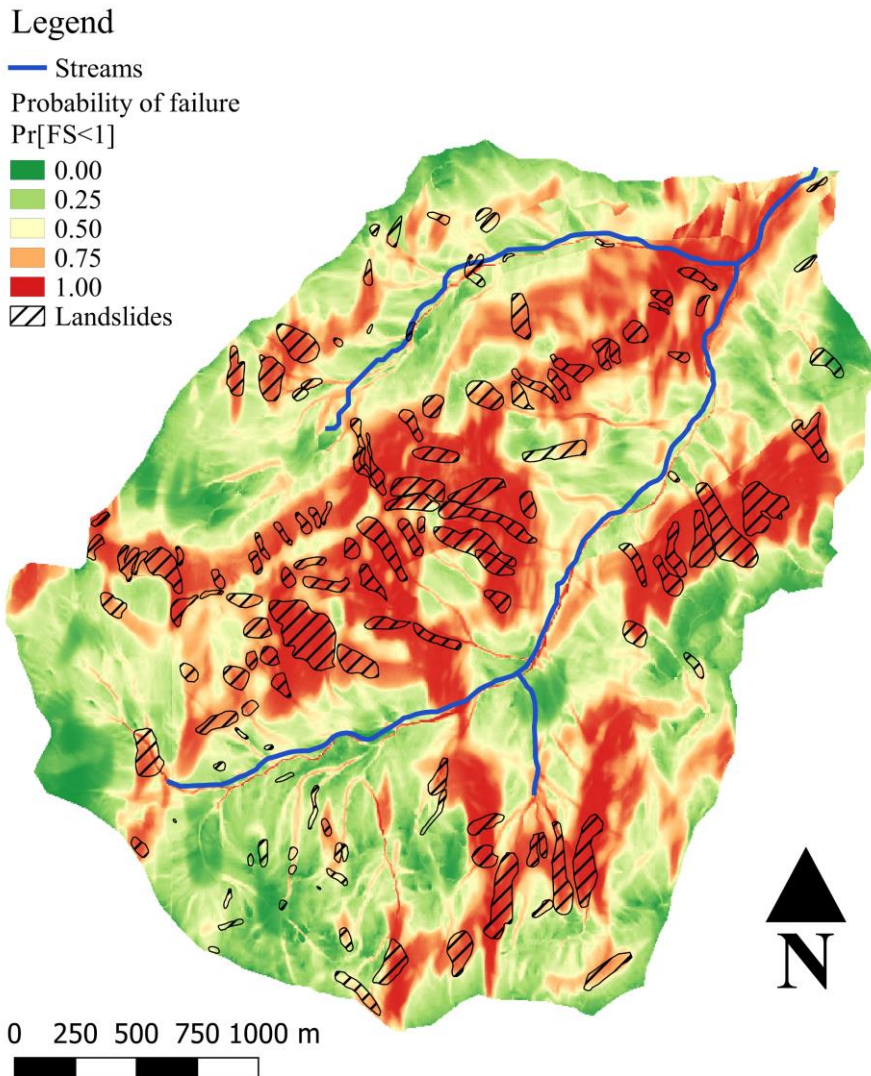


Figure 4.7. Probabilistic landslide hazard map with the landslide inventory. The result was obtained by applying MAP-SLAN: the model identifies most landslide areas.

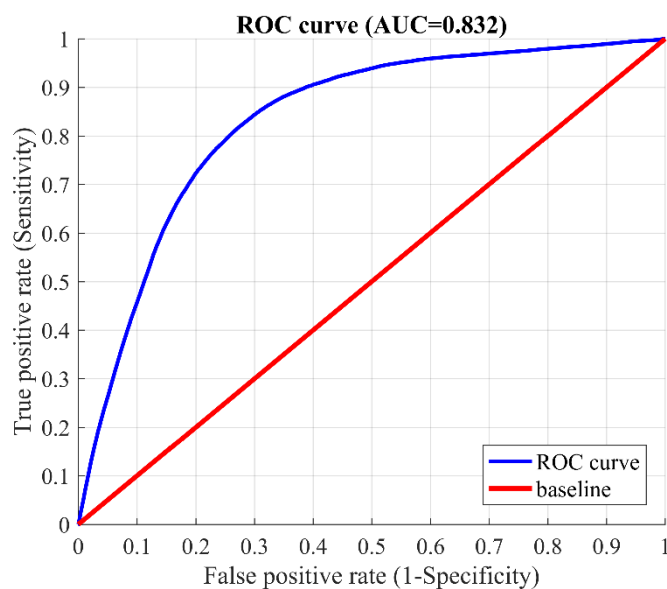


Figure 4.8. Receiver operating characteristic (ROC) curve for PRIMULA. The AUC is a quantitative index for model performance and corresponds to the area under the ROC curve. In the study case, it assumed a value of 0.832 indicating an excellent performance.

4.3.3 LW recruitment from hillslopes

Combining the landslide hazard map obtained by PRIMULA (Figure 4.7) and the forest map (Figure 4.9), we estimated the LW volume potentially produced by unstable hillslopes, according to its $cP(P^*)$ (Figure 4.10a and c). Repeating this operation for different P^* , we obtained a curve that relates the potential LW volume released by hillslopes with a compound probability of landslide occurrence, as shown in Figure 4.11. The graph indicates a susceptibility curve of the potential LW released by hillslopes. The maximum value of potential LW volume corresponds to the lowest value of cP and represents the most hazardous condition assuming that all woody material on the hillslopes is mobilised at the same time (except for those areas that result as unconditionally stable); this amount is $93,875 \text{ m}^3$ ($7,449 \text{ m}^3/\text{km}$). The minimum recruitable value of LW volume corresponds to the highest value of cP and represents the least conservative condition; this amount is

639 m³ (0.2 m³/km). The curve shows a sharp decreasing of LW volume with cP value in the 0.00-0.01 interval, and then a smoother decline. It can also be observed that values greater than 10,000 m³ are associated to a very low cP (less than 0.006) corresponding to a recurrence time of more than 150 years. It is also possible to evaluate the LW volume associated with a recurrence time corresponding to the time-span of the Italian landslide inventory, i.e. approximately 30-50 years. This value is around 8,000 m³. To compare the results, we estimated the LW volume that has been potentially mobilised by soil instabilities overlaying the forest map and landslide inventory map. Considering only the triggering area, the estimated LW volume resulted as 7,702 m³, which corresponds to a value of cP of 0.03 (Figure 4.11) that can be associated with a recurrence time of about 30 years.

In order to account for the processes responsible for LW storage on hillslopes and unchanneled valleys and obtain the LW volume recruited from hillslopes, the decay function described in section 2.2 was applied to the estimated LW volume mobilised by landslides (Figure 4.10b and d). The result is a curve of LW recruited from hillslopes representing a susceptibility curve of the potential recruitable LW (Figure 4.11). The maximum value is 5,986 m³, while the minimum is around 1 m³.

The curve is very similar to the one representing the LW volume released by hillslopes. The ratio between LW recruited and LW released by hillslopes is constant for almost the entire curve and equal to 16%.

Moreover, the LW stored in the channel network measured in field surveys by Rigon et al. (2012) is 838 m³ (106 m³/ha of channel area and 65.9 m³/km). This value corresponds to 11% of the LW volume mobilised by registered landslides and a value of the susceptibility curve corresponding to a cP of 0.13 (rounding off a recurrence time of 8 years).

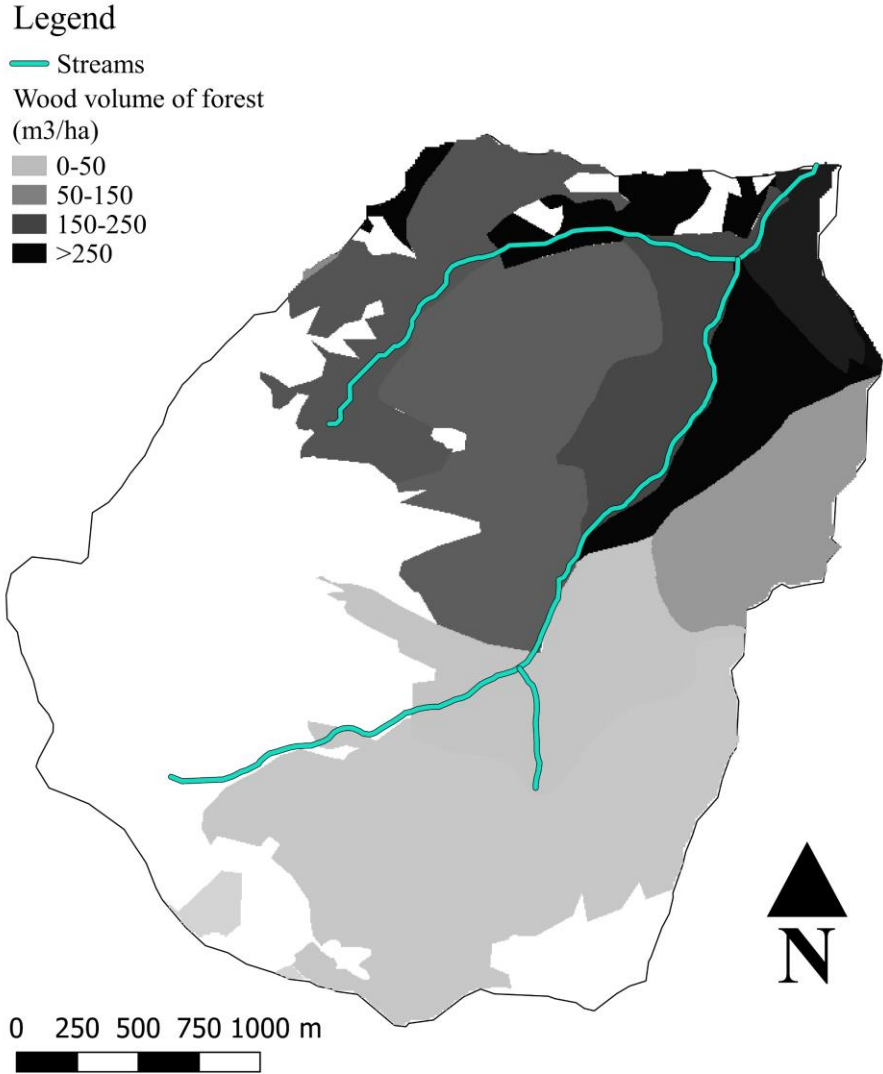


Figure 4.9. Map of forest stand volume (in m³ ha⁻¹).

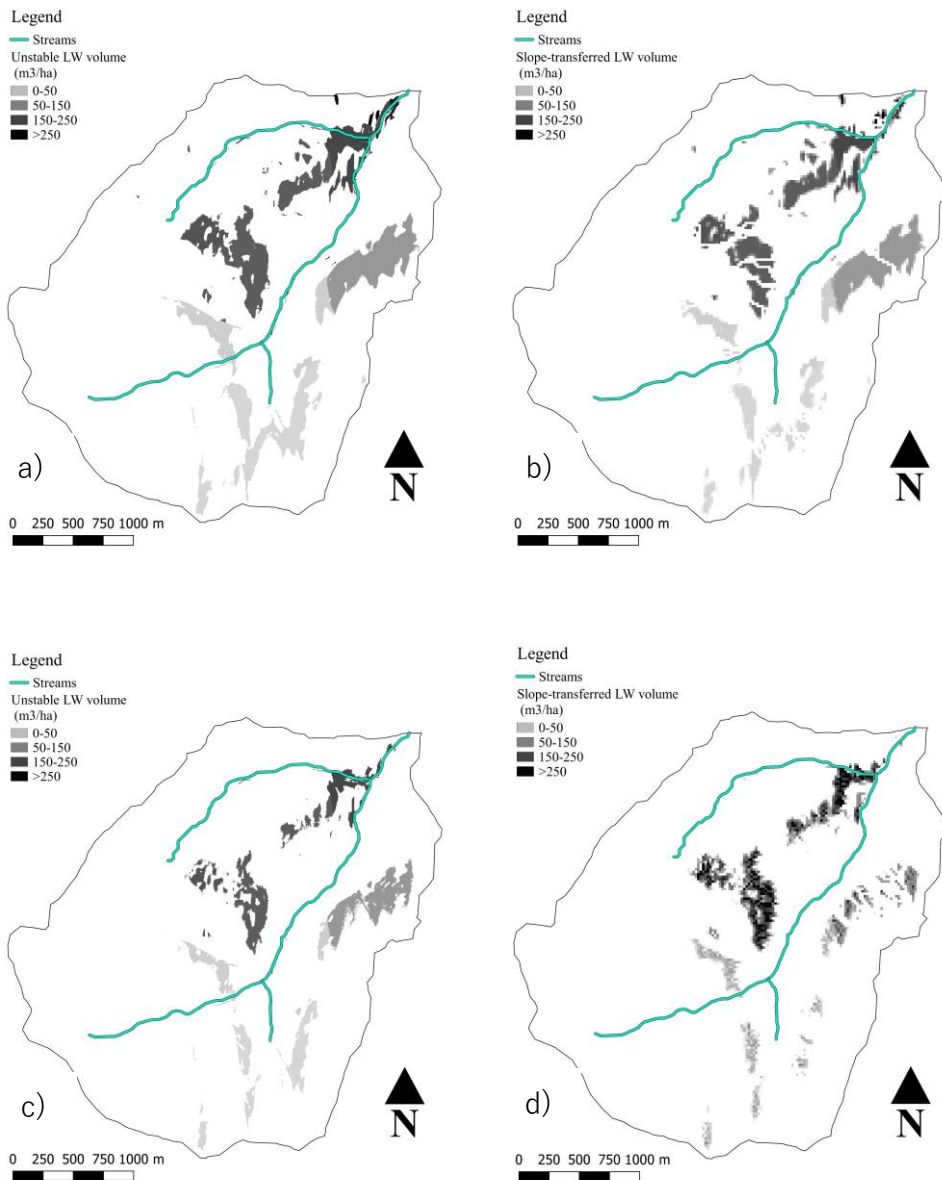


Figure 4.10. a) and b) Maps of potentially unstable LW volume and potential LW recruitment volume (in $m^3 ha^{-1}$) for $cP(P^*=0.90)$, respectively; c) and d) for $cP(P^*=0.95)$.

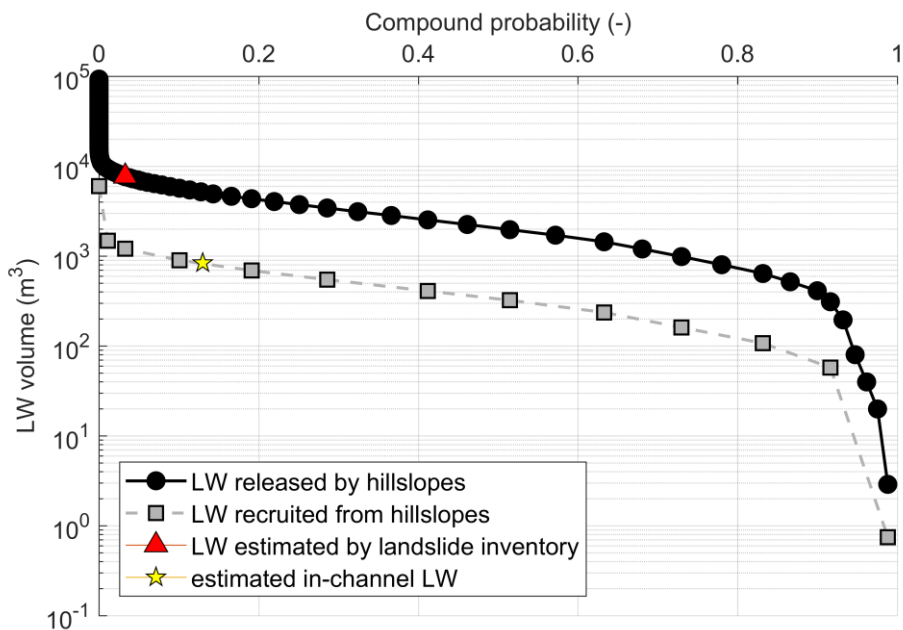


Figure 4.11. LW susceptibility curves of LW volumes released by landslides and recruited LW volume (solid line - black circles and dashed line - grey squares, respectively); the red triangle represents the LW volume estimated by inventoried landslides and the yellow star indicates in-channel LW volume estimated in field surveys by Rigon et al. (2012).

4.4 Discussion

4.4.1 Statistical analysis on landslide inventory

The statistical analysis of the landslide inventory plays a fundamental role in determining the main characteristics of mass movements. Such information is important not only to locate the most susceptible areas prone to instabilities within the catchment but also to identify the most common triggering mechanisms of slope failures. In the study area, the landslide inventory registered almost all events as debris flows. These mass movements begin as a rigid translational and/or rotational slide that involves the shallower soil layer and then liquefies and moves downslope (Iverson et al., 1997; Lancaster et al., 2003). According to this definition, PRIMULA correctly models the instability phenomena assuming the potential instabilities as a rigid block (Milledge et al., 2014). Moreover, debris flows from a forested mountain watershed strongly affect stream morphology (Benda et al., 2003a) and aquatic and terrestrial habitats (Lancaster et al., 2003) and typically contain a large fraction of woody material (Lancaster et al., 2003; Montgomery et al., 2003).

In addition, assuming that the soil-bedrock boundary defines the failure plane in shallow debris flows (Gabet and Mudd, 2006), it has been possible to estimate the volume of soil mass that affects both the runout distance and forested area involved (Denlinger and Iverson, 2001; Hungr, 1995; Iverson et al., 1998; Iverson and Denlinger, 2001; O'Brien and Julien, 1988). In the study case, the soil volume varied from 15 m³ to 50,000 m³ with a median of 6,658.4 m³. These values are comparable with debris flow inventories published in the literature (Table 4.3). Concerning the size of the landslides, the median values of length and width were 34.5 m and 110.8 m, respectively, which are much larger than those reported in the literature. Indeed, most common maximum values are 15 m for width and 40 m for length, as observed by several authors (Montgomery, 2001; Rice et al., 1969; Rickli and Graf, 2009; Warburton et al., 2008). We also observed that both width and length

exceeded the soil depth and that the length always exceeded the width as is commonly acknowledged in the literature (e.g. Gabet and Dunne, 2002; Larsen et al., 2010; Marchesini et al., 2009; Milledge et al., 2014). There is instead no conclusive explanation as to why the hillslopes exposed to the northwest, east and southeast are more prone to landslide hazard, despite the hillslope inclinations being comparable and within the range observed most commonly at sites where debris flows mobilise from landslides (20-60° ; Table 4.3).

Table 4.3. Data on debris flow characteristics in the scientific literature: minimum and maximum values of mass soil volume (V_{min} and V_{max}) in m^3 and hillslope inclination (θ_{min} and θ_{max}) in degrees.

V_{min}	V_{max}	θ_{min}	θ_{max}	Surveys	Location	References
4,000	60,000	12.0	40.0	11	Swiss Alps, Switzerland	Zimmermann (1990)
2,000	214,000	12.9	54.1	24	Swiss Alps, Switzerland	Rickenmann and Sheidl (2013)
7,000	136,000	14.0	31.6	6	Southern Rocky Mountains of British Columbia, Canada	Jackson et al. (1989)
214	14,800	-	-	26	Kamikamihori Valley, Japan	Okuda and Suwa (1984)
14	6,484	21.0	44.0	34	Western Uluguru Mountains, Tanzania	Temple and Rapp (1972)
60	39,630	24.0	48.0	49	Southwestern British Columbia, Canada	O'Loughlin (1972)
-	-	25.0	45.0	65	Hong Kong	Lumb (1975)

4.4.2 LW mobilised and recruited by hillslopes

The potential LW released by hillslopes has been obtained from the application of a slope stability analysis (PRIMULA), which is able to locate potential source areas of LW and the related failure probability. The slope stability model also takes into account the reinforcement effect of the forest and provides a probability of slope failure.

The slope stability analysis conducted provided a robust and reliable simulation of unstable areas in the study case and reliable values of LW potentially released by landslides. The performance of PRIMULA combined with its sub-models, as reported in section 3.2, showed that AUC, which is a measure of observation-prediction fit in spatial distribution modelling (Carrara et al., 2008; Frattini et al., 2010; Raia et al., 2014; Vorpahl et al., 2012; Yilmaz, 2009), corresponds to an excellent prediction (0.832) according to many authors (e.g. Cervi et al., 2010; Hosmer and Lemeshow, 2000; Pradhan, 2013; Zizioli et al., 2013). Similarly, the other performance indexes confirmed the positive goodness-of-fit: $MSR = 0.659$, $WMSR = 0.719$ and $I_{tot} = 0.609$.

On such a basis, the susceptibility curve of the potential LW released from hillslopes (Figure 4.11) can be considered highly reliable and robust, as confirmed by the LW volume estimated from the analysis of inventoried landslides. Such a value, in fact, corresponds to a probability of 0.03; this means about 30 years that can be considered coherent with the time-span in which most of the inventoried landslides occurred.

Unfortunately, there are not many studies for comparing the results, in terms of LW volume at hillslope level, with other sites because only the total recruitment volume is often reported or data refer to absolute values (m^3) that are difficult to compare. Lucia et al. (2015b) and Comiti et al. (2016) for two watersheds and their sub-catchment in Central Italy reported values of LW volume recruitment due to landslides varying between 0 and $971 m^3/km$. For Gravegnola catchments, the median value was $131 m^3/km \pm 223 m^3/km$, whereas for Pogliaschina catchment the median value was $0 m^3/km \pm 129$

m³/km. Hassan et al. (2016) for two watersheds and their sub-catchment on Graham Island (British Columbia, Canada) estimated LW volumes from landslides between 0 and about 190 m³/year.

The values obtained in this study varied between 0 and 751 m³/km and between 0 and 313 m³/year, for a probability of 0.988 and 0.011, respectively and are comparable with those presented by Lucia et al. (2015b) and partially with those by Hassan et al. (2016). In the first case, we have a comparable wood volume on the hillslopes (150-250 m³/ha) and a much longer recurrence time (500 years). In the second, the wood volume on hillslopes was much higher and recurrence time comparable (100 years). In the latter case, it must also be noted that trees were much older than in European forests (255-319 years), suggesting that although old forests could potentially release large amounts of LW, their reinforcement effect reduces the amount available. This emphasises the importance of adopting a slope stability model able to account for slope reinforcement due to vegetation and its time dynamics.

To appreciate if the results obtained by the proposed multi-dimensional approach are significantly better than less sophisticated methods, we also conducted a slope stability analysis with a limit equilibrium approach. We adopted a semi-three dimensional method, semi3D, proposed by Casadei et al. (2003a) and Chiaradia et al. (2016), which evaluated the factor of safety, FS , as follows:

$$FS = \frac{c_s + c_{rb} + \frac{A_{lat}}{A_{bas}} c_s + \frac{A_{lat}}{A_{bas}} c_{rl} + [(D\gamma_s - D_w\gamma_w + q_0) \cos \alpha] \tan \phi'}{(D\gamma_s + D_w\gamma_{sat} + q_0) \sin \alpha} \quad (4.4)$$

where c_s is the soil cohesion (in Pa). c_{rb} and c_{rl} are the contributions of plant roots to slope stability (in Pa), A_{lat} and A_{bas} are the lateral and basal surfaces (in m²), D is the average depth of the sliding surface (in m), D_w is the average height of seepage with respect to the sliding surface (in m), γ_s , γ_w and γ_{sat} are the unit weights of dry soil, water and saturated soil, respectively (in N

m^{-3}), q_0 is the tree surcharge per unit area (in N m^{-2}), α is the hillslope inclination (in rad) and ϕ' is the effective friction angle (in rad).

Semi3-D is not a standard in infinite slope model applications, but it is the most simplified model that can be adopted to include the spatial distribution of reinforcement induced by the presence of vegetation on hillslopes acting on both the basal and lateral landslide surfaces (Casadei et al., 2003b; Chiaradia et al., 2016).

As done when applying PRIMULA, an independent and random set of possible values of the input parameters was assumed. In addition, we set: (i) c'_{rb} as negligible; (ii) γ_{sat} was estimated by considering that all voids were completely filled by water and correspond to 40% of the total volume (Hammond et al., 1992); (iii) $q_0 = 275 \text{ N m}^{-2}$ for the forested area (Del Favero et al., 2000) and negligible for the rest of the catchment.

The goodness-of-fit was evaluated with the same performance indices adopted for PRIMULA and all resulted in slightly worse values: $\text{AUC} = 0.795$, $\text{MSR} = 0.602$, $\text{WMSR} = 0.700$ and $I_{\text{tot}} = 0.574$.

We then quantified the value of LW recruitment for different cP in the same way as already done for the results obtained by PRIMULA. While the minimum and maximum LW volume are substantially the same, the susceptibility curve is slightly different, except for very low probability values (Figure 4.12). The susceptibility curve obtained by PRIMULA produced a lower LW volume estimation than the infinite slope approach for cP greater than 0.91 and higher for the other probability values, until values lower than 0.01. In addition, the LW volume estimated from inventoried landslides matches the value for a probability value of 0.019, which corresponds to a recurrence time of more than 50 years that is longer than expected.

The multidimensional approach of PRIMULA thus proved to be slightly better than simpler approaches such as the infinite slope, which, however, provided LW estimations that are not entirely different in the present case.

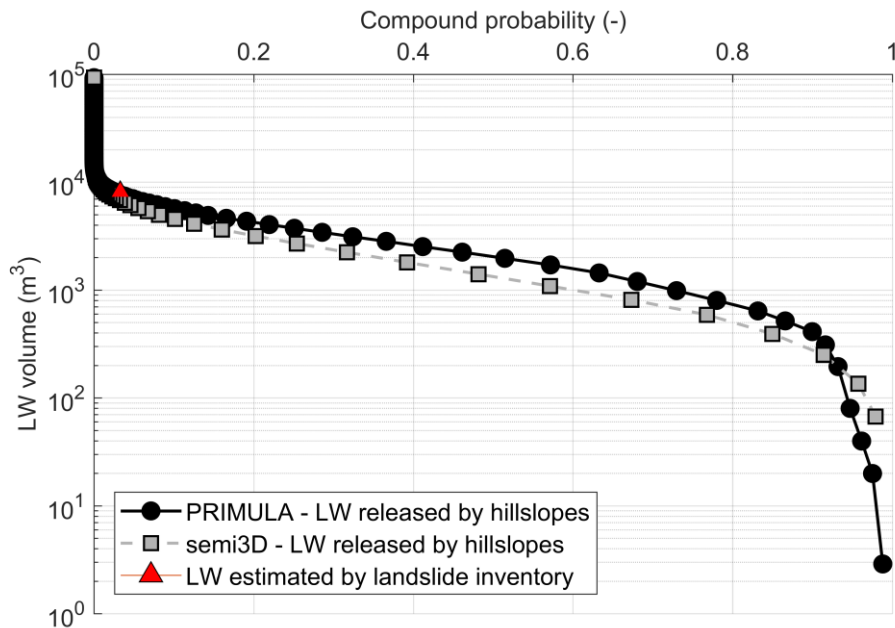


Figure 4.12. LW susceptibility curves of LW volumes released by landslides obtained estimating unstable areas by PRIMULA (solid line and black circles), by the infinite slope approach (dashed line and grey squares) and by inventoried landslides (red triangle).

The LW recruited from hillslopes obtained in this study by applying a decay function to LW mobilised by landslides, resulted as being a small part of what could potentially be released (16% for most of the probability values). This is in partial agreement with the observations of Amorfini et al. (2002) reported by Comiti et al. (2016), who observed that more than half of LW mobilised by landslides did not reach the channel network.

The studies distinguishing LW recruited from hillslopes with respect to other recruitment sources, and accounting for deposition on hillslopes and unchanneled valleys processes, are few. Benda et al. (2002) in the Van Duzen River watershed and its sub-catchments (California, USA) estimated, by in-channel surveys, LW volumes between 0 and 1,570 m³/km and between 0 and 12.2 m³/km year. In particular, they estimated 0 m³/km year in 12 sites out of 21, less than 4 m³/km year in 7 sites, 6 m³/km year and 12 m³/km year

in the other two. Investigating the same catchment as in this study, Rigon et al. (2012) estimated 54 m³/km, 133 m³/km and 351 m³/km for three different scenarios of landslide hazard, 1 (very likely, high frequency), 2 (medium probability and frequency), 3 (unlikely, low frequency), respectively. They also estimated in-channel LW recruitment by field survey and obtained 65.85 m³/km and 2.2 m³/km year.

In this study, the estimated values are in agreement with the variability reported by the above-mentioned authors: between 0-116 m³/km and 0-4 m³/km year, for probability values of 0.988 and 0.011, respectively.

The susceptibility curve of recruited LW volume is very similar to the curve obtained for the LW released from hillslopes: this suggests that the decay function just acts as scale factor, at least in the present case. Actually, the spatial distribution of the different forest types with respect to the channel network is rather uniform and the decay function factors (flow distance and upslope area) were not applied differently.

The outcomes of this study should be viewed under different perspectives:

- the probabilistic multidimensional approach developed by PRIMULA and the physically-based inclusion of the role of vegetation in the stability analysis represents a reliable and robust tool to study LW recruitment mechanisms in small headwater and forested catchments. This can be considered a significant improvement for a more accurate and precise prediction of LW recruitment from landslide-prone hillslopes, which is still considered very challenging and subject to great uncertainties (e.g. Comiti et al., 2016; Ruiz-Villanueva et al., 2016; Wohl et al., 2010). In addition, not many researches have so far been conducted on this topic (Wohl, 2017). Furthermore, the adopted approach and the good performance obtained without calibration, differently from statistical procedures and standard application of physically-based models (e.g. SHALSTAB in Mazzorana et al., 2009 and in Lucía et al., 2015a) allow it to be applied in different contexts, in particular, in areas with little available data.

- the possibility to estimate the sources of potential LW due to hillslope instabilities in a reliable way will allow the LW recruitment process from mass instabilities to be studied in more detail, distinguishing LW availability and its transport down hillslopes and unchanneled valleys, going beyond the empirical approach often adopted (Comiti et al., 2016; Kasprak et al., 2012; Mazzorana et al., 2009; Ruiz-Villanueva et al., 2014). Uncertainties in potential LW volume estimation, in fact, have hindered a clear description and validation of the transport process frequently based on empirical approaches (e.g. Rigon et al., 2012).

- the developed model establishes a link between LW recruitment volume and its probability, providing a robust and powerful tool both for fluvial geomorphologists/ecologists and civil/forest engineers, who traditionally have different perspectives (Comiti et al., 2016). The association of a probability of occurrence to a specific LW volume surely allows LW volume magnitude to be estimated and to calculate the residual hazard related to LW in small headwater catchments.

- the explicit inclusion of forest characteristics in the LW recruitment estimation makes it possible to simulate the consequences of different temporal and spatial forest management scenarios as well as to identify the most hazardous reaches for planning maintenance works or LW retention structures.

Finally, the method opens a new perspective of further refinement for estimating LW recruitment from hillslopes, both for estimation of the reinforcement exerted by vegetation and for tree volume quantification. The method could, in fact, easily incorporate a better description of the forest component obtained through supplementary field surveys, airborne LiDAR data and an allometry-based approach that are able to more accurately predict forest structure and tree-size distribution (Anfodillo et al., 2013; Eysn et al., 2015; Hyde et al., 2005, 2006).

4.5 Conclusions

It has long been noticed that colluvial processes such as landslides and debris flows are the main source of LW recruitment in lower-order mountain streams, although a quantitative approach is still lacking to distinguish the conditions where mass LW input dominates (Wohl, 2017). Focusing on mountainous-forested catchments of the European Alps where LW recruitment and dynamics must be managed to reduce flood hazards (Comiti et al., 2008b; Mazzorana et al., 2011b), we developed an innovative physically-based approach to reasonably predict recruitable LW with a defined probability of occurrence, able to account for forest characteristics. The procedure combines a multidimensional and probabilistic model to evaluate hillslope instabilities and topographic and forest stand characteristics for estimating the LW volume potentially produced by hillslopes. The model takes into account the wide spatial and, potentially, temporal variability of the input parameters required by the slope stability analysis and forest stand characteristics.

The model, applied to a small catchment in the Dolomites (Eastern Italian Alps) without any calibration and using readily available standard information (DEM, geological map, forest management map, etc.), proved to be satisfactory. The final model output is a susceptibility curve, which links the LW volume recruited from hillslopes with the expected probability of its occurrence. Such a result contributes filling some gaps in LW studies with particular reference to the quantitative prediction of LW recruitment within a given catchment in a spatially distributed form and for an assigned magnitude/probability. This will help in identifying the LW origin for single channel stretches and is fundamental for LW-related hazard estimations.

The slope stability model provided accurate performances, in terms of both unstable areas identification according to the landslide inventory (AUC = 0.832), and LW volume estimation in comparison with the LW volume produced by inventoried landslides (7,702 m³ corresponding to a recurrence

time of about 30 years in the susceptibility curve). Moreover, for a comparison, results were normalised for a unit length of channel and unit length of channel per year (0-751 m³/km and 0-25 m³/km year) and were in agreement with those reported in the few similar studies in the literature. In terms of LW recruited at the channel scale, results showed that most of the LW potentially mobilised by landslides does not reach the channel network (only about 16%). This agrees with the few data reported by other studies, as well as the data normalised for a unit length of channel and unit length of channel per year (0-116 m³/km and 0-4 m³/km year).

From a scientific perspective, the proposed model contributes to understanding and quantifying the transport process from hillslopes to channel networks. The possibility of comparing the estimation of in-channel LW volume (for instance by field surveys) with a reliable estimation of the potential LW volume released by hillslopes towards the same channel is, in fact, fundamental for studying the transport mechanisms down hillslopes and unchanneled incisions in more detail.

The results can be considered a useful tool for forest managers and technicians to map hazardous zones (Mazzorana et al., 2009, 2011b, 2011a; Rigon et al., 2012), to identify where LW retention structures should be installed (e.g. Schmocker and Weitbrecht, 2013), or where LW could be removed within river management programmes (Wohl et al., 2016). Indeed, modelling LW recruitment will be useful in planning a more sustainable forest management, for prioritizing watershed management interventions such as forest felling and wood retention structures, and for localizing and designing the most suitable sites for bioengineering works.

5 ROOT REINFORCEMENT IN A VINEYARD

Keywords:

Grapevine roots;

Root reinforcement;

Vineyards;

Slope stability;

Back analysis.

5.1 Introduction

Rainfall-induced shallow landslides are the most frequent gravitational processes affecting both cultivated steep terrains and natural slopes around the world (e.g. Beguería, 2006; Crosta et al., 2003; Glade, 2003; Lee and Pradhan, 2006; Mugagga et al., 2012; Reichenbach et al., 2014; Roering et al., 2003; Schmidt et al., 2001). These phenomena are typically translational slope failures of soil mantle or regolith a few metres thick (Hovius et al., 1997; Godt et al., 2009; Caine and Swanson, 2013). They are generally triggered by high-intensity and concentrated rainfall, which causes a sudden increase in soil water content, a decrease in soil suction and consequently a reduction of soil shear strength (Gasmo et al., 2000; Iverson, 2000; van Asch et al., 1999).

These phenomena frequently affect vineyards, typically located on sloping terrains, and involve anthropogenic soils. The consequences are a partial or complete destruction of grapevine fields, local structures and infrastructure and thus huge economic damages and more general impacts on the environment. Landslides are a serious threat in the context of European vineyards, in particular where grapevines have been cultivated for a long time, as in Germany, (Grunert, 2009), Slovenia (Komac and Zorn, 2009), Romania (Margarint et al., 2013), Spain (Ramos et al., 2007), Portugal (Pereira et al., 2012), France (Marre et al., 1997; Van Den Eeckhaut et al., 2010) and especially in Italy (Blahut et al., 2014; Bordoni et al., 2016; Camera et al., 2015; Cevasco et al., 2014; Fonte and Masciocco, 2009; Meisina and Scarabelli, 2007; Zizioli et al., 2013). Moreover, landslide risk is increasing in those areas where vineyards have been introduced more recently and have replaced natural vegetation (Guthey and Whiteman, 2009; Opperman et al., 2005). Indeed, the modifications of land use and agricultural practices have important effects on hydrological processes and on the mechanical structure of the soil (Greenway, 1987; Reichenbach et al., 2014; Schmidt et al., 2001).

Despite the risk for human safety, the direct and indirect economic loss, the impact on natural landscapes, and the social impact on local communities in terms of land and settlement abandonment, few studies have been carried out to date to highlight the role of grapevines on slope stability.

The beneficial effects of vegetation in preventing slope instabilities have been demonstrated by several studies (see section 1.1.3), and it is now clear that plants positively influence the triggering mechanisms via root strength, root anchorage, and evapotranspiration (e.g. Sidle and Bogaard, 2016). In particular, since the pioneering work of Endo and Tsuruta (1969), considerable attention has been focused on the quantification of the mechanical contribution of root reinforcement to soil shear strength (Bischetti et al., 2009; Fan and Su, 2008; Schwarz et al., 2010a; Wu et al., 1979) and the value of such reinforcement for different vegetation species growing in different environments. However, most of such studies have considered natural and/or forest species and sometimes pastures.

The aim of this study was to increase our knowledge of the role and limits of grapevine plants in stabilizing slopes in comparison with natural vegetation. In particular, drawing from the results obtained by Bordoni et al. (2016), we evaluated the mechanical root reinforcement of grapevine plants as a function of their size and spatial distribution along a cultivated hillslope in a typical vineyard context in Northern Italy (Oltrepo' Pavese, Lombardy). The results obtained by modelling the root reinforcement contribution according to the current state of knowledge were compared with those obtained by carrying out a back analysis on landslides that had occurred in steep-slope vineyards.

Indeed, back-analysis provides reliable estimates of the additional rooted-soil reinforcement necessary to stabilize the selected landslide area; however, it is not able to explain the spatial variability or the driving mechanisms occurring between plants and soil. On the other hand, modelling the root reinforcement at specific experimental sites by carrying out detailed field and laboratory measurements provides results liable to a certain degree

of generalization. In particular, modelling allows consideration of the wide variability and uncertainty linked to the mechanical properties and the spatial distribution of the roots, which remain a great challenge (Giadrossich et al., 2016; Loades et al., 2010). Moreover, such variability could be exaggerated in the case of vineyards by a great number of factors connected with their agricultural practices. In fact, the literature in the field of viticulture shows that a balance exists between the top growth and root growth in grapevines and that it is affected by cultivation practices (de Herralde et al., 2010; Saayman and Van Huyssteen, 1980; Southey, 1992; Van Zyl and Van Huyssteen, 1980). Additionally, some studies have demonstrated that grapevine root distribution can be affected by soil physical properties (Conradie, 1983), vine spacing (Archer and Strauss, 1985; Hunter, 1998), rootstock (Morano and Kliewer, 1994) and irrigation (Araujo et al., 1995).

In this study, we proposed a model that combines two sub-models: the first sub-model simulates the density of the roots in different diameter classes as a function of distance from the stem (Root Distribution Model, RDM; Ammer and Wagner, 2005; Moroni et al., 2003; Roering et al., 2003), whereas the second calculates the root reinforcement in terms of stress-strain behaviour (Root Bundle Model, RBMw, described in detail in section 1.2.1; Schwarz et al., 2013). In this way, guidelines for designing new vineyards (with plant spacing and density as a function of soil properties, steepness and the climatic conditions of sites) can be provided that consider landslide prevention in addition to wine-growing potential. This will also be useful to support decision-makers in conceiving rural and territorial sustainable development, such as land management practices, land use change, and landscapes.

5.2 Materials and methods

5.2.1 Quantification of root reinforcement

Quantification of root reinforcement has been developed and conceptualized through different methods: (i) direct shear tests in the field (e.g. Abe and Iwamoto, 1986; Docker and Hubble, 2008; Endo and Tsuruta, 1969; Wu and Watson, 1998) or pull-out tests in the field (e.g. Anderson et al., 1989; Mickovski et al., 2007; Schwarz et al., 2010c), (ii) direct shear tests in the laboratory (e.g. Abe and Ziemer, 1991; Mickovski et al., 2009; Waldron and Dakessian, 1981) or centrifuge test in the laboratory (Sonnenberg et al., 2007), (iii) back analysis (e.g. Gray and Megahan, 1981; O'Loughlin, 1974; Schwarz et al., 2010a; Swanston, 1970), and (iv) root reinforcement modelling (Abernethy and Rutherford, 2001; Cislighi et al., 2017; Schmidt et al., 2001; Schwarz et al., 2012a; Wu, 1984).

In general, field measurements provide a good reference, but they are very time consuming, and extensive data may be impractical to obtain (Schmidt et al., 2001). For example, direct shear tests are extremely burdensome and can only be carried out for shallower soil layers. Additionally, boundary conditions cannot be controlled, and determining the spatial variability of root reinforcement is unworkable. On the other hand, laboratory tests are suitable for studying physical processes under different boundary conditions, but they are affected by scaling problems. Back analyses on collapsed slopes have been adopted in several cases to obtain realistic limit values for the mechanical effects of root systems on slope stability (e.g. Casadei et al., 2003a; Montgomery et al., 2000; Schwarz et al., 2010a; Sidle and Ochiai, 2006). The results have provided important information about the range of root reinforcement values provided by different species or plant associations, although only in very specific contexts in terms of climate, soil and hydrologic combinations. Additionally, the reliability of such values depends on the data availability and the soundness of the assumptions involved in the slope stability model. Finally, modelling based on field and laboratory results (e.g.

Mao et al., 2012; Thomas and Pollen-Bankhead, 2010) consists of a general approach, able to provide the mechanical reinforcement because of root systems in several different sites and conditions. Such models generally consider: (i) the mechanical properties of single roots (tensile strength or resistance) with different diameters measured in the field or in the laboratory (e.g. Bischetti et al., 2005; De Baets et al., 2008; Hales et al., 2009) and (ii) the density of roots of different diameters, possibly at various depths and distances from stems obtained by digging trenches (Bohm, 1979) or core sampling (Roberts, 1976).

5.2.2 Modelling root density by a Root Distribution Model and root reinforcement by the Root Bundle Model

A Root Distribution Model, RDM, predicts the spatial distribution of root diameters (ϕ), which is strongly correlated with the stem diameter of the plant (θ) and the distance from the plant stem (d) (Ammer and Wagner, 2005; Bauhus and Bartsch, 1996; Brockway and Outcalt, 1998; Drexhage and Colin, 2001). In this study, we adopted the RDM introduced by Schwarz et al. (2010b) and further developed by Giadrossich et al. (2016). The model is based on the static fractal branching model (Tobin et al., 2007) and pipe theory (Shinozaki et al., 1964a, 1964b). First, it provides the density of fine roots with a diameter less than 1.5 mm, $\rho_{FR}(\theta, d)$, as a function of the plant stem (θ in m) and the distance from the stem (d in m) via the following equation:

$$\rho_{FR}(\theta, d) = \left(\frac{N_{FR}}{d_{\max} 2 \pi d} \right) \left(\frac{d_{\max} - d}{d_{\max}} \right) \quad d < d_{\max} \quad (5.1)$$

where N_{FR} is the total number of fine roots (diameter less than 1.5 mm), which is strongly correlated with θ through the pipe theory coefficient μ (Osawa and Allen, 1993) (in roots/m², equation 5.2), and d_{\max} (in m) is the maximum distance from the stem that the roots can reach. Such length is directly proportional to θ through a dimensionless proportionality constant (ψ)

empirically estimated by Roering et al. (2003) and Ammer and Wagner (2005) (equation 5.3).

$$N_{FR}(\Theta) = \mu \frac{\Theta^2 \pi}{4} \quad (5.2)$$

$$d_{\max}(\Theta) = \psi \Theta \quad (5.3)$$

Moreover, the RDM estimates the density of each diameter class of roots, $\rho_{CR}(\phi_i, \Theta, d)$, greater than 1.5 mm as a function of the considered root diameter (ϕ_i), the size of trees (Θ) and distance (d) via the following equation:

$$\rho_{CR}(\phi_i, \Theta, d) = \rho_{FR} \left(\frac{\ln(1 + \phi_{\max}) - \ln(1 + \phi_i)}{\ln(1 + \phi_{\max})} \right) \left(\frac{\phi_i}{\phi_0} \right)^\gamma \quad (5.4)$$

where γ is a dimensionless constant accounting for the decrease in the root density, ϕ_0 is the reference diameter, which assumes the value of 1 mm, and ϕ_{\max} is the maximum root diameter (in mm). ϕ_{\max} is, in turn, a function of the size of trees (Θ) and the distance (d) as shown in equations 5.3 and 5.5.

$$\phi_{\max}(\Theta, d) = \frac{d_{\max} - d}{\eta} \quad (5.5)$$

where η is a dimensionless self-similarity coefficient.

The empirical coefficients μ , ψ , η and γ need to be calibrated to minimize the differences between the observed and simulated root distribution data (Giadrossich et al., 2016; Moroni et al., 2003; Schwarz et al., 2010b; Vergani et al., 2016; Waldron and Dakessian, 1981; Wu et al., 1988).

Two different indices were estimated to evaluate such differences: the mean percentage error, *MPE* (equation 2.5 in section 2.2.7), and the root mean square error, *RMSE* (equation 2.6 in section 2.2.7).

The minimization of both indices was accomplished through the application of a standard gradient-based automatic optimization algorithm implemented in the MATLAB/Simulink software package (MATLAB R2015b, The MathWorks, Inc., Natick, Massachusetts, United States).

Despite a large number of published works, little information is available about the root distribution in diameter classes, which is necessary to provide the root reinforcement (Schwarz et al., 2013), and no information is available for grapevines.

Concerning the quantification of root reinforcement, one of the available methods for evaluating root reinforcement is the Root Bundle Model Weibull, RBMw (Schwarz et al., 2013). RBMw is a strain step loading fibre bundle model that considers the mechanical and geometrical properties in addition to the root distribution and the maximum resisting force (see the detailed description in section 1.2.1). The input parameters of the model are the maximum tensile force F_{\max} (in N), the Young's modulus E (in MPa), and the root length L (in mm). The application of RBMw requires the calibration of eight different parameters. Six of them (F_0 , E_0 , L_0 , ξ , α and β) are obtained by fitting laboratory test data and field measurements using nonlinear least square regressions, as suggested by Giadrossich et al. (2016), whereas the last two (λ and ω) are calibrated according to the procedure described in detail in Schwarz et al. (2013).

The combined application of the RDM and RBMw models allows the evaluation of the spatial distribution of root reinforcement both for a single plant and for an entire vineyard. RDM provides the root density by diameter classes at a specific distance from the stem based on the size of the grapevine trunk. RBMw gives a value of lateral root reinforcement as the ratio between the maximum tensile force and 1 m^2 of soil in vertical cross-section.

5.2.3 Back analysis

Back analysis was performed by adopting a 3-D approach that implements a limit equilibrium theory, assuming that each shallow landslide reacts as a rigid volume of thin soil sliding on a planar shear surface (Casadei et al., 2003a; Dietrich et al., 2007). The Factor of Safety, FS , is expressed according to Casadei et al. (2003a) and Chiaradia et al. (2016), as follows:

$$FS = \frac{C'_s + C'_{rb} + \frac{A_{lat}}{A_{bas}} C'_s + \frac{A_{lat}}{A_{bas}} C'_{rl} + [(D \gamma_s - D_w \gamma_w + q_0) \cos \theta] \tan \phi'}{(D \gamma_s + D_w \gamma_{sat} + q_0) \sin \theta} \quad (5.6)$$

where C'_s is the soil effective cohesion (in Pa), C'_{rb} is the basal root reinforcement (in Pa), C'_{rl} is the lateral root reinforcement (in Pa), D is the soil depth (in m), D_w is the groundwater level (in m), A_{lat} is the lateral area (in m²), A_{bas} is the basal area (in m²), γ_s is the unit weight of dry soil (in N/m³), γ_w is the unit weight of water (in N/m³), γ_{sat} is the unit weight of saturated soil (in N/m³), q_0 is the tree surcharge per unit area (in Pa), ϕ' is the effective friction angle (in rad) and θ is the slope steepness (in rad). The lateral area is the product of the scarp perimeter and the scarp depth.

The groundwater level was evaluated by adopting a steady state shallow subsurface flow described in several TOPMODEL applications (Beven and Freer, 2001; Beven and Kirkby, 1979; O'Loughlin, 1986) as follows:

$$D_w = \min \left(\frac{R a}{K_s D \cos \theta \sin^2 \theta b}, 1 \right) \quad (5.7)$$

where R is the steady-state recharge (in m/hr), a is the contributing area (in m²), b is the contour length of the lower bound to each contributing area (in m) and K_s is the saturated hydraulic conductivity (in m/hr).

To evaluate C'_{rb} the main assumptions in the slope stability analysis were the following: (i) FS equal to unity, (ii) negligible basal root reinforcement ($C'_{rb} =$

0), (iii) negligible tree surcharge ($q_0 = 0$) and (iv) rainfall amount R equal to the average critical events that triggered shallow landslides.

The back analysis was performed on the available landslide inventory data collected since 2009 for those phenomena that occurred in the corresponding vineyards.

5.2.4 Study area, experimental site and field work

The study area and the experimental site were located on the hills of the municipality of Santa Maria della Versa in the northeastern part of Oltrepò Pavese, the largest viticulture district in Lombardy, Northern Italy (Figure 5.1). The viticulture of this area is based on a group of major cultivars, such as Barbera and Croatina, and produces high-quality local CDO (“Controlled Designation of Origin”) red wines (Rossoni et al., 2015). Other grape cultivars are Chardonnay, Cortese, Uvarara, Vespolina, Pinot, Italian Riesling, Moscato and Malvasia (Failla, 1988; Rossoni et al., 2015).

The study area is 59 km² and is extensively cultivated with grapevines, which occupy approximately 60% of the territory (Figure 5.2a). Elevation ranges from 77 m to 350 m a.s.l (Figure 5.2b), while slope varies from 0° to 40° (Figure 5.2c). According to Koppen’s classification of world climates, the climatic regime is temperate/mesothermal, with a mean annual temperature of approximately 12° C and a mean annual precipitation of 684.4 mm, as monitored by a rain-gauge station (located at the Canevino station in the ARPA Lombardy monitoring network).

In the northern part of the area, bedrock materials are characterized by a Mio-Pliocenic succession consisting of arenaceous, conglomeratic, marly and evaporitic deposits (Monte Arzolo Sandstone, Rocca Ticozzi Conglomerates Sant'Agata Fossili Marls, and Gypsum formation). In this area, slopes are steep, with slope angles generally steeper than 20° . Superficial soils derived from bedrock weathering are sandy silts and clayey sandy silts with a thickness ranging between a few centimetres and 2.5 m. In the southern part of the area, bedrock is composed of Cretaceous flysch deposits (Val Luretta Formation) with a predominant clayey/marly component (Figure 5.2d). In this sector, slopes are less steep with slope angles generally between 10 and 20° . Superficial soils are predominantly silty clays with a thickness between 1 and 4 m.

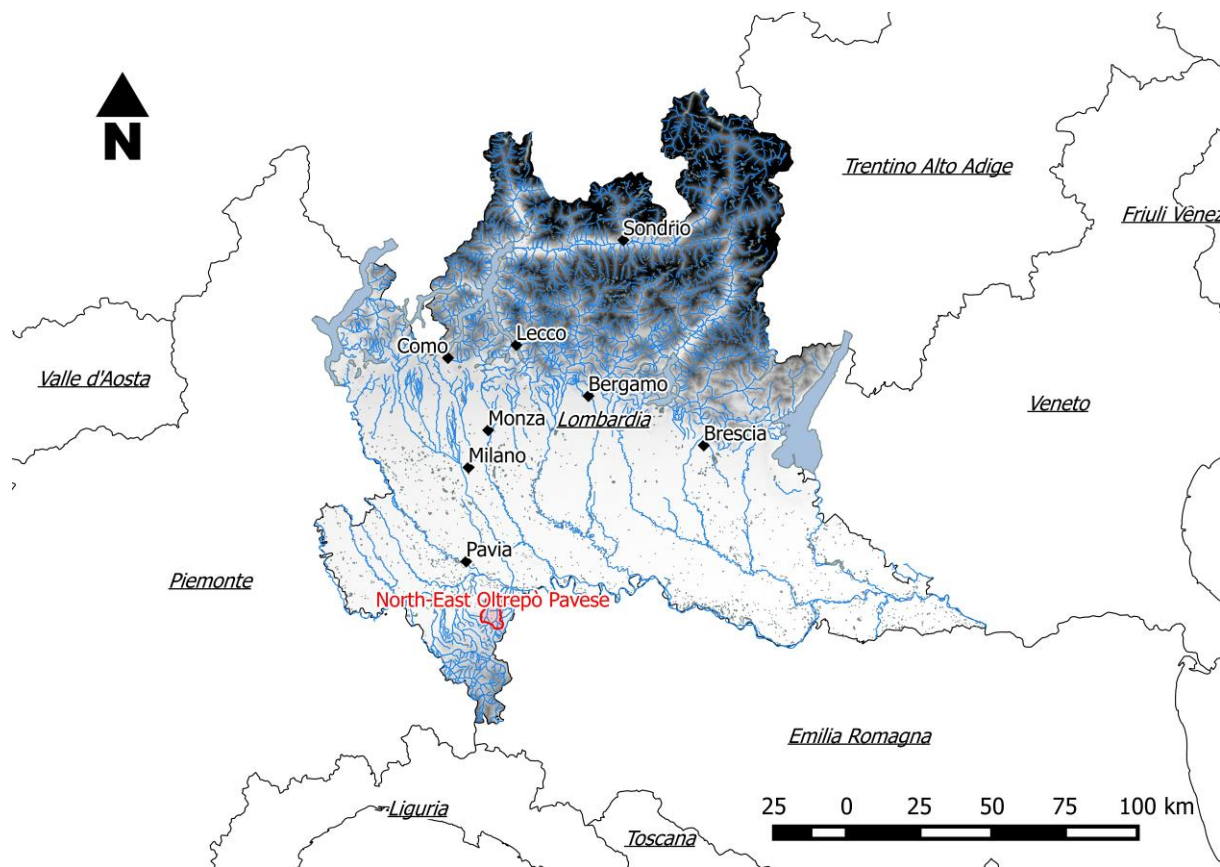


Figure 5.1. The study area is the northeastern part of Oltrepò Pavese that is situated about 70 km from Milano (Lombardy, North Italy) and covers 59 km² almost completely cultivated with grapevines.

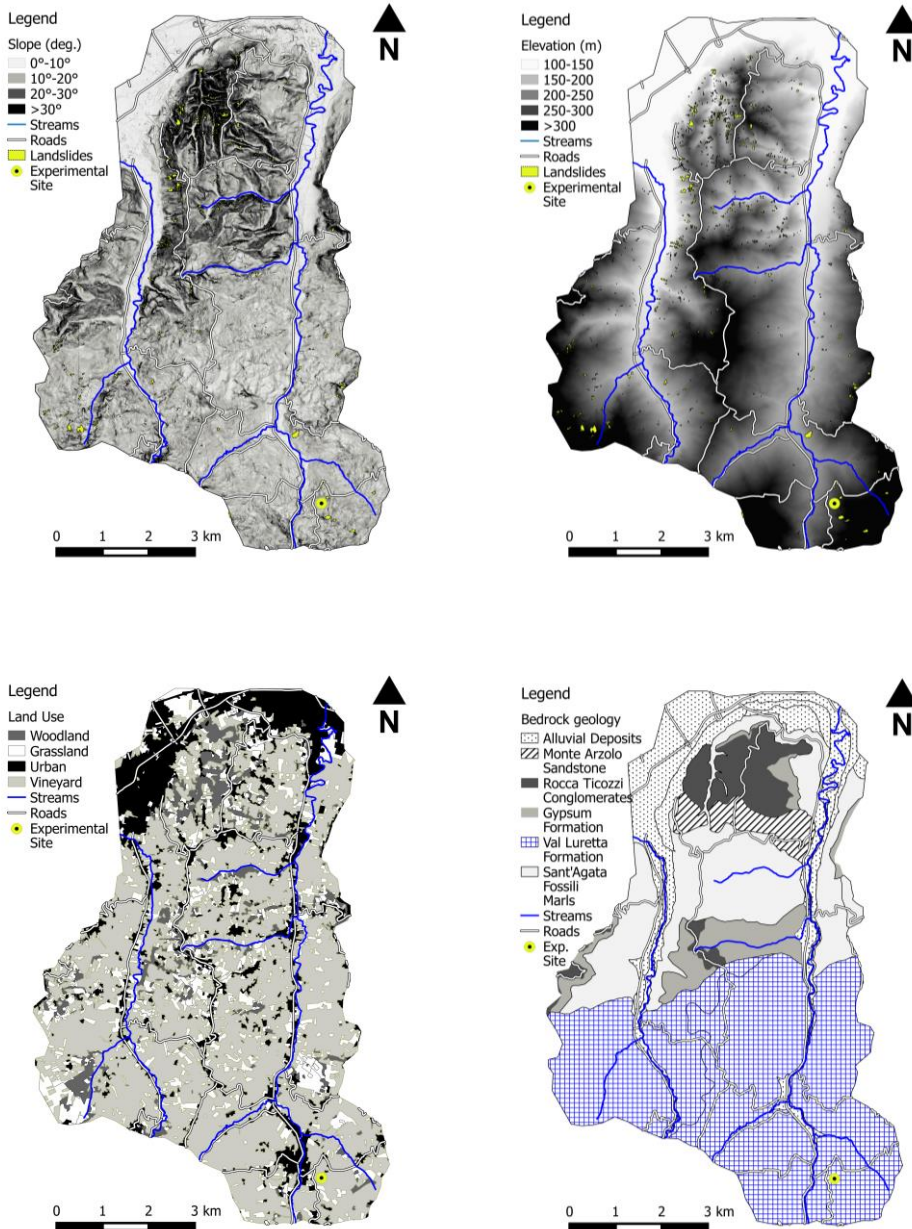


Figure 5.2. a) Digital elevation model and landslide inventory of the northeastern part of Oltrepò Pavese, b) topographic slope map, c) land use map, and d) geological map.

Shallow landslide inventory data, collected through field surveys and interpretation of aerial photographs and satellite images, have been available since 2009. This area is prone to rainfall-induced shallow landslides (Bordoni et al., 2015a; Meisina and Scarabelli, 2007; Zizioli et al., 2013) with a mean density of 15.36 phenomena per km². The first and most significant event in terms of the number of landslides occurred on 27–28 April 2009 and was characterized by an extreme rainfall event of 160 mm in 62 h (Zizioli et al., 2013). Further shallow landslide events occurred in 2013 and 2014 after rainfall events with cumulative rainfall amounts higher than 20 mm in 15 h. The average critical rainfall for most of the occurred landslides was 0.0015 m/h (Table 5.1).

Table 5.1. Main heavy rainfalls that led to severe landslides since 2009 (Bordoni et al., 2015a, 2015b; Zizioli et al., 2013).

Rainfall (mm)	Duration (h)	Date
160	62	27-28th April 2009
29.8	24	23rd-24th March 2013
24.6	15	30th March 2013
29.5	26	4-5th April 2013
34.6	47	18-20th January 2014
68.9	42	28th February-2nd March 2014

The instability phenomena can generally be classified as complex landslides that start as shallow rotational-translational failures and evolve into earth-flows according to the landslide classification reported by Cruden and Varnes (1996). The depth of the sliding surfaces settled between 0.90 m and 1.50 m at the contact between soil and bedrock or at the contact between soil horizons with different permeability, where a perched water table could form during triggering rainfalls. These features were detected in the entire study area, taking into account different bedrock types, soil textures and land use classes.

We identified an experimental vineyard planted 25 years ago in the context of a sub-area frequently affected by shallow landslides (Figure 5.2a) and

characterized by a silty clay soil developed above the Val Luretta Formation, with a depth of failure surface of 0.90 m. The variability in soil properties was low along the vertical profile, as shown in Table 5.2. The rootstock S04 (*Vitis berlandieri* x *Vitis riparia*) is typical of the entire area (Bordoni et al., 2016) and was grafted with Italian Riesling clones. The main characteristics of the experimental vineyard and of its soil are summarized in Table 5.2 and Table 5.3, respectively.

Table 5.2. Main characteristics of the soil.

Soil characteristic	
Gravel (%)	6.20 ± 4.73
Sand (%)	4.15 ± 0.70
Silt (%)	34.15 ± 4.16
Clay (%)	55.50 ± 4.44
Liquid limit w_L (%)	74.00 ± 2.97
Plasticity index PI (%)	53.43 ± 2.80
Soil unit weight γ_s (KN m ⁻³)	17.20
Soil porosity n (-)	0.53

Table 5.3. Main characteristics of the experimental vineyard at Santa Maria della Versa, Province of Pavia, Lombardy.

Vineyard characteristics	
Rootstock	S04 (<i>Vitis berlandieri</i> x <i>V. riparia</i>)
Scion	Italic Riesling
Age	25 years
Spacing between vine rows (m)	2.5
Spacing between grapevines (m)	2
Average diameter of stems	45.4 mm ± 6.5 mm.

The trench-profile method is the most commonly accepted method to measure the root distribution both in viticulture and forestry (Abdi et al., 2010; Abernethy and Rutherford, 2001; Bischetti et al., 2009; Bohm, 1979; Di Iorio et al., 2013; Schmid and Kazda, 2002). In viticulture, the profile wall is generally established approximately 0.3 m to 1 m from the vine trunk, although there seems to be no preferred distance (Smart et al., 2006). We adopted this method by excavating four different 0.50 x 1.10 m profiles for six grapevine plants in the experimental vineyard at four different distances from the grapevine stems 0.20 m, 0.40 m, 0.80 m and 1.30 m, along with the radial and vertical directions (Figure 5.3). The last distance corresponds to the middle point between two adjacent rows of grapevines.



Figure 5.3. The experimental procedure consisted of digging a trench wide 2 m × 1.3 m and a depth approximately 1.1 m with the use of an excavator, taking pictures of vertical profiles (0.50 m × 1.1 m) at different distances, collecting intact roots for measuring their length and for testing the maximum tension force in the laboratory.

To count the number of roots, digital images were taken, analysis was conducted (Bischetti et al., 2009; Hales et al., 2009; Vergani et al., 2014a), and roots were ranked in 1 mm diameter classes from 0.5 to 15.5 mm; the digital method is not capable of accurately identifying roots with a diameter smaller than 0.5 mm (Chiaradia et al., 2016; Vergani et al., 2014b).

All six selected grapevines were completely excavated, which allowed us to measure the length of the roots and collect samples of live roots with different diameters. The samples were carefully conserved in plastic containers in 15% alcohol to prevent deterioration (Bischetti et al., 2005). Tensile tests were performed in the laboratory within two weeks after the root collection using a device described in Bischetti et al. (2009) to measure the maximum tensile resistance and the Young's modulus as a function of the root diameter for each tested root.

5.3 Results

5.3.1 Root distribution

The root density in trenches at the same distance from the grapevine stems had a very small variability. The highest root density was measured in the closest trenches to the stem (212 ± 64 roots per m^2), and the root density decreased until 0.80 m from the stem (Figure 5.4): 110 ± 12 roots/ m^2 at 0.40 m and 78 ± 6 roots/ m^2 at 0.80 m. At 1.30 m, which was the midpoint between rows, the density increased to 96 ± 11 roots/ m^2 . Moreover, roots were ranked in four different categories (0.5-1 mm, 1-2 mm, 2-5 mm and >5 mm) based on several studies (e.g. Genet et al., 2008; Vergani et al., 2014a). The diameters ranged from 0.5 mm to 14.5 mm, with 62% of the roots in the 0.5-1 mm diameter class, regardless of the distance from the stem. Additionally, approximately 21% of the roots belonged to the diameter class from 1 to 2 mm, whereas the larger roots (with a diameter greater than 2 mm) accounted for only 17% of the total.

Root vertical distribution between trenches at the same distance showed a small variability, except for the profiles dug at 0.20 m from the stems (Figure 5.4). On average, only 12% of the total roots were found in the shallower layer (until 0.10 m depth), and approximately 70% were found in the first 0.50 m. The profiles closer to the grapevine stems showed a rapid decrease in the root numbers with depth, whereas the root number was rather constant at 0.80 m and particularly at 1.30 m (Figure 5.4).

Whereas the proportion of finer roots observed at each depth increment was rather constant, large roots greater than 5 mm in diameter were generally observed at a depth between 0.20 m and 0.60 m, which is the planting depth of the rooted grafts (Figure 5.5). The maximum rooting depth was 0.90 m in all profiles.

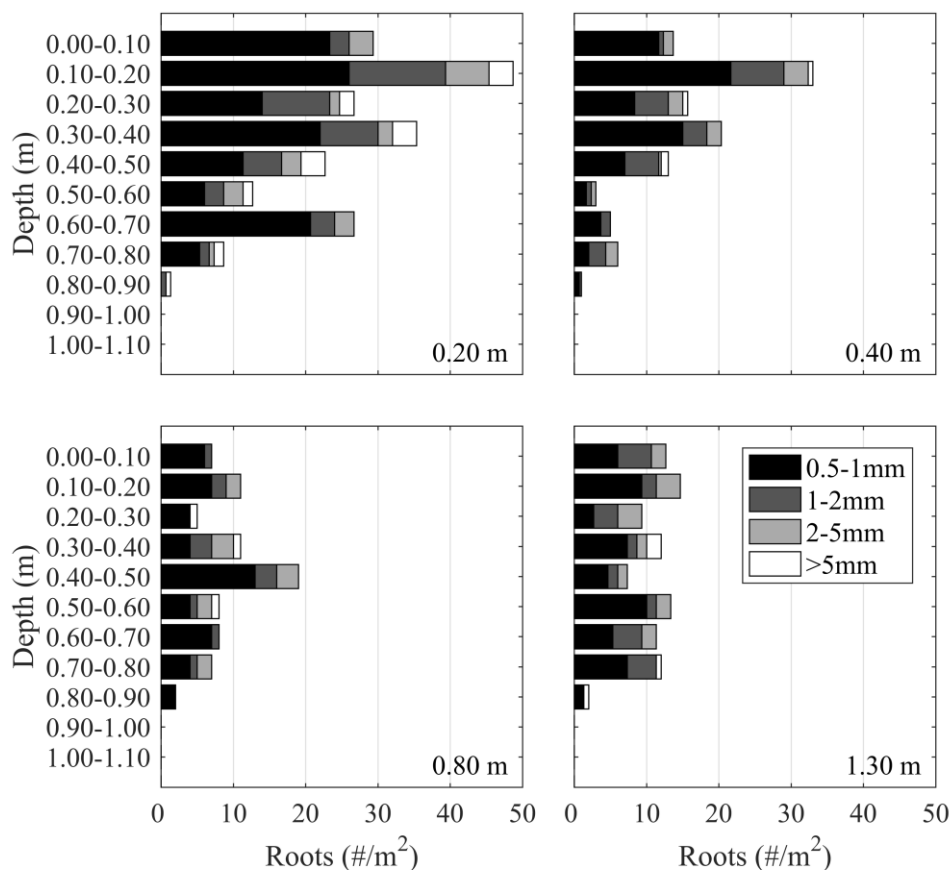


Figure 5.4. Average root density classified in four diameter classes (0.5–1 mm, 1–2 mm, 2–5 mm and >5 mm) at different distances from the vine trunk (0.20 m, 0.40 m, 0.80 m and 1.30 m).



Figure 5.5. At the planting depth of the rooted grafts, the larger roots with a diameter >5.5 mm are generally present. Such roots extend rather horizontally, in perpendicular direction respect the trunk to provide additional stability to the grapevine.

5.3.2 Calibration of RDM and RBMw

Both RDM and RBMw required calibration for the four parameters controlling the spatial distribution of roots. The values for the experimental site were obtained by minimizing the performance indices, $RMSE=3.12$ and $MPE=-10.45\%$.

The greatest discrepancy between field-observed and modelled values was obtained for the profiles at 1.30 m, where the root density was underestimated by approximately 20% in terms of MPE (Figure 5.6). The best-fit value for the pipe theory coefficient was 631 roots m^{-2} ; both the proportionality and the self-similarity coefficients assumed a value of 100, whereas the exponential coefficient was -2.4 (Table 5.4). The modelled root distribution as a function of distance from the stem is shown in Figure 5.6.

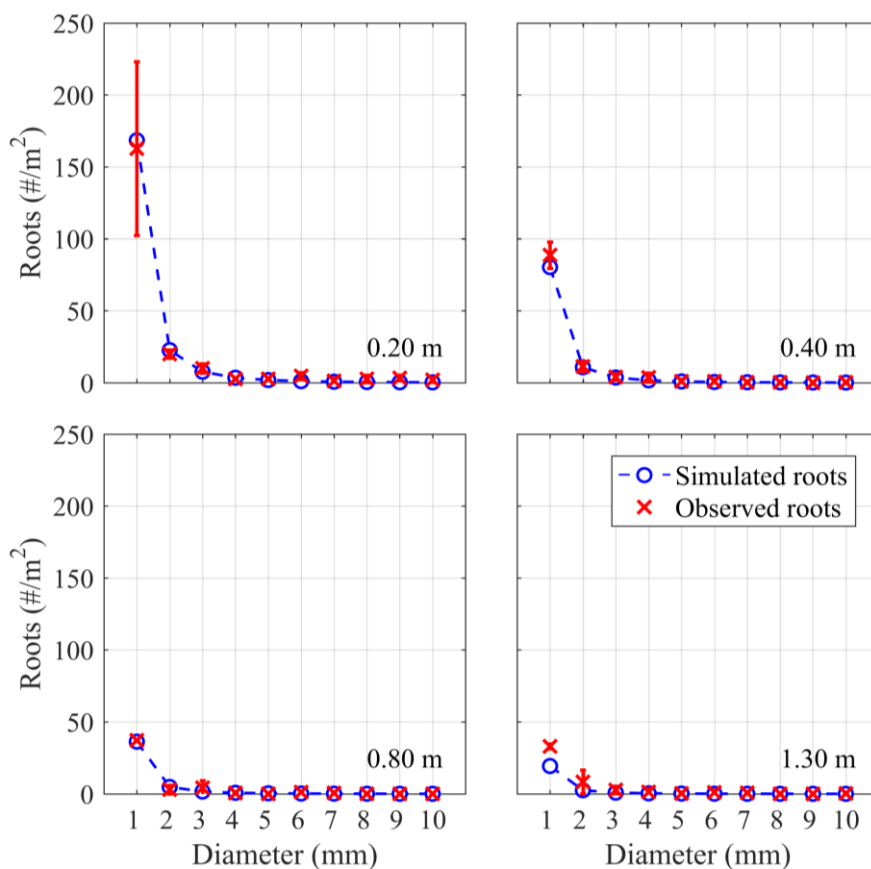


Figure 5.6. Discrepancies between the observed and the simulated number of roots divided into diameter classes at four distances from the vine trunk (0.20 m, 0.40 m, 0.80 m and 1.30 m).

Table 5.4. Optimal parameters of RDM (equations. 5.1-5.5) provided by the calibration procedure that minimized the differences between observed and simulated data.

Parameters of RDM	Value
μ [roots m ⁻²]	631
ψ [-]	100
η [-]	100
γ [-]	-2.4

Concerning RBMw, all input parameters were the coefficients of non-linear regressions for the maximum tensile force (equation 1.19 in section 1.2.1), the Young's modulus (equation 1.20 in section 1.2.1), the root length (equation 1.21 in section 1.2.1) and the Survival Weibull function (equation 1.25 in section 1.2.1).

The tensile tests were conducted on 34 roots with diameters that ranged from 0.26 mm to 5.77 mm. The measured maximum tensile forces ranged from 1.98 N to 158.49 N, with an average value of 39.43 N (Figure 5.7a). The measured Young's modulus varied from 5.05 MPa to 189.55 MPa, with an average value of 40.58 MPa (Figure 5.7b). Only four out of 34 tested roots showed Young's modulus greater than 100 MPa and were all very fine, with a diameter smaller than 0.5 mm. The maximum tensile force and Young's modulus had a strong correlation with the root diameter, as is the case for most tree species (e.g. Abe and Iwamoto, 1986; De Baets et al., 2008; Docker and Hubble, 2008). The tensile tests made in this study confirmed such behaviour, and the power function relationships obtained by fitting the measured data were robust ($R^2 = 0.650$ for the maximum tensile force and $R^2 = 0.551$ for Young's modulus; Figure 5.7a and Figure 5.7b).

To fit the non-linear regression between the length and the root diameter, field measurements were carefully conducted on the intact roots of each of the six examined plants. The diameters of these roots were representative of a root system and ranged from 3.4 mm to 20.9 mm. Their lengths varied between 0.40 m and 1.25 m. The fitted non-linear regression was a power function with a good correlation ($R^2 = 0.876$; Figure 5.7c). Additionally, the survival function was calibrated following the procedure described in detail by Schwarz et al. (2013), and satisfactory results were obtained (Figure 5.7d). All the fitted parameters of RBMw are reported in Table 5.5.

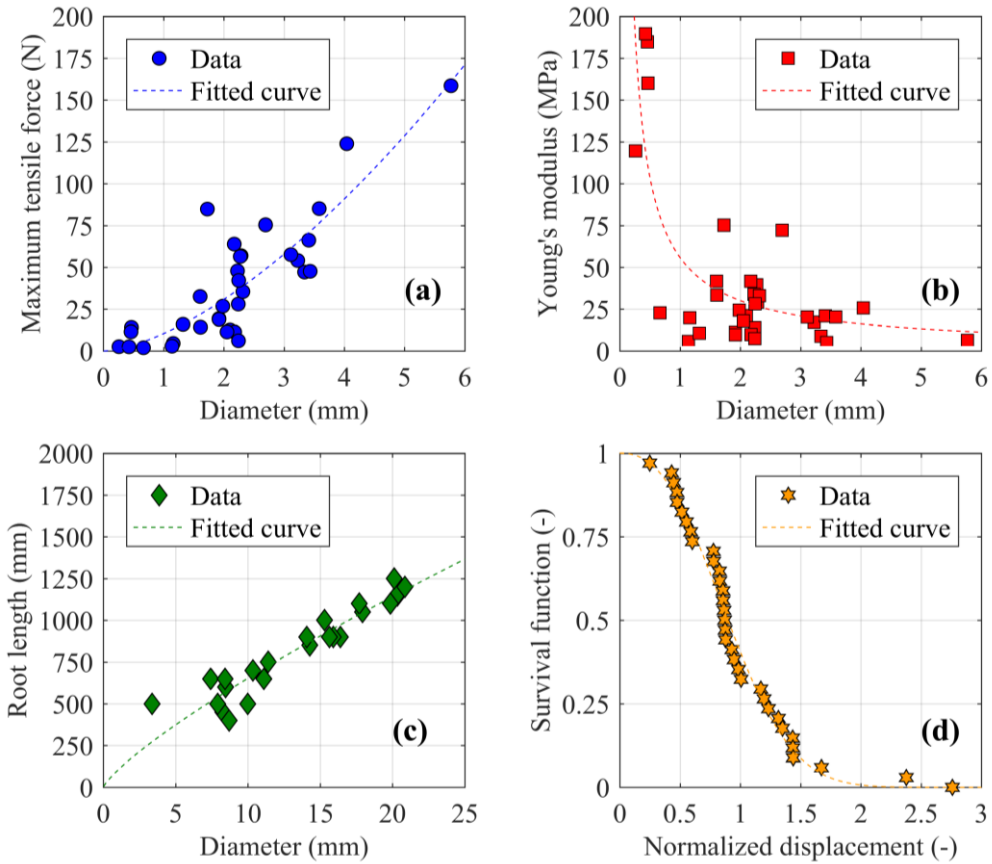


Figure 5.7. a) Maximum tensile force vs root diameter relationship provided by tensile tests in the laboratory, b) Young's modulus of elasticity vs diameter relationship provided by tensile tests in laboratory, c) root length vs diameter measured at the field, and d) survival function for laboratory tensile test data.

Table 5.5. Parameters of RBMw (equations 1.19, 1.20, 1.21 and 1.25 in section 1.2.1) provided by tensile tests in laboratory and field measurements.

Parameters of RBMw	Value	Parameters of RBMw	Value
F_0 [N]	10.419	L_0 [mm]	102.04
ξ [-]	1.562	α [-]	0.806
E_0 [MPa]	99.447	λ [-]	1.042
β [-]	-0.894	ω [-]	2.453

5.3.3 Application of RDM and RBMw at the stand scale

Once the two sub-models were calibrated, their combination led to estimates of the root reinforcement provided by the root systems of the considered grapevines at progressive distances from the stems.

The resistance initially increased until a peak was reached at a displacement of 20 mm for all the distances from the grapevine stems and then decreased to a nearly null value at a displacement of 200 mm (Figure 5.8). The peak value progressively decreased with increasing distance from the stem, from 8.33 N at 0.20 m to a value between 900 N and 1,750 N at a distance greater than 1 m.

These results show that the contribution of the roots to the soil strength between the rows was weaker by approximately an order of magnitude with respect to the points closest to the stems, from 8.33 kPa to 0.90 kPa.

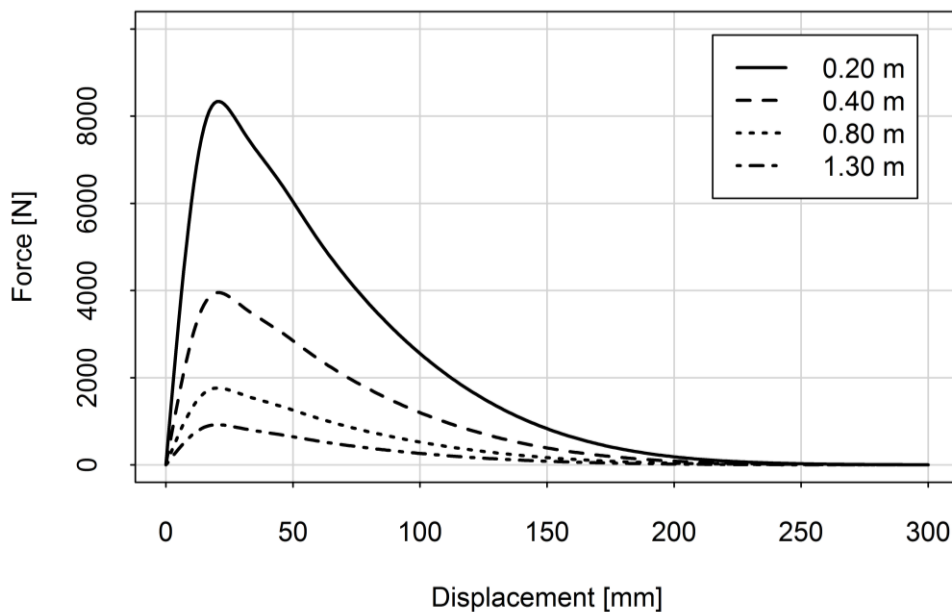


Figure 5.8. RBMw output as a function of different distances from stem: 0.20 m, 0.40 m, 0.80 m and 1.30 m. The tensile force is obtained considering all roots present in a vertical profile of 1 m².

5.3.4 Back analysis

A landslide inventory provided information on 906 landslides covering approximately 0.5 km², 1% of the total study area. Back analysis was conducted only on the 237 landslides that occurred in vineyards, approximately 26% of the total, which caused great economic damage over the last 7 years. Almost all these landslides were registered as shallow landslide events that affected the superficial soils above the weathered or non-weathered bedrock. Although they are uniformly located inside the study area, the hillslopes exposed to the west and northwest were generally more prone to such instabilities. Additionally, the hillslope inclination ranged from 10 to 45 degrees, with an average value of 28 degrees.

The basal area of the triggering zone ranged from 20 m² to 1,500 m², whereas the lateral area varied from 24 m² to 400 m². On average, the triggering zone covered 283 m² of the planar area and had a lateral surface equal to 125 m² (Figure 5.9). Therefore, the ratio between the lateral and the basal failure area (A_{lat}/A_{bas}), which is an input parameter for equation 5.6, ranged from 0.05 to 1.20, with a median value of 0.42.

The sliding surface depth for the considered shallow landslides ranged between 0.90 and 1.50 m. Because the failure planes reached a deeper depth than the maximum rooting depth of grapevines, in agreement with Bordoni et al. (2016), we verified the assumption that the basal root reinforcement was negligible ($C'_{rb} = 0$).

The main input parameters that characterized the soils (soil effective cohesion C'_s , unit weight of dry soil γ_s , saturated soil γ_{sat} and effective friction angle φ) were estimated through laboratory analysis on soil samples collected that corresponded to different bedrocks in the study area (Table 5.6).

The back-calculated average value of C'_{rl} was 5.96 kPa, as shown in Figure 5.10. The variability was quite large, and half of the values were in the range 2.63-11.64 kPa. The minimum estimated C'_{rl} was approximately 0 kPa, whereas the maximum reached approximately 25 kPa.

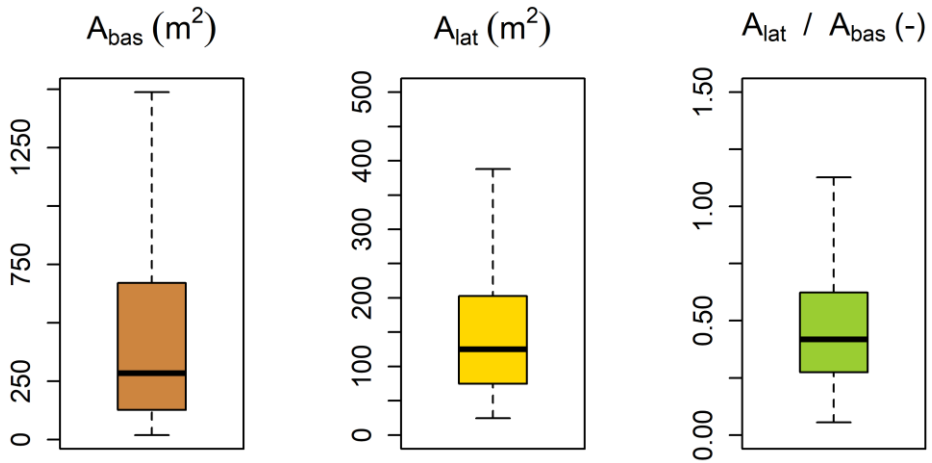


Figure 5.9. Analysis of landslide inventory: distribution of the planar size of the landslides as the basal and lateral failure area and their ratio.

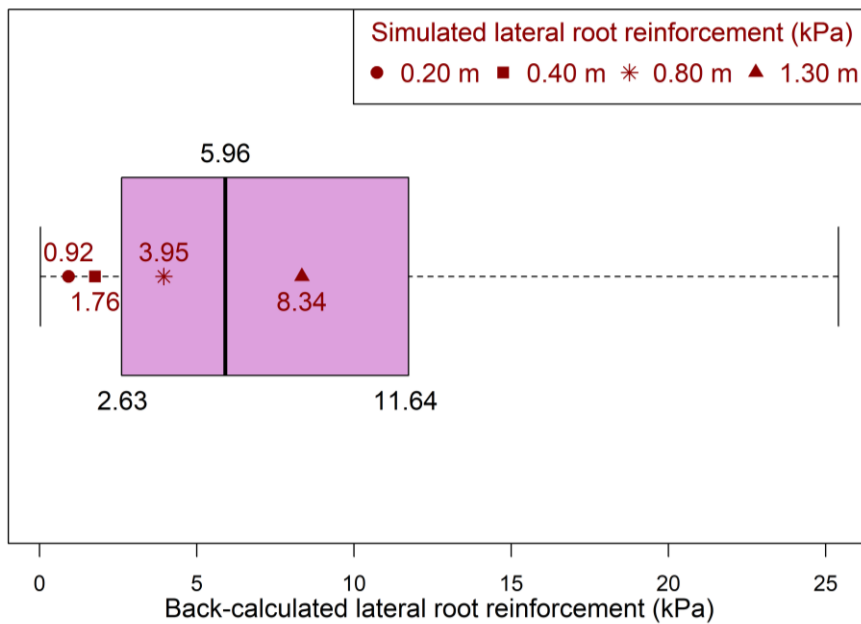


Figure 5.10. Back-calculated lateral root reinforcement values for each shallow landslides occurred in the study area since 2009. The median value is 6.45 kPa and the 50% of data ranges from 3.52 kPa and 11.52 kPa.

Table 5.6. Geotechnical characteristics of the colluvial soils involved in shallow landslides evaluated through laboratory analysis.

Bedrock geology	C_s (kPa)	γ_s (KN m⁻³)	γ_{sat} (KN m⁻³)	ϕ' (°)	Ks (m hr⁻¹)
Alluvial deposits	1.0 – 2.0	15.5	18	25.0 – 27.0	6.0 E-05
Monte Arzolo Sandstone	0.0 – 7.0	15.0 – 16.3	17.9	23.0 – 30.0	8.3E-05
Rocca Ticozzi Conglomerate	2.0	15.2 – 16.3	17.7	32	6.5 E-05
Gypsum Formation	4.0 – 7.0	15.7	17.8	25.0 – 27.0	5.8 E-05
Sant'Agata Fossili Marls	7.0 – 10.0	15.3 – 15.8	18	24.0 – 27.0	5.8 E-05
Val Luretta Formation	1.0 – 2.0	16.5	20.4	19.0 – 23.0	8.3 E-05

5.4 Discussion

5.4.1 Root distribution

The total number of roots observed in this study was similar to the values found in adjacent sites in northeast Oltrepò Pavese by Bordoni et al. (2016), which indicates that the experimental site can be considered representative of the geological and agricultural characteristics of the area and that these results can be considered typical of the situation in northeast Oltrepò Pavese. In fact, the root numbers of grapevines appear to be more controlled by rootstock type than by edaphic conditions, which affect the root system architecture (Gerós et al., 2015), and the studied rootstock, S04 (*Vitis berlandieri* × *V. riparia*), is the same in the entire area.

The total number of roots was also relatively similar to measurements in other studies, considering the distance from the stem and that very fine roots (diameters smaller than 0.5 mm) were excluded because of the limits of the image analysis (Table 5.7). Morlat and Jacquet (2003) counted 251 ± 20 roots/m² on a vertical profile at 0.15 m from the grapevine trunk, 171 ± 39 roots/m² at 0.80 m and 60 ± 6 roots/m² at 1.60 m when analysing a 25-year-old *Vitis vinifera* L. cv. Cabernet Sauvignon vineyard grafted onto S04 rootstock in the Loire Valley (France). Hunter (1998) observed approximately 160 roots/m² on a vertical profile at 0.30 m from the stem in a 14-year-old *Vitis vinifera* L. cv. Pinot noir vineyard with a plant spacing of 2 m × 2 m near Stellenbosch (Republic of South Africa). Swanepoel and Southey (1989) measured a range in root total number between 118 and 461 roots/m² in a 5-year-old Chenin blanc vineyard grafted on different rootstocks in the Upper Breed River Valley (Republic of South Africa).

The total number of grapevine roots was drastically smaller than that observed in European forests. Chiaradia et al. (2016) counted on average 175 roots/m², 200 roots/m² and 279 roots/m² for Sweet chestnut (*Castanea sativa* Mill.) in 42 trenches, for European beech (*Fagus sylvatica* L.) in 45

trenches and for Norway spruce (*Picea abies* L. H. Karst.) in 58 trenches, respectively.

Moreover, roots with a diameter ranging from 0.5 to 2 mm, which have water and nutrient foraging and uptake functions (de Herralde et al., 2010), represented the majority of the total, approximately 83%. Such a percentage is generally slightly smaller than those observed in most studies of grapevine cultivars (Morlat and Jacquet, 2003; Nagarajah, 1987; Swanepoel and Southey, 1989), except for the studies by Williams and Smith (1991) and by Hunter et al. (1995) that observed a portion less than 73%. Comparing the observations with forest species, our results agreed with measurements on European beech (*Fagus sylvatica* L.), whereas they were significant underestimates with respect to observations on Sweet chestnut (*Castanea sativa* Mill.) and Norway spruce (*Picea abies* L. H. Karst.) (Chiaradia et al., 2016; Vergani et al., 2014b).

The maximum rooting depth observed in our measurements, approximately 1 m, agrees with most studies in viticulture and seems to be related to the planting depth of rootstocks, although slightly deeper. Smart et al. (2006), who compared more than 200 trench-wall profiles from approximately 40 different combinations among rootstocks and scions, found that the root systems of grapevines develop within 1-2 m from the ground surface. Additionally, Nagarajah (1987) observed that maximum rooting ranged between 0.60 m and 1.20 m for fine soils, although a greater depth of more than 6 m has sometimes been observed (Branas and Vergnes, 1957; Doll, 1954; Seguin, 1972), which must be ascribed to site-specific conditions. For example, Archer and Strauss (1985) and Morano and Kliwer (1994) emphasized that the rooting depth increased with an increase in planting density. In any case, as for many liana-type plants, which develop tendrils, the function of the structural support of the root system is not so fundamental, and root development is driven by other factors (e.g., water content and nutrient availability). Finally, rooting has a genetic component, and *V. berlandieri* x *V. riparia* rootstock is known to be more superficial and

less vigorous than others, although there is not full agreement on this issue (Smart et al., 2006).

In terms of root distribution with depth, it is well known that the number of roots shows a drastic decline with depth (Morano and Kliewer, 1994; Morlat and Jacquet, 2003). The data obtained in this study agreed very well with most of the literature for profiles closer to the grapevine stems, whereas the root distribution seemed to be uniform at greater distances from the stems. This agrees with Williams and Smith (1991), who observed the same distribution throughout the soil profile to the maximum rooting depth, whereas Saayman and Van Huyssteen (1980) observed such behaviour only above a depth of 1 m, probably because of the uniformity of soil and the lack of an impervious soil layer at this location (Williams and Smith, 1991).

Approximately 70% of roots in our study were in the first 50 cm, which is in substantial agreement with the literature. Smart et al. (2006) emphasized that $63.2\% \pm 2.6\%$ of roots were found in the upper 0.60 m for grapevines growing in mostly deep fertile soils. Limiting the analysis to *V. berlandieri* x *V. riparia* rootstocks with a maximum depth similar to the one observed in this study, the cumulative number of roots at 0.60 m was higher.

Additionally, the number of roots in our study was usually smaller in the upper (0-0.20 m) and deeper (1-1.20 m) soil layers, which agrees with results from other authors (Cheng and Baumgartner, 2005; Swanepoel and Southey, 1989). Generally, a small number of roots in the most superficial layer (0.20 m – 0.30 m) of soil is strongly related to agronomical practices such as tilling and permanent sward (Ancel, 1986; Morlat and Jacquet, 2003; Saayman and Van Huyssteen, 1980; Soyer et al., 1984). Moreover, we observed that the distribution of the large roots (with diameters greater than 5.5 mm) was concentrated in the soil layer between 0.20 m and 0.60 m, which corresponds to the planting depth of the rooted grafts, as was also observed by Southey (1992).

In terms of the spatial distribution of root density, we observed a general decrease in the total number of roots with distance from the stems,

regardless if the distance was along the row or between the rows, which suggests a uniform 3-D distribution. This result agrees with the literature. Kozma (1967) found that the spatial distribution of roots around a grapevine trunk was relatively uniform. Cheng and Baumgartner (2005) found that the root biomass was lower in the centre of vineyard middles (approximately 0.90 m from the plant) than in the area closest to the vine trunk. Nagarajah (1987) observed that the root density in the vertical soil profile was higher at 0.30 m than at 0.90 m or 1.20 m from the trunk. For a thorough discussion of 3-D distributions, see Smart et al. (2006).

The increase in the root number that we observed at the midpoint between rows (1.30 m) seems to be because of the overlap between the root systems of different adjacent rows because grapevine roots can extend laterally for a great distance from the trunk (Smart et al., 2006). Analogously, the change in root distribution with depth, which is more uniform than for profiles closer to stems, can also be ascribed to roots overlapping.

Table 5.7. Root densities (N_R) measured in several studies characterized by a different distance from the vine trunk (D_{VT}), rootstock, soil texture, vine spacing (Δ) and cultivar. Reference and location: [1] Swanepoel and Southey (1989) Upper Breede River Valley (Republic of South Africa), [2] Hunter et al. (1995) in Upper Breede River Valley (Republic of South Africa), [3] Araujo et al. (1995) in California (U.S.A.), [4] Hunter (1998) in Upper Breede River Valley (Republic of South Africa), [5] Morlat and Jacquet (2003) in Loire Valley (France) and [6] Bordonni et al. (2016) in North-East Oltrepò Pavese (Lombardy, Italy).

N_R (roots m ⁻²)	D_{VT} (m)	Rootstock	Soil	Δ (m x m)	Age (years)	Vine	Ref.
277	0.5	Berlandieri 13/5	Silt loam	2.70 x 1.20	5	<i>Vitis berlandieri</i> Planch. cv Chenin blanc	[1]
394	0.5	101-14 Millardet et de Grasset	Silt loam	2.70 x 1.30	5	<i>Vitis riparia</i> Mich x <i>Vitis rupestris</i> Sch. cv Chenin blanc	[1]
167	0.5	775 Paulsen	Silt loam	2.70 x 1.40	5	<i>Vitis berlandieri</i> x <i>Vitis rupestris</i> cv Chenin blanc	[1]
461	0.5	1103 Paulsen	Silt loam	2.70 x 1.50	5	<i>Vitis berlandieri</i> x <i>Vitis rupestris</i> cv Chenin blanc	[1]
305	0.5	99 Richter	Silt loam	2.70 x 1.60	5	<i>Vitis berlandieri</i> x <i>Vitis rupestris</i> cv Chenin blanc	[1]
365	0.5	110 Richter	Silt loam	2.70 x 1.70	5	<i>Vitis berlandieri</i> x <i>Vitis rupestris</i> cv Chenin blanc	[1]

Root reinforcement in a vineyard

152	0.5	140 Ruggeri	Silt loam	2.70 x 1.80	5	<i>Vitis berlandieri</i> x <i>Vitis rupestris</i> cv Chenin blanc	[1]
118	0.5	US 12-6-8	Silt loam	2.70 x 1.90	5	Jacquez (<i>Vitis aestivalis</i> Mich. X <i>Vitis cinerea</i> Engel. X <i>Vitis vinifera</i> L.) x 99 R (<i>Vitis berlandieri</i> x <i>Vitis rupestris</i>) cv Chenin blanc	[1]
302	0.5	US 16-13-26	Silt loam	2.70 x 1.10	5	1202 Couderc (<i>Vitis vinifera</i> x <i>Vitis rupestris</i>) x 99 R (<i>Vitis berlandieri</i> x <i>Vitis rupestris</i>) cv Chenin blanc	[1]
103	0.3	99 Richter	Sandy clay loam	3.50 x 1.50	11	<i>Vitis vinifera</i> L. cv Cabernet Sauvignon	[2]
352 ± 37	0.3	-	Sandy loam	3.60 x 2.40	10	<i>Vitis vinifera</i> L. cv Thompson Seedless	[3]
584 ± 67	0.3	-	Sandy loam	3.60 x 2.41	10	<i>Vitis vinifera</i> L. cv Thompson Seedless	[3]
140.6	0.3	99 Richter	Sandy loam	3.00 x 3.00	14	<i>Vitis vinifera</i> L. cv. Pinot noir	[4]
160.13	0.3	99 Richter	Sandy loam	3.00 x 1.50	14	<i>Vitis vinifera</i> L. cv. Pinot noir	[4]

159.4	0.3	99 Richter	Sandy loam	2.00 x 2.00	14	<i>Vitis vinifera</i> L. cv. Pinot noir	[4]
281.1	0.3	99 Richter	Sandy loam	2.00 x 1.00	14	<i>Vitis vinifera</i> L. cv. Pinot noir	[4]
251.4	0.3	99 Richter	Sandy loam	1.00 x 1.00	14	<i>Vitis vinifera</i> L. cv. Pinot noir	[5]
328.2	0.3	99 Richter	Sandy loam	1.00 x 0.50	14	<i>Vitis vinifera</i> L. cv. Pinot noir	[5]
251 ± 20	0.15	S04	Silt loam	3.20 x 1.20	25	<i>Vitis vinifera</i> L. cv. Cabernet Sauvignon	[5]
171 ± 39	0.8	S04	Silt loam	3.20 x 1.20	25	<i>Vitis vinifera</i> L. cv. Cabernet Sauvignon	[5]
60 ± 6	1.6	S04	Silt loam	3.20 x 1.20	25	<i>Vitis vinifera</i> L. cv. Cabernet Sauvignon	[5]
132	0.3	S04	Silty clay loam	2.10 x 0.90	10	10 years old <i>Vitis berlandieri</i> / <i>Vitis riparia</i> vineyard	[6]
108	0.6	S04	Silty clay loam	2.10 x 0.90	10	10 years old <i>Vitis berlandieri</i> / <i>Vitis riparia</i> vineyard	[6]
264	0.3	S04	Silty clay loam	2.35 x 1.00	10-15	<i>Vitis berlandieri</i> x <i>Vitis riparia</i> vineyard cv Croatina	[6]
184	0.6	S04	Silty clay loam	2.35 x 1.00	10-15	<i>Vitis berlandieri</i> x <i>Vitis riparia</i> vineyard cv Croatina	[6]

Root reinforcement in a vineyard

322	0.5	S04 / 420 A	Silty clay loam	2.00 x 1.00	20-30	<i>Vitis berlandieri</i> x <i>Vitis riparia</i> vineyard cv Croatina, Uva Rara and Barbera	[6]
146	0.5	S04	Silt loam	2.25 x 0.80	1-6	<i>Vitis berlandieri</i> x <i>Vitis riparia</i> vineyard cv Croatina	[6]
108	0.95	S04 / 420 A	Silty clay loam	2.20 x 1.00	13-15	<i>Vitis berlandieri</i> x <i>Vitis riparia</i> vineyard cv Croatina, Uva Rara and Barbera	[6]
74	1.15	S04 / 420 A	Silty clay loam	2.20 x 1.00	13-15	<i>Vitis berlandieri</i> x <i>Vitis riparia</i> vineyard cv Croatina, Uva Rara and Barbera	[6]
110	0.65	S04 / 420 A	Silty clay loam	2.20 x 1.00	13-15	<i>Vitis berlandieri</i> x <i>Vitis riparia</i> vineyard cv Croatina, Uva Rara and Barbera	[6]
102	0.8	S04 / 420 A	Silty clay loam	2.35 x 2.00	20-25	<i>Vitis berlandieri</i> x <i>Vitis riparia</i> vineyard cv Croatina, Uva Rara and Barbera	[6]
170	0.65	S04 / 420 A	Silty clay loam	2.35 x 2.00	20-25	<i>Vitis berlandieri</i> x <i>Vitis riparia</i> vineyard cv Croatina, Uva Rara and Barbera	[6]

116	1.3	S04 / 420 A	Silty clay loam	2.35 x 2.00	20-25	<i>Vitis berlandieri</i> x <i>Vitis riparia</i> vineyard cv Croatina, Uva Rara and Barbera	[6]
110	0.3	S04 / 420 A	Silty clay loam	2.30 x 1.00	5-6	<i>Vitis berlandieri</i> x <i>Vitis riparia</i> vineyard cv Croatina, Uva Rara and Barbera	[6]
104	0.7	S04 / 420 A	Silty clay loam	2.30 x 1.00	5-6	<i>Vitis berlandieri</i> x <i>Vitis riparia</i> vineyard cv Croatina, Uva Rara and Barbera	[6]
176	0.2	S04 / 420 A	Silty clay loam	2.30 x 1.00	5-6	<i>Vitis berlandieri</i> x <i>Vitis riparia</i> vineyard cv Croatina, Uva Rara and Barbera	[6]
104	0.9	S04 / 420 A	Silty clay loam	2.30 x 1.00	5-6	<i>Vitis berlandieri</i> x <i>Vitis riparia</i> vineyard cv Croatina, Uva Rara and Barbera	[6]

5.4.2 Mechanical properties of roots and root system geometry

It is well known that the values of mechanical properties are strongly influenced by the diameter of roots (e.g. Bischetti et al., 2009; De Baets et al., 2008; Giadrossich et al., 2016). The measured maximum tensile forces (1.98-158.47 N for roots with diameters from 0.26 mm to 5.77 mm) were similar to those obtained by Bordoni et al. (2016) for roots of similar diameters collected in other test-sites of northeast Oltrepò Pavese. Such values are comparable with those measured for forest species, except for European beech (Chiaradia et al., 2016).

The relationships between root diameter and values of maximum tensile force and of Young's modulus (equations 1.19 and 1.20 in section 1.2.1) were slightly poor ($R^2 = 0.650$ and $R^2 = 0.551$, respectively) with respect to those reported by several studies (e.g. Chiaradia et al., 2016; Vergani et al., 2014b). On the other hand, the relationship between root diameter and root length was more robust with respect to the literature (e.g. Giadrossich et al., 2013; Schwarz et al., 2010b). Concerning Young's modulus, the stiffnesses of the grapevine roots were greater than those of the roots of Black Locust (*Robinia pseudoacacia* L.) and Chinese Arborvitae (*Platycladus orientalis*), as observed by Ji et al. (2012) in the Loess Plateau in China, but were much lower than those reported by Operstein and Frydman (2000) for several species of herbs and shrubs. Thomas and Pollen-Bankhead (2010) measured quite similar values for two species of trees, Oregon Ash (*Fraxinus latifolia* Benth.) and Eastern Sycamore (*Platanus occidentalis* L.), on stream banks in the U.S. states of Oregon and Mississippi.

Root lengths were underestimated with respect to some other species of plants, such as Spruce (*Picea abies* L.) (Schwarz et al., 2010b), Barley (*Hordeum vulgare* L.) and Western yellow pine (*Pinus ponderosa*) (Waldron and Dakessian, 1981).

5.4.3 Root reinforcement

Back-analysis carried out on the study area provided the additional cohesion needed for vineyards to contrast the triggers of slope failure under very severe hydrological conditions, which certainly caused several shallow landslides during the last years. On average, the back-calculated additional cohesion was 5.96 kPa, with a variability between 2.63 kPa and 11.64 kPa for 50% of cases. Such values mainly referred only to the root reinforcement estimated along the lateral failure surface because roots crossing the basal failure plane could rarely be found. Such values are in the range of published back-calculated values of 1 kPa to 17.5 kPa for different forest species and geological and hydrological conditions, as reported in Table 5.8.

The root reinforcement estimated through the combination of the two sub-models, RDM and RBMw, agreed with those obtained by the back analysis: from approximately 0.90 kPa between rows to 8.50 kPa near the vine trunk. The agreement between additional root strength modelled at the experimental sites and back-calculated values for a larger area confirms that the obtained results can be considered valid for the entire study area (North Oltrepò Pavese).

To evaluate the effect of root reinforcement on the stand scale, we calculated the root reinforcement for a part of the experimental vineyard with a plant spacing of 2.0 m x 2.5 m. As expected, the root reinforcement was higher along the rows of grapevines than between the rows (lines A and C in Figure 5.11); the average root reinforcement was approximately 3.4 kPa, with maximum values of 15 kPa nearest the grapevines. This range was similar to most of the root reinforcement values estimated by the back-analysis procedure (Figure 5.10). On the other hand, the root reinforcement had lower values ranging from 0 and 1 kPa along the inter-row direction (lines B and D in Figure 5.11), where the biomass was lower than in the area closest to the stem (Cheng and Baumgartner, 2005).

Table 5.8. Back-calculated root reinforcement values for different species and sites available in the literature.

Root reinforcement (kPa)	Vegetation type	Location	References
6.5	European beech (<i>Fagus sylvatica</i> L.)	Pre-Alps, Lombardy, Italy	Bischetti et al. (2004)
6.2-7.0	Sugar maple (<i>Acer saccharum</i>)	Cincinnati area, Ohio, U.S.A.	Riestedberg and Sovonick-Dunford (1983)
3.4-4.4	Hemlock (<i>Tsuga martensiana</i>) and spruce (<i>Picea sitchensis</i>)	Alaska, U.S.A.	Swanston (1970)
1.0-3.0	Douglas fir (<i>Pseudotsuga menziesii</i>)	British Columbia, Canada	O'Loughlin (1974)
3.0-17.5	Douglas fir (<i>Pseudotsuga menziesii</i>)	Western Oregon and Idaho, U.S.A.	Burroughs and Thomas (1977)
5.0	Yellow pine (<i>Pinus ponderosa</i>)	California, U.S.A.	Waldron and Dakessian (1981)
2.5-3.0	Alder (<i>Alnus</i> sp.), hemlock (<i>Tsuga</i> sp.), Douglas fir (<i>Pseudotsugamenziesii</i>) and cedar (<i>Thuja</i> sp.)	Washington, U.S.A.	Buchanan and Savigny (1990)

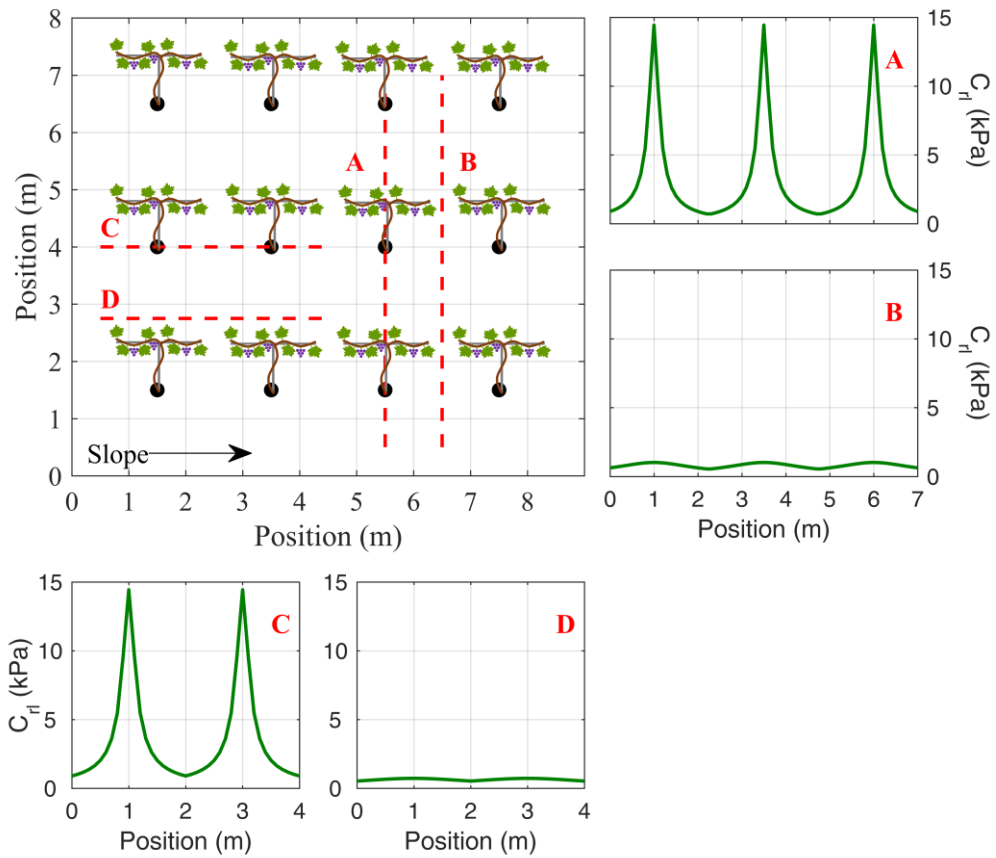


Figure 5.11. Application at stand scale of the combination between two sub-models (RDM and RBMw) to evaluate the spatial distribution of root reinforcement. The characteristics of the site are the same of the experimental vineyard (i.e. rootstock, cultivar, vine spacing, etc.). To better understand the variability of the root reinforcement, we considered four lines, two perpendicular (A and B) and two parallel (C and D) to the vine rows. The lines A and C show the trend of root reinforcement along a vine row, whereas the lines B and D along an inter-row.

5.5 Conclusions

Slope instabilities are common phenomena that affect steep terrain in areas with viticulture worldwide. Therefore, the design of vineyard plantations should consider the effects of their interactions with slope stability mechanisms in addition to agronomic and productivity parameters. In fact, the extension of vineyard cultivation to inappropriate sites and the adoption of more intensive practices to increase the economic return could increase the probability of slope failure and the resulting partial or total destruction of the plantations, as well as damages to structures and infrastructure.

It is well known that plants can stabilize the soil in principle, but in the case of grapevines, the quantification of such action is still lacking. In this work, we analysed in detail the root system of grapevines in an experimental vineyard located in Oltrepò Pavese, a wine-producing zone prone to slope failures and provided some data and a method suitable for adoption in other areas.

The results in terms of root density and 3-D distribution agreed with those reported by Bordoni et al. (2016) for a neighbouring area and agreed rather well with those reported in the literature for different contexts (e.g. Morlat and Jacquet, 2003; Hunter, 1998; Swanepoel and Southey, 1989), which suggests that they can be considered a general although approximate reference.

In terms of mechanical properties of grapevine roots, the only possible comparison was with Bordoni et al. (2016), who obtained very similar values. This was expected because both the studies considered the same rootstock in a similar area; more investigations are required to verify if different rootstocks, soil and climatic conditions, or agricultural practices (e.g. fertilization) can affect the mechanical properties of grapevine roots. Comparing grapevines with forest species, it was evident that root density was generally smaller, although more uniform in terms of 3-D distribution. Additionally, depth was more regular in grapevines than in forest species,

and generally, most of the grapevine roots did not deepen below the rootstock planting depth.

In terms of absolute values of additional root reinforcement, the average values obtained in this study for grapevines were within the range commonly estimated for many forest species. Looking at the spatial variability of root reinforcement, grapevines exhibited two traits that reflected the root spatial distribution and that can have a significant impact on slope stability: i) the root reinforcement decreased uniformly with distance from the plants, and ii) roots did not significantly stabilize the soil below the rootstock planting depth. Consequently, plantation design in terms of plant density, row distance and rootstock depth can seriously affect the stabilizing action of grapevines.

In conclusion, the methods and data provided in this study, in combination with slope stability models, will make it possible to evaluate the slope stability in vineyards as a function of plantation parameters (i.e., distance between vine row, distance between plants, density of plantation) and steepness, soil and climatic properties of the area. In this way, recommendations can be provided for reducing landslide susceptibility and avoiding economic losses.

Further development of this research will be directed to considering different agricultural practices and expanding the analysis to a larger scale.

6 ROOTED-SOIL UNDER COMPRESSION

Keywords:

Passive earth pressure;
Compression experiments;
Behaviour of compressed rooted-soils;
Slope stability;
Triggering mechanisms.

6.1 Introduction

Shallow landslides are a significant hazard in mountain areas due to their high frequencies and forecasting difficulties (Campbell, 1975; Kim et al., 2015; Mao et al., 2012). These phenomena control the landscape evolution as major landform-shaping processes (Anagnostopoulos et al., 2015; Istanbulluoglu and Bras, 2005; Milledge et al., 2014) and are often associated with numerous natural events such as soil instabilities (e.g. debris flow, soil slip) and various channel processes (i.e. large woody debris and sediment transport during floods, channelized debris flows) (Sidle and Ochiai, 2006). Predicting location, size and evolution of shallow landslides is a fundamental challenge at regional scales. Numerous methods have been developed over the years, from statistically-based approaches to physically-based spatially-distributed models (Brenning, 2005; Guzzetti et al., 1999; Mergili et al., 2014b; Montgomery and Dietrich, 1994; Pradhan, 2010). The latter provide a better understanding of triggering processes and thus are more suitable for designing appropriate measures for mitigating the consequences of these instability phenomena (van Beek and van Asch, 2004). Most of these models are based on the infinite slope stability model (Taylor, 1948), a simplified and well-known 2-D approach, or on a simple steady state assumption for hydrological soil conditions (Baum et al., 2002; Dietrich et al., 2001; Montgomery and Dietrich, 1994; Pack et al., 1998; Wu and Sidle, 1995). Additionally, some of these models include the beneficial effect on slope stability provided by vegetation through the root system, better known as root reinforcement (Burroughs and Thomas, 1977; Cohen and Schwarz, 2017; Hubble et al., 2013; Roering et al., 2003; Schmidt et al., 2001; Sidle et al., 1985). Roots increase the apparent soil cohesion and consequently augment the resistive forces that operate along the sliding surface (Wu and Sidle, 1995). This additional cohesion is known as basal root reinforcement. Although many studies have verified that the 2-D approach is suitable for the analysis of shallow landslide occurrences when the topography has a major

influence on the triggering mechanisms (Gorsevski et al., 2006b; Pack et al., 1998), some criticisms remain because of the absence of inter-slice interactions and the exclusion of lateral stresses (Casadei et al., 2003b; Duncan et al., 2014; Schmidt et al., 2001). For this reason, the resistant forces given by roots crossing the lateral surface of a landslide, so-called lateral root reinforcement (Burroughs, 1985; Chiaradia et al., 2016; Dietrich et al., 2007; Reneau and Dietrich, 1987; Schmidt et al., 2001), as well as lateral earth pressure forces (Dietrich et al., 2007) cannot be neglected.

Because of the significant limitations of the 2-D approach, 3-D limit equilibrium analysis have been developed and improved based on the pioneering work of Burroughs (1985). Burroughs proposed a simplified limit equilibrium force balance on a slope block with translation, assuming that failure occurs simultaneously with shearing at the boundaries without internal deformation. This model evaluates the Factor of Safety, FS , of each block as the relationship between the resistive and driving forces. The resistive forces are:

- (i) friction and soil cohesion on the basal area and the lateral faces;
- (ii) basal root reinforcement on the basal area;
- (iii) active earth pressure on the upslope side;
- (iv) saturated soil weight on the downslope side;
- (v) lateral root reinforcement on the lateral sides and upslope edge.

Terwilliger and Waldron (1991) included the lateral earth pressures due to the soil on the sides, top and toe of a sliding block inside their force equilibrium. To evaluate these pressures, they applied geotechnical theoretical calculations commonly used for the design of engineering structures such as retaining walls, sheet-pile walls, and braced and unbraced excavations (Bowles, 1997). Dietrich et al. (2007) proposed a simple 3-D force balance neglecting progressive failure, pore water pressure dynamics, and unequal stress-strain behaviour. They assumed vertical boundaries and characterised the shear resistance as the result of a combination of rooted-soil cohesion and friction. Recently, based on similar concepts, Milledge et

al. (2014) developed a multidimensional shallow landslide model, MD-STAB, to predict location and size of shallow landslides. Later, Bellugi et al. (2015a, 2015b) combined MD-STAB in a raster-based GIS and a spectral clustering search algorithm to predict size and location of shallow landslides across a natural landscape. More recently, Cislighi et al. (2017) and Dorren and Schwarz (2017) modified this approach by including a stochastic procedure for all input parameters and provided a probability of failure ($Pr[FS < 1]$) considering rectangular and elliptical landslide shapes, respectively. Cohen and Schwarz (2017) implemented force-displacement calculations of rooted soils under compression using the Discrete Element Method.

Although these approaches gave accurate results in different environmental contexts, they are all based on the assumption that the soil sliding mass behaves as a rigid block neglecting local failures, non-uniform stress field, and boundary conditions along the scarp and the toe prior to landsliding (Urciuoli et al., 2007). Furthermore, a soil element can support different stress configurations during landslide movement depending on time and location on the slope (Doglioni et al., 2013; Savage and Wasowski, 2006; Schwarz et al., 2015). Figure 6.1 illustrates the behaviour of three soil elements during the triggering of a shallow landslide schematically and located in three different positions of the sliding soil mass (A on the top, B in the central zone and C on the bottom), and in terms of displacement and soil stress configuration (D, E, F and G). The triggering mechanism consists in the formation of tension cracks above the soil element A because of local loss of shear strength (Figure 6.1, case 1 - soil configuration D). Subsequently, local failures continue to expand with increasing soil tensional forces within the tension crack (Figure 6.1, case 2 - soil configuration D). Simultaneously, the soil mass that breaks off along the failure surface increases the lateral compressive stress in the downslope zone of the landslide, around the soil element B. Once the resistive shear stress in each block has reached its maximum value, the failure surface expands downwards (Figure 6.1, case 2 - soil configurations E and F). As the soil mass

moves downward, compression of the soil elements increases at the toe of the landslide until the expansion of a runout (Figure 6.1, case 3 - soil configuration G). At the same time, the tension resistance remarkably decreases near the scarp (Figure 6.1, case 3 – soil configuration D).

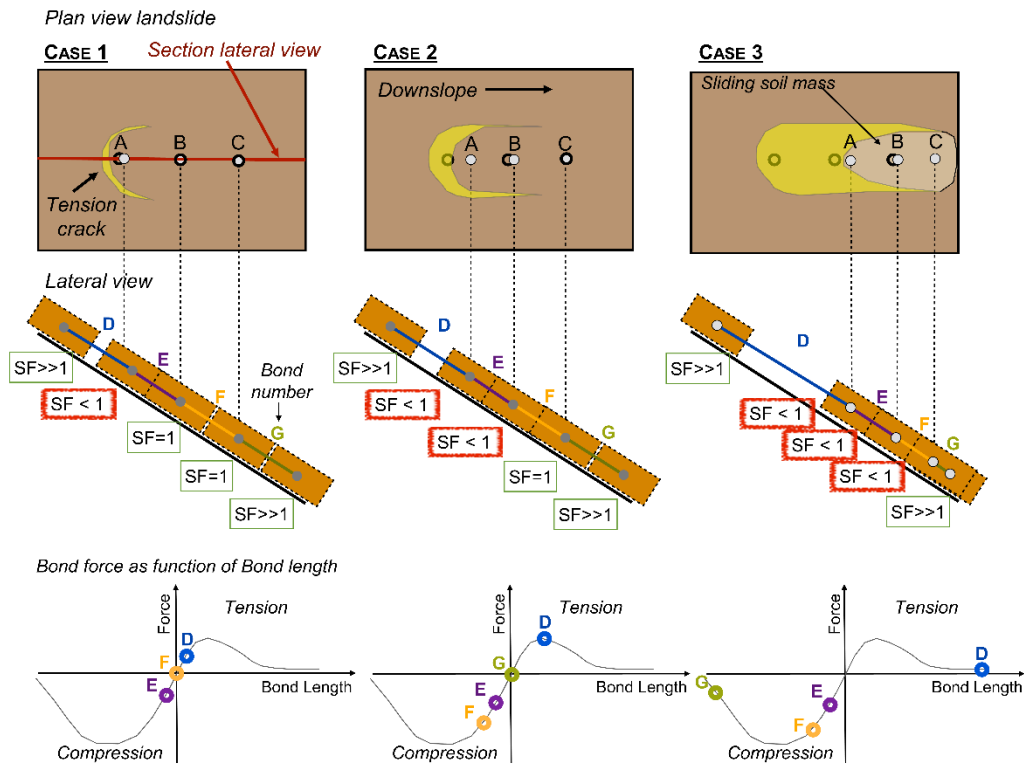


Figure 6.1. Schematic diagrams of the triggering mechanism during the formation of a shallow landslide: from the formation of tension cracks (case 1) to the compression phase (case 3). The points A, B and C represent three soil elements located at different places inside the landslide body, whereas D, E, F and G are the associated soil stress configurations showing displacement and stability of soil blocks along a downhill section. In particular, A-D indicate the tensile resistant near the scarp, B-E-F the increase in shear stress and C-G the compression stress during the failure.

Soil compression resistance has been generally evaluated as the passive earth force in the geotechnical literature. However, to be included into a slope stability analysis, this quantity requires a more thorough evaluation to prove

experimental measurements (Schwarz et al., 2015). Theoretical approaches for evaluating the passive earth force are numerous and date back to the eighteenth century (e.g. Coulomb, 1776; Culmann, 1886; Rankine, 1857; Rebhann, 1871); however, only few studies compared analytical calculations with field observations or laboratory experiments. Terzaghi (1920) measured the horizontal and vertical components of the passive earth force using a box of dry sands and a 0.05 m high wall on one side. Later, Fang et al. (1994, 1997, 2002) conducted experiments on a similar experimental setup with different cohesionless soils and with several backfill inclinations. Recently, Schwarz et al. (2015) investigated the effect of roots on compression resistance by compressing rooted and non-rooted soils using a custom-designed experimental laboratory setup. Notwithstanding these studies, data regarding the soil behaviour under compression are scarce and are usually limited to cohesionless soils in artificial conditions (i.e. in laboratory). In this context, our study aims to:

- (i) describe the behaviour between the compression force and the displacement in field experiments with cohesive soil;
- (ii) evaluate the differences between the passive earth force under dynamic and quasi-static conditions by interrupting the compression thrust at different time steps;
- (iii) compare the maximum measured passive earth resistance with theoretical calculations commonly used in geotechnical practice;
- (iv) verify which external factors mainly affect the resistive force;
- (v) measure the geometrical characteristics of the compressed wedge during the progression of the experiment.

These innovative measurements accurately illustrate the physical process of compression force mobilisation, typically occurring during the triggering mechanism of landslides. Finally, this study will be a crucial step to improve the 3-D slope stability approaches in order to upscale the analysis to larger scales (i.e. hillslope scale, watershed scale, regional scale).

6.2 Literature review of passive earth force

Estimating the passive earth force against retaining structures is an old and classic problem in soil mechanics. Several methods are available in the geotechnical literature such as limit equilibrium solutions (Krey, 1936; Patki et al., 2015), plasticity theory (Chen and Rosenfarb, 1973), method of slices (Janbu, 1957), empirical equations (e.g., Brinch Hansen, 1953), finite-element model (Duncan and Mokwa, 2001), and finite-difference computer method (Benmebarek et al., 2008). The first pioneering studies go back to the end of the eighteenth century and were developed by Coulomb (1776) and Rankine (1857). The general form of such theories is based on similar assumptions:

- (i) the soil is isotropic and homogeneous;
- (ii) the rupture surface is a plane and the compressed wedge has a planar surface (i.e. the backfill inclination β is null, see Figure 6.2 for a schematic of the compressed wedge);
- (iii) the friction resistance is distributed uniformly along the rupture plane;
- (iv) the failure of the wedge is a rigid body undergoing translation;
- (v) the failure is a plane strain problem.

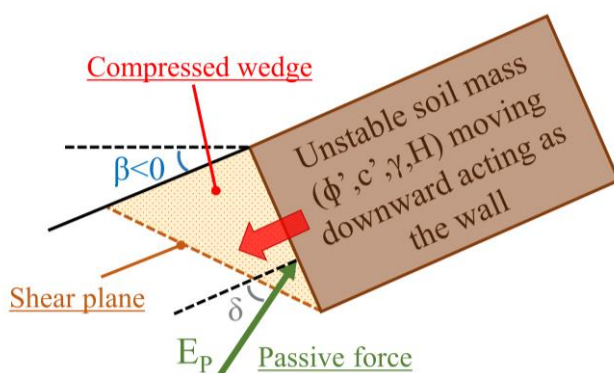


Figure 6.2. Schematic representation of the passive earth wedge (modified by Schwarz et al., 2015).

Coulomb's and Rankine's theories are widely accepted and commonly used in geotechnical practice. They provide closed form solution for evaluating the coefficient of passive earth pressure K_p . However, many authors observed and demonstrated that several assumptions are too constraining, such as a vertical retaining wall and a horizontal backfill (Benmeddour et al., 2012; Craig, 2013; Das, 2010; Fang et al., 1997; Kérisel and Absi, 1990; Terzaghi, 1943) and proposed modifications and improvements. Müller-Breslau (1906) generalized the Coulomb's theory, named gen-Coulomb hereafter, for cohesionless soils, considering also a backfill inclination (β), the frictional interaction angle between wall and soil (δ), and the angle of the internal face between wall and vertical direction (λ). Müller-Breslau proposed a closed form formulation for evaluating K_p :

$$K_p = \frac{\cos^2(\phi' + \lambda)}{\cos^2(\lambda) \cos(\delta - \lambda) \left[1 - \sqrt{\frac{\sin(\phi' + \delta) \sin(\phi' + \beta)}{\cos(\delta - \lambda) \cos(\beta - \lambda)}} \right]^2} \quad (6.1)$$

where ϕ' is the soil internal friction angle. Later, Terzaghi (1943) investigated the active and passive Rankine stress-state in a semi-infinite mass of cohesive soil with inclined backfill and developed a graphical method for solving retaining wall problems. Based on that study, Mazindrani and Ganjali (1997) proposed an analytical procedure for evaluating K_p (equation 6.2), easier to use, called gen-Rankine here:

$$K_p = \frac{1}{\cos^2(\phi')} \left\{ \begin{array}{l} 2 \cos^2(\beta) + 2 \left(\frac{c}{\gamma H} \right) \cos(\phi') \sin(\phi') + \\ \sqrt{4 \cos^2(\beta) [\cos^2(\beta) - \cos^2(\phi')] + 4 \left(\frac{c}{\gamma H} \right)^2 \cos^2(\phi')} \\ + 8 \left(\frac{c}{\gamma H} \right) \cos^2(\beta) \cos(\phi') \sin(\phi') \end{array} \right\} - 1 \quad (6.2)$$

where γ is the unit of soil weight, c is the soil cohesion and H is the soil depth. To calculate the passive earth force per unit length E_p , the formulation is:

$$E_p = \frac{1}{2} \gamma H^2 K_p + 2 c' H \sqrt{K_p} \quad (6.3)$$

where c' is the soil effective cohesion and K_p can be evaluated using equation 6.1 or equation 6.2.

Many researchers defined the sliding failure surface as a circular arc or combinations of straight lines and curves, based on the limit equilibrium of the soil wedge (Caquot and Kérisel, 1948; Janbu, 1957; Krey, 1936; Morrison Jr and Ebeling, 1995; Terzaghi, 1941), overcoming the planar restrictions of Coulomb's and Rankine's theories. Soubra et al. (1999) developed a variational limit equilibrium method that combines a moment equilibrium equation with a logarithmic spiral failure surface. Such wedge geometry provides more accurate prediction than the planar failure surface models (Kumar and Subba Rao, 1997). Soubra and Macuh (2002) developed a spreadsheet tool for the general case (i.e. sloping backfill, frictional and cohesive soil, uniform surcharge), described in more details in Appendix E, and called the log-spiral approach. In this case, the effects of soil weight, vertical surcharge loading, and cohesion are represented by different coefficients, $K_{p\gamma}$, K_{pq} , and K_{pc} , and the passive earth force can be expressed as follows:

$$E_p = K_{p\gamma} \frac{\gamma H^2}{2} + K_{pq} q H + K_{pc} c H \quad (6.4)$$

where q is the vertical surcharge loading.

Most studies on calculating passive earth force neglect the effects of the third dimension. Blum (1932) conducted the first study focused on this issue. Blum's formulation is an extension of the traditional one-block Coulomb's mechanism using the limit equilibrium solution neglecting the frictional forces acting on lateral planes. Later, Soubra et al. (2000) and Soubra and

Regenass (2000) investigated several translation failure wedges using the limit equilibrium analysis such as one-block mechanism, multi-block mechanism, and truncated multi-block mechanism. Their results emphasized that the truncated solid multi-block failure gave accurate and reliable solutions for the practical use when compared to Blum's approach. Meanwhile, Regenass et al. (2000) reviewed the numerical and experimental studies of the 3-D solution and proposed a synthesis based on the previous study of Horn (1972). They underlined a wide variability of the quantification of this factor, mainly due to different tested soils, different experimental setups, and the lack of a standard procedure. Nevertheless, they presented an empirical simple formulation:

$$K_{P3D} = K_P \left(1 + C \frac{H}{B} \right) \quad (6.5)$$

where B is the wall width and C is a shape factor (dimensionless) that varies in the literature from 0.04 to 1.37 with an average value of 0.52 for H/B less than 1 (Regenass et al., 2000).

Later, Škrabl and Macuh (2005) presented an approach based on 3-D, kinematically admissible, rotational and hyperbolic failure mechanisms composed of one central and two lateral bodies, and evaluated it using the framework of the limit analysis theory. Škrabl (2008) improved the previous version by implementing a 3-D logarithmic spiral. Another similar approach was proposed by Vrecl-Kojc and Škrabl (2007), who applied the upper bound theorem of limit analysis considering a kinematically admissible failure geometry subdivided into three simplified rigid blocks. The main difference as compared to other models is that the lateral parts are composed of a family of cone envelopes. Other studies used the explicit finite difference code FLAC^{3D} (Fast Lagrangian Analyses of Continua) to investigate the 3-D passive earth pressures induced by the translation of a rigid rough retaining wall for associative soils and the increase of the passive earth coefficient with decreasing the wall width (Benmebarek et al., 2008; Khelifa and

Benmebarek, 2014). More recently, Motta and Raciti (2014) estimated 3-D effects through a practical closed form solution only applicable for cohesionless soil.

6.3 Materials and methods

6.3.1 Study area

For the field measurements, we selected a study site located in a forested area (WGS84, latitude 46.8160 N, longitude 7.8235 E) on the north-facing slope of the Honegg ridge near the village of Schangnau in the Emmental (Canton of Bern, Swiss Prealps, Switzerland). The average elevation is around 1000 m a.s.l. and the mean slope is around 25°. The climate is humid continental, typical for Central Alpine north-facing slopes with annual precipitation ranging from 1500 and 1700 mm and mean annual air temperatures of around 6.5 °C (Meteo Swiss, 2015).

From the geological point of view, the study site is located at the southern boundary of the Molasse basin at the border of the Subalpine Molasse (clastic sedimentary rocks). Soil thickness is around 2 m on average and rocks fragments are generally present in soil depths between 0.30 and 0.50 m. The deeper soil layer mainly consists of Pleistocene moraine material that was deposited during the last glacial maximum by the Emme glacier and the shallower soil layer above it is composed of a Holocene weathered hillside regolith (geological map of Switzerland 1:25000, Swiss Federal Office of Topography, www.swisstopo.admin.ch, 2012). Moreover, it is likely that mudflow material was periodically deposited due to the high vulnerability of the study area to shallow landslides and debris flows.

The study area is almost completely covered by a coniferous forest where European spruce (*Picea abies* (L.) Karst) and silver fir (*Abies alba* Mill.) are the predominant species (respectively 70% and 30%); however, European beech (*Fagus sylvatica* L.) and sycamore maple (*Acer pseudoplatanus* L. [1753]) are also present. A nearly homogeneous forest canopy covers about 80% of the ground, seldom interrupted by small gaps. This forest is managed

as a protection forest for slope stabilization and for soil protection from erosion in agreement with the Swiss national directives (Frehner et al., 2005).

6.3.2 Soil properties

Soil properties of the study site were determined by analysing one cubic meter of soil excavated from the A horizon within the top 0.40 m as described in detail by Schwarz et al. (2015). Grain size distribution, Attenberg's consistency limits and Proctor compaction test were carried out in the laboratory to measure density and water content of soil subsamples (Table 6.1). According to the Unified Soil Classification System (USCS), the soil was classified as a clayey gravel (GC) with sand. Additionally, the coefficient of uniformity, CU_d , indicated that the first layer of soil was well graded and compressible and the plasticity index, PI , revealed that the consistency was sensitive to the variation of water content. In addition, direct shear tests were conducted to estimate several geotechnical parameters at three different soil water contents (sc-1, sc-2 and sc-3 in Table 6.2). Such properties are: bulk density prior the experiment ρ_B , porosity n , the water content θ with indices g and v indicating the gravimetric and volumetric values, respectively, the degree of saturation S_R , the effective angle of internal friction ϕ' and the effective cohesion c' .

Table 6.1. Mechanical properties of the soil in the experimental site. The parameters W_{Pr} , ρ_{Pr} and D_{Pr} are derived from a Proctor test according to SN 670330-2 on the material's fraction with particle size less than 4.0 mm; W_L , W_p and I_p are derived from testing the material fraction < 0.5 mm according to SN 670345-b. All other parameters are derived from testing the fraction < 0.5 mm according to SN 670004-2b (modified from Schwarz et al., 2015)

Symbol	Mechanical property	Unit of measure	Values
c_C	content of clay	% by mass	6.2
c_M	content of silt	% by mass	34.6
c_S	content of sand	% by mass	28.6
c_G	content of gravel	% by mass	30.7
C_{ud}	coefficient of uniformity	-	87.3
C_{Cd}	coefficient of curvature	-	0.9
W_L	water content at liquid limit	% by mass	33.2
W_P	water content at plastic limit	% by mass	22.5
I_P	plastic index	% by mass	15.3
W_{Pr}	optimum water content	% by mass	15.3
ρ_{Pr}	material's maximum density	$g\ cm^{-3}$	1.81
D_{Pr}	material's degree of compaction	%	86.7

Table 6.2. Soil shear parameters of the fraction < 0.5 mm for three samples with different water contents (sc-1, sc-2 and sc-3). v is shearing rate (in $mm\ s^{-1}$); ρ_B is bulk density measured prior to the experiment when the soil was formed in the device (in $g\ cm^{-3}$); n is porosity (in $m^3\ m^{-3}$); ϑ is water content with indices g and v indicating gravimetric and volumetric values, respectively (in % by mass); S_R is degree of saturation (in $m^3\ m^{-3}$); ϕ' is effective angle of internal friction (in deg); c' is effective cohesion (in $kN\ m^{-2}$). The direct shear tests were performed in accordance with the standard DIN 18137 (modified from Schwarz et al., 2015).

Symbol	v	ρ_B	n	θ_g	θ_v	S_R	ϕ'	c'
sc-1	0.04	1.57	0.420	19.43	0.304	0.725	23.7	21.6
sc-2	0.04	1.56	0.421	22.84	0.357	0.849	24.1	18.1
sc-3	0.04	1.56	0.424	27.22	0.423	0.998	27.1	13.5

6.4 Field measurements

6.4.1 Experimental equipment

The compression experiments were carried out using an experimental setup described in Schwarz et al. (2015) and specifically adjusted for field tests. Figure 6.3 shows a simplified diagram of the field setup. The compression machine is composed of a steel structure, a stiff plate and an electro-mechanic actuator. The dimensions of the steel structure are 1.10 m x 0.72 m x 0.60 m. The stiff plate is 0.02 m thick, 0.72 m wide and 0.38 m high and is attached to an in-feed slide. Inside the steel structure, an electro-mechanic actuator (MecVel, AV3 model) moves the stiff plate in horizontal direction through two sets of two roller bearings sliding on four tracks at a constant velocity of 5 mm s^{-1} to a maximum stroke of 0.40 m. The electric actuator requires a power supply of 400 V produced by a gasoline electric power generator (Kraftech, KT-8500W-Mobile). The compression machine is equipped with: (i) a displacement sensor (Burster GmbH, potentiometric displacement sensor model 8719, accuracy $\pm 0.05\%$) to measure the relative horizontal displacement; (ii) four load cells (Burster GmbH, miniature ring load cell model 8438, 50 kN, accuracy $<1\%$) located on the four edges of the stiff plate; and (iii) a data logger (Campbell Scientific, CR1000) to record and store the measurements at time intervals of 1 s. The displacement sensor was calibrated using five fixed points, whereas load cells were calibrated with known weights. In addition, five soil moisture sensors (Decagon, 10HS, $\pm 3\%$ accuracy by volume) were positioned at 0.10 m of depth and at 0.15 m and 0.30 m from the stiff plate to monitor the volumetric water content. The measurements were recorded every 60 s using another data logger (Decagon, Em50).

During each experiment, three scans of the ground surface were performed using a laser scanner (FARO, Focus 3D model). The scanner completes a scan in 30 minutes with a scan speed of $244,000 \text{ dots s}^{-1}$ and a resolution of

1.50 million dots m^{-2} . The accuracy is ± 2 mm for a distance between the scanner and an object in the range of 10-25 m.

To determine the effects of rainfall on the passive earth force, we irrigated the superficial ground during a number of compression experiments using a rain simulator. It consisted of a square aluminium plate (1.00 m x 1.00 m) with small tubes attached to 100 perforated holes. The tubes were mounted in a 0.10 m x 0.10 m square pattern and had inner diameters of 2 mm that led to a small cylindrical reservoir. During the irrigation, an electric motor moved the plate back and forth by 0.05 m in horizontal direction and a flow meter controlled the intensity of the rainfall. The rain simulator was fed by a water-filled tank through a hydraulic pump. According to Lange et al. (2009, 2011), the recommended distance between plate and soil surface lies between 0.30 m and 0.50 m.

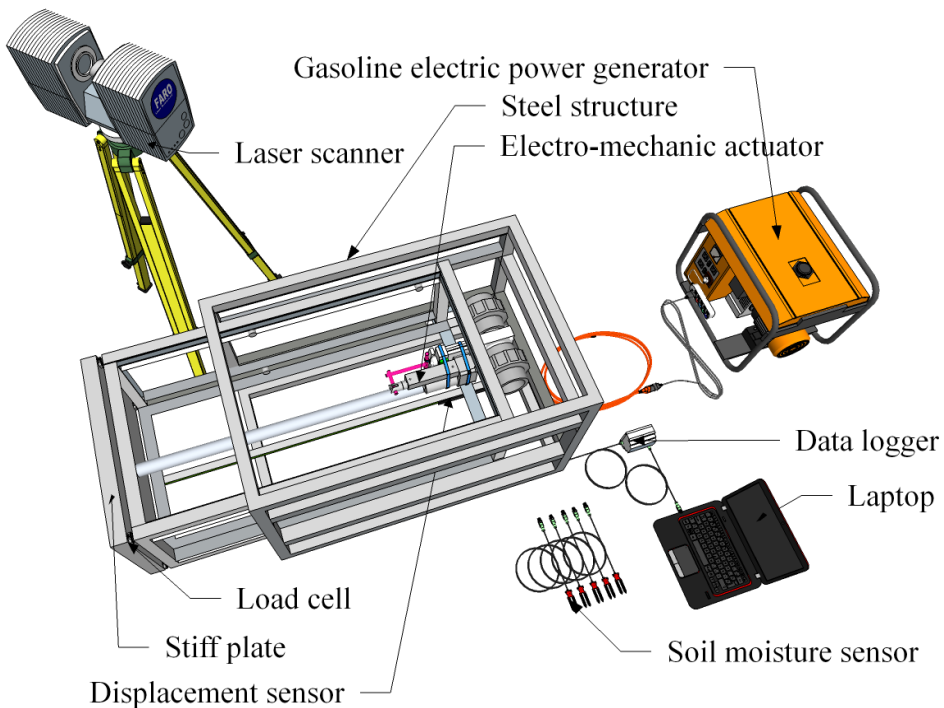


Figure 6.3. Schematic drawing of experimental equipment: the compression machine with sensors, data-logger and electric power generator and the laser scanner.

6.4.2 Experimental procedure

Experiments were conducted to measure the variation of the soil compression force, F_p , as a function of external factors such as H , β , θ and the displacement Δx . Figure 6.4 summarizes the experimental procedure with some photographs showing several field operations. First, we removed the upper 0.10 m of the superficial soil layer mainly composed of organic matter. Then, we manually excavated a trench 1.20 m x 1.00 m large and approximately 0.50 m deep with shovels and pickaxes, taking care not to damage the root system. Once the trench was excavated, we counted roots crossing the downslope profile and measured their diameter using an electronic calliper. Additionally, we assembled the compression machine with all sensors and the data logger and placed it into the trench. Then, we fixed the compression machine using a wooden plate and two wooden sticks on the upslope side and we filled and compacted the backfill with soil and stones. This anchorage served to avoid an uphill movement of the machine and to measure only the displacement in the same direction of the mechanical thrust. During the entire experiment, the inclination of the compression machine was monitored using an accelerometer sensing inclination. Five soil water content sensors were introduced into the soil. Before each experiment (“control”), the laser scanner scanned the soil surface in front of the compression machine creating a 3-D image.

The compression experiment consisted in a series of “loading step” during which the soil was displaced by 0.05 m. After every 0.05 m of displacement, the loading step was interrupted by “pause”. The experiment started through the activation of the electro-mechanic actuator that moved the compression plate toward the downhill soil with a constant velocity of 5 mm s^{-1} . The pauses allowed us to evaluate the behaviour of the compression force both in dynamic and quasi-static states. The displacement was repeated after a minimum pause of 25 minutes until a maximum displacement of 0.35 m was reached. Scans were conducted at the beginning (“control”), at the second pause (“pause-2”) and at the end of each experiment.

For the experiments with simulated rainfall, the irrigation started after “pause-2”. We positioned the rainfall simulator above the downslope wedge in front of the compression machine. Each irrigation event lasted for about 60 minutes and the volume flux density of irrigation was 70 mm h^{-1} . This amount of rainfall corresponds to the maximum hourly precipitation rate with a return period of 100 years for this region (Lange et al., 2009).



Figure 6.4. a) Flowchart of the experimental procedure; and b) photographs at different stages of an experiment.

6.4.3 Data processing

Effects of interface friction

The mobilisation of the compression resistance occurs when a soil wedge moves downward along a hillslope. This process depends on several factors, such as (i) amount and direction of movement, (ii) strength and stiffness of soil, and (iii) friction/adhesion between the pushing soil wedge and the compressed one (Duncan and Mokwa, 2001). The experimental design of this study allows us to measure the component of the compression force perpendicular to the stiff plate, $F_{P\perp}$, with four load cells located at its corners. However, the interfacial friction between the plate and the soil modifies the direction of the compression force (Bowles, 1997). To correct this effect, it is possible to evaluate the vector force F_P , oriented at an angle δ , known as the interface friction angle (Figure 6.2). This angle depends on soil properties such as the roughness of the interface and the relative shear displacement along the interface (Duncan and Mokwa, 2001). To estimate the magnitude of δ , and consequently F_P , we wrote a force balance acting on the plate (equation 6.6) and corrected $F_{P\perp}$, taking into account the component of compression force parallel to the plate (equation 6.7).

$$\delta = \arctan\left(\frac{W_{CM} \cos \alpha}{F_{P\perp} + W_{CM} \sin \alpha}\right) \quad (6.6)$$

where W_{CM} is the weight of the compression machine with one side on the ground and α is the inclination of the compression machine.

$$F_P = \frac{F_{P\perp}}{\cos \delta} \quad (6.7)$$

Effects of roots

The measured passive earth force includes the contribution of the root reinforcement. Root reinforcement under compression is mobilised across the shear plane that develops during the compression and leads to a complex bending-buckling-tensioning of the roots (Wu et al., 1988). To evaluate such contribution, Schwarz et al. (2015) proposed a fibre bundle model adapted to roots in compression, called Co-RBMw (Compressed - Root Bundle Model Weibull). They assumed that the maximum root-buckling force can be estimated as a function of root diameter using a two-parameter power law function:

$$F_{rb}^{ult} = F_0 \phi^\xi \quad (6.8)$$

where F_{rb}^{ult} is the maximum buckling-tensile force, ϕ is the root diameter, ξ is the empirical exponent, and F_0 is a multiplicative constant. This model considers the root reinforcement as a function of displacement, root diameter distribution, and the cumulative Weibull probability distribution of root strength within a single root diameter class. Thus, it estimates the total contribution of a root bundle to the compression force F_{rb-tot} by summing the force provided by each root diameter class i , $F_{rb-i}(\phi_i, \Delta x)$, multiplied by a survival function, S , as follows:

$$F_{rb-tot}(\Delta x) = \sum_{i=1}^{n_c} N_i F_{rb-i}(\phi_i, \Delta x) S(\Delta x^*_i) \quad (6.9)$$

where n_c is the number of root diameter class, N_i is the number of root in class diameter i , ϕ_i is the diameter of root class i , Δx is the displacement, and Δx^* is the normalized displacement respect than that measured when the compression force is maximum. $F_{rb-i}(\phi_i, \Delta x)$ is the individual root force that can be estimated using Hooke's law for elasticity:

$$F_{rb-i}(\phi_i, \Delta x) = k(\phi) \Delta x \quad F_{rb-i}(\phi_i, \Delta x) < F_{rb}^{ult}(\phi) \quad (6.10)$$

where k is the spring constant (dimensionless) that is a function of ϕ through the following linear relationship (k_i and k_p are the two linear parameters), empirically evaluated by Schwarz et al., (2011):

$$k(\phi) = k_i + k_p \phi \quad (6.11)$$

k incorporates the mechanical properties of the root-soil system under specific conditions (root diameter, tree species, forest stand characteristic, soil properties, soil confining pressure, soil density, moisture conditions).

The survival function S describes the probability that roots break with increasing displacement and assumes a Weibull probability distribution (Schwarz et al., 2015, 2013):

$$S(\Delta x_i^*) = \exp \left\{ - \left[\frac{\Delta x_i k(\phi)}{\lambda F_{rb}^{ult}(\phi)} \right]^\omega \right\} \quad (6.12)$$

where λ and ω are the scale and the shape dimensionless Weibull parameters.

The Co-RBMw model includes six different parameters (F_0 , ξ , k_i , k_p , ω and λ) that have to be calibrated. Values were estimated in Schwarz et al. (2011, 2013, 2015) and are: $F_0 = 6.5 \times 10^5$ N, $\xi = 1.67$, $k_i = 480$ N mm⁻¹, $k_p = 10.2 \times 10^5$ N mm⁻², $\omega = 1$ and $\lambda = 1$. The location of the soil profiles for the compression tests were chosen to minimize the influence of root reinforcement (as far as possible from tree stems).

Dynamic vs quasi-static force analysis

Our study includes the analysis of the differences between dynamic and quasi-static force measurements. As previously described, the experiment consists of a series of loading steps at a constant velocity of 5 mm s⁻¹ interrupted by pauses of 25 minutes. Excluding the effect of interface friction (equation 6.7) and the contribution of roots on soil resistance (equation 6.9), the corrected force corresponds to the dynamic compression force, F_{dyn} . The

alternation between loading steps and pauses generates a transition from dynamic to quasi-static state. As expected, F_{dyn} rapidly declines to a constant asymptotic value during the pause, while the compression machine keeps the displacement constant. The constant asymptotic value corresponds to the quasi-static compression force, called F_{q-s} hereafter. The decline of F_{dyn} assumes a behaviour that is described by a three-parameter negative exponential function as follows:

$$\frac{F_{dyn}(t)}{F_{dyn}^*} = a t^b + c \quad (6.13)$$

where F_{dyn}^* is the value of F_{dyn} at the interruption of the loading, t is the time, and a , b and c are the three coefficients of the exponential function. To compare measurements with theoretical calculations obtained by equations 6.3 and 6.4, we normalized the maximum values of F_{q-s} by the length of the stiff plate to obtain a compression force per unit length.

Geometry of compressed wedge

For each experiment, three scans were done at the start (control), at “pause 2”, and at the end of the experiment. We post-processed the scanner-created point clouds using the software PointCab (Point Cloud Software Company GmbH, 2015). The main output is a 3-D image and raster map with a resolution of 0.01 m. By overlapping raster maps, we were able to measure changes in the soil surface during the progression of the experiment and the extension of the compressed wedge in terms of its size and volume. The geometrical measurements consisted of 1-D geometrical characteristics such as the length, L , the width, W , and the discrepancy between the soil surface before and after the experiment, Δz . Figure 6.5 shows a plan-view photograph of an experiment and the post-processed raster in which the colour scale emphasizes the extension of the compressed wedge and the values of Δz . In terms of volume, a simple balance allows us to evaluate the 3-D volumetric difference, ΔV_{3D} , as follows:

$$\Delta V_{3D} = (V^* - V_M) + (V_S - V^*) = V_S - V_M \quad (6.14)$$

where V^* is the soil volume subject to passive earth pressure, V_M is the moved volume after the movement of the stiff plate, and V_S is the volume difference between the loading step 0 and the next scan.

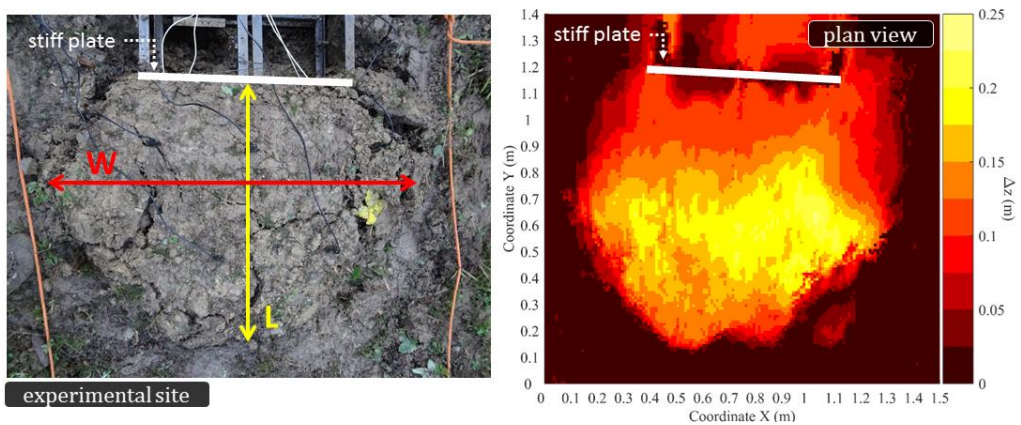


Figure 6.5. a) Plan view of the experimental site at the end of an experiment with a maximum displacement is approximately 0.35 m. The compressed wedge and cracks/fractures on the soil surface are clearly visible. b) The post-processed image of the soil surface scan. The colour scale emphasizes the extension of the compressed wedge and the value of discrepancy in terms of soil surface height.

Figure 6.6 shows a lateral view of the soil mass involved in the experiment in which V^* is the area bordered by the green line, V_M is the yellow area and V_S is the blue area.

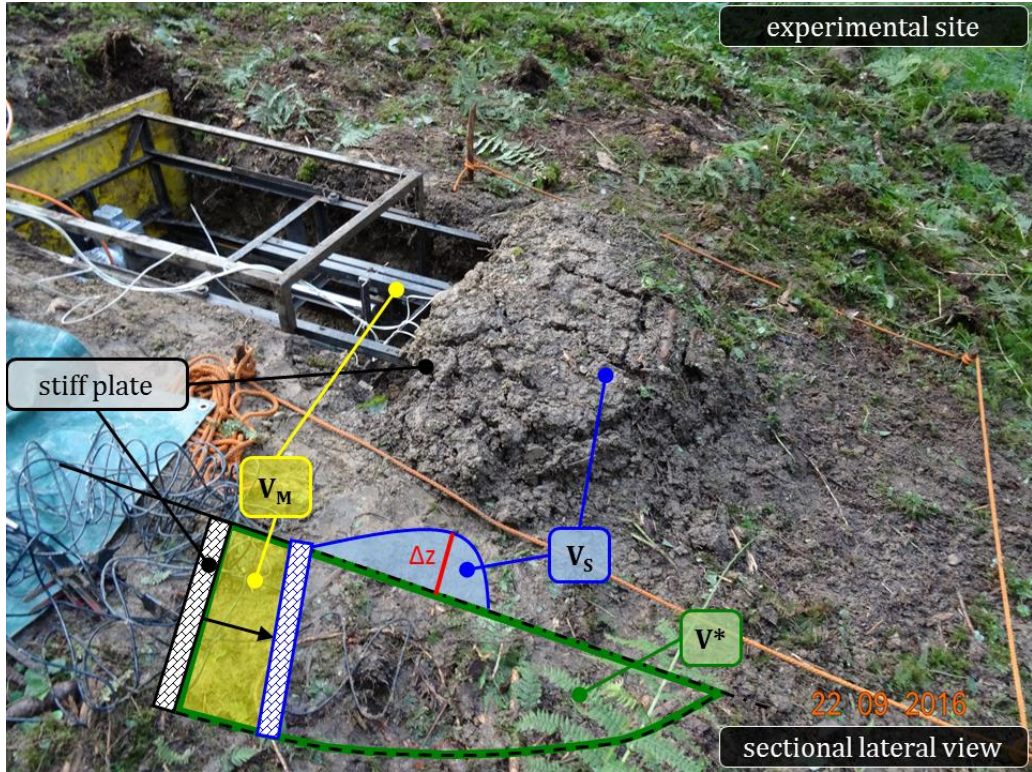


Figure 6.6. Photograph of the experiment at end of compression, and schematic of lateral view of the experiment. V^* is the unknown soil volume moved by the stiff plate, V_M is the moved soil volume, and V_S is the difference of soil volume between the condition of soil surface pre- and post-experiment.

6.5 Results

6.5.1 Experimental measurements

Eleven compression experiments were performed in September of 2016: four in natural condition (i.e. θv is almost constant) and seven tests with simulated rainfall.

H ranged between 0.38 m to 0.50 m with β varying from 13.4° to 28.1° . Soil moisture conditions were determined by measuring θv that ranged between 0.292 and 0.405 with an average value of 0.361 ± 0.040 . We evaluated the presence of roots using the Root Area Ratio (RAR, % by surface), the relationship between the total cross-sectional area of all roots and the soil area, a common indicator of root density (e.g. Bischetti et al., 2005; Docker and Hubble, 2008; Preti and Giadrossich, 2009). RAR varied from 0.12% to 5.22%. The force measurements taken by the four load cells located on the four vertexes of the stiff plate were summed to provide $F_{p\perp}$ exerted during the experiments. The corrections due to the frictional angle between the stiff steel plate and the compressed soil were almost negligible. The contribution of root reinforcement, however strongly depends on the presence of roots and the maximum value of F_{rb-tot} was estimated to be between 0.08 kN and 2.04 kN using Co-RBMw (equation 6.10).

The measured behaviour of the dynamic force as a function of displacement, $F_{dyn}(\Delta x)$ showed a typical rapid increase until the ultimate compression resistance is reached, followed by a moderate decline reaching a residual value (Figure 6.7a). The maximum values of F_{dyn} varied from 8.49 kN to 31.67 kN and occurred inside a range of Δx between 43.2 mm and 85.2 mm. If this displacement was normalized by H , it varied from 0.10 to 0.19 with an average value of 0.152 ± 0.026 . The residual compression force and the maximum dynamic force ascended from 2.72 kN to 22.58 kN. Moreover, the measurements of soil moisture during the experiments indicated that θv increased up to the ultimate passive earth force and slightly decreased to a residual constant value (Figure 6.7b).

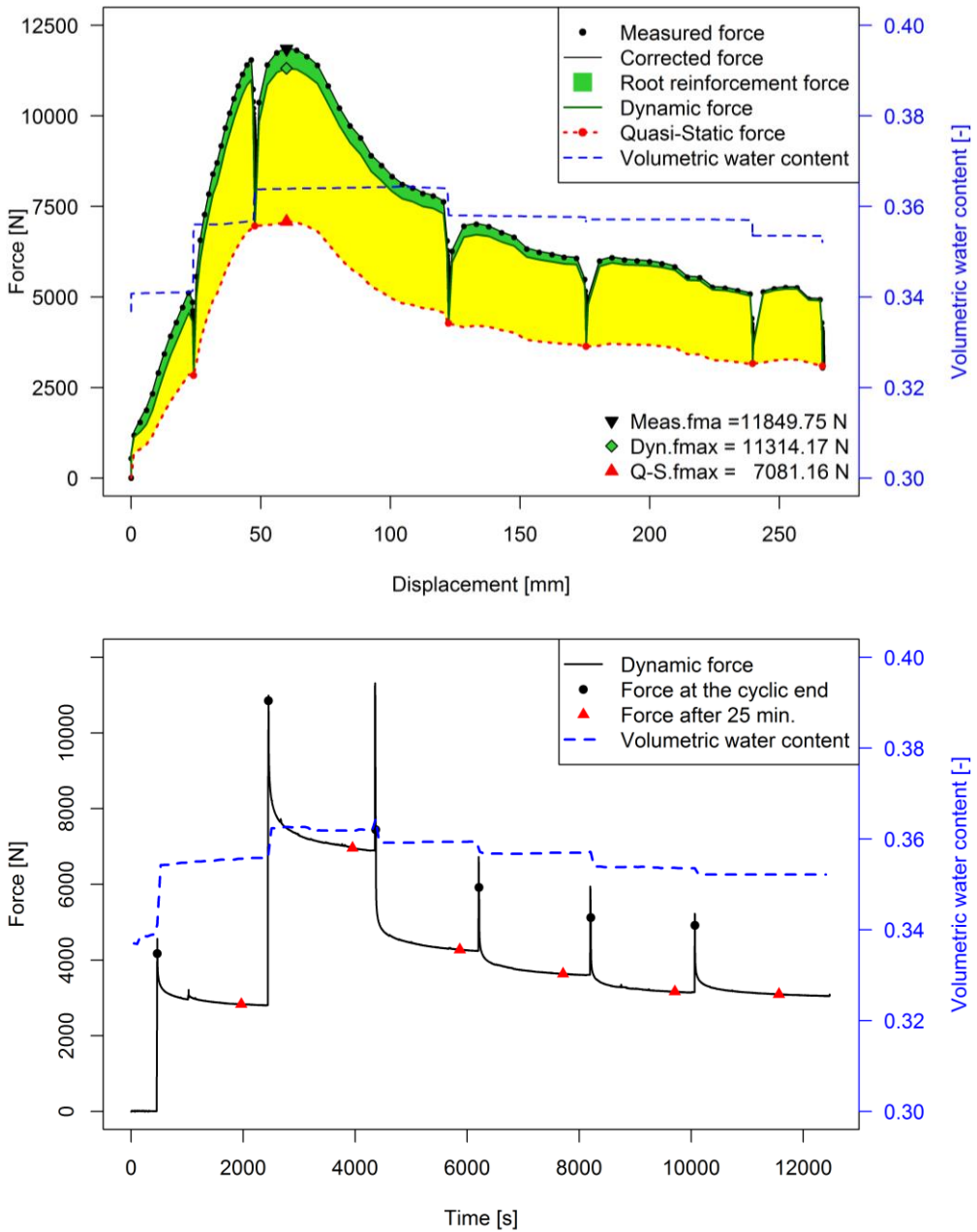


Figure 6.7. a) Force in function of displacement, and b) force in function of time. The dynamic force before the pause corresponds to the black circle and the quasi-static force at the end of the pause to the red triangle.

6.5.2 Friction between stiff plate and compressed soil wedge

As expressed in equation 6.6, it is possible to calculate δ by monitoring the inclination of the compression machine α during the experiment. The angle δ assumes a minimum value δ^{\min} at the same time $F_{p\perp}$ reaches its maximum value. The inclination α between “control” and the end of the experiment varied from 1.80° to 8.90° with an average value of $5.41^\circ \pm 2.08^\circ$. Consequently, δ^{\min} ranged from $0.042 \phi'$ to $0.159 \phi'$ with an average value of $0.094 \phi' \pm 0.032 \phi'$ (Figure 6.8). Furthermore, δ increased until a constant value δ^{res} ranging from $0.057 \phi'$ to $0.373 \phi'$ with an average value of $0.258 \phi' \pm 0.100 \phi'$ (Figure 6.8). These values were greater than δ^{\min} .

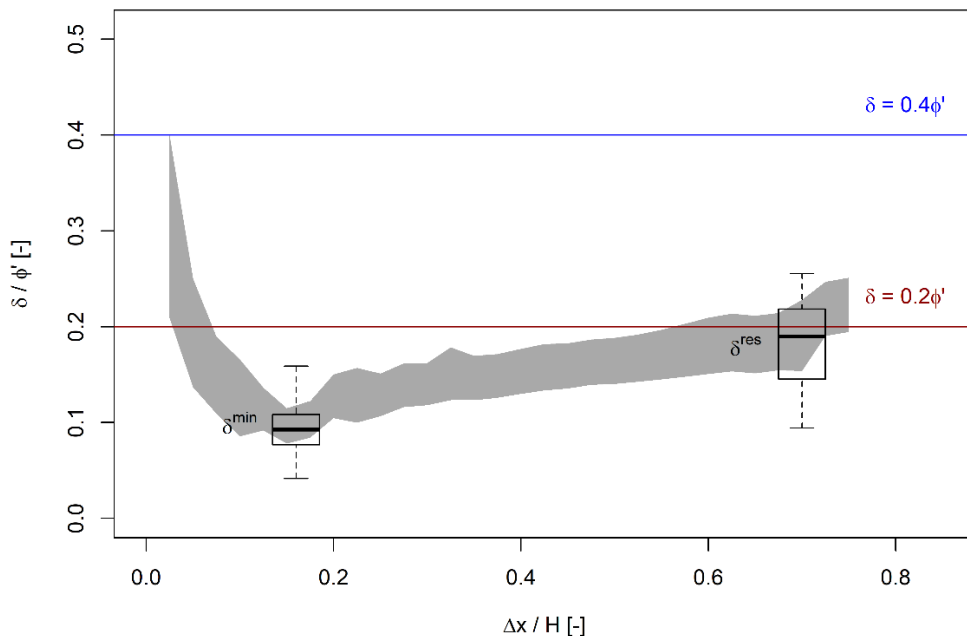


Figure 6.8. Evolution of friction angle between wall and soil, δ , during the experiment. The relationship between δ and the angle of soil internal friction is shown on the vertical axis and the relationship between displacement Δx and soil depth H on the horizontal axis. The grey area corresponds to the 95% confidence interval of all experiments, whereas the two boxplots refer to δ^{\min} the minimum value of friction angle and to δ^{res} at the end of the experiments.

6.5.3 Dynamic and quasi-static force

The procedure applied to estimate F_{q-s} consisted of calculating the difference between the monitored force at the end of each loading step (black circle in Figure 6.7b) and after a 25 minute pause (red triangle in Figure 6.7b) for each pause of every experiment. Figure 6.9 shows the behaviour of the normalized F_{dyn} for its maximum value F_{dyn}^* . A rapid decline of the compression force is clearly visible. The F_{dyn} / F_{dyn}^* curve declined until it reached a quasi-asymptotic value at the end of each pause, apparently reaching the quasi-static condition, denoted Γ for simplicity. This value indicated an evident difference between the two states and Γ varied from 0.471 to 0.784 with an average value of 0.614 ± 0.071 as shown in the boxplot in Figure 6.9. The variability of Γ is large, as shown by the presence of five outliers. They are, however equally distributed on both sides of the boxplot. Additionally, Γ was individually evaluated for each experiment taking the soil moisture condition into account (Figure 6.10): the first four in natural condition and the seven others in artificial soil moisture condition due to the simulated rainfall. Figure 6.10 shows that Γ is 0.60, on average, with moderate variability. However, exceptions were also evident: for example, experiment #05 was conducted on a rainy day and shows low Γ values, whereas during the second part of experiment #11, the steel structure of the compression machine nearly collapsed forcing us to stop the test. Although we collected several measurements under different soil moisture conditions, no generalities can be made about the differences between the unsaturated and saturated (i.e. after irrigation) conditions. F_{q-s} was evaluated reducing F_{dyn} by Γ and its maximum values ranged from 5.61 kN to 24.55 kN, as shown in Figure 6.11. Finally, we evaluated the soil stiffness as the ratio between the ultimate F_{q-s} and the corresponding Δx . The soil stiffness varied from 0.094 kN mm^{-1} to 0.310 kN mm^{-1} with an average value of $0.171 \text{ kN mm}^{-1} \pm 0.070 \text{ kN mm}^{-1}$ and increased with increasing soil depth. We then grouped the experiments in three different classes 0.36-0.42 m, 0.42-0.46 m and 0.46-0.50 m. Inside these classes, the soil stiffness had a small standard deviation and assumed

average values equal to $0.107 \text{ kN mm}^{-1} \pm 0.011 \text{ kN mm}^{-1}$, $0.207 \text{ kN mm}^{-1} \pm 0.022 \text{ kN mm}^{-1}$ and 0.310 kN mm^{-1} , respectively.

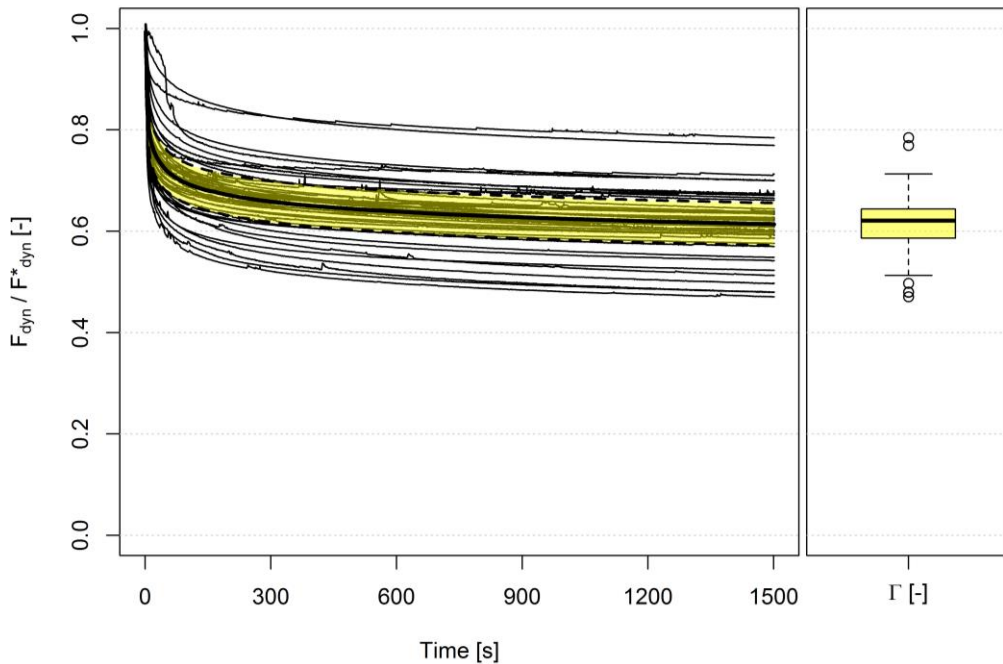


Figure 6.9. Normalized dynamic force vs time during 25 minutes of pause. On the right, boxplot displays the variability of the minimum values of normalized dynamic force.

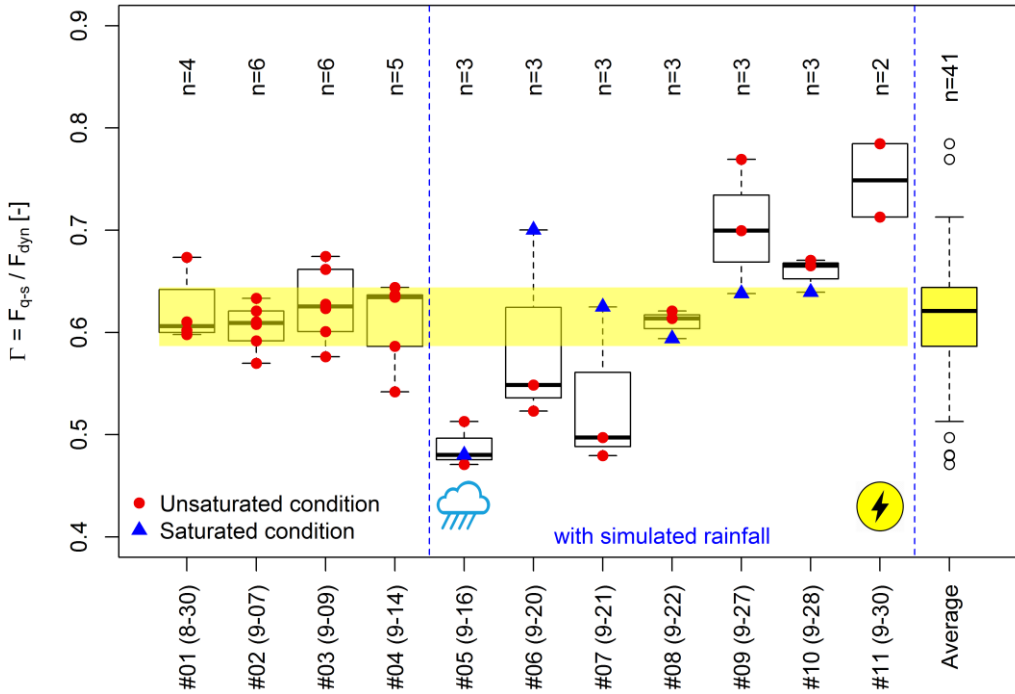


Figure 6.10. Evaluation of the ratio between dynamic force at the end of the pause (i.e. quasi-static force) and maximum dynamic force, named Γ , for the eleven experiments: four in natural soil moisture condition and seven in artificial condition influenced by the simulated rainfall. The yellow strip represents the range in which the 50% of the values are measured; the red circles indicate when the measure has been recorded in unsaturated condition, and the blue triangles pinpoints the saturated condition after the irrigation. The rainfall icon indicates that the experiment was conducted on a rainy day, whereas the thunder electric problems. On the right, the yellow boxplot indicates the distribution of Γ values.

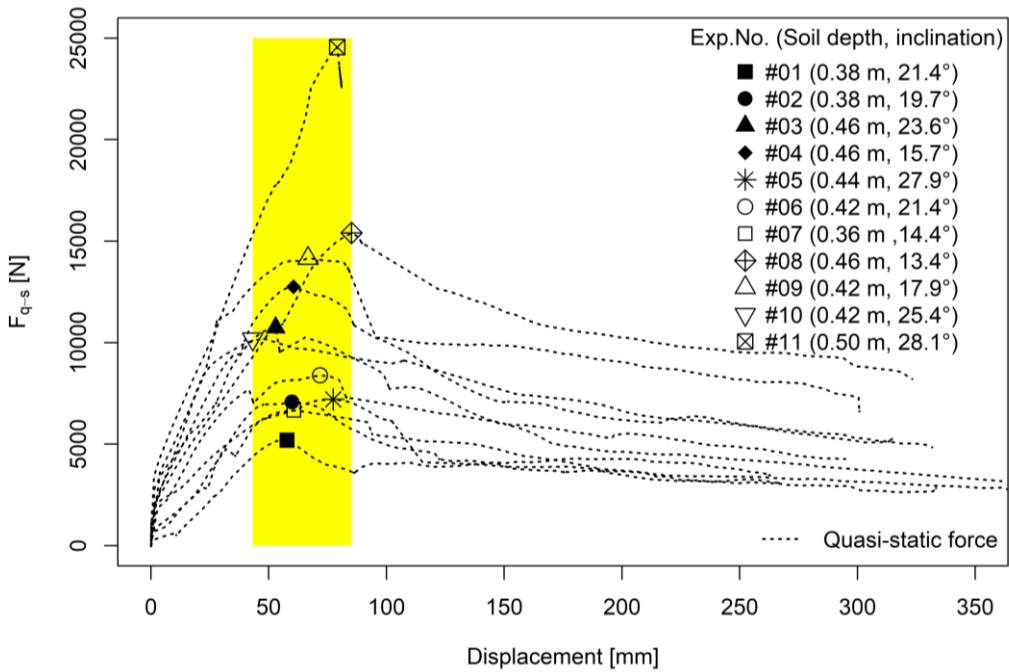


Figure 6.11. Quasi-static force in function of the displacement. The yellow areas are the range of displacement at the ultimate compression force.

A statistical analysis was performed to verify which factors influence the maximum values of F_{q-s} . Kendall's τ and Spearman's ρ were calculated to estimate a rank-based measure of association/correlation. Pearson's product-moment correlation, PPMC, and Pearson's r were performed to measure the linear relationship between F_{q-s} and other external factors. These factors are: H , β , Δx and the normalized displacement at the maximum force Δx_{peak} and $\Delta x_{peak}/H$, θ_v at "control" and at the ultimate compression force $\theta_{v-start}$ and θ_{v-peak} and the difference between the inclination of the machine at "control" and at the end of the experiment, $\Delta \alpha$. For these statistical analyses, all the samples need to be normally distributed. Therefore, Shapiro-Wilk tests were conducted excluding experiment #11 (outlier data) verifying normal distribution. The statistics indicated that maximum F_{q-s} correlated significantly with H ($t = 2.863$,

PPMC's p-value = 0.021, $r = 0.711$, $\tau = 0.629$ and $\rho = 0.779$), but did not correlate to the other factors (Table 6.3).

Table 6.3. Results of statistical analysis to estimate the correlation between F_{q-s} and other factors.

Variable	Shapiro-Wilk test	PPMC	r	τ	ρ
F_{q-s}	W = 0.924 p-value = 0.391	-	-	-	-
H	W = 0.889 p-value = 0.166	$t_8 = 2.863$ p-value = 0.021	0.711	0.629	0.779
β	W = 0.965 p-value = 0.842	$t_8 = 1.261$ p-value = 0.243	0.407	0.225	0.298
Δx_{peak}	W = 0.975 p-value = 0.930	$t_8 = 0.785$ p-value = 0.455	0.267	0.244	0.284
$\Delta x_{peak}/H$	W = 0.918 p-value = 0.344	$t_8 = -0.225$ p-value = 0.828	-0.079	0.111	0.054
θv_{start}	W = 0.949 p-value = 0.662	$t_8 = 0.664$ p-value = 0.526	0.228	0.244	0.224
θv_{peak}	W = 0.965 p-value = 0.838	$t_8 = 0.743$ p-value = 0.478	0.254	0.289	0.321
$\Delta \alpha$	W = 0.973 p-value = 0.916	$t_8 = 0.384$ p-value = 0.711	0.134	0.111	0.127

6.5.4 Passive earth force comparison

Maximum passive earth force per length unit was computed using different geotechnical theories including the soil cohesion component, plate-soil cohesion/adhesion contribution, interface inclination and plate width. We selected three general formulations widely used in practice and already described in section 6.2: gen-Rankine (equations 6.1 6.3), gen-Coulomb (equations 6.2 and 6.3), and log-spiral approach (equation 6.4). The measurements were normalized by the plate width and the difference between observation and theory was estimated using two indicators: root mean square error, *RMSE* (equation 2.6 in section 2.2.7), and mean absolute percent error, *MAPE*. The comparison is shown in Figure 6.12. It is evident that the gen-Rankine provided the closest estimates and was the most accurate for this application. Additionally, no particular trend in terms of underestimation or overestimation was evident and the performance indexes assumed the lowest values (*RMSE* = 5.89 kN and *MAPE* = 26.96%). The other two theories considerably overestimated the observations. Specifically, the gen-Coulomb provided values up to 70% larger than the observed ones (*RMSE* = 9.07 kN and *MAPE* = 70.30%), whereas the log-spiral yielded even greater values (*RMSE* = 24.57 kN and *MAPE* = 167.41%). Figure 6.12 also shows the range of the computed values. Although the gen-Rankine provided the most accurate estimates, the values ranged between 10.39 kN and 18.67 kN, smaller than the observations and despite that the gen-Coulomb's values were overestimated, the range from 15.58 kN to 29.92 kN was similar to the observed ones. An extremely wide range was obtained for the log-spiral approach, ranging from 20.78 kN to 66.56 kN.

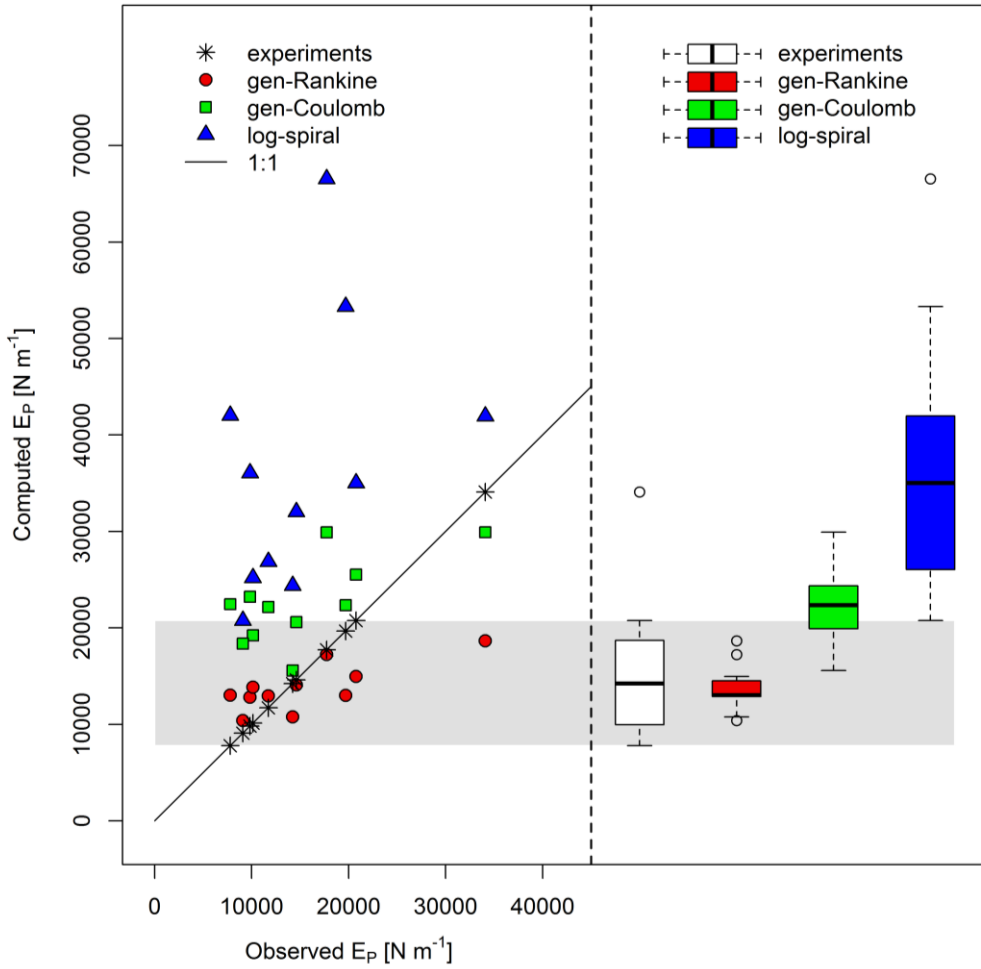


Figure 6.12. Comparison and variability between observed measurements and theoretical calculations of E_p .

6.5.5 Geometry of compressed wedge

The extension of the compressed wedge induced by the compression machine gradually varied with increasing Δx . We measured the geometrical features at two stages: at “pause-2” (Figure 6.13) and at the end of the experiment (“end” in Figure 6.13). Δz ranged from 0.068 m to 0.123 m with an average value $0.087 \text{ m} \pm 0.018 \text{ m}$ at “pause-2” and increased to 0.150 - 0.250 m with an average value of $0.209 \text{ m} \pm 0.026 \text{ m}$, reaching values greater than 83.74% to 253.10% towards the end of the experiment. L ranged from 0.359 m to 0.525 m approximately 11% more than the dimension of H and increased up to 0.385 m to 0.651 m, around 22% more on average. In terms of lateral expansion, W varied from 0.777 m to 1.092 m up to 0.990 m to 1.222 m. Figure 6.13 is an example of the post-processing of three subsequent scans and shows six boxplots with the differences between the two stages for the three 1-D geometrical features. Concerning the behaviour of the compressed wedge in terms of volume (3-D), the analysis clearly showed how the compressed wedge volume initially decreased and then expanded once the maximum resistance force was reached. As shown in Figure 6.14, ΔV_{3D} assumed negative values at “pause-2” varying between -0.013 m^3 and -0.001 m^3 with an average of $-0.004 \text{ m}^3 \pm 0.003 \text{ m}^3$. However, at the end of the experiments, ΔV_{3D} had positive values one order of magnitude greater, ranging from 0.010 m^3 to 0.079 m^3 with an average of $0.038 \text{ m}^3 \pm 0.021 \text{ m}^3$.

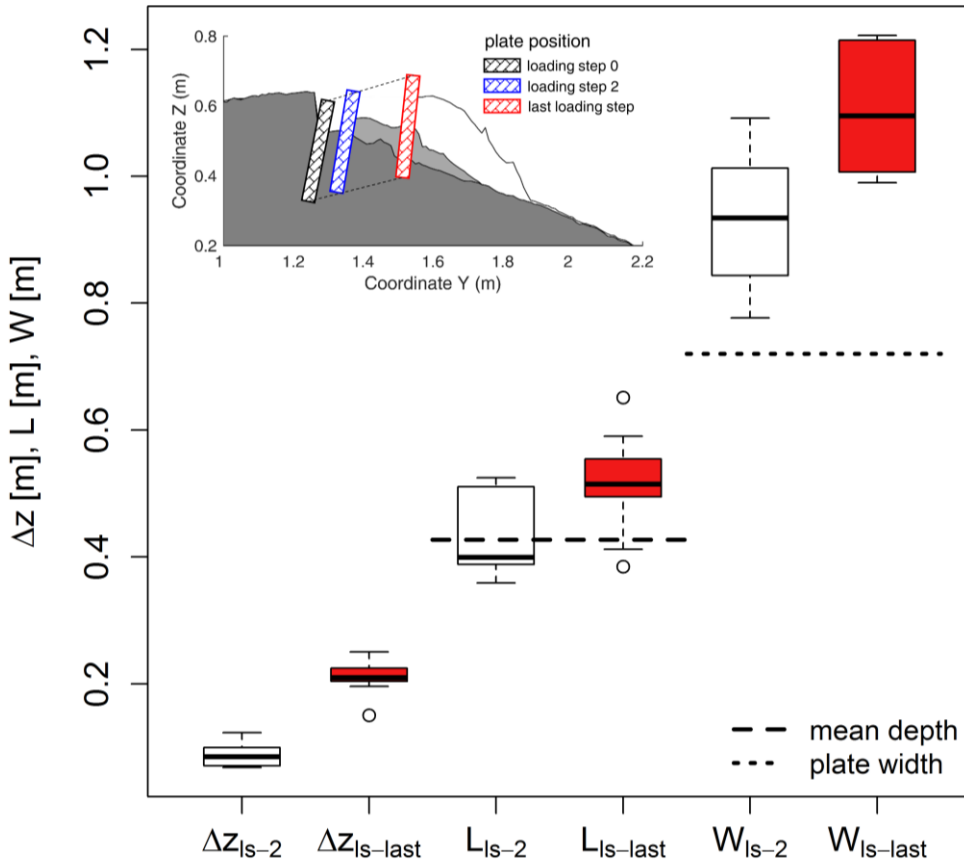


Figure 6.13. 1-D geometrical measurements at two different stages: at “p-2” that corresponds to “pause-2” and at “end” that indicates the final condition of the experiment. Example of post-processing of experiment #01, in which the dark-grey area indicates the soil surface before the experiment, the light-grey at “pause-2” and the white at the end of the experiments. Additionally, the position of the plate has been included.

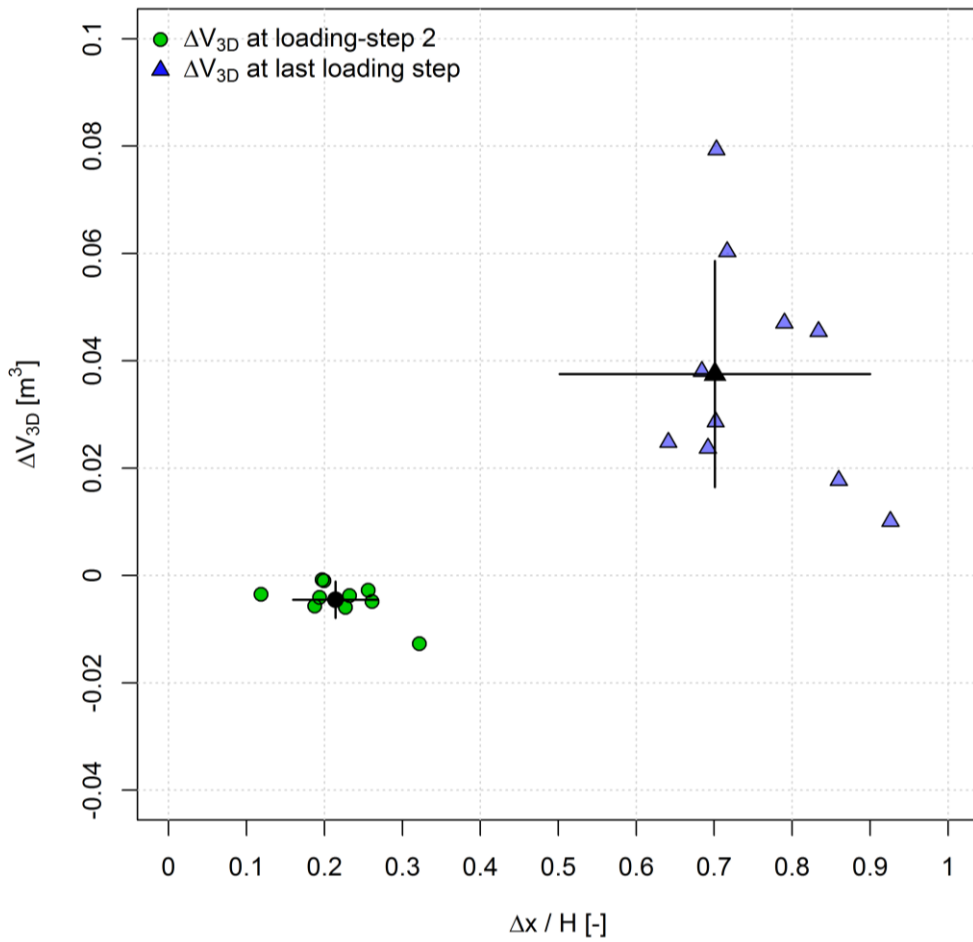


Figure 6.14. 3-D geometrical characteristics of the compressed wedge versus the normalized displacement. Error bars show the variability of the values.

6.5.6 Influence of water content

Seven of the eleven experiments were performed under saturated condition by adding water using a rainfall-simulator at a rate of 70 mm h^{-1} for about 60 minutes after “pause-2”. We fitted a curve on the decline of the compressive force during “pause-2” for each experiment using a three-parameter negative exponential function (equation 6.11). This function yielded an excellent fit with R^2 near unity and $RMSE$ of approximated 0.001. The fitted coefficients a , b and c varied from -0.12 to 1.33 for a , from -0.17 to 0.12 for b and from -0.36 to 0.95 for c . All $F_{\text{dyn}} / F_{\text{dyn}}^*$ fitted curves for each experiment, described with red lines, are shown in Figure 6.15 as a function of time. This procedure allowed not only to describe the decline of compression force, but also to assess the effects of the rainfall comparing the fitted curves with the measurements under irrigation (points black in Figure 6.15). Furthermore, we calculated their maximum difference, Δ . The average value of Δ was $-10.04\% \pm 3.72\%$ excluding experiment #05, because it was conducted during a natural rainfall event and therefore the initial soil water content was already high prior to irrigation. In that case, estimated Δ was -25.60% . It is interesting that the curves declined remarkably after approximately 11-12 minutes after initial irrigation except for experiment #05.

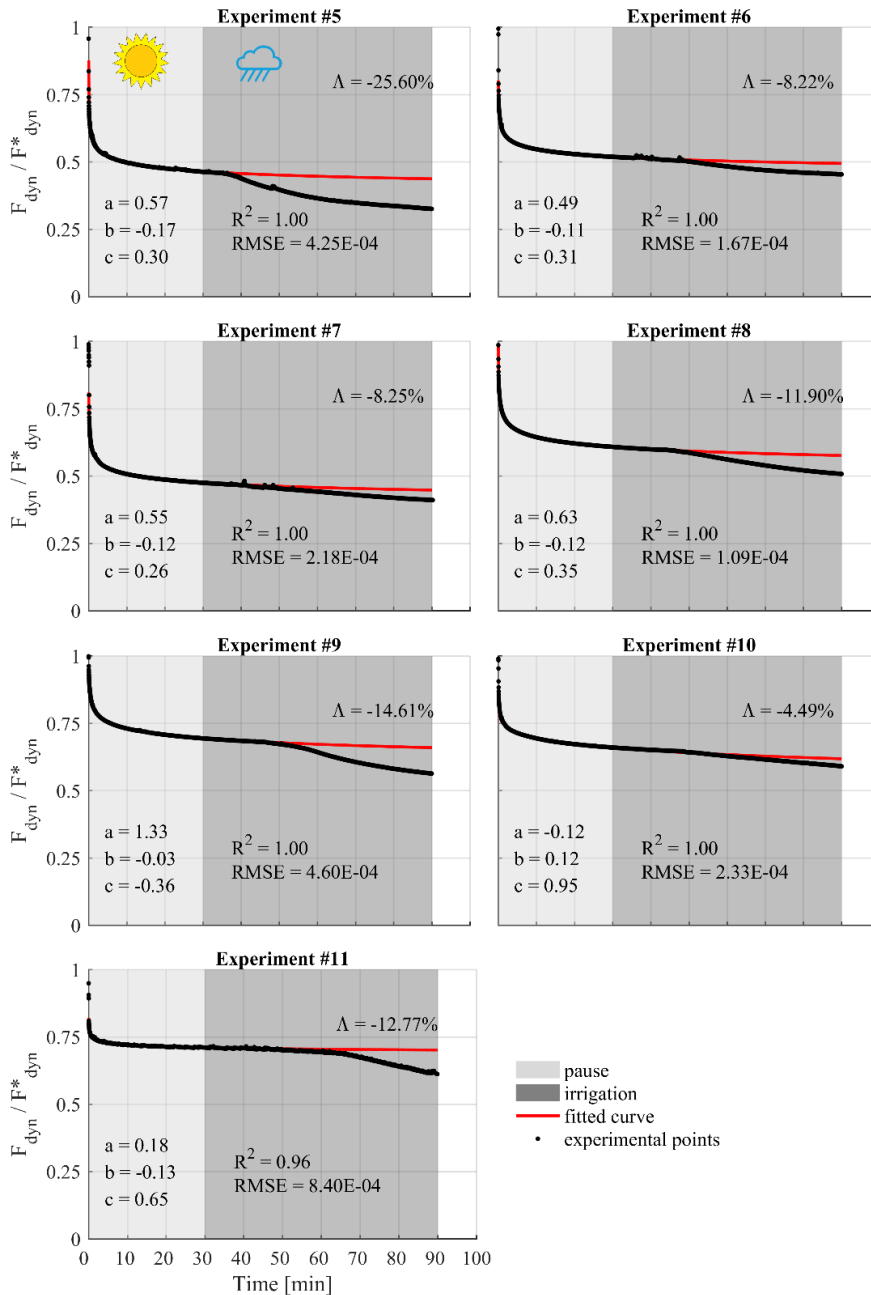


Figure 6.15. Decline of compression force (F_{dyn}/F_{dyn}^*) during the “pause-2” and the simulated rainfall. The black points represent the measured values, the red line is the fitted curve before the artificial rainfall, the light-grey area corresponds to the dry soil condition, whereas the grey area the wet-saturated condition.

6.6 Discussion

6.6.1 Experimental measurements

Our experiments showed measurements of passive earth force as a function of multiple factors including soil depth, slope, and soil moisture. Statistical analysis indicated that the maximum value of the compression resistance is strongly affected by soil depth (Table 6.3). We noticed that the force-displacement curves behaved similarly in all the experiments despite wide differences in terms of compression peak forces (Figure 6.11). The shape of these curves is comparable to results obtained for dense soils in many experimental studies.

Force-displacement behaviour measured in this study can be compared to a few other similar studies. Fang et al. (2002) investigated the differences, in terms of magnitude and behaviour under compression, between sands with different densities. Their experimental setup consisted of a retaining wall 1.00 m wide, 0.55 m high, with a 0.12 m thick movable stiff plate, already used in previous studies (Fang et al., 1994, 1997). Their results showed similar behaviour for medium dense and dense sand; however, they found that the mobilisation of the ultimate compression resistance occurred at a displacement between 0.015-0.030 $\Delta x/H$. This range of displacement is an order of magnitude less than that obtained in our experiments.

Wilson and Elgamal (2010) conducted another interesting experiment that is described in detail in Wilson (2009). To account for the contribution of the passive earth resistance against excessive displacement occurring along bridge abutments and piles, they measured force-displacement behind a 1.70 m high vertical wall section inside a wider container filled with dense well-graded silty sand. As in our case, the passive earth force increased with increasing displacement until an ultimate value of 0.035 $\Delta x/H$ was reached, followed by a slight decrease dropping to a residual state.

Gutberlet et al. (2013) provided similar results exploring the differences in terms of passive earth forces analysing different sands and combinations of

them. They used a sandbox with a movable 0.225 m high wall on one side that moved against the soil driven by an electric step motor. They clearly recorded a peak in compression force for dense materials and observed that the complete mobilisation required a displacement of $0.02 \Delta x/H$ for quartz sand and $0.05 \Delta x/H$ for crushed gabbro. Mixing the two materials, the mobilisation always occurred within this range of displacement.

Regarding displacement at peak compression, Schwarz et al. (2015) measured similar values in laboratory experiments with the same soil material used here. However, their force-displacement curve showed a continuous increase of force with no peak value, probably due to the different setup of the laboratory experiment: soil was confined in a box and the compression plate movement was horizontal. Moreover, our force-displacement curves confirmed that soil stiffness substantially depends on soil depth (Terzaghi et al., 1996). Figure 6.11 shows that soil stiffness, evaluated as the ratio between the ultimate compression resistance and the mobilised displacement, increased with increasing soil depth classes. Our study is in agreement with Wilson and Elgamal's (2010), who conducted numerical and experimental studies on different types of backfilled soils and showed an extensive range of variation of soil stiffness as a function of soil depth.

6.6.2 Measured passive earth force vs theoretical calculations

The comparison between our quasi-static measurements of the ultimate passive earth force and the theoretical calculations showed that the gen-Rankine provides the most accurate and consistent values. Both the gen-Coulomb and the log-spiral approach yielded generally larger values approximately 1.68 and 2.67 times more than the measured ones, respectively. Our results disagree with a large part of the geotechnical literature.

Experimental and numerical studies emphasized that theories assuming a non-linear sliding surface such as the log-spiral approach, are considered

more accurate than others that are based on a planar failure surface for the case of cohesionless soils (Caquot and Kérisel, 1948; Soubra, 2000; Terzaghi, 1943; Zhu and Qian, 2000). Although almost all experiments were conducted on granular soils and in the laboratory, they indicated that the gen-Rankine generally underestimates the passive earth resistance, whereas the gen-Coulomb produces a significant overestimation (Bowles, 1997; Duncan and Mokwa, 2001; Fang et al., 1994, 1997; Narain et al., 1969). For dense sands, the log-spiral approach provided good estimates of the compression resistance peak in several studies (e.g., Fang et al., 2002; Wilson and Elgamal, 2010).

In our study, the tested soil was classified as clayey gravel (GC) according to the USCS soil classification with high cohesion (i.e. $c' \approx 15$ kPa) and a low friction angle (i.e. $\phi' \approx 24^\circ$) values. These characteristics were the causes of the discrepancies between observations and calculations. In particular, the contribution of the cohesion component on E_p was most substantial approximately 97% for the log-spiral approach and 89% for the gen-Rankine and the gen-Coulomb. It was confirmed that the linear behaviour was caused by the cohesion component when computing E_p using the selected geotechnical theories in function of H and fixing the other input parameters, (equations 6.3 and 6.4), as shown in Figure 6.16. Additionally, Figure 6.16 shows the variability of theoretical calculations as a function of three different hydrological soil conditions (Table 6.3). It seems that if the gen-Rankine and the gen-Coulomb exhibited a moderate variability in terms of computed force, the log-spiral approach was highly sensitive to soil moisture conditions.

Each theoretical calculation has some limitations including the range of backfill inclination. In Figure 6.17, we showed the calculation of E_p as a function of β using the selected theories and the same set of input parameters. The gen-Rankine's calculations showed a symmetrical behaviour with respect to the longitudinal axis. Whether the backfill inclination is -30° or $+30^\circ$, the passive earth resistance assumes the same

value. This fact is clearly incorrect for positive values of β , whereas it is feasible for negative values (Fang et al., 1997). Regarding the other theories, the gen-Rankine provides estimates of E_p for all the considered ranges of β , even though the gen-Rankine's K_p becomes complex when the square root term in equation 6.2 becomes negative. This generally happens in case of cohesionless soils, when $|\beta|$ is greater than ϕ' and the cohesion term is not high enough to obtain K_p as a real number. Similar problems occur using both the gen-Coulomb and the log-spiral approach. For the gen-Coulomb's theory, K_p becomes complex only when $\beta < -\phi'$. On the other hand, K_p obtained with the log-spiral approach becomes indeterminate for $|\beta| > \phi'$, because the log-spiral slip surface degenerates to a planar surface with radii approaching infinity and violating optimization constraints (Soubra and Macuh, 2002). In addition, Macuh and Škrabl (2010) verified that in case of interface friction and inclined backfill, K_{pc} values are not admissible if obtained applying the basic corresponding state theorem (equation A-14) developed by Caquot (1934).

Therefore, Soubra and Macuh (2002) suggested reasonable practical limitations for obtaining K_p values similar to those given by Kérisel and Absi (1990) (i.e. $\phi' \leq 40^\circ$, $1/3 \leq \delta/\phi' \leq 2/3$, $\beta/\phi' \leq 1/3$ and $\lambda = 0^\circ$).

Our comparison did not consider 3-D effects because of the difficulty to find field evidence of 3-D failure mechanisms in the soil and because of the lack of scientific contributions adapted for soils with characteristics similar to our study site. However, we can estimate that the theoretical calculations, if corrected for the 3-D effects, would yield values approximately 30% greater when applying the empirical simple formulation in equation 6.5 considering an average value of the shape parameter, $C=0.52$ as proposed by Regenass et al. (2000). Other estimates are available from numerical simulations: Benmebarek et al. (2008) estimated that the passive earth pressure coefficients ratio K_{p-3D} / K_{p-2D} increases with decreasing B/H . This ratio reaches a value twice as high for $B/H \leq 1$, whereas it reaches a value of 1 for $B/H \gg 10$. Khelifa and Benmebarek (2014) further found that the passive

earth pressure increased with decreasing wall width and decreased with decreasing angle of dilation of the soil.

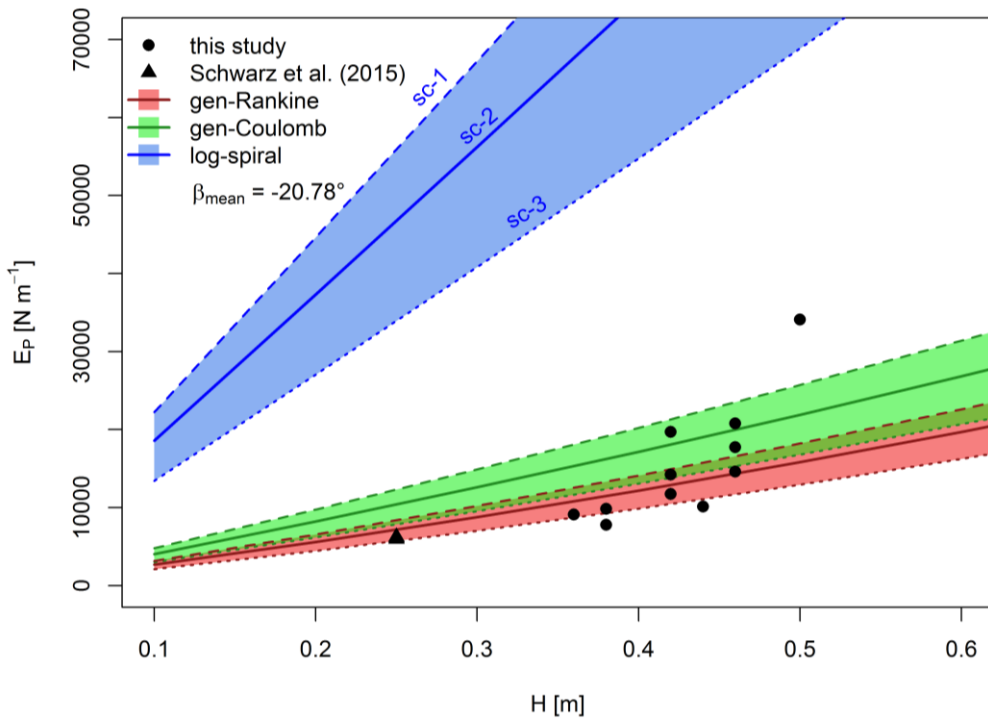


Figure 6.16. Passive earth force at different soil depths. Symbols indicate the measured quasi-static forces during experiments in the field (this study) and in the laboratory (Schwarz et al., 2015). The coloured stripes represent theoretical calculations, whereas the different line types indicate different soil water content (sc-1, sc-2 and sc-3 as described in detail in Table 6.2), with a fixed inclination equal to -20.78° corresponding to the average of those measured during the field experiments.

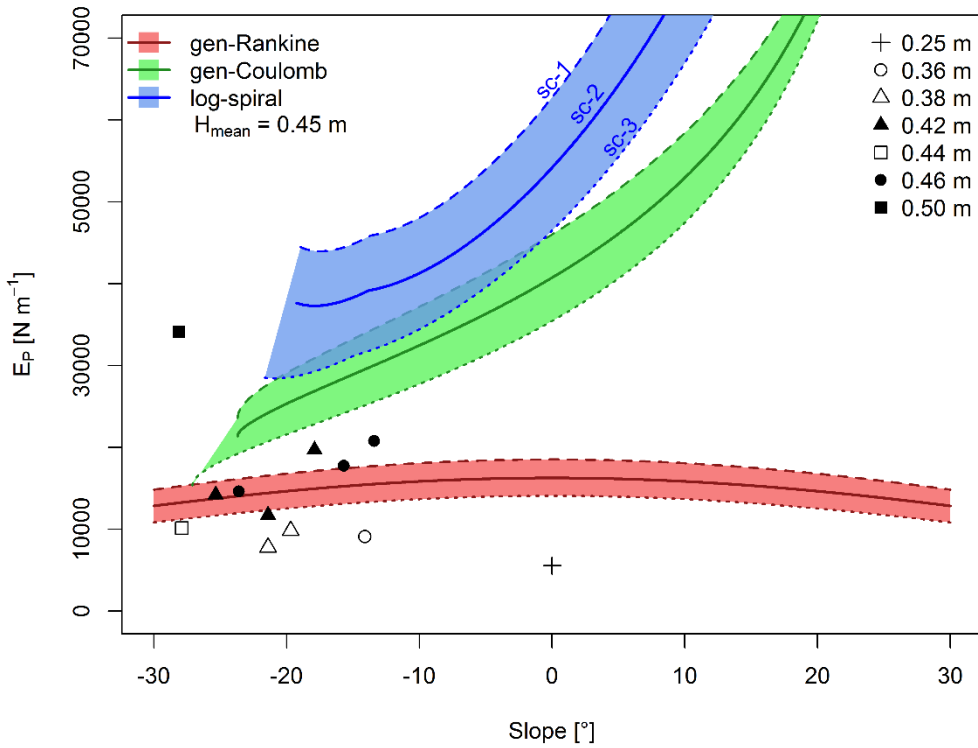


Figure 6.17. Passive earth force at different inclinations of backfill. Symbols indicate the measured quasi-static forces during experiments in the field (this study) whereas the coloured stripes represent the theoretical calculations. The different line types indicate different soil water contents content (sc-1, sc-2 and sc-3 as described in detail in Table 6.2) with a fixed depth of 0.45 m corresponding to the average of those measured during the field experiments.

6.6.3 Friction between stiff plate and compressed soil wedge

Our observations of the angle of friction between stiff plate and the soil showed an inverse dependence with respect to the expected compression resistance, being in agreement with Rowe and Peaker (1965) and Narain et al. (1969). Indeed, these authors underlined that the wall friction angle changes with the displacement and mainly depends on the instantaneous direction of wall displacement at each stage of deformation. In addition, Sherif et al. (1982) indicated that the maximum wall friction does not occur simultaneously with the maximum shearing resistance along the rupture surface. Although this factor is fundamental for a reliable estimate of passive resistance, only few studies focused on quantifying the interface friction during a compression test. Potyondy (1961) conducted interface shear tests on a variety of structural materials and soils, obtaining a wide range of values. For the interface between steel and soils, the typical maximum value of δ ranged from 11° to 22° (Bowles, 1997; Duncan and Mokwa, 2001) and was comparable to our observations at the end of the experiment. However, our measurements of δ^{\min} around 2° - 3° were similar to those obtained by Wilson and Elgamal (2010). In addition, our results underlined how values greater than 0.4-0.5 times ϕ' yield an overestimation of EP computed using Coulomb's theory, as already indicated by several authors (Duncan and Mokwa, 2001; Morgenstern and Eisenstein, 1970).

6.6.4 Dynamic vs quasi-static force

Evaluating both F_{dyn} and the quasi-static force, $F_{\text{q-s}}$, means increasing the knowledge on how and how much of such force is mobilised during the compression phase occurring at the toe of a landslide during its failure. Our results showed that the difference between F_{dyn} and $F_{\text{q-s}}$ of approximately 60% was considerable and were in agreement with results of Schwarz et al. (2015). F_{dyn} was completely mobilised at low displacement, around 15% of H , but rapidly decreased once displacement stopped (first loading step). This decay behaved as a negative exponential function, probably caused by the

rheological properties of soil (Ghezzehei and Or, 2003, 2001). Understanding the effects of the rheological properties of soil and the force redistribution on a slope during the initial phase of a landslide failure is fundamental to include and quantify in numerical models. For instance, the interplay between displacement rate and changes in suction and pore water pressure at the toe of the landslide determine the development of the failure. In the case of a soil with an initial relative low water content, deformation is slow and the pore water pressure/suction at the moment of maximum passive earth force mobilisation is low resulting in an arrest of the sliding mass. Conversely, a landslide with an initial relative high soil water content produces high values of pore water contents before the dilatation phase along the passive earth failure plan, resulting in fluidization and runout of the soil mass.

6.6.5 Effects of water

Passive earth force strongly depends on soil type and soil density, but also on soil moisture. Poterasu (2013) investigated this aspect in detail through compression experiments on fractions of Kaolin clay content (6 to 10%). Poterasu showed that the behaviour of passive earth force was associated to pore volume saturation ranging from 5% to 100%. Her results underlined that collapsing mechanisms of the clay-water bridges between the grains of the granular material were responsible for a significant reduction in soil stiffness and strength. Because the range of soil moisture in our experiments was limited ($\theta_v = 0.292-0.405$), we did not find a relationship between volumetric water content and ultimate compression force. However, our observations showed that the water content increased during compression, probably due to the reduction of pore volume. This evidence was also highlighted in the study conducted by Iverson et al. (2000). They explained that the contraction associated with aggregate crushing is probably the main cause of excess pore pressure and responsible for soil weakening and landslide acceleration. Concerning the effects of rainfall, statistical analysis

performed on the dataset of the seven field experiments with simulated rainfall did not yield a strong correlation between the soil moisture condition and the measured ultimate resistant force or variation from dynamic to quasi-static state. However, in terms of timing of the hydrological process, it was possible to notice how the initial water content influenced the decline of F_{dyn} during the simulated rainfall (Figure 6.15). For example, experiment #05 showed a remarkable decline shortly after the beginning of the irrigation, whereas the other experiments displayed a decline only after several minutes. Moreover, rainfall intensity and initial pore water pressure inside the subsoil affected this hydrological behaviour. Based to the hydrological soil condition, this evidence could have affected the measurements.

6.6.6 Implications for slope stability analysis

The triggering mechanisms of shallow landslides are a central issue of many studies that proposed and developed a wide range of slope stability analysis such limit equilibrium approach and numerical models, tested through laboratory or field experiments (Askarinejad et al., 2012; Bordoni et al., 2015a; Iverson, 2000). Despite the uninterrupted effort to improve knowledge about hydrological and mechanical processes and soil evolution by the scientific community, the heterogeneity of rooted-soils in space and in time impedes and creates enormous difficulties to characterise large areas. The present study is an integral part of the modelling development started with the pioneering work of Burroughs (1985), and continued until Cohen and Schwarz (2017). In particular, the study investigated and included the quantification of the compression resistance as a crucial contribution to the limit equilibrium calculations and as a contrasting trigger mechanism (Dietrich et al., 2007). Most physically-based limit equilibrium models evaluate the lateral earth force using geotechnical theoretical calculations developed for the design of geotechnical structures (Milledge et al., 2014; Terwilliger and Waldron, 1991); usually without taking timing and location of earth pressure mobilisation into account. Nevertheless, few studies

proposed alternative approaches developed through numerical or experimental analysis at slope scales. For example, Savage and Smith (1986) proposed an application of the Mohr-Coulomb theory through an integration of hyperbolic differential equations for stress and velocity fields in a 2-D semi-infinite space. Their model predicted longitudinal tensile stresses at the upper part of the soil mass and compression stresses at the toe of the instable mass. Furthermore, Savage and Wasowski (2006) validated the model on a real case in Southern Italy. Sdao and Simeone (2007) and later Doglioni et al. (2013) developed a simple analytical model of the passive force at the toe of a landslide based on the Mohr-Coulomb criteria representing the stress state in infinite slopes. They evaluated the backward passive failure surface and the contribution of the strength at the toe. Besides compression force measurements, our observations related them to the displacement underlining a non-linear behaviour.

Considering the role of displacement in force balance improves modelling results (Cohen and Schwarz, 2017) and allows preventing the assumption that maximum active and passive earth forces simultaneously reach the ultimate state, as shown by Askarinejad et al. (2012).

Another important output of this study is the 1-D and 3-D geometrical characterisations of the compressed wedge. Our measurements did not detect a clear sliding failure surface or a shear zone, but the 1-D characterisation showed that the maximum length of the compressed wedge was of the same order of magnitude as the soil depth as suggested by several authors (Capilleri et al., 2015; Fang et al., 1994; Wilson and Elgamal, 2010). Therefore, in the case of finite volume methods, the resolution of the discretization should be at least as large as the expected depth of the sliding surface.

Further studies are needed to assess the variability of force-displacement curves under field conditions and to model this behaviour taking soil depth, soil properties, presence of roots and the effects of water into account.

6.7 Conclusions

Since the calculations of the passive earth force has a vast application in slope stability analysis, it is worthwhile to quantify this measure through field experiments and to investigate which geotechnical theories guarantee accurate predictions. Field measurements were conducted using a specific experimental equipment on a clayey gravel soil in a coniferous forest site susceptible to shallow landslides. Our measurements clearly showed that the behaviour of the compression force during the experiment was a function of several factors, such as dynamics, soil properties, soil depth, backfill inclination and soil water content. Additionally, our results underlined that:

1. the force-displacement curves assumed identical shapes with an initial increase until an ultimate condition is reached, followed by a decrease reaching a residual condition;
2. the maximum dynamic compression force varied from 8.49 kN to 31.67 kN for clayey gravel soils with different combinations of soil depths (0.38 m - 0.50 m) and slope inclinations (13.4° - 28.1°);
3. the quasi-static compression forces were approximately 61.4% lower than the dynamic ones, and the maximum values varied from 5.61 kN to 24.55 kN;
4. comparing observations of passive earth force and computed theoretical calculations, the gen-Rankine's theory provided the most accurate predictions, whereas the gen-Coulomb's and the log-spiral approach largely overestimated them;
5. the effects of rainfall on the dynamic compression force caused a decrease of the resistance by around 10% with an initial average soil moisture of 36%;
6. the compressed wedge initially decreased its dimension until the ultimate compression state, then dilatancy and visible cracks on the surface occurred with a subsequent volume expansion.

Notations

E_p	Passive earth force per unit length (N m^{-1})
γ	Unit weight of soil (KN m^{-3})
c'	Soil effective cohesion (Pa)
c	Soil cohesion (Pa)
ϕ'	Internal friction angle of soil (rad)
β	Backfill inclination (rad)
δ	Frictional interaction angle between wall and soil (rad)
λ	Angle of the internal face between wall and vertical direction (rad)
H	Soil depth (m)
q	Vertical surcharge loading (KN m^{-3})
K_p	2-D coefficient of passive earth pressure (-)
$K_{p\gamma}$	Coefficients of passive earth pressure due to soil weight (-)
K_{pc}	Coefficients of passive earth pressure due to soil cohesion (-)
K_{pq}	Coefficients of passive earth pressure due to surcharge (-)
B	Width of plate (m)
K_{p3D}	3-D coefficient of passive earth pressure (-)
θ_V	Volumetric water content ($\text{m}^3 \text{m}^{-3}$)
Δx	Displacement (mm)
$F_{p\perp}$	Measured compression force perpendicular to the plate (N)
W_{CM}	Weight of the compression machine with one side on the ground (N)
α	Inclination of compression machine (rad)

$\Delta \alpha$	Difference between inclination of machine at control and at the end of experiment (rad)
F_p	Measured compression force (N)
F_{rb}^{ult}	Maximum buckling-tensile force (N)
ϕ	Root diameter (mm)
ξ	Empirical exponent of $F_{rb}^{ult}-\phi$ curve (-)
F_0	Multiplicative coefficient of $F_{rb}^{ult}-\phi$ curve (-)
F_{rb-i}	Contribution of root diameter class i to root reinforcement under compression (N)
F_{rb-tot}	Root reinforcement under compression (N)
N_i	Number of roots in diameter class i (-)
n_c	Number of diameter class (-)
Δx^*	Normalized displacement than that measured at maximum value of compression force (-)
S	Survival function (-)
k	Spring constant function
k_i	Intercept of spring constant function (-)
k_p	Multiplicative coefficient of spring constant function (mm^{-1})
F_{dyn}	Dynamic compression force (N)
F_{dyn}^*	Dynamic compression force at end of loading step (N)
F_{q-s}	Quasi-static compression force (N)
t	Time (s)
a	Multiplicative coefficient of three-parameter negative exponential function (-)

b	Empirical exponent of three-parameter negative exponential function (-)
c	Intercept of three-parameter negative exponential function (-)
L	Length of compressed wedge (m)
W	Width of compressed wedge (m)
Δz	Height of compressed wedge (m)
ΔV_{3D}	Volumetric difference (m ³)
V^*	Soil volume subject to passive earth pressure (m ³)
V_M	Soil volume moved by stiff plate (m ³)
V_S	Soil surface volume difference (m ³)

7 CONCLUSIVE REMARKS

The present dissertation focused on the assessment of the shallow landslide susceptibility of vegetated hillslopes through the development of a 3-D probabilistic physically-based spatially-distributed model. Such issue claims significant challenge for the international scientific community and requests a multidisciplinary approach, from physics to biology, from geotechnics to forest science.

The main results presented in the document can be summarised by the following points.

(1) Role of forests in preventing and in reducing shallow landslide hazard

This work summarized the effects of the forests against the hydrogeological hazards, especially the shallow landslides, through a detailed review of previous studies and by synthesizing original data (*Chapter 1*). This background underlines the importance of the contribution of the root systems in reinforcing the soil mantle. Additionally, the chapter points out the difficulties and the open issues that remain in quantifying this stabilizing effect, known as root reinforcement, and in predicting hillslope stability of vegetated areas.

(2) Development of a 3-D probabilistic model of hillslope stability

This work introduced a modular approach combining a 3-D limit equilibrium analysis and a stochastic process (*Chapter 2*). The 3-D slope stability analysis is a geotechnical solution that allows us to overcome the limitations of the 2-D infinite slope theory, the most commonly used both in scientific research and in practical applications. In particular, the proposed model takes into account all forces acting on a slip surface and allows considering in a thoughtful way the presence of the root systems in the soil. To account for the variability of the input parameters, a stochastic procedure has been included through a Monte Carlo simulation. In this way, the intrinsic spatial and temporal variability and the uncertainties of measurements of the input parameters can be considered. This modular approach has been called

PRobabilistic Multidimensional shallow Landslide Analysis, PRIMULA, and represents a fundamental basis for theoretical improvements and a powerful instrument for forest and land use planning sector.

(3) Investigation of a rooted-soil compression component

Among the theoretical insights, one of the main results concerns the compression component of the rooted soil (*Chapter 6*). In particular, this study presented the first attempt to measure the compression force acting on a soil mass during a trigger mechanism of the shallow landslide. Field experiments have been designed and conducted to improve the accuracy of 3-D limit equilibrium analysis and to compare with the geotechnical formulations, commonly used in practice.

(4) Scenario studies

From a practical perspective, PRIMULA has been applied to three scenario cases, demonstrating its potentiality. In particular, this work has been applied to obtain the assessment of the impact of forest management on slope stability (*Chapter 3*); the quantification of the large wood recruitment in mountainous catchments (*Chapter 4*); and the design of new vineyards in areas prone to hillslope instabilities (*Chapter 5*).

APPENDIX A

Location	Dominant species	Density [tree ha ⁻¹]	Age [years]	Tree height [m]	DBH [m]	MAP [mm yr ⁻¹]	I _c [%]	References
Alicant, SE-Spain	Aleppo pine					302		Abdelli, (1999)
Alicant, SE-Spain	Aleppo pine					302		Abdelli, (1999)
Alicant, SE-Spain	Kermes oak					302		Abdelli, (1999)
Skogaby, SW-Sweden	Norway spruce		35			1100	45	Alavi et al. (2001)
Aragón, NE-Spain	Scots pine	1080		19	0.186	931	26.1	Alvera (1976)
Aragón, NE-Spain	Scots pine	1080		19	0.186	931		Alvera (1977)
Nancy, France	European beech	1300	30	12.5	0.087	719	16.9	Aussenac (1968)
Nancy, France	Grand fir	620	35	23	0.303	719	40	Aussenac (2000)
Nancy, France	Norway spruce	2160	30	12.5	0.12	719	34	Aussenac (2000)

Appendix A

Nancy, France	Scots pine	1520	28	13	0.17	719	30	Aussenac (2000)
Frankfurt, Germany	Scots pine		28			620	36	Balázs (1982)
Segeberg, N-Germany	Scots pine		37			880	33	Balázs (1982)
Segeberg, N-Germany	Scots pine		97			880	36.75	Balázs (1982)
Frankfurt, Germany	Scots pine		119			620	44	Balázs (1982)
Frankfurt, Germany	European larch		28			620	37	Balázs (1982)
Segeberg, N-Germany	European larch		28			880	21.75	Balázs (1982)
Segeberg, N-Germany	European larch		49			880	17.25	Balázs (1982)
Frankfurt, Germany	European larch		51			620	34.2	Balázs (1982)
Lombardy, N-Italy	Norway spruce		80			1267	23.6	Balestrini and Tagliaferri (2001)
Lombardy, N-Italy	Silver fir		180			1342	22.3	Balestrini and Tagliaferri (2001)
Tarragona, NE-Spain	Evergreen oak	6009				570	12.9	Bellot and Escarre (1998)

Prades, NE-Spain	Evergreen oak	18200			570	35.1	Bellot et al. (1999)
Prades, NE-Spain	Evergreen oak	8460	9		570	12.9	Bellot et al. (1999)
Murcia, SE-Spain	Aleppo pine				228	27.6	Belmonte (1997)
Murcia, SE-Spain	Prickly juniper				228	30.4	Belmonte (1997)
Murcia, SE-Spain	Rosemary				228	23.6	Belmonte (1997)
Murcia, SE-Spain	Thyme				228	31.6	Belmonte (1997)
Hocksolling, N-Germany	European beech	245	120	25	1066	18	Benecke (1984)
Solling, N-Germany	Norway spruce	595	85	24.4	1066	29	Benecke (1984)
Solling, N-Germany	European beech		120		1066	19	Benecke and Van Der Ploeg (1978)
Solling, N-Germany	Norway spruce		90		1066	28	Benecke and Van Der Ploeg (1978)
Frankfurt, Germany	European beech		30		681.5	9	Brechtel (1970)
Frankfurt, Germany	European beech		61		681.5	23	Brechtel (1970)
Frankfurt, Germany	European beech		111		681.5	20	Brechtel (1970)

Appendix A

Frankfurt, Germany	European larch		18		681.5	31	Brechtel (1970)	
Frankfurt, Germany	European larch		41		681.5	26	Brechtel (1970)	
Frankfurt, Germany	Norway spruce		25		681.5	33	Brechtel (1970)	
Frankfurt, Germany	Oak		17		681.5	5	Brechtel (1970)	
Frankfurt, Germany	Oak		54		681.5	22	Brechtel (1970)	
Frankfurt, Germany	Oak		165		681.5	17	Brechtel (1970)	
Frankfurt, Germany	Scots pine		18		681.5	23	Brechtel (1970)	
Frankfurt, Germany	Scots pine		46		681.5	25	Brechtel (1970)	
Frankfurt, Germany	Scots pine		109		681.5	22	Brechtel (1970)	
Salamanca, W-Spain	Evergreen oak			8.4	0.249	432	36.4	Calabuig et al. (1977)
Bristol, United Kingdom	Apple tree	1900	17		820	15.2	Calheiros De Miranda and Butler (1986)	
Istanbul, Turkey	Crimean pine		42	15	1061	31	Çepel (1967)	

Istanbul, Turkey	Oriental beech		50	15		1045	17	Çepel (1967)
Istanbul, Turkey	Sessile oak		54	12		1020	20	Çepel (1967)
Harz, N-Germany	Norway spruce		15	4	0.05	1300	4	Delfs (1954)
Harz, N-Germany	Norway spruce		30	11	0.08	1300	17	Delfs (1954)
Harz, N-Germany	Norway spruce		60	17	0.19	1300	22	Delfs (1954)
Harz, N-Germany	Norway spruce		80	23	0.315	1300	32	Delfs (1954)
Lozère, S-France	European beech	4270	50	13	0.102	1900	14.8	Didon-Lescot (1998)
Lozère, S-France	Norway spruce	395	60	14	0.27	1900	16	Didon-Lescot (1998)
North Holland, Netherlands	Oak	3000		9.6		850	25	Dolman (1987)
Almeria, SE-Spain	Black pine	1375	16	3.5	0.058	396	3.4	Domingo et al. (1994)
Almeria, SE-Spain	Laurel-leaf cistus	670	16	1.5	0.083	396	28.1	Domingo et al. (1994)
Almeria, SE-Spain	Maritime pine	110	16	10	0.128	395	12.6	Domingo et al. (1994)

Appendix A

Almeria, SE-Spain	Silver broom	207	16	1	0.124	396	20.6	Domingo et al. (1994)
Almeria, SE-Spain	Albaida			7		300	40	Domingo et al. (1998)
Almeria, SE-Spain	Retama broom			1.7		300	21	Domingo et al. (1998)
Var, SE-France	Heath					967	5.4	Duwig (1994)
Sauerland-Rothaargebirge, Germany	European beech		100			1216	8	Eidmann (1959)
Sauerland-Rothaargebirge, Germany	Norway spruce					1216	26	Eidmann (1959)
Agueda basin, N-Portugal	Maritime pine	400	50		0.321	1600	14.1	Ferreira (1996)
Agueda basin, N-Portugal	Tasmania bluegum	1760	7		0.127	1600	13.2	Ferreira (1996)
Agueda basin, N-Portugal	Tasmania bluegum	1792	10		0.135	1600	12.4	Ferreira (1996)
Agueda basin, N-Portugal	Tasmania bluegum	1664	5		0.073	1600	11.4	Ferreira (1996)

NE-Scotland, United Kingdom	Scots pine	1870	44	15	700	42.4	Gash et al. (1980)	
Cheviot Hills, United Kingdom	Sitka spruce	3600	29	12.9	850	31.7	Gash et al. (1980)	
Plynlimon, United Kingdom	Sitka spruce	4250	33	8.9	2650	26.7	Gash et al. (1980)	
Göttingen, Central Germany	European beech		120	30	812	16	Gerke (1985)	
Tuscany, N-Italy	European beech				0.285	2027	24.8	Giacomin and Trucchi (1992)
Tuscany, N-Italy	European beech				0.285	2027	21.8	Giacomin and Trucchi (1992)
Madrid, Spain	Atlas cedar		45	25	453		González del Tánago et al. (1988)	
Madrid, Spain	Silver poplar		35	35	453		González del Tánago et al. (1988)	
Huesca, NE-Spain	Rosemary				497		González-Hidalgo et al. (1997)	
Berkshire, United Kingdom	Peduncul ate oak			22		24.9	Herbst et al. (2008)	
Kiel, N-Germany	European beech	154	97	27	697	10.9	Hörmann et al. (1996)	
Delta Rhone, SE- France	Stone pine	800	33	11.5	494	27.1	Ibrahim et al. (1982)	

Appendix A

Calabria, S-Italy	Corsican pine	1533	35		0.231	1179	58	lovino et al. (1998)
Calabria, S-Italy	Corsican pine	867	35		0.257	1179	47	lovino et al. (1998)
Calabria, S-Italy	Downy oak	3250	7		0.022	1021	26.3	lovino et al. (1998)
Calabria, S-Italy	Downy oak	1934	5		0.025	1021	15.2	lovino et al. (1998)
Scotland, United Kingdom	Sitka spruce		50	20		2200	28	Johnson (1990)
Ljubljana, Slovenia	Scots pine			11.7	0.135	1394	3.9	Kermavnar and Vilhar (2017)
Ljubljana, Slovenia	Sessile oak			21.9	0.334	1394	18	Kermavnar and Vilhar (2017)
Ljubljana, Slovenia	Sycamore			15.8	0.176	1394	7.1	Kermavnar and Vilhar (2017)
Hainich national park, C-Germany	European beech	428	107	36	0.33	652.3	33.2	Krämer (2010)
Hainich national park, C-Germany	European beech	216	145	38	0.46	652.3	29.8	Krämer (2010)
Hainich national park, C-Germany	European beech	228	193	41	0.37	652.3	33	Krämer (2010)
Hainich national park, C-Germany	European beech	224	143	39	0.46	652.3	26.2	Krämer (2010)

Hainich national park, C-Germany	European beech	436	79	29	0.28	652.3	31.6	Krämer (2010)
Hainich national park, C-Germany	European beech	532	98	32	0.27	652.3	31.2	Krämer (2010)
Hainich national park, C-Germany	European beech	776	79	31	0.25	652.3	35.6	Krämer (2010)
Hainich national park, C-Germany	European beech	660	102	29	0.25	652.3	28.4	Krämer (2010)
Hainich national park, C-Germany	European beech	468	93	28	0.28	652.3	28.8	Krämer (2010)
Hainich national park, C-Germany	Small-leaved lime & Largeleaf linden	392	117	29	0.31	652.3	29.6	Krämer (2010)
Hainich national park, C-Germany	Small-leaved lime & Largeleaf linden	332	90	28	0.31	652.3	31.8	Krämer (2010)
Hainich national park, C-Germany	Small-leaved lime & Largeleaf linden	484	115	27	0.26	652.3	32.4	Krämer (2010)

Appendix A

Sicily, Italy	Sweet chestnut	258		7	0.1	667	18.4	Leonardi et al. (1993)
Sicily, Italy	Sweet chestnut	288		5	0.05	964	24.8	Leonardi et al. (1993)
Montpellier, S-France	Evergreen oak	6885				908	30.9	Limousin et al. (2008)
Montpellier, S-France	Evergreen oak	5464				908	20.2	Limousin et al. (2008)
Barcelona, SE-Spain	Scots pine	2400	33	10	0.143	850	23.8	Llorens (1997); Llorens et al. (1997)
E-Pyrenees, Spain	Scots pine					850	17	Llorens (1997); Llorens et al. (1997)
Bordeaux, France	Maritime pine	800	18	12.6		920	17.4	Loustau et al. (1992a, 1992b)
Lokorsko, Bulgaria	Black locust		28			483.5	17.8	Malvolti (2002)
Nestos, Greece	Black locust		14			437.8	18.6	Malvolti (2002)
Gödöllő, Hungary	Black locust		37			575.6	11.9	Malvolti (2002)
Kecskemét, Hungary	Black locust		22			456.1	17.6	Malvolti (2002)
Càceres, W-Spain	Evergreen oak	3045			0.255	516	26.5	Mateos Rodríguez and Schnabel (1998)

Pindous Mountains Range, C-Greece	Balkan beech		130	25	0.34	1456	11.5	Michopoulos et al. (2001)
Pindous Mountains Range, C-Greece	Greek fir		140	25	0.3	1634	31.7	Michopoulos et al. (2001)
Valsain, Guadarrama Range, C-Spain	Scots pine	269	120	30	0.38	877	16.5	González-Cascón et al. (1994); Minaya-Gallego et al. (1997)
Freiburg, SW-Germany	Douglas fir		5			850	2	Mitscherlich and Moll (1970)
Freiburg, SW-Germany	Douglas fir	2308	13	9.1	0.109	850	32	Mitscherlich and Moll (1970)
Freiburg, SW-Germany	Douglas fir	2016	29	17.2	0.157	850	33	Mitscherlich and Moll (1970)
Freiburg, SW-Germany	Douglas fir	1257	35	19.9	0.222	850	36	Mitscherlich and Moll (1970)
Freiburg, SW-Germany	Douglas fir	533	40	24.5	0.307	850	36	Mitscherlich and Moll (1970)
Freiburg, SW-Germany	European beech	1167	40	7.5	0.173	850	24	Mitscherlich and Moll (1970)
Freiburg, SW-Germany	European beech	848	80	16.93455 189	0.203653 302	850	30	Mitscherlich and Moll (1970)
Steppe, Eastern Europe	Aspen		20			500	18	Molchanov (1963)

Appendix A

Steppe, Eastern Europe	Aspen	40	500	17	Molchanov (1963)
Steppe, Eastern Europe	Aspen	60	500	13	Molchanov (1963)
Steppe, Eastern Europe	Aspen	80	500	10	Molchanov (1963)
Steppe, Eastern Europe	European ash	20	500	21	Molchanov (1963)
Steppe, Eastern Europe	European ash	40	500	20	Molchanov (1963)
Steppe, Eastern Europe	European ash	60	500	17	Molchanov (1963)
Steppe, Eastern Europe	European ash	80	500	13	Molchanov (1963)
Moscow, Russia	Scots pine	20	550	23	Molchanov (1963)
Moscow, Russia	Scots pine	40	550	27	Molchanov (1963)
Moscow, Russia	Scots pine	60	550	25	Molchanov (1963)
Moscow, Russia	Scots pine	80	550	25	Molchanov (1963)
Moscow, Russia	Scots pine	100	550	22	Molchanov (1963)

Moscow, Russia	Scots pine	120	550	19	Molchanov (1963)
Moscow, Russia	Scots pine	140	550	18	Molchanov (1963)
Moscow, Russia	Scots pine	160	550	18	Molchanov (1963)
Steppe, Eastern Europe	Strandzha oak	20	550	9	Molchanov (1963)
Steppe, Eastern Europe	Strandzha oak	40	550	12	Molchanov (1963)
Steppe, Eastern Europe	Strandzha oak	60	550	12	Molchanov (1963)
Steppe, Eastern Europe	Strandzha oak	80	550	11	Molchanov (1963)
Steppe, Eastern Europe	Strandzha oak	100	550	11	Molchanov (1963)
Steppe, Eastern Europe	Strandzha oak	120	550	11	Molchanov (1963)
Steppe, Eastern Europe	Strandzha oak	140	550	11	Molchanov (1963)
Steppe, Eastern Europe	Strandzha oak	160	550	11	Molchanov (1963)
Steppe, Eastern Europe	Strandzha oak	220	550	12	Molchanov (1963)

Appendix A

Salamanca, W-Spain	Pyrenean oak	820		13	0.152	1580	14.3	Moreno et al. (2001)
Salamanca, W-Spain	Pyrenean oak	405		17	0.254	1245	13.4	Moreno et al. (2001)
Salamanca, W-Spain	Pyrenean oak	1043		8.5	0.11	872	14.2	Moreno et al. (2001)
Salamanca, W-Spain	Pyrenean oak	740		12	0.165	720	15.8	Moreno et al. (2001)
Càceres, W-Spain	Sweet chestnut					444.5	19.1	Moreno et al. (2001)
Emilia-Romagna, NW-Italy	European beech	4356	40	12.8	0.103	1800	19.8	Mosello et al. (2002)
Veneto, NW-Italy	European beech	345	110	24.5	0.362	1900	12.5	Mosello et al. (2002)
Calabria, S-Italy	European beech	327	110	25	0.397	1500	22.6	Mosello et al. (2002)
Abruzzo, C-Italy	European beech	889	110	19.9	0.243	1300	20.3	Mosello et al. (2002)
Campania, SW-Italy	European beech	228	100	27.6	0.52	1250	10.9	Mosello et al. (2002)
Piedmont, NW-Italy	European beech	1200	55	15.4	0.178	1500	7.9	Mosello et al. (2002)
Friuli-Venezia Giulia, NE-Italy	European hornbeam					1100	18.8	Mosello et al. (2002)

Tuscany, C-Italy	Evergreen oak	2366	50	12.2	0.127	900	18.8	Mosello et al. (2002)
Emilia-Romagna, N-Italy	Sessile oak	2131	45	12.9	0.125	1200	7.2	Mosello et al. (2002)
Emilia-Romagna, N-Italy	Turkey oak	2131	45	12.9	0.125	1200	7.5	Mosello et al. (2002)
Sicily, S-Italy	Turkey oak	847	50	15.2	0.196	800	23.625	Mosello et al. (2002)
Lazio, C-Italy	Turkey oak	1623	35	14.1	0.141	1000	2.2	Mosello et al. (2002)
Marche, C-Italy	Turkey oak	4299	35	12.4	0.106	1250	15.4	Mosello et al. (2002)
Trentino-Alto Adige, N-Italy	Norway spruce	391	200	28.6	0.422	800	21.2	Mosello et al. (2002)
Friuli-Venezia Giulia, NE-Italy	Norway spruce	554	110	29.4	0.352	1500	21.8	Mosello et al. (2002)
Lombardy, N-Italy	Norway spruce	1031	80	18.8	0.228	1300	18.9	Mosello et al. (2002)
Pindous Mountains Range, C-Greece	Evergreen oak		80			1150	35.8	Michopoulos et al. (2001)
Hampshire, United Kingdom	European beech			21		800	15	Neal et al. (1993)
Évora, S-Portugal	Holm oak	30		7.3		665	6.2	Pereira 2009

Appendix A

Tras-os-Montes, N-Portugal	Sweet chestnut	67		10	0.412	1133	10.1	Portela and Pires (1995)
Tras-os-Montes, N-Portugal	Sweet chestnut	67		9	0.392	1133	5.4	Portela and Pires (1995)
Languedoc, SE-France	Stone pine	800			0.202	648	27.8	Rapp and Ibrahim (1978)
Languedoc, SE-France	Aleppo pine	660		12		770		Rapp and Romane (1968)
Languedoc, SE-France	Evergreen oak	525		15		478.5		Rapp and Romane (1968)
Languedoc, SE-France	Evergreen oak	1440		11		810.5		Rapp and Romane (1968)
Montseny Range, NE-Spain	European beech	50	70	20	0.207	1214	19.7	Ferrés et al. (1984)
Montseny Range, NE-Spain	Silver fir	1034	160	25	0.318	1021	16.1	Ferrés et al. (1984)
Montseny Range, NE-Spain	Evergreen oak	2546	90	12	0.186	849		Rodà et al. (1990)
Montseny Range, NE-Spain	Evergreen oak	2127		6	0.113	876	21.9	Rodrigo et al. (2003)
Montseny Range, NE-Spain	Evergreen oak	1753		6.4	0.12	876	22.6	Rodrigo et al. (2003)
Hampshire, United Kingdom	Corsican pine			20		800	35	Rutter et al. (1975)

Hampshire, United Kingdom	Douglas fir			24		800	39	Rutter et al. (1975)
Oxford, United Kingdom	European hornbeam			15		800	36	Rutter et al. (1975)
Oxford, United Kingdom	Norway spruce			17		800	48	Rutter et al. (1975)
Oxford, United Kingdom	Pedunculate oak			15		800	18	Rutter et al. (1975)
Salamanca, W-Spain	Scots pine	1700		9	0.198	985	8.5	Santa Regina (1995)
Lazio, C-Italy	Turkey oak	2375					67.5	Scarascia-Mugnozza et al. (1988)
S-Belgium	Oaks					1100	17	Schnock (1971)
Dragonja, SW-Slovenia	Manna ash	3100	35	8	0.07	1318.6	28.4	Šraj et al. (2008)
Rokawa, SW-Slovenia	Oriental hornbeam	825	35	12.32	0.14	1150	25.4	Šraj et al. (2008)
Burgos-Logroño, C-Spain	European beech	526	50	22	0.15	895	29	Tarazona et al. (1996)
Burgos-Logroño, C-Spain	Scots pine	581	50	15	0.35	895	48.4	Tarazona et al. (1996)
S-Scotland, United Kingdom	Sitka spruce	3000		10	0.15	1000	29.1	Teklehaimanot et al. (1991)
S-Scotland, United Kingdom	Sitka spruce	625		10	0.15	1000	29.4	Teklehaimanot et al. (1991)

Appendix A

S-Scotland, United Kingdom	Sitka spruce	277		10	0.15	1000	13.9	Teklehaimanot et al. (1991)
S-Scotland, United Kingdom	Sitka spruce	156		10	0.15	1000	9.7	Teklehaimanot et al. (1991)
Corse, France	Corsican pine	302	140	38		1612		Ulrich et al. (1995)
Mirailles, Aude, S-France	Silver fir	449	80	28		1210	26.4	Ulrich et al. (1995)
Hautes Alpes, SE-France	Silver fir	366		27		1063	37.9	Ulrich et al. (1995)
Pinhal da Carrasquiera, C-Portugal	Maritime pine	312	60	23.9	0.337	800	17.1	Valente et al. (1997)
Herdade da Espirra, C-Portugal	Tasmania n bluegum	1010	7	16.5	0.142	800	10.8	Valente et al. (1997)
Pinhal da Carrasqueira, C-Portugal	Maritime pine	312	60		0.337	600	17.1	Valente et al. (1997)
Portucel, C-Portugal	Tasmania n bluegum	1010	7	16.5	0.142	600	10.8	Valente et al. (1997)
Aubure, France	Norway spruce	575	90	25		1400	34.2	Viville et al. (1993)

SW-Georgia, U.S.A.	Chapman oak	1411	50	8.5	0.14	830	17.4	Bryant et al. (2005)
SW-Georgia, U.S.A.	Loblolly pine	370	43	15.3	0.246	830	22.3	Bryant et al. (2005)
SW-Georgia, U.S.A.	Longleaf pine	2050	13	8	0.1	830	17.6	Bryant et al. (2005)
SW-Georgia, U.S.A.	Sweetgum	1100	65	13.8	0.17	830	17.7	Bryant et al. (2005)
SW-Georgia, U.S.A.	White oak	711		11.65	0.158	830	18.6	Bryant et al. (2005)
S-Central Washington State, U.S.A.	Douglas fir		500	60		2467	23.9	Link et al. (2004)
S-British Columbia, Canada	Lodgepole pine		125			590	24	Moore et al. (2008)
S-British Columbia, Canada	Lodgepole pine		125			590	31	Moore et al. (2008)
S-Ontario, Canada	Northern red oak	442			0.27725	785	18.8	Price and Carlyle-Moses (2003)
S-Washington State, U.S.A.	Douglas fir		25	20		2500	21	Pypker et al. (2005)
S-Washington State, U.S.A.	Western hemlock	441	450	65		2500	24	Pypker et al. (2005)
C-Oregon, U.S.A.	Western hemlock		450			2300	32.7	Pypker et al. (2006)

Appendix A

N-California, U.S.A.	California redwood	538	120		1285	17.7	Reid and Lewis (2009)
N-California, U.S.A.	California redwood	475	120		1285	22.4	Reid and Lewis (2009)
S-Georgia, U.S.A.	Southern live oak	278		0.366	950	37	Van Stan et al. (2016)

APPENDIX B

Location	Dominant species	Mean elevation [m]	Mean steepness [-]	MAP [mm yr ⁻¹]	DBH [m]	WRB soil classification	USDA soil classification	Silvicultural system
Averara (BG)	Silver fir	1075	0.91	1400	0.33	Cambisols on porphyry bedrock	loamy sand	High forest
Cusio (BG)	Silver fir	1284	0.40	1400	0.31	Cambisols on sandstone, siltstone and mudstone	loamy sand	High forest
Boario (BS)	Sweet chestnut	595	0.64	1350	0.13	Cambisols on alluvial deposits	loamy sand	Coppice
Casargo (LC)	Sweet chestnut	980	0.35	1550	0.2	Umbrisols on conglomerates and sandstone	loamy sand	Coppice
Crandola (LC)	Sweet chestnut	1012	0.61	1550	0.18	Regosols on conglomerates and sandstone	sandy loam	Coppice
Villa di Chiavenna (SO)	Sweet chestnut	776	0.46	1350	0.31	Regosols on alluvial deposits	loamy sand	Coppice

Appendix B

Brenta (VA)	Sweet chestnut	850	0.50	1250	0.2	Cambisols on marls and sandstone	clay loam	Coppice
Valduggia (VC)	Sweet chestnut	700	0.35	1019	0.16	Cambisols on limestone and dolomite	loamy sand	Coppice
Oneta (BG)	Fraxinus excelsior L.	646	0.16	1800	0.23	Cambisols on mudstone, marls and limestone	loamy sand	Coppice
Prestine (BS)	Common ash	867	0.46	1390	0.19	Cambisols on sandstone, marls, siltstone, mudstone and limestone	loam	High forest
Pasturo (LC)	Common ash	700	0.61	1600	0.06	Cambisols on alluvial deposits	loam	Coppice
Vararo (VA)	Common ash	790	0.64	1250	0.25	Leptosols on marls and limestone	loamy sand	High forest
Malegno (BS)	Common ash	807	0.65	890	0.06	Cambisols on limestone	clay loam	Coppice
Artogne (BS)	European beech	1197	0.63	1350	0.23	Podzol on phyllites and mica-schists	loamy sand	Coppice

Gianico (BS)	European beech	964	0.47	1350	0.24	Cambisols on phyllites and mica-schists	loamy sand	Coppice
Montemezzo (CO)	European beech	1370	0.53	1750	0.14	Cambisols on granite bedrock	loamy sand	Coppice
Moggio (LC)	European beech	949	0.26	1680	0.34	Cambisols on dolomite	loamy sand	Coppice
Morterone (LC)	European beech	1266	0.38	1800	0.22	Cambisols on marls and limestone	clay	Coppice
Castione della Presolana (BG)	European larch	1464	0.47	1500	0.55	Cambisols on mudstone, marls and limestone	clay	High forest
Montemezzo (CO)	European larch	1562	0.42	1750	0.23	Umbrisols on granite bedrock	loamy sand	High forest
Fino del Monte (BG)	Norway spruce	931	0.42	1500	0.34	Leptosols on dolomite	loam	High forest
Castione della Presolana (BG)	Norway spruce	1477	0.53	1500	0.37	Cambisols on mudstone, marls and limestone	clay	High forest
Incudine (BS)	Norway spruce	1209	0.40	1040	0.37	Cambisols on alluvial deposits	loamy sand	High forest
Montemezzo (CO)	Norway spruce	1548	0.56	1750	0.24	Umbrisols on granite bedrock	loamy sand	High forest

Appendix B

Piuro (SO)	Norway spruce	1095	0.77	1350	0.46	Umbrisols on basaltic bedrock	loamy sand	High forest
Villa di Chiavenna (SO)	Norway spruce	1085	0.48	1350	0.22	Regosols on paragneiss	loamy sand	High forest
Ponte Nossa (BG)	Black locust	454	0.30	980	0.11	Leptosols on dolomite	loam	Coppice
Opera (MI)	Black locust	98	n.a.	970	0.1	Cambisols on conglomerates	loamy sand	Coppice
Broni (PV)	Black locust	71	n.a.	685	0.12	Vertisols on conglomerates	clay	Coppice

APPENDIX C

This appendix summarizes the major equations of the 3D slope stability analysis incorporated in PRIMULA, which is completely described by Milledge et al. (2014). The model uses the Rankine method at both the upslope and downslope wedges to estimate the earth pressure coefficients. The active K_A and the passive K_P earth pressure coefficients of rooted soils are obtained through the Rankine solution for cohesive soils on hillslopes and defined as follows.

$$K_P, K_A = \frac{1}{\cos^2 \phi'} \left\{ \begin{array}{l} 2 \cos^2 \theta + 2 \left(\frac{C'_{rl}}{\gamma_s z} \right) \cos \phi' \sin \phi' \pm \\ \left[\begin{array}{l} 4 \cos^2 \theta (\cos^2 \theta - \cos^2 \phi') \\ + 4 \left(\frac{C'_{rl}}{\gamma_s z} \right)^2 \cos^2 \phi' \\ + 8 \left(\frac{C'_{rl}}{\gamma_s z} \right) \cos^2 \theta \sin \phi' \cos \phi' \end{array} \right]^{0.5} \end{array} \right\} - 1 \dots\dots\dots(A1)$$

The resistance and driving forces, shown in Figure 2.2, are described as follows.

- The basal resistance force F_{rb} that acts along the base of the block is the product of the normal force on the failure surface and the tangent of the friction angle, considering basal root cohesion negligible. F_{rb} is described as follows.

$$F_{rb} = \left[\begin{array}{l} (\gamma_s - \gamma_w m) \cos^2 \theta l \\ - \frac{1}{2} (K_P - K_A) z (\gamma_s - \gamma_w m^2) \sin(\delta - \theta) \end{array} \right] z w \tan \phi' \dots\dots\dots(A2)$$

- The shear resistance on two parallel and vertical cross-slope sides of the element, F_{rl} , can be predicted from the standard earth pressure theory and has the following form.

$$F_{rl} = \frac{1}{2} K_0 (\gamma_s - \gamma_w m^2) l z^2 \cos \theta \tan \phi' + C'_{rl} l z \cos \theta \quad (\text{A3})$$

- The passive earth pressure from the downslope wedge, F_{rd} , is defined as follows.

$$F_{rd} = \frac{1}{2} K_p z^2 (\gamma_s - \gamma_w m^2) w \cos(\delta - \theta) \quad (\text{A4})$$

- The central block weight force acting downslope along the failure surface, F_{dc} that corresponds to the driving stress integrated over the frontal surface of the block is as follows.

$$F_{dc} = \gamma_s z w l \sin \theta \cos \theta \quad (\text{A5})$$

- The active earth pressure from the upslope wedge represents the net driving force on the upslope margin and has a negative effect on the block stability:

$$F_{du} = \frac{1}{2} K_A z^2 (\gamma_s - \gamma_w m^2) w \cos(\delta - \theta) \quad (\text{A6})$$

where the Rankine method assumes that $\delta = \theta$.

APPENDIX D

This appendix briefly describes the Root Distribution Model, RDM, which predicts the spatial distribution of the root density. Introduced by Schwarz et al. (2010b), the RDM is based on a static fractal branching model (Tobin et al., 2007) and pipe theory, which demonstrates the strong correlation between the total number of fine roots and an allometric parameter (Osawa and Allen, 1993). In this model, the total number of fine roots N_{fr} and the maximum distance from the stem where coarse roots are found d_{max} are evaluated as follows.

$$N_{fr} = \mu DBH \quad (B1)$$

$$d_{max} = a_0 DBH \quad (B2)$$

The coefficient μ is the pipe theory coefficient, and a_0 is a proportionality constant empirically estimated by authors such as Roering et al. (2003) and Ammer and Wagner (2005) to estimate the fine root density D_{fr} as a function of the distance from a single tree stem d_{stem} . The model proposes the following equations:

$$D_{fr}(d_{stem}, DBH) = \begin{cases} \frac{N_{fr}}{d_{max}} \left[\alpha + (1 - \alpha) \frac{d_{stem}}{m DBH} \right], & d_{stem} < \chi DBH \\ \frac{N_{fr}}{d_{max}} \left(\frac{1}{2 \pi d_{stem}} \right), & d_{stem} \geq \chi DBH \end{cases} \quad (B3)$$

where α and χ are two empirical coefficients. Schwarz et al. (2012a) calibrated α as 0.7 and χ as 5. The coarse root density is evaluated as a function of root diameter between the fine root diameter (0.5-1.5 mm) and maximum root diameter ϕ_{max} , which is calculated based on empirical root distribution data (Moroni et al., 2003; Schwarz et al., 2010b; Waldron and

Dakessian, 1981; Wu et al., 1988). The resulting root distribution function is as follows:

$$N_{roots}(\phi_i, \phi_{max}) = D_{fr} \frac{[\ln(1 + \phi_{max}) - \ln(1 + \phi_i)]}{\ln(1 + \phi_{max})} \left(\frac{\phi_i}{\phi_0} \right)^\lambda \quad (B4)$$

where ϕ_i is the mean diameter of roots in class i , ϕ_0 is the reference diameter equal to 1 and λ assumes a value of -1. ϕ_{max} is mainly a function of distance and can be evaluated as follows:

$$\phi_{max}(d_{stem}) = \frac{d_{max} - d_{stem}}{BD} CSA_{fr} PF \quad (B5)$$

where BD is the average value of branching distance (0.09 m for the coniferous forest in Schwarz et al. 2012a), CSA_{fr} is the mean cross-sectional area of fine roots (equal to $\pi/4$) and PF is a constant proportionality factor (0.28 mm^{-1} for the coniferous forest in Schwarz et al. 2012a). The model requires that the root distribution of a single tree is (i) radially symmetrical and (ii) not influenced by neighbouring trees.

APPENDIX E

This appendix reports in details the equations for the log-spiral method developed by Soubra and Macuh (2002) for sloping backfill including friction and cohesion strength.

$$K_{P\gamma} = \frac{2}{\left(\frac{l}{r_0}\right)^2} \frac{f_1 - f_2 - f_3}{g_4} \quad (\text{E.1})$$

$$K_{Pq} = \frac{1}{r_0} \frac{f_6}{f_4} \quad (\text{E.2})$$

$$K_{Pc} = \frac{1}{r_0} \frac{f_7 - f_5}{f_4} \quad (\text{E.3})$$

$$f_1 = - \left\{ \frac{e^{3(\theta_1 - \theta_0)\tan(\phi')} [3 \tan(\phi') \sin(\theta_1) - \cos(\theta_1)]}{3 [9 \tan^2(\phi')] - 3 \tan(\phi') \sin(\theta_0) + \cos(\theta_0)} \right\} \quad (\text{E.4})$$

$$f_2 = - \frac{1}{6} \frac{L}{r_0} \left[2 \sin(\theta_0) - 2 \frac{l}{r_0} \sin(\lambda) + \frac{L}{r_0} \cos(\beta) \right] \cos(\theta_1 - \beta) e^{(\theta_1 - \theta_0)\tan(\phi')} \quad (\text{E.5})$$

$$f_3 = - \frac{1}{6} \frac{l}{r_0} \sin(\theta_0 - \lambda) \left[2 \sin(\theta_0) - \frac{l}{r_0} \sin(\lambda) \right] \quad (\text{E.6})$$

$$g_4 = \cos(\delta - \lambda) \left[\cos(\theta_0) - \frac{1}{3} \frac{l}{r_0} \cos(\lambda) \right] - \sin(\delta - \lambda) \left[\sin(\theta_0) - \frac{1}{3} \frac{l}{r_0} \sin(\lambda) \right] \quad (\text{E.7})$$

$$f_4 = \cos(\delta - \lambda) \left[\cos(\theta_0) - \frac{1}{2} \frac{l}{r_0} \cos(\lambda) \right] - \sin(\delta - \lambda) \left[\sin(\theta_0) - \frac{1}{2} \frac{l}{r_0} \sin(\lambda) \right] \quad (\text{E.8})$$

$$f_5 = \frac{l}{r_0} \frac{\tan(\delta)}{\tan(\phi')} \sin(\lambda - \theta_0) \quad (\text{E.9})$$

$$f_6 = \frac{L}{r_0} \left[-\sin(\theta_0) + \frac{l}{r_0} \sin(\lambda) - \frac{1}{2} \frac{L}{r_0} \cos(\beta) \right] \quad (\text{E.10})$$

$$f_7 = \frac{1}{2 \tan(\phi')} \left[e^{2(\theta_1 - \theta_0) \tan(\phi')} - 1 \right] \quad (\text{E.11})$$

$$f_8 = \frac{L}{r_0} \left[\sin(\beta - \theta_0) + \frac{l}{r_0} \sin(\lambda - \beta) - \frac{1}{2} \frac{L}{r_0} \right] \quad (\text{E.12})$$

where

$$\frac{l}{r_0} = - \frac{e^{(\theta_1 - \theta_0) \tan(\phi')} \cos(\theta_1 - \beta) + \cos(\theta_0 - \beta)}{\cos(\beta - \lambda)} \quad (\text{E.13})$$

$$\frac{L}{r_0} = \frac{e^{3(\theta_1 - \theta_0) \tan(\phi')} [\sin(\theta_1) - \cos(\theta_1) \tan(\lambda)] - \sin(\theta_0) + \cos(\theta_0) \tan(\lambda)}{\sin(\beta) \tan(\lambda) + \cos(\beta)} \quad (\text{E.14})$$

The results obtained with equation E.3 indicate that the coefficient K_{Pc} respects the Caquot's theorem of corresponding states (Caquot, 1934) through the following relationship:

$$K_{Pc} = \frac{K_{Pq0} - \frac{1}{\cos(\delta)}}{\tan(\phi')} \quad (\text{E.15})$$

where

$$K_{Pq0} = - \frac{1}{\frac{l}{r_0}} \frac{f_8}{f_4} \quad (\text{E.16})$$

REFERENCES

- ✓ Abbe, T.B., Brooks, A.P., 2011. Geomorphic, engineering and ecological considerations when using wood in river restoration, in: *Stream Restoration in Dynamic Fluvial Systems: Scientific Approaches, Analyses, and Tools*. AGU, Washington, D.C., pp. 419–451.
- ✓ Abbe, T.B., Montgomery, D.R., 1996. Large woody debris jams, channel hydraulics and habitat formation in large rivers. *Regul. Rivers Res. Manag.* 12, 201–221.
- ✓ Abdelli, F., 1999. Análisis comparativo de distintas comunidades vegetales a la distribución del agua de lluvia, a la conservación del agua en el suelo ya la recarga de acuíferos en medios semiáridos (Master thesis). International Center for Advanced Mediterranean Agronomic Studies, Zaragoza, Spain.
- ✓ Abdi, E., Majnounian, B., Genet, M., Rahimi, H., 2010. Quantifying the effects of root reinforcement of Persian Ironwood (*Parrotia persica*) on slope stability; a case study: Hillslope of Hyrcanian forests, northern Iran. *Ecol. Eng.* 36, 1409–1416. doi:10.1016/j.ecoleng.2010.06.020
- ✓ Abdi, E., Majnounian, B., Rahimi, H., Zobeiri, M., 2009. Distribution and tensile strength of Hornbeam (*Carpinus betulus*) roots growing on slopes of Caspian Forests, Iran. *J. For. Res.* 20, 105–110. doi:10.1007/s11676-009-0019-x
- ✓ Abe, K., Iwamoto, M., 1986. Preliminary experiment on shear in soil layers with a large-direct-shear apparatus. *J. Jpn. For. Soc.* 68, 61–65.
- ✓ Abe, K., Ziemer, R.R., 1991. Effect of tree roots on a shear zone: modeling reinforced shear stress. *Can. J. For. Res.* 21, 1012–1019.
- ✓ Abernethy, B., Rutherford, I.D., 2001. The distribution and strength of riparian tree roots in relation to riverbank reinforcement. *Hydrol. Process.* 15, 63–79.
- ✓ Agnoletti, M., Anderson, S., 2000. Forest history: international studies on socioeconomic and forest ecosystem change: report No. 2 of the IUFRO task force on environmental change. CABI.
- ✓ Alavi, G., Jansson, P.-E., Hällgren, J.-E., Bergholm, J., 2001. Interception of a dense spruce forest, performance of a simplified canopy water balance model. *Nord. Hydrol.* 32, 265–284.
- ✓ Alvera, B., 1976. Contribución al estudio de la interceptación de las precipitaciones atmosféricas en el pinar de San Juan de la Peña. *Publicaciones Cent. Piren. Biol. Exp.* 7, 95–100.
- ✓ Alvera, B., 1977. Interceptación de las precipitaciones atmosféricas en un pinar altoaragonés. 1er año de observaciones (1971-1972). *Publicaciones Cent. Piren. Biol. Exp.* 8, 7–13.
- ✓ Ammann, M., Böll, A., Rickli, C., Speck, T., Holdenrieder, O., 2009. Significance of tree root decomposition for shallow landslides. *For. Snow Landsc. Res.* 82, 79.
- ✓ Ammer, C., Wagner, S., 2005. An approach for modelling the mean fine-root biomass of Norway spruce stands. *Trees* 19, 145–153. doi:10.1007/s00468-004-0373-4

- ✓ Amorfini, A., Bartelletti, A., Preti, F., 2002. Analisi dell'evento alluvionale del 19 giugno 1996 in Alta Garfagnana e degli interventi di sistemazione dei versanti. *Quad. Idronomia Mont.* 18, 39–64.
- ✓ Anagnostopoulos, G.G., Fatichi, S., Burlando, P., 2015. An advanced process-based distributed model for the investigation of rainfall-induced landslides: The effect of process representation and boundary conditions. *Water Resour. Res.* 51, 7501–7523. doi:10.1002/2015WR016909
- ✓ Ancel, J., 1986. Effects de la non culture sur le système racinaire de la vigne et sur quelques caractéristiques du sol, in: *Annales ANPP, 2 E Symp. Int. Sur La Non Culture de La Vigne et Les Autres Techniques D'entretien Du Sol*, Montpellier (France). pp. 337–344.
- ✓ Anderson, B.G., Rutherford, I.D., Western, A.W., 2006. An analysis of the influence of riparian vegetation on the propagation of flood waves. *Environ. Model. Softw.* 21, 1290–1296. doi:10.1016/j.envsoft.2005.04.027
- ✓ Anderson, C.J., Coutts, M.P., Ritchie, R.M., Campbell, D.J., 1989. Root extraction force measurements for Sitka spruce. *Forestry* 62, 127–137.
- ✓ Anderson, N.H., Sedell, J.R., Roberts, L.M., Triska, F.J., 1978. The role of aquatic invertebrates in processing of wood debris in coniferous forest streams. *Am. Midl. Nat.* 100, 64–82.
- ✓ Andréassian, V., 2004. Waters and forests: from historical controversy to scientific debate. *J. Hydrol.* 291, 1–27. doi:10.1016/j.jhydrol.2003.12.015
- ✓ Anfodillo, T., Carrer, M., Simini, F., Popa, I., Banavar, J.R., Maritan, A., 2013. An allometry-based approach for understanding forest structure, predicting tree-size distribution and assessing the degree of disturbance. *Proceedings of the Royal Society B: Biological Sciences* 280, 20122375. doi:10.1098/rspb.2012.2375
- ✓ Antón, A., Elosegi, A., García-Arberas, L., Díez, J., Rallo, A., 2011. Restoration of dead wood in Basque stream channels: effects on brown trout population: Restoration of dead wood in Basque stream channels. *Ecol. Freshw. Fish* 20, 461–471. doi:10.1111/j.1600-0633.2010.00482.x
- ✓ Araujo, F., Williams, L.E., Grimes, D.W., Matthews, M.A., 1995. A comparative study of young “Thompson Seedless” grapevines under drip and furrow irrigation. I. Root and soil water distributions. *Sci. Hortic.* 60, 235–249.
- ✓ Archer, E., Strauss, H.C., 1985. Effect of plant density on root distribution of three-year-old grafted 99 Richter grapevines. *South Afr. J. Enol. Vitic.* 6, 25–30.
- ✓ Archer, E., Strauss, H.C., others, 1990. The effect of vine spacing on some physiological aspects of *Vitis vinifera* L.(cv. Pinot noir). *South Afr. J. Enol. Vitic.* 11, 76–87.
- ✓ Arnone, E., Dialynas, Y.G., Noto, L.V., Bras, R.L., 2014. Parameter uncertainty in shallow rainfall-triggered landslide modeling at basin scale: a probabilistic approach. *Procedia Earth Planet. Sci.* 9, 101–111. doi:10.1016/j.proeps.2014.06.003
- ✓ Arnone, E., Noto, L.V., Lepore, C., Bras, R.L., 2011. Physically-based and distributed approach to analyze rainfall-triggered landslides at watershed scale. *Geomorphology* 133, 121–131. doi:10.1016/j.geomorph.2011.03.019

-
- ✓ Askarinejad, A., Casini, F., Bischof, P., Beck, A., Springman, S.M., 2012. Rainfall induced instabilities: a field experiment on a silty sand slope in northern Switzerland. *Ital. Geotech. J.* 3, 50–71.
 - ✓ Aşkın, T., Kızılkaya, R., Yılmaz, R., Olekhov, V., Mudrykh, N., Samofalova, I., 2012. Soil exchangeable cations: A geostatistical study from Russia. *Eurasian J. Soil Sci.* 1, 34–39.
 - ✓ Aussenac, G., 1968. Interception des précipitations par le couvert forestier. *Ann. Sci. For.* 25, 135–156. doi:10.1051/forest/19680302
 - ✓ Aussenac, G., 2000. Interactions between forest stands and microclimate: ecophysiological aspects and consequences for silviculture. *Ann. For. Sci.* 57, 287–301.
 - ✓ Badoux, A., Böckli, M., Rickenmann, D., Rickli, C., Ruiz-Villanueva, V., Zurbrügg, S., Stoffel, M., 2015. Large wood transported during the exceptional flood event of 24 July 2014 in the Emme catchment (Switzerland), in: *Proceedings of the 3rd International Conference Wood in World Rivers*. Padova, Italy.
 - ✓ Baeza, C., Corominas, J., 2001. Assessment of shallow landslide susceptibility by means of multivariate statistical techniques. *Earth Surf. Process. Landf.* 26, 1251–1263. doi:10.1002/esp.263
 - ✓ Balasubramanyan, S., Manivannan, M.I., 2008. Root pattern studies in acid lime in silt clay soils. *Asian J. Hortic.* 3, 241–245.
 - ✓ Balázs, A., 1982. Interzeptions-Verdunstung des Waldes im Winterhalbjahr als Bestimmungsgrosse des nutzbaren Wasserdargebotes, in: de Haar, U., Hoffmann, D. (Eds.), *Wasser aus dem Wald, Wasser für den Wald/herausgegeben*.
 - ✓ Balestrini, R., Tagliaferri, A., 2001. Atmospheric deposition and canopy exchange processes in alpine forest ecosystems (northern Italy). *Atmos. Environ.* 35, 6421–6433.
 - ✓ Bassanelli, C., Bischetti, G.B., Chiaradia, E.A., Rossi, L., Vergani, C., 2013. The contribution of chestnut coppice forests on slope stability in abandoned territory: a case study. *J. Agric. Eng.* 44, 68–73. doi:10.4081/jae.2013.s2.e13
 - ✓ BassiriRad, H., 2005. *Nutrient acquisition by plants: an ecological perspective*. Springer Science & Business Media.
 - ✓ Bathurst, J.C., Bovolo, C.I., Cisneros, F., 2010. Modelling the effect of forest cover on shallow landslides at the river basin scale. *Ecol. Eng.* 36, 317–327. doi:10.1016/j.ecoleng.2009.05.001
 - ✓ Bauhus, J., Bartsch, N., 1996. Fine-root growth in beech (*Fagus sylvatica*) forest gaps. *Can. J. For. Res.* 26, 2153–2159.
 - ✓ Baum, R.L., Coe, J.A., Godt, J.W., Harp, E.L., Reid, M.E., Savage, W.Z., Schulz, W.H., Brien, D.L., Chleborad, A.F., McKenna, J.P., Michael, J.A., 2005. Regional landslide-hazard assessment for Seattle, Washington, USA. *Landslides* 2, 266–279. doi:10.1007/s10346-005-0023-y
 - ✓ Baum, R.L., Savage, W.Z., Godt, J.W., 2002. TRIGRS—A Fortran program for transient rainfall infiltration and grid-based regional slope-stability analysis, version 2.0. *US Geol. Surv. Open-File Rep.* 2008-1159 75.
-

References

- ✓ Beckman, N.D., Wohl, E., 2014. Carbon storage in mountainous headwater streams: The role of old-growth forest and logjams. *Water Resour. Res.* 50, 2376–2393. doi:10.1002/2013WR014167
- ✓ Beguería, S., 2006. Changes in land cover and shallow landslide activity: A case study in the Spanish Pyrenees. *Geomorphology* 74, 196–206. doi:10.1016/j.geomorph.2005.07.018
- ✓ Bellot, J., Àvila, A., Rodrigo, A., 1999. Throughfall and stemflow, in: *Ecology of Mediterranean Evergreen Oak Forests*, Ecological Studies. Springer, pp. 209–222.
- ✓ Bellot, J., Escarre, A., 1998. Stemflow and throughfall determination in a resprouted Mediterranean holm-oak forest. *Ann. Sci. For.* 55, 847–865.
- ✓ Bellugi, D., Milledge, D.G., Dietrich, W.E., McKean, J.A., Perron, J.T., Sudderth, E.B., Kazian, B., 2015a. A spectral clustering search algorithm for predicting shallow landslide size and location: A shallow landslide search algorithm. *J. Geophys. Res. Earth Surf.* 120, 300–324. doi:10.1002/2014JF003137
- ✓ Bellugi, D., Milledge, D.G., Dietrich, W.E., Perron, J.T., McKean, J., 2015b. Predicting shallow landslide size and location across a natural landscape: Application of a spectral clustering search algorithm. *J. Geophys. Res. Earth Surf.* 120, 2552–2585. doi:10.1002/2015JF003520
- ✓ Belmonte, F., 1997. *Interceptación en bosque y matorral mediterráneo semiárido: balance hídrico y distribución espacial de la lluvia neta* (PhD dissertation). Universidad de Murcia, Murcia, Spain.
- ✓ Benda, L., Dunne, T., 1997. Stochastic forcing of sediment supply to channel networks from landsliding and debris flow. *Water Resour. Res.* 33, 2849–2863.
- ✓ Benda, L., Miller, D., Bigelow, P., Andras, K., 2003a. Effects of post-wildfire erosion on channel environments, Boise River, Idaho. *For. Ecol. Manag.* 178, 105–119. doi:10.1016/S0378-1127(03)00056-2
- ✓ Benda, L., Veldhuisen, C., Black, J., 2003b. Debris flows as agents of morphological heterogeneity at low-order confluences, Olympic Mountains, Washington. *Geol. Soc. Am. Bull.* 115, 1110–1121.
- ✓ Benda, L.E., Bigelow, P., Worsley, T.M., 2002. Recruitment of wood to streams in old-growth and second-growth redwood forests, northern California, U.S.A. *Can. J. For. Res.* 32, 1460–1477. doi:10.1139/x02-065
- ✓ Benda, L.E., Cundy, T.W., 1990. Predicting deposition of debris flows in mountain channels. *Can. Geotech. J.* 27, 409–417.
- ✓ Benda, L.E., Sias, J.C., 2003. A quantitative framework for evaluating the mass balance of in-stream organic debris. *For. Ecol. Manag.* 172, 1–16.
- ✓ Benecke, P., 1984. *Wasserumsatz eines Buchen- und eines Fichtenwaldökosystems im Hochsolling*. Sauerländer.
- ✓ Benecke, P., Van Der Ploeg, R.R., 1978. *Wald und Wasser. II. Quantifizierung des Wasserumsatzes am Beispiel eines Buchen und eines Fichtenaltbestandes im Solling*. *Forstarchiv* 49.

-
- ✓ Benmebarek, S., Khelifa, T., Benmebarek, N., Kastner, R., 2008. Numerical evaluation of 3D passive earth pressure coefficients for retaining wall subjected to translation. *Comput. Geotech.* 35, 47–60. doi:10.1016/j.compgeo.2007.01.008
 - ✓ Benmeddour, D., Mellas, M., Frank, R., Mabrouki, A., 2012. Numerical study of passive and active earth pressures of sands. *Comput. Geotech.* 40, 34–44. doi:10.1016/j.compgeo.2011.10.002
 - ✓ Berger, F., Rey, F., 2004. Mountain protection forests against natural hazards and risks: new French developments by integrating forests in risk zoning. *Nat. Hazards* 33, 395–404.
 - ✓ Beven, K., Freer, J., 2001. A dynamic TOPMODEL. *Hydrol. Process.* 15, 1993–2011. doi:10.1002/hyp.252
 - ✓ Beven, K.J., Kirkby, M.J., 1979. A physically based, variable contributing area model of basin hydrology. *Hydrological Sciences-Bulletin-des Sciences Hydrologiques* 24, 43–69.
 - ✓ Bischetti, G.B., Bassanelli, C., Chiaradia, E.A., Minotta, G., Vergani, C., 2016. The effect of gap openings on soil reinforcement in two conifer stands in northern Italy. *For. Ecol. Manag.* 359, 286–299. doi:10.1016/j.foreco.2015.10.014
 - ✓ Bischetti, G.B., Chiaradia, E.A., 2010. Calibration of distributed shallow landslide models in forested landscapes. *J. Agric. Eng.* 41, 23–35.
 - ✓ Bischetti, G.B., Chiaradia, E.A., Epis, T., Morlotti, E., 2009. Root cohesion of forest species in the Italian Alps. *Plant Soil* 324, 71–89. doi:10.1007/s11104-009-9941-0
 - ✓ Bischetti, G.B., Chiaradia, E.A., Simonato, T., 2004. The role of root reinforcement on May 2002 shallow slope failures in St. Giulio creek catchment (Northern Italy), in: *Internationales Symposium. Presented at the Proceedings of the 1st Congress INTERPRAEVENT 2004, Research Society INTERPRAEVENT, Riva del Garda (Trient, Italy)*, pp. 57–67.
 - ✓ Bischetti, G.B., Chiaradia, E.A., Simonato, T., Speziali, B., Vitali, B., Vullo, P., Zocco, A., 2005. Root strength and root area ratio of forest species in Lombardy (Northern Italy). *Plant Soil* 278, 11–22. doi:10.1007/s11104-005-0605-4
 - ✓ Blahut, J., Glade, T., Sterlacchini, S., 2014. Debris flows risk analysis and direct loss estimation: the case study of Valtellina di Tirano, Italy. *J. Mt. Sci.* 11, 288–307. doi:10.1007/s11629-013-2806-2
 - ✓ Blum, H., 1932. Wirtschaftliche Dalbenformen und deren Berechnung. *Bautechnik* 10, 122–135.
 - ✓ Bohm, W., 1979. Methods of studying root systems. *Methods Stud. Root Syst.*
 - ✓ Bordoni, M., Meisina, C., Valentino, R., Bittelli, M., Chersich, S., 2015a. Site-specific to local-scale shallow landslides triggering zones assessment using TRIGRS. *Nat. Hazards Earth Syst. Sci.* 15, 1025–1050. doi:10.5194/nhess-15-1025-2015
 - ✓ Bordoni, M., Meisina, C., Valentino, R., Lu, N., Bittelli, M., Chersich, S., 2015b. Hydrological factors affecting rainfall-induced shallow landslides: From the field monitoring to a simplified slope stability analysis. *Eng. Geol.* 193, 19–37. doi:10.1016/j.enggeo.2015.04.006
 - ✓ Bordoni, M., Meisina, C., Vercesi, A., Bischetti, G.B., Chiaradia, E.A., Vergani, C., Chersich, S., Valentino, R., Bittelli, M., Comolli, R., Persichillo, M.G., Cislaghi, A., 2016. Quantifying the
-

- contribution of grapevine roots to soil mechanical reinforcement in an area susceptible to shallow landslides. *Soil Tillage Res.* 163, 195–206. doi:10.1016/j.still.2016.06.004
- ✓ Borga, M., Dalla Fontana, G., Da Ros, D., Marchi, L., 1998. Shallow landslide hazard assessment using a physically based model and digital elevation data. *Environ. Geol.* 35, 81–88.
 - ✓ Borga, M., Dalla Fontana, G., Cazorzi, F., 2002. Analysis of topographic and climatic control on rainfall-triggered shallow landsliding using a quasi-dynamic wetness index. *J. Hydrol.* 268, 56–71.
 - ✓ Bowles, J.E., 1997. *Foundation analysis and design*, 5th edition. ed. The McGraw-Hill Companies, Inc., Singapore.
 - ✓ Bracken, L.J., Croke, J., 2007. The concept of hydrological connectivity and its contribution to understanding runoff-dominated geomorphic systems. *Hydrol. Process.* 21, 1749–1763. doi:10.1002/hyp.6313
 - ✓ Bragg, D.C., 2000. Simulating catastrophic and individualistic large woody debris recruitment for a small riparian system. *Ecology* 81, 1383–1394.
 - ✓ Branas, J., Vergnes, A., 1957. Morphologie du système racinaire. *Prog. Agric. Vitic.* 1, 3–13.
 - ✓ Brang, P., Schönenberger, W., Frehner, M., Schwitter, R., Thormann, J.-J., Wasser, B., 2006. Management of protection forests in the European Alps: an overview. *For. Snow Landsc. Res.* 80, 23–44.
 - ✓ Brang, P., Schönenberger, W., Ott, E., Gardner, B., 2001. Forests as protection from natural hazards, in: *The Forests Handbook*. pp. 53–81.
 - ✓ Braudrick, C.A., Grant, G.E., 2000. When do logs move in rivers? *Water Resour. Res.* 36, 571–583.
 - ✓ Braudrick, C.A., Grant, G.E., Ishikawa, Y., Ikeda, H., 1997. Dynamics of wood transport in streams: a flume experiment. *Earth Surf. Process. Landf.* 22, 669–683.
 - ✓ Brechtel, H.M., 1970. Wald und Retention-Einfache Methoden zur Bestimmung der lokalen Bedeutung des Waldes für die Hochwasserdämpfung. *Dtsch. Gewässerkd. Mitteilungen* 14, 91–103.
 - ✓ Brenning, A., 2005. Spatial prediction models for landslide hazards: review, comparison and evaluation. *Nat. Hazards Earth Syst. Sci.* 5, 853–862.
 - ✓ Breuer, L., Eckhardt, K., Frede, H.-G., 2003. Plant parameter values for models in temperate climates. *Ecol. Model.* 169, 237–293. doi:10.1016/S0304-3800(03)00274-6
 - ✓ Brinch Hansen, J., 1953. Earth pressure calculation.
 - ✓ Broadmeadow, S., Nisbet, T., 2010. Opportunity mapping for woodland to reduce flooding in the Yorkshire & the Humber Region. *For. Res. Monogr.* 1.
 - ✓ Brockway, D.G., Outcalt, K.W., 1998. Gap-phase regeneration in longleaf pine wiregrass ecosystems. *For. Ecol. Manag.* 106, 125–139.
 - ✓ Brotto, E., 2008. *Le organizzazioni forestali nello Stato*. Provincia autonoma di Trento. Giunta.

-
- ✓ Bryant, M.L., Bhat, S., Jacobs, J.M., 2005. Measurements and modeling of throughfall variability for five forest communities in the southeastern US. *J. Hydrol.* 312, 95–108. doi:10.1016/j.jhydrol.2005.02.012
 - ✓ Buchanan, P., Savigny, K.W., 1990. Factors controlling debris avalanche initiation. *Can. Geotech. J.* 27, 659–675.
 - ✓ Burroughs, E.R., 1985. Landslide hazard rating for portions of the Oregon Coast Range, in: *Proceedings of the Symposium on Effects of Forest Land Use on Erosion and Slope Stability* (May 7-11, 1984). University of Hawaii, Honolulu, pp. 265–274.
 - ✓ Burroughs, E.R., Thomas, B.R., 1977. Declining root strength in Douglas-fir after felling as a factor in slope stability. USDA Forest Service, Intermountain Forest and Range Experiment Station Research Paper INT-190.
 - ✓ Burylo, M., Hudek, C., Rey, F., 2011. Soil reinforcement by the roots of six dominant species on eroded mountainous marly slopes (Southern Alps, France). *Catena* 84, 70–78. doi:10.1016/j.catena.2010.09.007
 - ✓ Büsgen, M., Münch, E., Thomson, T., 1929. *The structure and life of forest trees*. Chapman & Hall.
 - ✓ Böhm, W., 1979. *Methods of studying root systems*, Ecological Studies. Springer, Berlin, Germany.
 - ✓ Cadol, D., Wohl, E., Goode, J.R., Jaeger, K.L., 2009. Wood distribution in neotropical forested headwater streams of La Selva, Costa Rica. *Earth Surf. Process. Landf.* 34, 1198–1215. doi:10.1002/esp.1800
 - ✓ Caine, N., Swanson, F.J., 2013. Geomorphic coupling of hillslope and channel systems in two small mountain basins, in: *Fluvial Geomorphology. Geomorphology: Critical Concepts in Geography*. Routledge, pp. 189–203.
 - ✓ Calabuig, E.L., Gago Gamallo, M.L., Gómez-Gutiérrez, J.M., 1977. Influencia de la encina (*Quercus rotundifolia* Lam.) en la distribución del agua de lluvia. *Anu. Cent. Edafol. Biol. Apl. CSIC* 4, 143–159.
 - ✓ Calheiros De Miranda, R.A., Butler, D.R., 1986. Interception of rainfall in a hedgerow apple orchard. *J. Hydrol.* 87, 245–253.
 - ✓ Camera, C., Apuani, T., Masetti, M., 2015. Modeling the stability of terraced slopes: an approach from Valtellina (Northern Italy). *Environ. Earth Sci.* 74, 855–868. doi:10.1007/s12665-015-4089-0
 - ✓ Cammeraat, E., van Beek, R., Kooijman, A., 2005. Vegetation succession and its consequences for slope stability in SE Spain. *Plant Soil* 278, 135–147. doi:10.1007/s11104-005-5893-1
 - ✓ Campbell, R.H., 1975. Soil slips, debris flows, and rainstorms in the Santa Monica Mountains and vicinity, southern California (No. 2330–7102). U.S. Government Publishing Office.
 - ✓ Canadell, J., Jackson, R.B., Ehleringer, J.R., Mooney, H.A., Sala, O.E., Schulze, E.-D., 1996. Maximum rooting depth of vegetation types at the global scale. *Oecologia* 108, 583–595.
 - ✓ Capilleri, P.P., Motta, E., Todaro, M., Massimino, M.R., Raciti, E., 2015. Studio sperimentale del comportamento di un terreno incoerente in stato passivo soggetto a un carico applicato da una
-

- piastra rigida. Presented at the Incontro Annuale dei Ricercatori di Ingegneria Geotecnica, IARG 2015, Cagliari.
- ✓ Caquot, A.I., 1934. Équilibre des massifs à frottement interne: stabilité des terres, pulvérulentes ou cohérentes. Gauthier-Villars.
 - ✓ Caquot, A.I., Kérisel, J.L., 1948. Tables for the calculation of passive pressure, active pressure and bearing capacity of foundations. Gauthier-Villars, Paris, France.
 - ✓ Carrara, A., Cardinali, M., Detti, R., Guzzetti, F., Pasqui, V., Reichenbach, P., 1991. GIS techniques and statistical models in evaluating landslide hazard. *Earth Surf. Process. Landf.* 16, 427–445.
 - ✓ Carrara, A., Crosta, G., Frattini, P., 2008. Comparing models of debris-flow susceptibility in the alpine environment. *Geomorphology* 94, 353–378. doi:10.1016/j.geomorph.2006.10.033
 - ✓ Casadei, M., Dietrich, W.E., Miller, N.L., 2003a. Controls on shallow landslide size. *Debris-Flow Hazards Mitig. Mech. Predict. Assess.* 91–101.
 - ✓ Casadei, M., Dietrich, W.E., Miller, N.L., 2003b. Testing a model for predicting the timing and location of shallow landslide initiation in soil-mantled landscapes. *Earth Surf. Process. Landf.* 28, 925–950. doi:10.1002/esp.470
 - ✓ Cattiau, V., Mari, E., Renaud, J.-P., 1995. Forêt et protection contre les chutes de rochers. *Ingénieries Eau – Agric. – Territ.* 3, 45–54.
 - ✓ Cavalli, M., Trevisani, S., Comiti, F., Marchi, L., 2013. Geomorphometric assessment of spatial sediment connectivity in small Alpine catchments. *Geomorphology* 188, 31–41. doi:10.1016/j.geomorph.2012.05.007
 - ✓ Cervi, F., Berti, M., Borgatti, L., Ronchetti, F., Manenti, F., Corsini, A., 2010. Comparing predictive capability of statistical and deterministic methods for landslide susceptibility mapping: a case study in the northern Apennines (Reggio Emilia Province, Italy). *Landslides* 7, 433–444. doi:10.1007/s10346-010-0207-y
 - ✓ Cazzuffi, D., Cardile, G., Giofrè, D., 2014. Geosynthetic engineering and vegetation growth in soil reinforcement applications. *Transp. Infrastruct. Geotechnol.* 1, 262–300. doi:10.1007/s40515-014-0016-1
 - ✓ Çepel, N., 1967. Interzeption (= Niederschlagsverdunstung im Kronenraum) in einem Buchen-, einem Eichen- und einem Kiefernbestand des Belgrader Waldes bei Istanbul. *Forstwiss. Cent.* 86, 301–314.
 - ✓ Cervi, F., Berti, M., Borgatti, L., Ronchetti, F., Manenti, F., Corsini, A., 2010. Comparing predictive capability of statistical and deterministic methods for landslide susceptibility mapping: a case study in the northern Apennines (Reggio Emilia Province, Italy). *Landslides* 7, 433–444. doi:10.1007/s10346-010-0207-y
 - ✓ Cevasco, A., Pepe, G., Brandolini, P., 2014. The influences of geological and land use settings on shallow landslides triggered by an intense rainfall event in a coastal terraced environment. *Bull. Eng. Geol. Environ.* 73, 859–875. doi:10.1007/s10064-013-0544-x

-
- ✓ Chatré, B., Lanzinger, G., Macaluso, M., Mayrhofer, W., Morandini, M., Onida, M., Polajnar, B., 2010. The Alps: people and pressures in the mountains, the facts at a glance. Presented at the Permanent Secretariat of the Alpine Convention (ed): Vademedum, Innsbruck, Austria.
 - ✓ Chen, C.-Y., Huang, W.-L., 2013. Land use change and landslide characteristics analysis for community-based disaster mitigation. *Environ. Monit. Assess.* 185, 4125–4139. doi:10.1007/s10661-012-2855-y
 - ✓ Chen, W.F., Rosenfarb, J.L., 1973. Limit analysis solution of earth pressure problems. *Soils Found., Japanese Society of Soil Mechanics and Foundation Engineering* 13, 45–60.
 - ✓ Cheng, J.D., Lin, L.L., Lu, H.S., 2002. Influences of forests on water flows from headwater watersheds in Taiwan. *For. Ecol. Manag.* 165, 11–28.
 - ✓ Cheng, X., Baumgartner, K., 2005. Overlap of grapevine and cover-crop roots enhances interactions among grapevines, cover crops, and arbuscular mycorrhizal fungi, in: *Soil Environment and Vine Mineral Nutrition: Symposium Proceedings and Related Papers*. San Diego, CA: American Society of Enology and Viticulture. pp. 171–174.
 - ✓ Chiaradia, E.A., Vergani, C., Bischetti, G.B., 2016. Evaluation of the effects of three European forest types on slope stability by field and probabilistic analyses and their implications for forest management. *For. Ecol. Manag.* 370, 114–129. doi:10.1016/j.foreco.2016.03.050
 - ✓ Chirico, G.B., Borga, M., Tarolli, P., Rigon, R., Preti, F., 2013. Role of vegetation on slope stability under transient unsaturated conditions. *Procedia Environ. Sci.* 19, 932–941. doi:10.1016/j.proenv.2013.06.103
 - ✓ Chow, V.T., Maidment, D.R., Mays, L.W., 1988. *Applied hydrology*.
 - ✓ Cislighi, A., Chiaradia, E.A., Bischetti, G.B., 2017. Including root reinforcement variability in a probabilistic 3D stability model. *Earth Surf. Process. Landf.* 42, 1789–1806. doi:10.1002/esp.4127
 - ✓ Claessens, L., Heuvelink, G.B.M., Schoorl, J.M., Veldkamp, A., 2005. DEM resolution effects on shallow landslide hazard and soil redistribution modelling. *Earth Surf. Process. Landf.* 30, 461–477. doi:10.1002/esp.1155
 - ✓ Cohen, D., Lehmann, P., Or, D., 2009. Fiber bundle model for multiscale modeling of hydromechanical triggering of shallow landslides. *Water Resour. Res.* 45, W10436. doi:10.1029/2009WR007889
 - ✓ Cohen, D., Schwarz, M., 2017. Tree-root control of shallow landslides. *Earth Surf. Dynam.* 5, 451–477. doi:10.5194/esurf-5-451-2017
 - ✓ Cohen, D., Schwarz, M., Or, D., 2011. An analytical fiber bundle model for pullout mechanics of root bundles. *J. Geophys. Res.* 116. doi:10.1029/2010JF001886
 - ✓ Comiti, F., Andreoli, A., Mao, L., Lenzi, M.A., 2008a. Wood storage in three mountain streams of the Southern Andes and its hydro-morphological effects. *Earth Surf. Process. Landf.* 33, 244–262. doi:10.1002/esp.1541
-

References

- ✓ Comiti, F., Lucía, A., Rickenmann, D., 2016. Large wood recruitment and transport during large floods: A review. *Geomorphology* 269, 23–39. doi:10.1016/j.geomorph.2016.06.016
- ✓ Comiti, F., Mao, L., Preciso, E., Picco, L., Marchi, L., Borga, M., 2008b. Large wood and flash floods: evidence from the 2007 event in the Davča basin (Slovenia), in: *Proceeding of the 2nd Monitoring, Simulation, Prevention and Remediation of Dense Debris Flows*. WIT Press, pp. 173–182. doi:10.2495/DEB080181
- ✓ Conradie, W.J., 1983. Liming and choice of rootstocks as cultural techniques for vines in acid soils. *South Afr. J. Enol. Vitic.* 1, 39–44.
- ✓ Coppin, N.J., Richards, I.G., 1990. *Use of vegetation in civil engineering*. Construction Industry Research and Information Association London.
- ✓ Coulomb, C.A., 1776. *Essai sur une application des règles de maximis & minimis à quelques problèmes de statique, relatifs à l'architecture*, Memoires de l'Academie Royale pres Divers Savants. Paris, France.
- ✓ Craig, R.F., 2013. *Soil mechanics*. Springer.
- ✓ Crockford, R.H., Richardson, D.P., 1998a. Litterfall, litter and associated chemistry in a dry sclerophyll eucalypt forest and a pine plantation in south-eastern Australia: 1. Litterfall and litter. *Hydrol. Process.* 12, 365–384.
- ✓ Crockford, R.H., Richardson, D.P., 1998b. Litterfall, litter and associated chemistry in a dry sclerophyll eucalypt forest and a pine plantation in south-eastern Australia: 2. Nutrient recycling by litter, throughfall and stemflow. *Hydrol. Process.* 12, 385–400.
- ✓ Crosta, G.B., Dal Negro, P., Frattini, P., 2003. Soil slips and debris flows on terraced slopes. *Nat. Hazards Earth Syst. Sci.* 3, 31–42.
- ✓ Crosta, G.B., Frattini, P., 2003. Distributed modelling of shallow landslides triggered by intense rainfall. *Nat. Hazards Earth Syst. Sci.* 3, 81–93.
- ✓ Cruden, D.M., Varnes, D., 1996. *Landslide types and processes*, in: *Landslides, Investigation and Mitigation*, Ed. AK Turner and RL Schuster. Transportation Research Board, Special Report. National Academy Press, Washington, D. C., pp. 36–75.
- ✓ Culmann, K., 1886. *Die graphische Statik*. Meyer & Zeller, Zurich, Switzerland.
- ✓ Cutler, D.F., Gasson, P.E., Farmer, M.C., 1990. The wind blown tree survey: analysis of results. *Arboric. J.* 14, 265–286.
- ✓ Czarnomski, N.M., Dreher, D.M., Snyder, K.U., Jones, J.A., Swanson, F.J., 2008. Dynamics of wood in stream networks of the western Cascades Range, Oregon. *Can. J. For. Res.* 38, 2236–2248.
- ✓ D'Amato Avanzi, G., Galanti, Y., Giannecchini, R., Lo Presti, D., Puccinelli, A., 2013. Estimation of soil properties of shallow landslide source areas by dynamic penetration tests: first outcomes from Northern Tuscany (Italy). *Bulletin of Engineering Geology and the Environment* 72, 609–624. <https://doi.org/10.1007/s10064-013-0535-y>

-
- ✓ Daniels, H.E., 1945. The statistical theory of the strength of bundles of threads. I, in: Proceedings of the Royal Society of London A: Mathematical, Physical and Engineering Sciences. The Royal Society, pp. 405–435.
 - ✓ Danjon, F., Barker, D.H., Drexhage, M., Stokes, A., 2007. Using three-dimensional plant root architecture in models of shallow-slope stability. *Ann. Bot.* 101, 1281–1293. doi:10.1093/aob/mcm199
 - ✓ Das, B.M., 2010. Principles of geotechnical engineering. Cengage Learning, Stamford, Connecticut, USA.
 - ✓ Davidovic, N., Prolovic, V., Stojic, D., 2010. Modeling of soil parameters spatial uncertainty by geostatistics. *Facta Univ. - Ser. Archit. Civ. Eng.* 8, 111–118. doi:10.2298/FUACE1001111D
 - ✓ Day, S.D., Wiseman, P.E., Dickinson, S.B., Harris, J.R., 2010. Contemporary concepts of root system architecture of urban trees. *Arboric. Urban For.* 36, 149–159.
 - ✓ De Baets, S., Poesen, J., 2010. Empirical models for predicting the erosion-reducing effects of plant roots during concentrated flow erosion. *Geomorphology* 118, 425–432. <https://doi.org/10.1016/j.geomorph.2010.02.011>
 - ✓ De Baets, S., Poesen, J., Reubens, B., Wemans, K., De Baerdemaeker, J., Muys, B., 2008. Root tensile strength and root distribution of typical Mediterranean plant species and their contribution to soil shear strength. *Plant Soil* 305, 207–226. doi:10.1007/s11104-008-9553-0
 - ✓ de Herralde, F., Savé, R., Aranda, X., Biel, C., 2010. Grapevine roots and soil environment: Growth, distribution and function, in: *Methodologies and Results in Grapevine Research*. Springer, pp. 1–20.
 - ✓ Del Favero, R., 2002. I tipi forestali della Lombardia. Cierre edizioni, Milano.
 - ✓ Del Favero, R., Carraro, G., Disegna, M., Savio, D., Zen, S., Abramo, E., Andrich, O., Corona, P., Cassol, M., Lasen, C., 2000. Biodiversità e indicatori nei tipi forestali del Veneto.
 - ✓ del Río, M., Pretzsch, H., Alberdi, I., Bielak, K., Bravo, F., Brunner, A., Condés, S., Ducey, M.J., Fonseca, T., von Lüpke, N., Pach, M., Peric, S., Perot, T., Souidi, Z., Spathelf, P., Sterba, H., Tijardovic, M., Tomé, M., Vallet, P., Bravo-Oviedo, A., 2016. Characterization of the structure, dynamics, and productivity of mixed-species stands: review and perspectives. *Eur. J. For. Res.* 135, 23–49. doi:10.1007/s10342-015-0927-6
 - ✓ Delfs, F., 1954. Niederschlagszurückhaltung (Interception) in verschieden alten Fichtenbeständen. *Wald Wasser* 31–36.
 - ✓ Denlinger, R.P., Iverson, R.M., 2001. Flow of variably fluidized granular masses across three-dimensional terrain: 2. Numerical predictions and experimental tests. *J. Geophys. Res.* 106, 553–566.
 - ✓ Dewitte, O., Demoulin, A., 2005. Morphometry and kinematics of landslides inferred from precise DTMs in West Belgium. *Nat. Hazards Earth Syst. Sci.* 5, 259–265.
-

- ✓ Dhakal, A.S., Sidle, R.C., 2003. Long-term modelling of landslides for different forest management practices. *Earth Surf. Process. Landf.* 28, 853–868. doi:10.1002/esp.499
- ✓ Dhakal, A.S., Sullivan, K., 2014. Shallow groundwater response to rainfall on a forested headwater catchment in northern coastal California: implications of topography, rainfall, and throughfall intensities on peak pressure head generation. *Hydrol. Process.* 28, 446–463. doi:10.1002/hyp.9542
- ✓ Di Iorio, A., Lasserre, B., Scippa, G.S., Chiatante, D., 2005. Root system architecture of *Quercus pubescens* trees growing on different sloping conditions. *Ann. Bot.* 95, 351–361. doi:10.1093/aob/mci033
- ✓ Di Iorio, A., Montagnoli, A., Terzaghi, M., Scippa, G.S., Chiatante, D., 2013. Effect of tree density on root distribution in *Fagus sylvatica* stands: a semi-automatic digitising device approach to trench wall method. *Trees* 27, 1503–1513. doi:10.1007/s00468-013-0897-6
- ✓ Didon-Lescot, J.F., 1998. The importance of throughfall in evaluating hydrological and biogeochemical fluxes: example of a catchment (Mont-Lozère, France). Presented at the Proceedings of the International Conference on Catchment Hydrological and Biochemical Processes in Changing Environment, Liblice, Liblice, Czech Republic, pp. 17–20.
- ✓ Dietrich, W.E., Bellugi, D., Real De Asua, R., 2001. Validation of the shallow landslide model, SHALSTAB, for forest management. *Land Use Watersheds Hum. Influ. Hydrol. Geomorphol. Urban For. Areas* 195–227.
- ✓ Dietrich, W.E., McKean, J., Bellugi, D., Perron, T., 2007. The prediction of shallow landslide location and size using a multidimensional landslide analysis in a digital terrain model, in: Proceedings of the 4th International Conference on Debrisflow Hazards Mitigation: Mechanics, Prediction, and Assessment (DFHM-4). Chengdu, China. pp. 10–13.
- ✓ Dislich, C., Huth, A., 2012. Modelling the impact of shallow landslides on forest structure in tropical montane forests. *Ecol. Model.* 239, 40–53. doi:10.1016/j.ecolmodel.2012.04.016
- ✓ Dobson, M., 1995. Tree root system. *Arboric. Res. Inf. Note* 130, 1–6.
- ✓ Docker, B.B., Hubble, T.C.T., 2008. Quantifying root-reinforcement of river bank soils by four Australian tree species. *Geomorphology* 100, 401–418. doi:10.1016/j.geomorph.2008.01.009
- ✓ Doglioni, A., Galeandro, A., Simeone, V., 2013. A simple model for passive failure compression structure at the toe of landslide, in: *Landslide Science and Practice*. Springer, pp. 177–181.
- ✓ Doll, C.C., 1954. Studies of Concord grape roots in loess soil, in: Proceedings of the American Society of Horticultural Science. pp. 175–182.
- ✓ Dolman, A.J., 1987. Summer and winter rainfall interception in an oak forest. Predictions with an analytical and a numerical simulation model. *J. Hydrol.* 90, 1–9.
- ✓ Domingo, F., Puigdefabregas, J., Moro, M.J., Bellot, J., 1994. Role of vegetation cover in the biogeochemical balances of a small afforested catchment in southeastern Spain. *J. Hydrol.* 159, 275–289.

-
- ✓ Domingo, F., Sánchez, G., Moro, M.J., Brenner, A.J., Puigdefábregas, J., 1998. Measurement and modelling of rainfall interception by three semi-arid canopies. *Agric. For. Meteorol.* 91, 275–292.
 - ✓ Dorren, L.K.A., Berger, F., le Hir, C., Mermin, E., Tardif, P., 2005. Mechanisms, effects and management implications of rockfall in forests. *For. Ecol. Manag.* 215, 183–195. doi:10.1016/j.foreco.2005.05.012
 - ✓ Dorren, L.K.A., Schwarz, M., 2016. Quantifying the stabilizing effect of forests on shallow landslide-prone slopes, in: Renaud, F.G., Sudmeier-Rieux, K., Estrella, M., Nehren, U. (Eds.), *Ecosystem-Based Disaster Risk Reduction and Adaptation in Practice*. Springer International Publishing, Cham, pp. 255–270. doi:10.1007/978-3-319-43633-3_11
 - ✓ Drexhage, M., Colin, F., 2001. Estimating root system biomass from breast - height diameters. *Forestry* 74, 491–497.
 - ✓ Duan, J., Grant, G.E., 2000. Shallow landslide delineation for steep forest watersheds based on topographic attributes and probability analysis, in: *Terrain Analysis: Principles and Applications*. Wiley & Sons, New York, pp. 311–329.
 - ✓ Duncan, J.M., Mokwa, R.L., 2001. Passive earth pressures: theories and tests. *J. Geotech. Geoenvironmental Eng.* 127, 248–257.
 - ✓ Duncan, J.M., Wright, S.G., Brandon, T.L., 2014. *Soil strength and slope stability*. John Wiley & Sons.
 - ✓ Dunne, T., 1991. Stochastic aspects of the relations between climate, hydrology and landform evolution. *Trans. Jpn. Geomorphol. Union* 12, 1–24.
 - ✓ Dupuy, L., Fourcaud, T., Stokes, A., 2005. A numerical investigation into the influence of soil type and root architecture on tree anchorage. *Plant Soil* 278, 119–134. doi:10.1007/s11104-005-7577-2
 - ✓ Duwig, C., 1994. *Eléments de modélisation de l'interception des pluies par 4 espèces d'arbres de type méditerranéen* (Master of Advanced Studies Thesis). Université Joseph Fourier, Grenoble, France.
 - ✓ Eaton, B.C., Hassan, M.A., 2013. Scale-dependent interactions between wood and channel dynamics: Modeling jam formation and sediment storage in gravel-bed streams. *J. Geophys. Res. Earth Surf.* 118, 2500–2508. doi:10.1002/2013JF002917
 - ✓ Eidmann, F.E., 1959. Die Interception in Buchen- und Fichtenbeständen; Ergebnis mehrjähriger Untersuchungen im Rothargebirge (Sauerland). Presented at the Symposium of Hannoversch-Münden, pp. 5–25.
 - ✓ Ekanayake, J.C., Phillips, C.J., 1999. A method for stability analysis of vegetated hillslopes: an energy approach. *Can. Geotech. J.* 36, 1172–1184.
 - ✓ Endo, T., Tsuruta, T., 1969. The effect of the tree roots upon the shear strength of soil, Annual Report of the Hokkaido Branch, Forest Place Experimental Station. Sapporo, Japan.
 - ✓ Ennos, A., 1993. The scaling of root anchorage. *J. Theor. Biol.* 161, 61–75.
-

References

- ✓ Ermini, L., Catani, F., Casagli, N., 2005. Artificial Neural Networks applied to landslide susceptibility assessment. *Geomorphology* 66, 327–343. doi:10.1016/j.geomorph.2004.09.025
- ✓ Erskine, W.D., Webb, A.A., 2003. Desnagging to resnagging: new directions in river rehabilitation in southeastern Australia. *River Res. Appl.* 19, 233–249. doi:10.1002/rra.750
- ✓ European Commission, 2012. Report from the Commission to the European Parliament, the Council, the European Economic and Social Committee and the Committee of the Regions: The implementation of the Soil Thematic Strategy and ongoing activities.
- ✓ Eysn, L., Hollaus, M., Lindberg, E., Berger, F., Monnet, J.-M., Dalponte, M., Kobal, M., Pellegrini, M., Lingua, E., Mongus, D., Pfeifer, N., 2015. A benchmark of LiDAR-based single tree detection methods using heterogeneous forest data from the Alpine space. *Forests* 6, 1721–1747. doi:10.3390/f6051721
- ✓ Failla, O., 1988. L'evoluzione della viticoltura oltrepadana: vecchi e nuovi vitigni. *Oltrepò Pavese Aspetti Vitic. Enol. Ed Econ. Ed. Tecnos Pavia* 177–192.
- ✓ Fan, C.-C., Su, C.-F., 2008. Role of roots in the shear strength of root-reinforced soils with high moisture content. *Ecol. Eng.* 33, 157–166. doi:10.1016/j.ecoleng.2008.02.013
- ✓ Fang, Y.-S., Chen, J.-M., Chen, C.-Y., 1997. Earth pressures with sloping backfill. *J. Geotech. Geoenvironmental Eng.* 123, 250–259.
- ✓ Fang, Y.-S., Chen, T.-J., Wu, B.-F., 1994. Passive earth pressures with various wall movements. *J. Geotech. Eng.* 120, 1307–1323.
- ✓ Fang, Y.-S., Ho, Y.-C., Chen, T.-J., 2002. Passive earth pressure with critical state concept. *J. Geotech. Geoenvironmental Eng.* 128, 651–659.
- ✓ Fannin, R.J., Eliadorani, A., Wilkinson, J.M.T., 2005. Shear strength of cohesionless soils at low stress. *Géotechnique* 55, 467–478.
- ✓ Fannin, R.J., Wise, M.P., 2001. An empirical-statistical model for debris flow travel distance. *Can. Geotech. J.* 38, 982–994. doi:10.1139/cgj-38-5-982
- ✓ Ferreira, A.J.D., 1996. Processos hidrológicos e hidroquímicos em povoamentos de *Eucalyptus globulus* Labill. e *Pinus pinaster* Aiton (PhD dissertation). Universidade de Aveiro, Aveiro, Portugal.
- ✓ Ferrés, L., Rodà, F., Verdú, A.M.C., Terradas, J., 1984. Circulación de nutrientes en algunos ecosistemas forestales del Montseny (Barcelona). *Mediterránea Ser. Estud. Biológicos* 7, 139–166.
- ✓ Finér, L., Ohashi, M., Noguchi, K., Hirano, Y., 2011. Factors causing variation in fine root biomass in forest ecosystems. *For. Ecol. Manag.* 261, 265–277. doi:10.1016/j.foreco.2010.10.016
- ✓ Fitter, A.H., 1987. An architectural approach to the comparative ecology of plant root systems. *New Phytol.* 106, 61–77.
- ✓ Fonte, N., Masciocco, L., 2009. A simplified physically-based approach for the assessment of hazard related to shallow landslides in Southern Piedmont (Italy). *Geogr. Fis. E Din. Quat.* 32, 193–202.

-
- ✓ Food and Agriculture Organization, 2014. World reference base for soil resources 2014 international soil classification system for naming soils and creating legends for soil maps. FAO, Rome.
 - ✓ Forbes, K., Broadhead, J., 2011. Forests and landslides: the role of trees and forests in the prevention of landslides and rehabilitation of landslide-affected areas in Asia. Food and Agriculture Organization of the United Nations (FAO), Bangkok.
 - ✓ Frattini, P., Crosta, G., Carrara, A., 2010. Techniques for evaluating the performance of landslide susceptibility models. *Eng. Geol.* 111, 62–72. doi:10.1016/j.enggeo.2009.12.004
 - ✓ Freer, J., McDonnell, J.J., Beven, K.J., Peters, N.E., Burns, D.A., Hooper, R.P., Aulenbach, B., Kendall, C., 2002. The role of bedrock topography on subsurface storm flow: THE ROLE OF BEDROCK TOPOGRAPHY ON SUBSURFACE STORM FLOW. *Water Resour. Res.* 38, 5-1-5–16. doi:10.1029/2001WR000872
 - ✓ Frehner, M., Wasser, B., Schwitler, R., 2005. Nachhaltigkeit und Erfolgskontrolle im Schutzwald [Sustainability and control method in protection forests] (No. Wegleitung fr Pflegemassnahmen in Wldern mit Schutzfunktion. Bundesamt fr Umwelt, Wald und Landschaft, Bern, Switzerland, 564 pp). Wegleitung fr Pflegemassnahmen in Wldern mit Schutzfunktion. Bundesamt fr Umwelt, Wald und Landschaft, Bern, Switzerland.
 - ✓ Frei, M., Böll, A., Graf, F., Heinimann, H.R., Springman, S., 2003. Quantification of the influence of vegetation on soil stability. Lee C. F. and Tham L. G. (eds), Hong Kong, China, pp. 872–877.
 - ✓ Frey, W., Thee, P., 2002. Avalanche protection of windthrow areas: A ten year comparison of cleared and uncleared starting zones. *For. Snow Landsc. Res.* 77, 2.
 - ✓ Fuchu, D., Lee, C.F., Sijing, W., 1999. Analysis of rainstorm-induced slide-debris flows on natural terrain of Lantau Island, Hong Kong. *Engineering Geology* 51, 279–290.
 - ✓ Gabet, E.J., Dunne, T., 2002. Landslides on coastal sage-scrub and grassland hillslopes in a severe El Nino winter: The effects of vegetation conversion on sediment delivery. *Geol. Soc. Am. Bull.* 114, 983–990.
 - ✓ Gabet, E.J., Mudd, S.M., 2006. The mobilization of debris flows from shallow landslides. *Geomorphology* 74, 207–218. doi:10.1016/j.geomorph.2005.08.013
 - ✓ Gale, M.R., Grigal, D.F., 1987. Vertical root distributions of northern tree species in relation to successional status. *Can. J. For. Res.* 17, 829–834.
 - ✓ Galve, J.P., Cevasco, A., Brandolini, P., Soldati, M., 2015. Assessment of shallow landslide risk mitigation measures based on land use planning through probabilistic modelling. *Landslides* 12, 101–114. doi:10.1007/s10346-014-0478-9
 - ✓ Gash, J.H.C., Wright, I.R., Lloyd, C.R., 1980. Comparative estimates of interception loss from three coniferous forests in Great Britain. *J. Hydrol.* 48, 89–105.
 - ✓ Gasmo, J.M., Rahardjo, H., Leong, E.C., 2000. Infiltration effects on stability of a residual soil slope. *Comput. Geotech.* 26, 145–165.
-

References

- ✓ Genet, M., Kokutse, N., Stokes, A., Fourcaud, T., Cai, X., Ji, J., Mickovski, S., 2008. Root reinforcement in plantations of *Cryptomeria japonica* D. Don: effect of tree age and stand structure on slope stability. *For. Ecol. Manag.* 256, 1517–1526. doi:10.1016/j.foreco.2008.05.050
- ✓ Genet, M., Stokes, A., Salin, F., Mickovski, S.B., Fourcaud, T., Dumail, J.-F., van Beek, R., 2005. The influence of cellulose content on tensile strength in tree roots. *Plant Soil* 278, 1–9. doi:10.1007/s11104-005-8768-6
- ✓ George, D.L., Iverson, R.M., 2011. A two-phase debris-flow model that includes coupled evolution of volume fractions, granular dilatancy, and pore-fluid pressure. *Ital. J. Eng. Geol. Environ.* 415–424.
- ✓ Gerbore, E., 1997. I boschi nel medioevo. *Uomini E Boschi Val. D'Aosta*.
- ✓ Gerhold, H.D., Johnson, A.D., 2003. Root dimensions of landscape tree cultivars. *J. Arboric.* 29, 322–326.
- ✓ Gerke, H., 1985. Kronendurchlass, Stammabfluss und Interzeptionsverdunstung eines Buchenaltbestandes und deren Beziehungen zum Freiflächenniederschlag. *Wald Wasser* 5, 59–76.
- ✓ Gerós, H., Chaves, M.M., Gil, H.M., Delrot, S., 2015. Grapevine in a changing environment: a molecular and ecophysiological perspective. John Wiley & Sons.
- ✓ Gerrits, A.M.J., Pfister, L., Savenije, H.H.G., 2010. Spatial and temporal variability of canopy and forest floor interception in a beech forest. *Hydrol. Process.* 24, 3011–3025. doi:10.1002/hyp.7712
- ✓ Ghavasieh, A.-R., Poulard, C., Paquier, A., 2006. Effect of roughened strips on flood propagation: Assessment on representative virtual cases and validation. *J. Hydrol.* 318, 121–137. doi:10.1016/j.jhydrol.2005.06.009
- ✓ Ghestem, M., Sidle, R.C., Stokes, A., 2011. The influence of plant root systems on subsurface flow: implications for slope stability. *BioScience* 61, 869–879. doi:10.1525/bio.2011.61.11.6
- ✓ Ghezzehei, T.A., Or, D., 2001. Rheological properties of wet soils and clays under steady and oscillatory stresses. *Soil Sci. Soc. Am. J.* 65, 624–637.
- ✓ Ghezzehei, T.A., Or, D., 2003. Stress-induced volume reduction of isolated pores in wet soil. *Water Resour. Res.* 39. doi:10.1029/2001WR001137
- ✓ Giacomini, A., Trucchi, P., 1992. Rainfall interception in a beech coppice (Acquerino, Italy). *J. Hydrol.* 137, 141–147.
- ✓ Giadrossich, F., Cohen, D., Schwarz, M., Seddaiu, G., Contran, N., Lubino, M., Valdés-Rodríguez, O.A., Niedda, M., 2016. Modeling bio-engineering traits of *Jatropha curcas* L. *Ecol. Eng.* 89, 40–48. doi:10.1016/j.ecoleng.2016.01.005
- ✓ Giadrossich, F., Schwarz, M., Cohen, D., Cislighi, A., Vergani, C., Hubble, T., Phillips, C., Stokes, A., 2017. Methods to measure the mechanical behaviour of tree roots: a review. *Ecol. Eng.*
- ✓ Giadrossich, F., Schwarz, M., Cohen, D., Preti, F., Or, D., 2013. Mechanical interactions between neighbouring roots during pullout tests. *Plant Soil* 367, 391–406. doi:10.1007/s11104-012-1475-1

-
- ✓ Gilman, E.F., 1988. Predicting root spread from trunk diameter and branch spread. *J. Arboric.* 14, 85–89.
 - ✓ Gippel, C.J., Finlayson, B.L., O'Neill, I.C., 1996. Distribution and hydraulic significance of large woody debris in a lowland Australian river. *Hydrobiologia* 318, 179–194.
 - ✓ Glade, T., 2003. Landslide occurrence as a response to land use change: a review of evidence from New Zealand. *Catena* 51, 297–314.
 - ✓ Glenz, C., 2005. Process-based, spatially-explicit modelling of riparian forest dynamics in Central Europe—Tool for decision-making in river restoration (PhD dissertation). Université de Lausanne, Lausanne, Switzerland.
 - ✓ Godt, J.W., Baum, R.L., Lu, N., 2009. Landsliding in partially saturated materials. *Geophys. Res. Lett.* 36, 1–5. doi:10.1029/2008GL035996
 - ✓ Godt, J.W., Baum, R.L., Savage, W.Z., Salciarini, D., Schulz, W.H., Harp, E.L., 2008. Transient deterministic shallow landslide modeling: requirements for susceptibility and hazard assessments in a GIS framework. *Engineering Geology* 102, 214–226. doi:10.1016/j.enggeo.2008.03.019
 - ✓ Gómez, H., Kavzoglu, T., 2005. Assessment of shallow landslide susceptibility using artificial neural networks in Jabonosa River Basin, Venezuela. *Eng. Geol.* 78, 11–27. doi:10.1016/j.enggeo.2004.10.004
 - ✓ Gómez, J.B., Moreno, Y., Pacheco, A.F., 1998. Probabilistic approach to time-dependent load-transfer models of fracture. *Phys. Rev. E* 58, 1528–1532.
 - ✓ González del Tánago, M., Garcia, M.J., Ortega, L., Pardillo, G., Tourné, M., 1988. Intercepción y calidad del agua de lluvia bajo diferentes condiciones de cubierta vegetal. *Ecología* 2, 99–110.
 - ✓ González-Cascón, M.R., Lopez-Arias, M., Serrano-Játiva, M., Minaya-Gallego, M.T., 1994. Balance de entradas/salidas de cationes en una pequeña cuenca forestal de *Pinus sylvestris* en la Sierra de Guadarrama. *Ecología* 8, 157–166.
 - ✓ González-Hidalgo, J.C., Raventos, J., Echevarria, M.T., 1997. Comparison of sediment ratio curves for plants with different architectures. *Catena* 29, 333–340.
 - ✓ Gorsevski, P.V., Gessler, P.E., Boll, J., Elliot, W.J., Foltz, R.B., 2006a. Spatially and temporally distributed modeling of landslide susceptibility. *Geomorphology* 80, 178–198. doi:10.1016/j.geomorph.2006.02.011.
 - ✓ Gorsevski, P.V., Gessler, P.E., Foltz, R.B., Elliot, W.J., 2006b. Spatial prediction of landslide hazard using logistic regression and ROC analysis. *Trans. GIS* 10, 395–415.
 - ✓ Graf, F., Frei, M., Böll, A., 2009. Effects of vegetation on the angle of internal friction of a moraine. *For. Snow Landsc. Res.* 82, 61–77.
 - ✓ Graham, R.C., Wood, H.B., 1991. Morphologic development and clay redistribution in lysimeter soils under chaparral and pine. *Soil Sci. Soc. Am. J.* 55, 1638–1646.
 - ✓ Gray, D.H., Leiser, A.T., 1982. Biotechnical slope protection and erosion control. Van Nostrand Reinhold Company Inc.
-

References

- ✓ Gray, D.H., Megahan, W.F., 1981. Forest vegetation removal and slope stability in the Idaho batholith. USDA For. Serv. Res. Pap. INT USA 271.
- ✓ Gray, D.H., Ohashi, H., 1983. Mechanics of fiber reinforcement in sand. *J. Geotech. Eng.* 109, 335–353.
- ✓ Gray, D.H., Sotir, R.B., 1996. *Biotechnical and soil bioengineering slope stabilization: a practical guide for erosion control.* John Wiley & Sons.
- ✓ Greenway, D.R., 1987. Vegetation and slope stability. *Slope Stab. Geotech. Eng. Geomorphol.* MG Anderson KS Richards.
- ✓ Greenwood, J.R., Norris, J.E., Wint, J., 2004. Assessing the contribution of vegetation to slope stability. *Proc. ICE-Geotech. Eng.* 157, 199–207.
- ✓ Gregory, S., Boyer, K.L., Gurnell, A.M., 2003. Ecology and management of wood in world rivers. Presented at the International Conference of Wood in World Rivers (2000: Corvallis, Or.), American Fisheries Society.
- ✓ Griffiths, D.V., Huang, J., Fenton, G.A., 2009. Influence of spatial variability on slope reliability using 2-D random fields. *J. Geotech. Geoenvironmental Eng.* 135, 1367–1378.
- ✓ Grunert, J., 2009. Landslides in the Upper Middle Rhine valley and in Rheinhessen as indicators for climate change? Presented at the Proceedings of the International Conference “Landslide Processes,” Strasbourg, France.
- ✓ Günther, A., Reichenbach, P., Malet, J.-P., Van Den Eeckhaut, M., Hervás, J., Dashwood, C., Guzzetti, F., 2013. Tier-based approaches for landslide susceptibility assessment in Europe. *Landslides* 10, 529–546. doi:10.1007/s10346-012-0349-1
- ✓ Günther, A., Hervás, J., Van Den Eeckhaut, M., Malet, J.-P., Reichenbach, P., 2014. Synoptic pan-European landslide susceptibility assessment: the ELSUS 1000 v1 Map, in: Sassa, K., Canuti, P., Yin, Y. (Eds.), *Landslide Science for a Safer Geoenvironment.* Springer International Publishing, Cham, pp. 117–122. doi:10.1007/978-3-319-04999-1_12.
- ✓ Gurnell, A.M., Piégay, H., Swanson, F.J., Gregory, S.V., 2002. Large wood and fluvial processes. *Freshw. Biol.* 47, 601–619.
- ✓ Gutberlet, C., Katzenbach, R., Hutter, K., 2013. Experimental investigation into the influence of stratification on the passive earth pressure. *Acta Geotech.* 8, 497–507. doi:10.1007/s11440-013-0270-3
- ✓ Guthey, G.T., Whiteman, G., 2009. Social and ecological transitions: winemaking in California. *Emergence Complex. Organ.* 11, 37–48.
- ✓ Guthrie, R.H., 2002. The effects of logging on frequency and distribution of landslides in three watersheds on Vancouver Island, British Columbia. *Geomorphology* 43, 273–292.
- ✓ Guthrie, R.H., Hockin, A., Colquhoun, L., Nagy, T., Evans, S.G., Ayles, C., 2010. An examination of controls on debris flow mobility: Evidence from coastal British Columbia. *Geomorphology* 114, 601–613. doi:10.1016/j.geomorph.2009.09.021

-
- ✓ Guzzetti, F., Carrara, A., Cardinali, M., Reichenbach, P., 1999. Landslide hazard evaluation: a review of current techniques and their application in a multi-scale study, Central Italy. *Geomorphology* 31, 181–216.
 - ✓ Guzzetti, F., Reichenbach, P., Cardinali, M., Galli, M., Ardizzone, F., 2005. Probabilistic landslide hazard assessment at the basin scale. *Geomorphology* 72, 272–299. doi:10.1016/j.geomorph.2005.06.002
 - ✓ Gyssels, G., Poesen, J., Bochet, E., Li, Y., 2005. Impact of plant roots on the resistance of soils to erosion by water: a review. *Progress in Physical Geography* 29, 189–217. <https://doi.org/10.1191/0309133305pp443ra>
 - ✓ Hales, T.C., Cole-Hawthorne, C., Lovell, L., Evans, S.L., 2013. Assessing the accuracy of simple field based root strength measurements. *Plant Soil* 372, 553–565. doi:10.1007/s11104-013-1765-2
 - ✓ Hales, T.C., Ford, C.R., Hwang, T., Vose, J.M., Band, L.E., 2009. Topographic and ecologic controls on root reinforcement. *J. Geophys. Res.* 114. doi:10.1029/2008JF001168
 - ✓ Hamilton, L.S., 1992. The protective role of mountain forests. *GeoJournal*, Kluwer Academic Publishers 27, 13–22.
 - ✓ Hammond, C., Hall, D., Miller, S., Swetik, P., 1992. Level I Stability Analysis (LISA) Documentation for Version 2.0 (General Technical Report No. INT-285). USDA Forest Service Intermountain Research Station.
 - ✓ Haneberg, W.C., 2004. A rational probabilistic method for spatially distributed landslide hazard assessment. *Environ. Eng. Geosci.* 10, 27–43.
 - ✓ Haneberg, W.C., Cole, W.F., Kasali, G., 2009. High-resolution lidar-based landslide hazard mapping and modeling, UCSF Parnassus Campus, San Francisco, USA. *Bull. Eng. Geol. Environ.* 68, 263–276. doi:10.1007/s10064-009-0204-3
 - ✓ Haque, U., Blum, P., da Silva, P.F., Andersen, P., Pilz, J., Chalov, S.R., Malet, J.-P., Auflič, M.J., Andres, N., Poyiadji, E., Lamas, P.C., Zhang, W., Peshevski, I., Pétursson, H.G., Kurt, T., Dobrev, N., García-Davalillo, J.C., Halkia, M., Ferri, S., Gaprindashvili, G., Engström, J., Keellings, D., 2016. Fatal landslides in Europe. *Landslides* 13, 1545–1554. doi:10.1007/s10346-016-0689-3.
 - ✓ Harmon, M.E., Franklin, J.F., Swanson, F.J., Sollins, P., Gregory, S., Lattin, J., Anderson, N., Cline, S., Aumen, N.G., Sedell, J., 1986. Ecology of coarse woody debris in temperate ecosystems. *Adv. Ecol. Res.* 15, 133–302.
 - ✓ Harr, D.R., 1986. Effects of clearcutting on rain-on-snow runoff in Western Oregon - a new look at old studies. *Water Resour. Res.* 22, 1095–1100.
 - ✓ Hassan, M.A., Bird, S., Reid, D., Hogan, D., 2016. Simulated wood budgets in two mountain streams. *Geomorphology* 259, 119–133. doi:10.1016/j.geomorph.2016.02.010
 - ✓ Hathaway, R.L., Penny, D., 1975. Root strength in some *Populus* and *Salix* clones. *N. Z. J. Bot.* 13, 333–344.
-

References

- ✓ Helliwell, D.R., 1986. The extent of tree roots. *Arboric. J.* 10, 341–347. doi:10.1080/03071375.1986.9756343
- ✓ Herbst, M., Rosier, P.T.W., McNeil, D.D., Harding, R.J., Gowing, D.J., 2008. Seasonal variability of interception evaporation from the canopy of a mixed deciduous forest. *Agric. For. Meteorol.* 148, 1655–1667. doi:10.1016/j.agrformet.2008.05.011
- ✓ Hess, T.M., Holman, I.P., Rose, S.C., Rosolova, Z., Parrott, A., 2010. Estimating the impact of rural land management changes on catchment runoff generation in England and Wales. *Hydrol. Process.* n/a-n/a. doi:10.1002/hyp.7598
- ✓ Hewlett, J.D., Hibbert, A.R., 1967. Factors affecting the response of small watersheds to precipitation in humid areas. *For. Hydrol.* 1, 275–290.
- ✓ Highland, L., Bobrowsky, P.T., 2008. *The landslide handbook: a guide to understanding landslides.* US Geological Survey Reston.
- ✓ Ho, J.-Y., Lee, K.T., Chang, T.-C., Wang, Z.-Y., Liao, Y.-H., 2012. Influences of spatial distribution of soil thickness on shallow landslide prediction. *Eng. Geol.* 124, 38–46. doi:10.1016/j.enggeo.2011.09.013
- ✓ Hodgkins, E.J., Nichols, N.G., 1977. Extent of main lateral roots in natural longleaf pine as related to position and age of the trees. *For. Sci.* 23, 161–166.
- ✓ Hörmann, G., Branding, A., Clemen, T., Herbst, M., Hinrichs, A., Thamm, F., 1996. Calculation and simulation of wind controlled canopy interception of a beech forest in Northern Germany. *Agric. For. Meteorol.* 79, 131–148. doi:10.1016/0168-1923(95)02275-9
- ✓ Horn, A., 1972. Résistance et déplacement de culées de ponts chargées latéralement. Presented at the 5th European conf on soil mec hand found engrg, Madrid, pp. 143–5.
- ✓ Hosmer, D.W., Lemeshow, S., 2000. *Applied logistic regression.* John Wiley and Sons, New York 375.
- ✓ Hovius, N., Stark, C.P., Allen, P.A., 1997. Sediment flux from a mountain belt derived by landslide mapping. *Geology* 25, 231–234.
- ✓ Huang, J.-C., Kao, S.-J., Hsu, M.-L., Lin, J.-C., 2006. Stochastic procedure to extract and to integrate landslide susceptibility maps: an example of mountainous watershed in Taiwan. *Nat. Hazards Earth Syst. Sci.* 6, 803–815.
- ✓ Hubble, T.C.T., Airey, D.W., Sealey, H.K., De Carli, E.V., Clarke, S.L., 2013. A little cohesion goes a long way: estimating appropriate values of additional root cohesion for evaluating slope stability in the Eastern Australian highlands. *Ecol. Eng.* 61, 621–632. doi:10.1016/j.ecoleng.2013.07.069
- ✓ Hudak, A.T., Crookston, N.L., Evans, J.S., Hall, D.E., Falkowski, M.J., 2008. Nearest neighbor imputation of species-level, plot-scale forest structure attributes from LiDAR data. *Remote Sens. Environ.* 112, 2232–2245. doi:10.1016/j.rse.2007.10.009

-
- ✓ Hundecha, Y., Bárdossy, A., 2004. Modeling of the effect of land use changes on the runoff generation of a river basin through parameter regionalization of a watershed model. *J. Hydrol.* 292, 281–295. doi:10.1016/j.jhydrol.2004.01.002
 - ✓ Hungr, O., 1995. A model for the runout analysis of rapid flow slides, debris flows, and avalanches. *Can. Geotech. J.* 32, 610–623. doi:10.1139/t95-063
 - ✓ Hungr, O., Leroueil, S., Picarelli, L., 2014. The Varnes classification of landslide types, an update. *Landslides* 11, 167–194. doi:10.1007/s10346-013-0436-y.
 - ✓ Hunter, J.J., 1998. Plant spacing implications for grafted grapevine 1. Soil characteristics, root growth, dry matter partitioning, dry matter composition and soil utilisation. *South Afr. J. Enol. Vitic.* 19, 25–34.
 - ✓ Hunter, J.J., Ruffner, H.P., Volschenk, C.G., Le Roux, D.J., 1995. Partial defoliation of *Vitis vinifera* L. cv. Cabernet Sauvignon/99 Richter: effect on root growth, canopy efficiency; grape composition, and wine quality. *Am. J. Enol. Vitic.* 46, 306–314.
 - ✓ Hyde, P., Dubayah, R., Peterson, B., Blair, J., Hofton, M., Hunsaker, C., Knox, R., Walker, W., 2005. Mapping forest structure for wildlife habitat analysis using waveform lidar: validation of montane ecosystems. *Remote Sensing of Environment* 96, 427–437. doi:10.1016/j.rse.2005.03.005
 - ✓ Hyde, P., Dubayah, R., Walker, W., Blair, J.B., Hofton, M., Hunsaker, C., 2006. Mapping forest structure for wildlife habitat analysis using multi-sensor (LiDAR, SAR/InSAR, ETM+, Quickbird) synergy. *Remote Sensing of Environment* 102, 63–73. doi:10.1016/j.rse.2006.01.021
 - ✓ Imaizumi, F., Sidle, R.C., Kamei, R., 2008. Effects of forest harvesting on the occurrence of landslides and debris flows in steep terrain of central Japan. *Earth Surf. Process. Landf.* 33, 827–840. doi:10.1002/esp.1574
 - ✓ Iovino, F., Cinnirella, S., Veltri, A., Callegari, G., 1998. Processus hydriques dans des écosystèmes forestiers. *Écologie* 29, 369–375.
 - ✓ Iroumé, A., Andreoli, A., Comiti, F., Ulloa, H., Huber, A., 2010. Large wood abundance, distribution and mobilization in a third order Coastal mountain range river system, southern Chile. *For. Ecol. Manag.* 260, 480–490. doi:10.1016/j.foreco.2010.05.004
 - ✓ ISPRA, 2006. Progetto IFFI - Inventario dei fenomeni franosi in Italia. Istituto Superiore per la Protezione e la Ricerca Ambientale, Roma.
 - ✓ Istanbulluoglu, E., Bras, R.L., 2005. Vegetation-modulated landscape evolution: Effects of vegetation on landscape processes, drainage density, and topography. *J. Geophys. Res.* 110. doi:10.1029/2004JF000249
 - ✓ Iverson, R.M., 1997. The physics of debris flows. *Rev. Geophys.* 35, 245–296.
 - ✓ Iverson, R.M., 2000. Landslide triggering by rain infiltration. *Water Resour. Res.* 36, 1897–1910.
 - ✓ Iverson, R.M., Denlinger, R.P., 2001. Flow of variably fluidized granular masses across three-dimensional terrain 1. Coulomb mixture theory. *J. Geophys. Res.* 106, 537–552.
-

References

- ✓ Iverson, R.M., Reid, M.E., Iverson, N.R., LaHusen, R.G., Logan, M., Mann, J.E., Brien, D.L., 2000. Acute sensitivity of landslide rates to initial soil porosity. *Science* 290, 513–516.
- ✓ Iverson, R.M., Reid, M.E., LaHusen, R.G., 1997. Debris-flow mobilization from landslides. *Annu. Rev. Earth Planet. Sci.* 25, 85–138.
- ✓ Iverson, R.M., Schilling, S.P., Vallance, J.W., 1998. Objective delineation of lahar-inundation hazard zones. *Geol. Soc. Am. Bull.* 110, 972–984.
- ✓ Jackson, L.E.J., Hungr, O., Gardner, J.S., Mackay, C., 1989. Cathedral mountain debris flows, Canada. *Bull. Int. Assoc. Eng. Geol.-Bull. Assoc. Int. Géologie Ing.* 40, 35–54.
- ✓ Jackson, R.B., Canadell, J., Ehleringer, J.R., Mooney, H.A., Sala, O.E., Schulze, E.D., 1996. A global analysis of root distributions for terrestrial biomes. *Oecologia* 108, 389–411.
- ✓ Jakob, M., 2000. The impacts of logging on landslide activity at Clayoquot Sound, British Columbia. *Catena* 38, 279–300.
- ✓ Janbu, N., 1957. Earth pressure and bearing capacity calculations by generalized procedure of slices, in: *Proceedings of the 4th International Conference SMFE*. London, pp. 207–212.
- ✓ Jarque, C.M., Bera, A.K., 1980. Efficient tests for normality, homoscedasticity and serial independence of regression residuals. *Econ. Lett.* 6, 255–259. doi:10.1016/0165-1765(80)90024-5
- ✓ Ji, J., Kokutse, N., Genet, M., Fourcaud, T., Zhang, Z., 2012. Effect of spatial variation of tree root characteristics on slope stability. A case study on Black Locust (*Robinia pseudoacacia*) and Arborvitae (*Platycladus orientalis*) stands on the Loess Plateau, China. *Catena* 92, 139–154. doi:10.1016/j.catena.2011.12.008
- ✓ Johnson, R.C., 1990. The interception, throughfall and stemflow in a forest in highland Scotland and the comparison with other upland forests in the UK. *J. Hydrol.* 118, 281–287.
- ✓ Kail, J., Hering, D., Muhar, S., Gerhard, M., Preis, S., 2007. The use of large wood in stream restoration: experiences from 50 projects in Germany and Austria: Large wood in stream restoration. *J. Appl. Ecol.* 44, 1145–1155. doi:10.1111/j.1365-2664.2007.01401.x
- ✓ Kaplan, S., Garrick, B.J., 1981. On the quantitative definition of risk. *Risk Anal.* 1, 11–27.
- ✓ Kasprak, A., Magilligan, F.J., Nislow, K.H., Snyder, N.P., 2012. A LiDAR-derived evaluation of watershed-scale large woody debris sources and recruitment mechanisms: Coastal Maine, U.S.A. *River Res. Appl.* 28, 1462–1476. doi:10.1002/rra.1532
- ✓ Keijsers, J.G.S., Schoorl, J.M., Chang, K.-T., Chiang, S.-H., Claessens, L., Veldkamp, A., 2011. Calibration and resolution effects on model performance for predicting shallow landslide locations in Taiwan. *Geomorphology* 133, 168–177. doi:10.1016/j.geomorph.2011.03.020
- ✓ Keim, R.F., Skaugset, A.E., 2003. Modelling effects of forest canopies on slope stability. *Hydrol. Process.* 17, 1457–1467. doi:10.1002/hyp.5121
- ✓ Keller, E.A., Swanson, F.J., 1979. Effects of large organic material on channel form and fluvial processes. *Earth Surf. Process.* 4, 361–380.

-
- ✓ Kérisel, J., Absi, E., 1990. Active and passive earth pressure tables. CRC Press - Taylor & Francis Group.
 - ✓ Kermavnar, J., Vilhar, U., 2017. Canopy precipitation interception in urban forests in relation to stand structure. *Urban Ecosyst.* doi:10.1007/s11252-017-0689-7
 - ✓ Kerr, G., Haufe, J., 2011. Thinning practice: a silvicultural guide. Forestry Commission 1.
 - ✓ Kerry, R., Oliver, M.A., 2004. Average variograms to guide soil sampling. *Int. J. Appl. Earth Obs. Geoinformation* 5, 307–325. doi:10.1016/j.jag.2004.07.005
 - ✓ Khelifa, T., Benmebarek, S., 2014. Dilation effect on 3D passive earth pressure coefficients for retaining wall. *Acad. Platf. J. Eng. Sci.* 2, 1–6.
 - ✓ Khuder, H., Stokes, A., Danjon, F., Gouskou, K., Lagane, F., 2007. Is it possible to manipulate root anchorage in young trees? *Plant Soil* 294, 87–102. doi:10.1007/s11104-007-9232-6
 - ✓ Kim, D., Im, S., Lee, C., Woo, C., 2013. Modeling the contribution of trees to shallow landslide development in a steep, forested watershed. *Ecol. Eng.* 61, 658–668. doi:10.1016/j.ecoleng.2013.05.003.
 - ✓ Kim, M.S., Onda, Y., Kim, J.K., Kim, S.W., 2015. Effect of topography and soil parameterisation representing soil thicknesses on shallow landslide modelling. *Quat. Int.* 384, 91–106. doi:10.1016/j.quaint.2015.03.057
 - ✓ Kitamura, Y., Namba, S., 1981. The function of tree roots upon landslide prevention presumed through the uprooting test. *Bull. For. For. Prod. Res. Inst. Jpn.*
 - ✓ Krey, D.K., 1936. Erddruck, Erdwiderstand und Tragfähigkeit des Baugrundes, Gesichtspunkte für die Berechnung, praktische Beispiele und 118 Erddrucktabellen. Ernst.
 - ✓ Komac, B., Zorn, M., 2009. Statistical landslide susceptibility modeling on a national scale: the example of Slovenia. *Rev Roum Géogr* 53, 179–195.
 - ✓ Köstler, J.N., Brückner, E., Bibelriether, H., 1968. Die Wurzeln der Waldbaume. Untersuchungen Zur Morphol. Waldbaume Mitteleur. Verl. Paul Parey Hambg. Berl. 284, 3–4.
 - ✓ Kozłowski, T.T., 1971. Cambial growth, root growth, and reproductive growth. Elsevier.
 - ✓ Kozma, P., 1967. Szolotermesztes I. Mezogazdasagi Kiado, Budapest.
 - ✓ Krämer, I., 2010. Rainfall partitioning and soil water dynamics along a tree species diversity gradient in a deciduous old-growth forest in Central Germany (Dissertation zur Erlangung des Doktorgrades der Mathematisch-Naturwissenschaftlichen Fakultäten der Georg). Universität Göttingen, Rostock, Germany.
 - ✓ Krey, D.K., 1936. Erddruck, Erdwiderstand und Tragfähigkeit des Baugrundes, Gesichtspunkte für die Berechnung, praktische Beispiele und 118 Erddrucktabellen. Ernst.
 - ✓ Kumar, J., Subba Rao, K.S., 1997. Passive pressure coefficients, critical failure surface and its kinematic admissibility. *Géotechnique* 47, 185–192.
 - ✓ Kupferschmid Albisetti, A.D., Brang, P., Schönenberger, W., Bugmann, H., 2003. Decay of *Picea abies* snag stands on steep mountain slopes. *For. Chron.* 79, 247–252.
-

References

- ✓ Kuriakose, S.L., van Beek, L.P.H., van Westen, C.J., 2009. Parameterizing a physically based shallow landslide model in a data poor region. *Earth Surf. Process. Landf.* 34, 867–881. doi:10.1002/esp.1794.
- ✓ Lancaster, S.T., Hayes, S.K., Grant, G.E., 2001. Modeling sediment and wood storage and dynamics in small mountainous watersheds, in: Dorava, J.M., Montgomery, D.R., Palcsak, B.B., Fitzpatrick, F.A. (Eds.), *Water Science and Application*. American Geophysical Union, Washington, D. C., pp. 85–102. doi:10.1029/WS004p0085
- ✓ Lancaster, S.T., Hayes, S.K., Grant, G.E., 2003. Effects of wood on debris flow runout in small mountain watersheds. *Water Resour. Res.* 39, 1168–1188. doi:10.1029/2001WR001227
- ✓ Lange, B., Germann, P.F., Lüscher, P., 2011. Runoff-generating processes in hydromorphic soils on a plot scale: free gravity-driven versus pressure-controlled flow. *Hydrol. Process.* 25, 873–885. doi:10.1002/hyp.7873
- ✓ Lange, B., Luescher, P., Germann, P., 2009. Significance of tree roots for preferential infiltration in stagnic soils. *Hydrol. Earth Syst. Sci.* 13, 1809–1821.
- ✓ Lanni, C., Borga, M., Rigon, R., Tarolli, P., 2012. Modelling shallow landslide susceptibility by means of a subsurface flow path connectivity index and estimates of soil depth spatial distribution. *Hydrol. Earth Syst. Sci.* 16, 3959–3971. doi:10.5194/hess-16-3959-2012
- ✓ Larsen, I.J., Montgomery, D.R., Korup, O., 2010. Landslide erosion controlled by hillslope material. *Nat. Geosci.* 3, 247–251. doi:10.1038/ngeo776
- ✓ Larsen, M.C., Torres-Sánchez, A.J., 1998. The frequency and distribution of recent landslides in three montane tropical regions of Puerto Rico. *Geomorphology* 24, 309–331.
- ✓ Le, H.D., Smith, C., Herbohn, J., 2014. What drives the success of reforestation projects in tropical developing countries? The case of the Philippines. *Glob. Environ. Change* 24, 334–348. doi:10.1016/j.gloenvcha.2013.09.010
- ✓ Lee, S., Pradhan, B., 2006. Probabilistic landslide hazards and risk mapping on Penang Island, Malaysia. *J. Earth Syst. Sci.* 115, 661–672.
- ✓ Lee, S., Ryu, J.-H., Won, J.-S., Park, H.-J., 2004. Determination and application of the weights for landslide susceptibility mapping using an artificial neural network. *Eng. Geol.* 71, 289–302. doi:10.1016/S0013-7952(03)00142-X
- ✓ Leonardi, S., Rapp, M., Failla, M., Guarnaccia, D., 1993. Interception of rainfall, input and leaching of nutrients within two *Castanea sativa* Mill. stands at the Etna volcano. *Oecologia Mont.* 2, 7–12.
- ✓ Liang, W.-L., Kosugi, K., 'ichirou, Mizuyama, T., 2007. Heterogeneous soil water dynamics around a tree growing on a steep hillslope. *Vadose Zone J.* 6, 879. doi:10.2136/vzj2007.0029
- ✓ Liao, Z., Hong, Y., Kirschbaum, D., Adler, R.F., Gourley, J.J., Wooten, R., 2011. Evaluation of TRIGRS (transient rainfall infiltration and grid-based regional slope-stability analysis)'s predictive skill for hurricane-triggered landslides: a case study in Macon County, North Carolina. *Nat. Hazards* 58, 325–339. doi:10.1007/s11069-010-9670-y

-
- ✓ Limousin, J.-M., Rambal, S., Ourcival, J.-M., Joffre, R., 2008. Modelling rainfall interception in a mediterranean *Quercus ilex* ecosystem: Lesson from a throughfall exclusion experiment. *J. Hydrol.* 357, 57–66. doi:10.1016/j.jhydrol.2008.05.001
 - ✓ Link, T.E., Unsworth, M., Marks, D., 2004. The dynamics of rainfall interception by a seasonal temperate rainforest. *Agric. For. Meteorol.* 124, 171–191. doi:10.1016/j.agrformet.2004.01.010
 - ✓ Lisle, T.E., 1995. Effects of coarse woody debris and its removal on a channel affected by the 1980 eruption of Mount St. Helens, Washington. *Water Resour. Res.* 31, 1797–1808. doi:10.1029/95WR00734
 - ✓ Liu, S., 1997. A new model for the prediction of rainfall interception in forest canopies. *Ecol. Model.* 99, 151–159.
 - ✓ Llorens, P., 1997. Rainfall interception by a *Pinus sylvestris* forest patch overgrown in a Mediterranean mountainous abandoned area II. Assessment of the applicability of Gash's analytical model. *J. Hydrol.* 199, 346–359.
 - ✓ Llorens, P., Poch, R., Latron, J., Gallart, F., 1997. Rainfall interception by a *Pinus sylvestris* forest patch overgrown in a Mediterranean mountainous abandoned area I. Monitoring design and results down to the event scale. *J. Hydrol.* 199, 331–345.
 - ✓ Loades, K.W., Bengough, A.G., Bransby, M.F., Hallett, P.D., 2010. Planting density influence on fibrous root reinforcement of soils. *Ecol. Eng.* 36, 276–284. doi:10.1016/j.ecoleng.2009.02.005
 - ✓ Losey, S., Wehrli, A., 2013. Schutzwald in der Schweiz. Vom Proj. SilvaProtect-CH Zum Harmon. Schutzwald Bern Bundesamt Umw.
 - ✓ Loustau, D., Berbigier, P., Granier, A., 1992a. Interception loss, throughfall and stemflow in a maritime pine stand. II. An application of Gash's analytical model of interception. *J. Hydrol.* 138, 469–485.
 - ✓ Loustau, D., Berbigier, P., Granier, A., Moussa, F.E.H., 1992b. Interception loss, throughfall and stemflow in a maritime pine stand. I. Variability of throughfall and stemflow beneath the pine canopy. *J. Hydrol.* 138, 449–467.
 - ✓ Lu, N., Godt, J., 2008. Infinite slope stability under steady unsaturated seepage conditions. *Water Resour. Res.* 44, W11404. doi:10.1029/2008WR006976
 - ✓ Lucía, A., Antonello, A., Campana, D., Cavalli, M., Crema, S., Franceschi, S., Marchese, E., Niedrist, M., Schneiderbauer, S., Comiti, F., 2015a. Monitoring and modeling large wood recruitment and transport in a mountain basin of North-Eastern Italy, in: Lollino, G., Arattano, M., Rinaldi, M., Giustolisi, O., Marechal, J.-C., Grant, G.E. (Eds.), *Engineering Geology for Society and Territory - Volume 3*. Springer International Publishing, Switzerland, pp. 155–158. doi:10.1007/978-3-319-09054-2_31
 - ✓ Lucía, A., Comiti, F., Borga, M., Cavalli, M., Marchi, L., 2015b. Dynamics of large wood during a flash flood in two mountain catchments. *Nat. Hazards Earth Syst. Sci.* 15, 1741–1755. doi:10.5194/nhess-15-1741-2015
-

References

- ✓ Lumb, P., 1975. Slope failures in Hong Kong. *Q. J. Eng. Geol. Hydrogeol.* 8, 31–65.
- ✓ Luo, Y., He, S., Chen, F., Li, X., He, J., 2015. A physical model considered the effect of overland water flow on rainfall-induced shallow landslides. *Geoenvironmental Disasters* 2, 1–11. doi:10.1186/s40677-015-0017-6
- ✓ Macuh, B., Škrabl, S., 2010. Passive earth pressure determination: application of the corresponding state theorem for calculating upper-bound values. *Acta Geotech. Slov.* 2.
- ✓ Malvolti, M.E., 2002. Final Report - B.L.o.R.I.D.A.R. Black Locust (*Robinia pseudoacacia* L.) Resources Investigation for Degraded areas Rehabilitation (INCO Copernicus Contract N° ERB IC 15-CT 98-135). CNR-Institute for Agroforestry, Italy.
- ✓ Mao, L., Andreoli, A., Iroumé, A., Comiti, F., Lenzi, M.A., 2013. Dynamics and management alternatives of in-channel large wood in mountain basins of the southern Andes. *Bosque Valdivia* 34, 15–16. doi:10.4067/S0717-92002013000300008
- ✓ Mao, Z., Bourrier, F., Stokes, A., Fourcaud, T., 2014. Three-dimensional modelling of slope stability in heterogeneous montane forest ecosystems. *Ecol. Model.* 273, 11–22. doi:10.1016/j.ecolmodel.2013.10.017
- ✓ Mao, Z., Saint-André, L., Genet, M., Mine, F.-X., Jourdan, C., Rey, H., Courbaud, B., Stokes, A., 2012. Engineering ecological protection against landslides in diverse mountain forests: Choosing cohesion models. *Ecol. Eng.* 45, 55–69. doi:10.1016/j.ecoleng.2011.03.026
- ✓ Marchesini, I., Cencetti, C., De Rosa, P., 2009. A preliminary method for the evaluation of the landslides volume at a regional scale. *Geoinformatica* 13, 277–289. doi:10.1007/s10707-008-0060-5
- ✓ Marcus, W.A., Fonstad, M.A., 2008. Optical remote mapping of rivers at sub-meter resolutions and watershed extents. *Earth Surf. Process. Landf.* 33, 4–24. doi:10.1002/esp.1637
- ✓ Margarint, M.C., Juravle, D.T., Grozavu, A., 2013. Large landslide risk assessment in hilly areas. A case study of Huși town region (North-East of Romania). *Ital. J. Eng. Geol. Environ.* 275–286. doi:10.4408/IJEGE.2013-06.B-25
- ✓ Marre, A., Laurain, M., Guérémy, P., 1997. Relations spatiales et temporelles entre les formations superficielles et les mouvements de terrain sur la côte de l'Île-de-France (Champagne): un moyen de préparer les cartes des aléas. *Géologie Fr.* 2, 39–49.
- ✓ Mateos Rodríguez, A.B., Schnabel, S., 1998. Medición de la interceptación de las precipitaciones por la encina (*Quercus rotundifolia* Lam.): Metodología e instrumentalización. *Norba Rev. Geogr.*
- ✓ Mazindrani, Z.H., Ganjali, M.H., 1997. Lateral earth pressure problem of cohesive backfill with inclined surface. *J. Geotech. Geoenvironmental Eng.* 123, 110–112.
- ✓ Mazzorana, B., Comiti, F., Volcan, C., Scherer, C., 2011a. Determining flood hazard patterns through a combined stochastic–deterministic approach. *Nat. Hazards* 59, 301–316. doi:10.1007/s11069-011-9755-2

-
- ✓ Mazzorana, B., Hübl, J., Zischg, A., Largiader, A., 2011b. Modelling woody material transport and deposition in alpine rivers. *Nat. Hazards* 56, 425–449. doi:10.1007/s11069-009-9492-y
 - ✓ Mazzorana, B., Zischg, A., Largiader, A., Hübl, J., 2009. Hazard index maps for woody material recruitment and transport in alpine catchments. *Nat. Hazards Earth Syst. Sci.* 9, 197–209.
 - ✓ McClung, D., Schaerer, P.A., 2006. *The avalanche handbook*. The Mountaineers Books.
 - ✓ McClung, D.M., 2001. Characteristics of terrain, snow supply and forest cover for avalanche initiation caused by logging. *Ann. Glaciol.* 32, 223–229.
 - ✓ McKean, J., Roering, J., 2004. Objective landslide detection and surface morphology mapping using high-resolution airborne laser altimetry. *Geomorphology* 57, 331–351. doi:10.1016/S0169-555X(03)00164-8
 - ✓ Meisina, C., Scarabelli, S., 2007. A comparative analysis of terrain stability models for predicting shallow landslides in colluvial soils. *Geomorphology* 87, 207–223. doi:10.1016/j.geomorph.2006.03.039
 - ✓ Melchiorre, C., Frattini, P., 2012. Modelling probability of rainfall-induced shallow landslides in a changing climate, Otta, Central Norway. *Clim. Change* 113, 413–436. doi:10.1007/s10584-011-0325-0
 - ✓ Meloni, F., Lingua, E., Motta, R., 2006. Analisi della funzione protettiva delle foreste: l'esempio della "Carta delle foreste di protezione diretta della Valle d'Aosta." *For.-J. Silvic. For. Ecol.* 3, 420.
 - ✓ Mergili, M., Marchesini, I., Alvioli, M., Metz, M., Schneider-Muntau, B., Rossi, M., Guzzetti, F., 2014a. A strategy for GIS-based 3-D slope stability modelling over large areas. *Geosci. Model Dev.* 7, 2969–2982. doi:10.5194/gmd-7-2969-2014
 - ✓ Mergili, M., Marchesini, I., Rossi, M., Guzzetti, F., Fellin, W., 2014b. Spatially distributed three-dimensional slope stability modelling in a raster GIS. *Geomorphology* 206, 178–195. doi:10.1016/j.geomorph.2013.10.008
 - ✓ Michopoulos, P., Baloutsos, G., Nakos, G., Economou, A., 2001. Effects of bulk precipitation pH and growth period on cation enrichment in precipitation beneath the canopy of a beech (*Fagus moesiaca*) forest stand. *Sci. Total Environ.* 281, 79–85.
 - ✓ Mickovski, S.B., Bengough, A.G., Bransby, M.F., Davies, M.C.R., Hallett, P.D., Sonnenberg, R., 2007. Material stiffness, branching pattern and soil matric potential affect the pullout resistance of model root systems. *Eur. J. Soil Sci.* 58, 1471–1481. doi:10.1111/j.1365-2389.2007.00953.x
 - ✓ Mickovski, S.B., Hallett, P.D., Bransby, M.F., Davies, M.C.R., Sonnenberg, R., Bengough, A.G., 2009. Mechanical reinforcement of soil by willow roots: impacts of root properties and root failure mechanism. *Soil Sci. Soc. Am. J.* 73, 1276. doi:10.2136/sssaj2008.0172
 - ✓ Milledge, D.G., Bellugi, D., McKean, J.A., Densmore, A.L., Dietrich, W.E., 2014. A multidimensional stability model for predicting shallow landslide size and shape across landscapes: predicting landslide size and shape. *J. Geophys. Res. Earth Surf.* 119, 2481–2504. doi:10.1002/2014JF003135
-

References

- ✓ Milledge, D.G., Griffiths, D.V., Lane, S.N., Warburton, J., 2012. Limits on the validity of infinite length assumptions for modelling shallow landslides. *Earth Surf. Process. Landf.* 37, 1158–1166. doi:10.1002/esp.3235
- ✓ Miller, D., Luce, C., Benda, L., 2003. Time, space, and episodicity of physical disturbance in streams. *For. Ecol. Manag.* 178, 121–140. doi:10.1016/S0378-1127(03)00057-4
- ✓ Minaya-Gallego, M.T., López-Arias, M., González-Fernández, F., Rodríguez-Pena, J.A., 1997. Balance hídrico anual en una cuenca de *Pinus sylvestris*, in: *Congresos Forestales*. pp. 419–424.
- ✓ Mitscherlich, G., Moll, W., 1970. Untersuchungen über die Niederschlags- und bodenfeuchtigkeitsverhältnisse in einigen nadel- und laubholzbeständen in der nähe von Freiburg/br. *Allg. Forst Jagdztg.* 141, 49–60.
- ✓ Molchanov, A.A., 1963. The hydrological role of forests. (*Gidrologicheskaya rol'lesa*). Translated from Russian. Israel Program for Scientific Translations.
- ✓ Montgomery, D.R., 2001. Slope distributions, threshold hillslopes, and steady-state topography. *Am. J. Sci.* 301, 432–454.
- ✓ Montgomery, D.R., Collins, B.D., Buffington, J.M., Abbe, T.B., 2003. Geomorphic effects of wood in rivers, in: *Ecology and Management of Wood in World Rivers*. American Fisheries Society, pp. 1–27.
- ✓ Montgomery, D.R., Dietrich, W.E., 1994. A physically based model for the topographic control. *Water Resour. Res.* 30, 1153–1171.
- ✓ Montgomery, D.R., Piégay, H., 2003. Wood in rivers: interactions with channel morphology and processes. *Geomorphology* 51, 1–5.
- ✓ Montgomery, D.R., Schmidt, K.M., Greenberg, H.M., Dietrich, W.E., 2000. Forest clearing and regional landsliding. *Geology* 28, 311–314.
- ✓ Moore, J.R., 2000. Differences in maximum resistive bending moments of *Pinus radiata* trees grown on a range of soil types. *For. Ecol. Manag.* 135, 63–71.
- ✓ Moore, R.D., Winkler, R.D., Carlyle-Moses, D.E., Spittlehouse, D., Giles, T., Phillips, J., Leach, J.A., Eaton, B.C., Owens, P., Peticrew, E., 2008. Watershed response to the McLure forest fire: presentation summaries from the Fishtrap Creek workshop, March 2008. *Streamline Watershed Manag. Bull.* 12, 1–11.
- ✓ Moos, C., Bebi, P., Graf, F., Mattli, J., Rickli, C., Schwarz, M., 2016. How does forest structure affect root reinforcement and susceptibility to shallow landslides?: A Case Study in St. Antönien, Switzerland. *Earth Surf. Process. Landf.* 41, 951–960. doi:10.1002/esp.3887
- ✓ Morano, L., Kliewer, W.M., 1994. Root distribution of three grapevine rootstocks grafted to Cabernet Sauvignon grown on a very gravelly clay loam soil in Oakville, California. *Am. J. Enol. Vitic.* 45, 345–348.

-
- ✓ Moreno, G., Gallardo, J.F., Bussotti, F., 2001. Canopy modification of atmospheric deposition in oligotrophic *Quercus pyrenaica* forests of an unpolluted region (central-western Spain). *For. Ecol. Manag.* 149, 47–60.
 - ✓ Morgan, B.A., Wieczorek, G.F., Campbell, R.H., Gori, P.L., 1997. Debris-flow hazards in areas affected by the June 27, 1995 storm in Madison County, Virginia, USGS Open File Report.
 - ✓ Morgenstern, N.R., Eisenstein, Z., 1970. Methods of estimating lateral loads and deformations, in: *Lateral Stresses in the Ground and Design of Earth-Retaining Structures*. ASCE, pp. 51–102.
 - ✓ Morlat, R., Jacquet, A., 2003. Grapevine root system and soil characteristics in a vineyard maintained long-term with or without interrow sward. *Am. J. Enol. Vitic.* 54, 1–7.
 - ✓ Moroni, M.T., Worledge, D., Beadle, C.L., 2003. Root distribution of *Eucalyptus nitens* and *E. globulus* in irrigated and droughted soil. *For. Ecol. Manag.* 177, 399–407.
 - ✓ Morrison Jr, E.E., Ebeling, R.M., 1995. Limit equilibrium computation of dynamic passive earth pressure. *Can. Geotech. J.* 32, 481–487.
 - ✓ Mosello, R., Brizzio, M.C., Kotzias, D., Marchetto, A., Rembges, D., Tartari, G., 2002. The chemistry of atmospheric deposition in Italy in the framework of the National Programme for Forest Ecosystems Control (CONECOFOR). *J. Limnol.* 61, 77–92.
 - ✓ Motta, E., Raciti, E., 2014. A closed form solution for a three dimensional passive earth pressure coefficient. *Riv. Ital. Geotec.* 3, 18–27.
 - ✓ Motta, R., Haudemand, J.-C., 2000. Protective forests and silvicultural stability: an example of planning in the aosta valley. *Mt. Res. Dev.* 20, 180–187.
 - ✓ Mugagga, F., Kakembo, V., Buyinza, M., 2012. Land use changes on the slopes of Mount Elgon and the implications for the occurrence of landslides. *Catena* 90, 39–46. doi:10.1016/j.catena.2011.11.004
 - ✓ Müller-Breslau, H.F.B., 1906. *Erddruck auf stuetzmauern*. A. Kröner, Stuttgart, Germany.
 - ✓ Nagarajah, S., 1987. Effects of soil texture on the rooting patterns of Thompson Seedless vines on own roots and on Ramsey rootstock in irrigated vineyards. *Am. J. Enol. Vitic.* 38, 54–59.
 - ✓ Naghdi, R., Maleki, S., Abdi, E., Mousavi, R., Nikooy, M., others, 2013. Assessing the effect of *Alnus* roots on hillslope stability in order to use in soil bioengineering. *J. For. Sci.* 59, 417–423.
 - ✓ Nakamura, F., Swanson, F.J., 1993. Effects of coarse woody debris on morphology and sediment storage of a mountain stream system in western Oregon. *Earth Surf. Process. Landf.* 18, 43–61.
 - ✓ Nandi, A., Shakoor, A., 2010. A GIS-based landslide susceptibility evaluation using bivariate and multivariate statistical analyses. *Eng. Geol.* 110, 11–20. doi:10.1016/j.enggeo.2009.10.001
 - ✓ Narain, J., Saran, S., Nandakumaran, P., 1969. Model study of passive pressure in sand. *J. Soil Mech. Found. Div.*
 - ✓ Naranjo, J.L., van Westen, C.J., Soeters, R., 1994. Evaluating the use of training areas in bivariate statistical landslide hazard analysis: a case study in Colombia. *ITC J.* 3, 292–300.
-

References

- ✓ Neal, C., Robson, A.J., Bhardwaj, C.L., Conway, T., Jeffery, H.A., Neal, M., Ryland, G.P., Smith, C.J., Walls, J., 1993. Relationships between precipitation, stemflow and throughfall for a lowland beech plantation, Black Wood, Hampshire, southern England: findings on interception at a forest edge and the effects of storm damage. *J. Hydrol.* 146, 221–233.
- ✓ Nefeslioglu, H.A., Gokceoglu, C., Sonmez, H., 2008. An assessment on the use of logistic regression and artificial neural networks with different sampling strategies for the preparation of landslide susceptibility maps. *Eng. Geol.* 97, 171–191. doi:10.1016/j.enggeo.2008.01.004
- ✓ Negadi, K., Arab, A., Elbokl, M.K., Setti, F., 2015. Triaxial compression tests of soil reinforced with fibers. *J. Chem. Mater. Res.* 3, 15–20.
- ✓ Neuhäuser, B., Damm, B., Terhorst, B., 2012. GIS-based assessment of landslide susceptibility on the base of the Weights-of-Evidence model. *Landslides* 9, 511–528. doi:10.1007/s10346-011-0305-5
- ✓ Nilaweera, N.S., Nutalaya, P., 1999. Role of tree roots in slope stabilisation. *Bull. Eng. Geol. Environ.* 57, 337–342.
- ✓ Normaniza, O., Barakbah, S.S., 2006. Parameters to predict slope stability - Soil water and root profiles. *Ecol. Eng.* 28, 90–95. doi:10.1016/j.ecoleng.2006.04.004
- ✓ Norris, J.E., 2005. Root reinforcement by hawthorn and oak roots on a highway cut-slope in Southern England. *Plant Soil* 278, 43–53. doi:10.1007/s11104-005-1301-0
- ✓ O'Brien, J.S., Julien, P.Y., 1988. Laboratory analysis of mudflow properties. *J. Hydraul. Eng.* 114, 877–887.
- ✓ O'Loughlin, C., Ziemer, R.R., 1982. The importance of root strength and deterioration rates upon edaphic stability in steepland forests, in: *Carbon Uptake and Allocation in Subalpine Ecosystems as a Key to Management*. R.H. Waring, Oregon State University, Corvallis, Oregon, pp. 70–78.
- ✓ O'Loughlin, C.L., 1972. An investigation of the stability of the steepland forest soils in the coast mountains, southwest British Columbia (PhD dissertation). University of British Columbia, Vancouver, Canada.
- ✓ O'Loughlin, C.L., 1974. The effect of timber removal on the stability of forest soils. *J. Hydrol. NZ* 13, 121–134.
- ✓ O'Loughlin, C.L., Watson, A., 1979. Root-wood strength deterioration in radiata pine after clearfelling. *N. Z. J. For. Sci.* 9, 284–293.
- ✓ O'Loughlin, E.M., 1986. Prediction of surface saturation zones in natural catchments by topographic analysis. *Water Resour. Res.* 22, 794–804.
- ✓ Okimura, T., 1994. Prediction of the shape of a shallow failure on a mountain slope: The three-dimensional multi-planar sliding surface method. *Geomorphology* 9, 223–233.
- ✓ Okimura, T., Ichikawa, R., 1985. A prediction method for surface failures by movements of infiltrated water in a surface soil layer. *Nat. Disaster Sci.* 7, 41–51.

-
- ✓ Okuda, S., Suwa, H., 1984. Some relationships between debris flow motion and micro-topography for the Kamikamihori fan, North Japan Alps. *Catchment Exp. Fluv. Geomorphol.*, Geo Books, Norwich, England 447–464.
 - ✓ Operstein, V., Frydman, S., 2000. The influence of vegetation on soil strength. *Proc. Inst. Civ. Eng.-Ground Improv.* 4, 81–89.
 - ✓ Opperman, J.J., Lohse, K.A., Brooks, C., Kelly, N.M., Merenlender, A.M., 2005. Influence of land use on fine sediment in salmonid spawning gravels within the Russian River Basin, California. *Can. J. Fish. Aquat. Sci.* 62, 2740–2751. doi:10.1139/f05-187
 - ✓ Orris, G.J., Williams, J.W., 1984. Landslide length-width ratios as an aid in landslide identification and verification. *Bull. Assoc. Eng. Geol.* XXI, 371–375.
 - ✓ Osawa, A., Allen, R.B., 1993. Allometric theory explains self-thinning relationships of mountain beech and red pine. *Ecology* 1020–1032.
 - ✓ Pack, R.T., Tarboton, D.G., Goodwin, C.N., 1998. The SINMAP approach to terrain stability mapping, in: *Proceedings of the 8th Congress of the International Association of Engineering Geology*, Vancouver, British Columbia, Canada. pp. 21–25.
 - ✓ Panagos, P., Van Liedekerke, M., Jones, A., Montanarella, L., 2012. European soil data centre: response to European policy support and public data requirements. *Land Use Policy* 29, 329–338. doi:10.1016/j.landusepol.2011.07.003.
 - ✓ Parise, M., Jibson, R.W., 2000. A seismic landslide susceptibility rating of geologic units based on analysis of characteristics of landslides triggered by the 17 January, 1994 Northridge, California earthquake. *Eng. Geol.* 58, 251–270.
 - ✓ Park, D.W., Nikhil, N.V., Lee, S.R., 2013. Landslide and debris flow susceptibility zonation using TRIGRS for the 2011 Seoul landslide event. *Nat. Hazards Earth Syst. Sci.* 13, 2833–2849. doi:10.5194/nhess-13-2833-2013
 - ✓ Pathak, S., Nilsen, B., 2004. Probabilistic rock slope stability analysis for Himalayan conditions. *Bull. Eng. Geol. Environ.* 63, 25–32. doi:10.1007/s10064-003-0226-1
 - ✓ Patki, M.A., Mandal, J.N., Dewaikar, D.M., 2015. Computation of passive earth pressure coefficients for a vertical retaining wall with inclined cohesionless backfill. *Int. J. Geo-Eng.* 6. doi:10.1186/s40703-015-0004-5
 - ✓ Paudel, P.P., Moriwaki, K., Morita, K., Kubota, T., Omura, H., 2003. An assessment of shallow landslides mechanism induced by rainfall in Hakoishi Area. *Kyushu For. Res* 56, 122–128.
 - ✓ Penna, D., Borga, M., Aronica, G.T., Brigandi, G., Tarolli, P., 2014. The influence of grid resolution on the prediction of natural and road-related shallow landslides. *Hydrol. Earth Syst. Sci.* 18, 2127–2139. doi:10.5194/hess-18-2127-2014
 - ✓ Pereira, S., Zêzere, J.L., Bateira, C., 2012. Technical Note: Assessing predictive capacity and conditional independence of landslide predisposing factors for shallow landslide susceptibility models. *Nat. Hazards Earth Syst. Sci.* 12, 979–988. doi:10.5194/nhess-12-979-2012
-

References

- ✓ Persichillo, M.G., Bordoni, M., Meisina, C., 2017. The role of land use changes in the distribution of shallow landslides. *Sci. Total Environ.* 574, 924–937. doi:10.1016/j.scitotenv.2016.09.125
- ✓ Persichillo, M.G., Bordoni, M., Meisina, C., Bartelletti, C., Barsanti, M., Giannecchini, R., D'Amato Avanzi, G., Galanti, Y., Cevasco, A., Brandolini, P., Galve, J.P., 2016. Shallow landslides susceptibility assessment in different environments. *Geomat. Nat. Hazards Risk* 1–24. doi:10.1080/19475705.2016.1265011
- ✓ Phillips, C., Marden, M., Basher, L.R., 2017. Geomorphology and forest management in New Zealand's erodible steeplands: An overview. *Geomorphology*. doi:10.1016/j.geomorph.2017.07.031
- ✓ Piacentini, D., Troiani, F., Soldati, M., Notarnicola, C., Savelli, D., Schneiderbauer, S., Strada, C., 2012. Statistical analysis for assessing shallow-landslide susceptibility in South Tyrol (south-eastern Alps, Italy). *Geomorphology* 151–152, 196–206. doi:10.1016/j.geomorph.2012.02.003
- ✓ Piégay, H., Thévenet, A., Citterio, A., 1999. Input, storage and distribution of large woody debris along a mountain river continuum, the Drome River, France. *Catena* 35, 19–39.
- ✓ Piussi, P., 1994. *Selvicoltura generale, Scienze forestali e ambientali*. UTET.
- ✓ Pollen, N., 2007. Temporal and spatial variability in root reinforcement of streambanks: Accounting for soil shear strength and moisture. *Catena* 69, 197–205. doi:10.1016/j.catena.2006.05.004
- ✓ Pollen, N., Simon, A., 2005. Estimating the mechanical effects of riparian vegetation on stream bank stability using a fiber bundle model. *Water Resour. Res.* 41, W07025. doi:10.1029/2004WR003801
- ✓ Pollen, N., Simon, A., Collison, A., 2004. Advances in assessing the mechanical and hydrologic effects of riparian vegetation on streambank stability. *Riparian Veg. Fluv. Geomorphol.* 125–139.
- ✓ Pollen-Bankhead, N., Simon, A., Jaeger, K., Wohl, E., 2009. Destabilization of streambanks by removal of invasive species in Canyon de Chelly National Monument, Arizona. *Geomorphology* 103, 363–374. doi:10.1016/j.geomorph.2008.07.004
- ✓ Polomski, J., Kuhn, N., 2001. Wurzelhabitus und Standfestigkeit der Waldbäume. *Forstwiss. Cent. Ver. Mit Tharandter Forstl. Jahrb.* 120, 303–317.
- ✓ Portela, E., Pires, A.L., 1995. Nutrient deposition and leaching by rainwater in low and intensively managed chestnut groves. Presented at the Proceedings of the Conference on Erosion and Land Degradation in the Mediterranean, University of Aveiro, Aveiro, Portugal, pp. 307–317.
- ✓ Poterasu, A., 2013. Experimental investigation of the passive Earth pressure on retaining wall when the backfill is collapsible soil (Master thesis). Concordia University.
- ✓ Potyondy, J.G., 1961. Skin friction between various soils and construction materials. *Géotechnique* 11, 339–353.

-
- ✓ Pradhan, B., 2010. Remote sensing and GIS-based landslide hazard analysis and cross-validation using multivariate logistic regression model on three test areas in Malaysia. *Adv. Space Res.* 45, 1244–1256. doi:10.1016/j.asr.2010.01.006
 - ✓ Pradhan, B., 2013. A comparative study on the predictive ability of the decision tree, support vector machine and neuro-fuzzy models in landslide susceptibility mapping using GIS. *Comput. Geosci.* 51, 350–365. doi:10.1016/j.cageo.2012.08.023
 - ✓ Preti, F., 2006. Stabilità dei versanti vegetati. *G Sauli P Cornellini F Preti Cura Di* 3, 137–168.
 - ✓ Preti, F., 2013. Forest protection and protection forest: Tree root degradation over hydrological shallow landslides triggering. *Ecol. Eng.* 61, 633–645. doi:10.1016/j.ecoleng.2012.11.009
 - ✓ Preti, F., Dani, A., Laio, F., 2010. Root profile assessment by means of hydrological, pedological and above-ground vegetation information for bio-engineering purposes. *Ecol. Eng.* 36, 305–316. doi:10.1016/j.ecoleng.2009.07.010
 - ✓ Preti, F., Giadrossich, F., 2009. Root reinforcement and slope bioengineering stabilization by Spanish Broom (*Spartium junceum* L.). *Hydrol. Earth Syst. Sci.* 13, 1713–1726.
 - ✓ Price, A.G., Carlyle-Moses, D.E., 2003. Measurement and modelling of growing-season canopy water fluxes in a mature mixed deciduous forest stand, southern Ontario, Canada. *Agric. For. Meteorol.* 119, 69–85. doi:10.1016/S0168-1923(03)00117-5
 - ✓ Pypker, T.G., Bond, B.J., Link, T.E., Marks, D., Unsworth, M.H., 2005. The importance of canopy structure in controlling the interception loss of rainfall: Examples from a young and an old-growth Douglas-fir forest. *Agric. For. Meteorol.* 130, 113–129. doi:10.1016/j.agrformet.2005.03.003
 - ✓ Pypker, T.G., Unsworth, M.H., Bond, B.J., 2006. The role of epiphytes in rainfall interception by forests in the Pacific Northwest. II. Field measurements at the branch and canopy scale. *Can. J. For. Res.* 36, 819–832. doi:10.1139/x05-286
 - ✓ Qiu, C., Esaki, T., Xie, M., Mitani, Y., Wang, C., 2007. Spatio-temporal estimation of shallow landslide hazard triggered by rainfall using a three-dimensional model. *Environ. Geol.* 52, 1569–1579. doi:10.1007/s00254-006-0601-x
 - ✓ Raia, S., Alvioli, M., Rossi, M., Baum, R.L., Godt, J.W., Guzzetti, F., 2014. Improving predictive power of physically based rainfall-induced shallow landslide models: a probabilistic approach. *Geosci. Model Dev.* 7, 495–514. doi:doi:10.5194/gmd-7-495-2014
 - ✓ Ramos, M.C., Cots-Folch, R., Martínez-Casasnovas, J.A., 2007. Sustainability of modern land terracing for vineyard plantation in a Mediterranean mountain environment – The case of the Priorat region (NE Spain). *Geomorphology* 86, 1–11. doi:10.1016/j.geomorph.2006.08.004
 - ✓ Rankine, W.J.M., 1857. On the stability of loose earth. *Philos. Trans. R. Soc. Lond.* 147, 9–27.
 - ✓ Rapp, M., Ibrahim, M., 1978. Egouttement, écoulement et interception des précipitations par un peuplement de *Pinus pinea* L. *Oecologia Plant.* 13, 321–330.
-

References

- ✓ Rapp, M., Romane, F., 1968. Contribution a l'étude du bilan de l'eau dans les écosystèmes méditerranéens. 1. Egouttement des précipitations sous des peuplements de *Quercus ilex* L. et de *Pinus halepensis*. *Oecologia Plant.* 3, 271–284.
- ✓ Raspa, G., Moscatelli, M., Stigliano, F., Patera, A., Marconi, F., Folle, D., Vallone, R., Mancini, M., Cavinato, G.P., Milli, S., Costa, J.F.C.L., 2008. Geotechnical characterization of the upper Pleistocene–Holocene alluvial deposits of Roma (Italy) by means of multivariate geostatistics: Cross-validation results. *Eng. Geol.* 101, 251–268. doi:10.1016/j.enggeo.2008.06.007
- ✓ Rebhann, G., 1871. *Theorie des Erddruckes und der Futtermauern*. C. Gerold's sohn.
- ✓ Refice, A., Capolongo, D., 2002. Probabilistic modeling of uncertainties in earthquake-induced landslide hazard assessment. *Comput. Geosci.* 28, 735–749.
- ✓ Regenass, P., Meksaouine, M., Kastner, R., Soubra, A.-H., Bourdeau, Y., 2000. Étude de la butée sur un écran de largeur limitée en sol frottant. *Rev. Fr. Génie Civ.* 4, 543–575.
- ✓ Reichenbach, P., Busca, C., Mondini, A.C., Rossi, M., 2014. The Influence of land use change on landslide susceptibility zonation: the Briga catchment test site (Messina, Italy). *Environ. Manage.* 54, 1372–1384. doi:10.1007/s00267-014-0357-0
- ✓ Reid, L.M., Lewis, J., 2009. Rates, timing, and mechanisms of rainfall interception loss in a coastal redwood forest. *J. Hydrol.* 375, 459–470. doi:10.1016/j.jhydrol.2009.06.048
- ✓ Reneau, S.L., Dietrich, W.E., 1987. Size and location of colluvial landslides in a steep forested landscape. *IAHS-AISH Publ.* 39–48.
- ✓ Rice, R.M., Crobett, E.S., Bailey, R.G., 1969. Soil slips related to vegetation, topography, and soil in southern California. *Water Resour. Res.* 5, 647–659.
- ✓ Rickenmann, D., Sheidl, C., 2013. Debris-flow runout and deposition on the fan, in: Schneuwly-Bollschweiler, M., Stoffel, M., Rudolf-Miklau, F. (Eds.), *Dating Torrential Processes on Fans and Cones*, *Advances in Global Change Research*. Springer Netherlands, Dordrecht, pp. 75–93.
- ✓ Rickli, C., Graf, F., 2009. Effects of forests on shallow landslides—case studies in Switzerland. *For. Snow Landsc. Res.* 82, 33–44.
- ✓ Riestenberg, M.M., 1994. Anchoring of thin colluvium by roots of sugar maple and white ash on hillslopes in Cincinnati (No. U.S. Geological Survey Bulletin 2059-E). United States Government Printing Office, Washington, D. C.
- ✓ Riestenberg, M.M., Sovonick-Dunford, S., 1983. The role of woody vegetation in stabilizing slopes in the Cincinnati area, Ohio. *Geol. Soc. Am. Bull.* 94, 506–518.
- ✓ Rigon, E., Comiti, F., Lenzi, M.A., 2012. Large wood storage in streams of the Eastern Italian Alps and the relevance of hillslope processes. *Water Resour. Res.* 48, W01518. doi:10.1029/2010WR009854
- ✓ Roberts, J., 1976. A study of root distribution and growth in a *Pinus sylvestris* L. (Scots pine) plantation in East Anglia. *Plant Soil* 44, 607–621.

-
- ✓ Robinson, M., Cognard-Plancq, A.-L., Cosandey, C., David, J., Durand, P., Führer, H.-W., Hall, R., Hendriques, M.O., Marc, V., McCarthy, R., McDonnell, M., Martin, C., Nisbet, T., O’Dea, P., Rodgers, M., Zollner, A., 2003. Studies of the impact of forests on peak flows and baseflows: a European perspective. *For. Ecol. Manag.* 186, 85–97. doi:10.1016/S0378-1127(03)00238-X
 - ✓ Rodà, F., Avila, A., Bonilla, D., 1990. Precipitation, throughfall, soil solution and streamwater chemistry in a holm-oak (*Quercus ilex*) forest. *J. Hydrol.* 116, 167–183. doi:10.1016/0022-1694(90)90121-D
 - ✓ Rodrigo, A., Avila, A., Rodà, F., 2003. The chemistry of precipitation, throughfall and stemflow in two holm oak (*Quercus ilex* L.) forests under a contrasted pollution environment in NE Spain. *Sci. Total Environ.* 305, 195–205.
 - ✓ Roering, J.J., 2008. How well can hillslope evolution models “explain” topography? Simulating soil transport and production with high-resolution topographic data. *Geol. Soc. Am. Bull.* 120, 1248–1262.
 - ✓ Roering, J.J., Schmidt, K.M., Stock, J.D., Dietrich, W.E., Montgomery, D.R., 2003. Shallow landsliding, root reinforcement, and the spatial distribution of trees in the Oregon Coast Range. *Can. Geotech. J.* 40, 237–253. doi:10.1139/t02-113
 - ✓ Rosso, R., Rulli, M.C., Vannucchi, G., 2006. A physically based model for the hydrologic control on shallow landsliding. *Water Resour. Res.* 42, W06410. doi:10.1029/2005WR004369
 - ✓ Rossoni, M., Labra, M., Imazio, S., Grassi, F., Scienza, A., Sala, F., 2015. Genetic relationships among grapevine cultivars grown in Oltrepò Pavese (Italy). *Vitis* 42, 31.
 - ✓ Rowe, P.W., Peaker, K., 1965. Passive earth pressure measurements. *Géotechnique* 15, 57–78.
 - ✓ Ruiz-Villanueva, V., Díez-Herrero, A., Ballesteros, J.A., Bodoque, J.M., 2014. Potential large woody debris recruitment due to landslides, bank erosion and floods in mountain basins: A quantitative estimation approach. *River Res. Appl.* 30, 81–97. doi:10.1002/rra.2614
 - ✓ Ruiz-Villanueva, V., Piégay, H., Gurnell, A.M., Marston, R.A., Stoffel, M., 2016. Recent advances quantifying the large wood dynamics in river basins: new methods and remaining challenges. *Rev. Geophys.* 54, 611–652. doi:10.1002/2015RG000514
 - ✓ Rutter, A.J., Morton, A.J., Robins, P.C., 1975. A predictive model of rainfall interception in forests. II. Generalization of the model and comparison with observations in some coniferous and hardwood stands. *J. Appl. Ecol.* 367–380.
 - ✓ Saayman, D., Van Huyssteen, L., 1980. Soil preparation studies: I. The effect of depth and method of soil preparation and of organic material on the performance of *Vitis vinifera* (var. Chenin blanc) on hutton/sterkspruit Soil. *South Afr. J. Enol. Vitic.* 1, 107–121.
 - ✓ Sakals, M.E., Innes, J.L., Wilford, D.J., Sidle, R.C., Grant, G.E., 2006. The role of forests in reducing hydrogeomorphic hazards. *For. Snow Landsc. Res.* 80, 11–22.
 - ✓ Sakals, M.E., Sidle, R.C., 2004. A spatial and temporal model of root cohesion in forest soils. *Can. J. For. Res.* 34, 950–958.
-

References

- ✓ Santa Regina, I., 1995. Ciclos biogeoquímicos en bosques de la Sierra de Béjar (Salamanca). Retorno de bioelementos por medio del agua de lluvia. *Pirineos* 145–146, 65–80.
- ✓ Santacana, N., Baeza, B., Corominas, J., De Paz, A., Marturiá, J., 2003. A GIS-based multivariate statistical analysis for shallow landslide susceptibility mapping in La Pobla de Lillet area (Eastern Pyrenees, Spain). *Nat. Hazards* 30, 281–295.
- ✓ Savage, W., Wasowski, J., 2006. A plastic flow model for the Acquara–Vadoncello landslide in Senerchia, Southern Italy. *Eng. Geol.* 83, 4–21. doi:10.1016/j.enggeo.2005.06.024
- ✓ Savage, W.Z., Smith, W.K., 1986. A model for the plastic flow of landslides (U.S. Geological survey professional paper 1385 No. 1385). Washington, D.C., U.S.A.
- ✓ Scarascia-Mugnozza, G., Valentini, R., Spinelli, R.E.G., 1988. Osservazioni sul ciclo dell'acqua in un bosco ceduo di *Quercus cerris* L. *Ann. Dell'Accademia Ital. Sci. For.* 37, 3–21.
- ✓ Schenk, H.J., Jackson, R.B., 2002. Rooting depths, lateral root spreads and below-ground/above-ground allometries of plants in water-limited ecosystems. *J. Ecol.* 90, 480–494.
- ✓ Schlosser, F., Long, N.T., 1974. Recent results in French research on reinforced earth. *J. Constr. Div.* 100.
- ✓ Schmid, I., Kazda, M., 2002. Root distribution of Norway spruce in monospecific and mixed stands on different soils. *For. Ecol. Manag.* 159, 37–47.
- ✓ Schmidt, K.M., Roering, J.J., Stock, J.D., Dietrich, W.E., Montgomery, D.R., Schaub, T., 2001. The variability of root cohesion as an influence on shallow landslide susceptibility in the Oregon Coast Range. *Can. Geotech. J.* 38, 995–1024. doi:10.1139/cgj-38-5-995
- ✓ Schmocker, L., Weitbrecht, V., 2013. Driftwood: risk analysis and engineering measures. *J. Hydraul. Eng.* 139, 683–695. doi:10.1061/(ASCE)HY.1943-7900.0000728
- ✓ Schnock, G., 1971. Le Bilan de l'eau dans l'écosystème forêt: application à une chênaie mêlée de haute Belgique, in: *Productivité Des Écosystèmes Forestiers*. UNESCO, Paris, France.
- ✓ Schnorbus, M., Alila, Y., 2004. Forest harvesting impacts on the peak flow regime in the Columbia Mountains of southeastern British Columbia: an investigation using long-term numerical modeling. *Water Resour. Res.* 40. doi:10.1029/2003WR002918
- ✓ Schoeneberger, P.J., 2002. Field book for describing and sampling soils, Version 3.0. Government Printing Office.
- ✓ Schönenberger, W., Brang, P., 2004. Silviculture in mountain forests. *Encycl. For. Sci.* 3, 1085–1094.
- ✓ Schönenberger, W., Noack, A., Thee, P., 2005. Effect of timber removal from windthrow slopes on the risk of snow avalanches and rockfall. *For. Ecol. Manag.* 213, 197–208. doi:10.1016/j.foreco.2005.03.062
- ✓ Schwarz, M., Cohen, D., Or, D., 2011. Pullout tests of root analogs and natural root bundles in soil: Experiments and modeling. *J. Geophys. Res.* 116, 14. doi:10.1029/2010JF001753

-
- ✓ Schwarz, M., Cohen, D., Or, D., 2012a. Spatial characterization of root reinforcement at stand scale: Theory and case study. *Geomorphology* 171–172, 190–200. doi:10.1016/j.geomorph.2012.05.020
 - ✓ Schwarz, M., Thormann, J.J., Zurcher, K., Feller, K., 2012b. Quantifying root reinforcement in protection forests: implications for slope stability and forest management, in: 12th Congress Interpraevent. Grenoble, France, pp. 791–802.
 - ✓ Schwarz, M., Giadrossich, F., Cohen, D., 2013. Modeling root reinforcement using a root-failure Weibull survival function. *Hydrol. Earth Syst. Sci.* 17, 4367–4377. doi:10.5194/hess-17-4367-2013
 - ✓ Schwarz, M., Lehmann, P., Or, D., 2010a. Quantifying lateral root reinforcement in steep slopes - from a bundle of roots to tree stands. *Earth Surf. Process. Landf.* 35, 354–367. doi:10.1002/esp.1927
 - ✓ Schwarz, M., Preti, F., Giadrossich, F., Lehmann, P., Or, D., 2010b. Quantifying the role of vegetation in slope stability: A case study in Tuscany (Italy). *Ecol. Eng.* 36, 285–291. doi:10.1016/j.ecoleng.2009.06.014
 - ✓ Schwarz, M., Cohen, D., Or, D., 2010c. Root-soil mechanical interactions during pullout and failure of root bundles. *Journal of Geophysical Research: Earth Surface* (2003–2012) 115, 19. doi:10.1029/2009JF001603
 - ✓ Schwarz, M., Phillips, C., Marden, M., McIvor, I.R., Douglas, G.B., Watson, A., 2016. Modelling of root reinforcement and erosion control by “Veronese” poplar on pastoral hill country in New Zealand. *N. Z. J. For. Sci.* 46. doi:10.1186/s40490-016-0060-4
 - ✓ Schwarz, M., Rist, A., Cohen, D., Giadrossich, F., Egorov, P., Büttner, D., Stolz, M., Thormann, J.-J., 2015. Root reinforcement of soils under compression. *J. Geophys. Res. Earth Surf.* 120, 2103–2120. doi:10.1002/2015JF003632
 - ✓ Sdao, F., Simeone, V., 2007. Mass movements affecting Goddess Mefitis sanctuary in Rossano di Vaglio (Basilicata, southern Italy). *J. Cult. Herit.* 8, 77–80. doi:10.1016/j.culher.2006.10.004
 - ✓ Seguin, G., 1972. Répartition dans l’espace du système racinaire de la vigne. *Comptes Rendus Seances L’academie Sci.* 274, 2178–2180.
 - ✓ Seo, J.I., Nakamura, F., Nakano, D., Ichyanagi, H., Chun, K.W., 2008. Factors controlling the fluvial export of large woody debris, and its contribution to organic carbon budgets at watershed scales. *Water Resour. Res.* 44, W04428, 1–13. doi:10.1029/2007WR006453
 - ✓ Sherif, M.A., Ishibashi, I., Lee, C.D., 1982. Earth pressure against rigid retaining walls. *J. Geotech. Geoenvironmental Eng.* 108.
 - ✓ Shewbridge, S.E., Sitar, N., 1989. Deformation characteristics of reinforced sand in direct shear. *J. Geotech. Eng.* 115, 1134–1147.
 - ✓ Shimamura, M., Togari, A., 2006. Railway shelter-woods in Japan. *For. Snow Landsc. Res.* 80, 129–134.
-

References

- ✓ Shinozaki, K., Yoda, K., Hozumi, K., Kira, T., 1964a. A quantitative analysis of plant form - the pipe model theory. I. Basic analyses. *Jpn. J. Ecol., The Ecological Society of Japan* 14, 97–105.
- ✓ Shinozaki, K., Yoda, K., Hozumi, K., Kira, T., 1964b. A quantitative analysis of plant form - the pipe model theory. II. Further evidence of the theory and its application in forest ecology. *Jpn. J. Ecol., The Ecological Society of Japan* 14, 133–139.
- ✓ Sholtes, J.S., Doyle, M.W., 2011. Effect of channel restoration on flood wave attenuation. *J. Hydraul. Eng.* 137, 196–208.
- ✓ Sidle, R.C., Bogaard, T.A., 2016. Dynamic earth system and ecological controls of rainfall-initiated landslides. *Earth-Sci. Rev.* 159, 275–291. doi:10.1016/j.earscirev.2016.05.013
- ✓ Sidle, R.C., Ochiai, H., 2006. Landslides: processes, prediction, and land use. American Geophysical Union.
- ✓ Sidle, R.C., Pearce, A.J., O’Loughlin, C.L., 1985. Hillslope stability and land use, Water Resources Monograph Series 11. American Geophysical Union, Washington, D.C.
- ✓ Sidle, R.C., Terry, P.K.K., 1992. Shallow landslide analysis in terrain with managed vegetation, in: Proceedings of the Chengdu Symposium, July 1992. Presented at the Erosion, Debris Flows and Environment in Mountain Regions, IAHS Publ., Chengdu, China, pp. 289–298.
- ✓ Sidle, R.C., Ziegler, A.D., 2017. The canopy interception–landslide initiation conundrum: insight from a tropical secondary forest in northern Thailand. *Hydrol. Earth Syst. Sci.* 21, 651–667. doi:10.5194/hess-21-651-2017
- ✓ Sidle, R.C., Ziegler, A.D., Negishi, J.N., Nik, A.R., Siew, R., Turkelboom, F., 2006. Erosion processes in steep terrain - Truths, myths, and uncertainties related to forest management in Southeast Asia. *For. Ecol. Manag.* 224, 199–225. doi:10.1016/j.foreco.2005.12.019
- ✓ Silva, J.S., Rego, F.C., 2003. Root distribution of a Mediterranean shrubland in Portugal. *Plant Soil* 255, 529–540.
- ✓ Simon, A., Collison, A.J.C., 2002. Quantifying the mechanical and hydrologic effects of riparian vegetation on streambank stability. *Earth Surf. Process. Landf.* 27, 527–546. doi:10.1002/esp.325
- ✓ Simoni, S., Zanotti, F., Bertoldi, G., Rigon, R., 2008. Modelling the probability of occurrence of shallow landslides and channelized debris flows using GEOtop-FS. *Hydrol. Process.* 22, 532–545. doi:10.1002/hyp.6886
- ✓ Singh, R.P., 1987. Rainfall interception by *Pinus wallichiana* plantation in temperate region of Himachal Pradesh, India. *Indian For.* 113, 559–566.
- ✓ Sinun, W., Meng, W.W., Douglas, I., Spencer, T., 1992. Throughfall, stemflow, overland flow and throughflow in the Ulu Segama rain forest, Sabah, Malaysia. *Philos. Trans. R. Soc. Lond. B Biol. Sci.* 335, 389–395.
- ✓ Škrabl, S., 2008. The limit values and the distribution of three-dimensional passive earth pressures. *Acta Geotech. Slov.* 1, 23–34.

-
- ✓ Škrabl, S., Macuh, B., 2005. Upper-bound solutions of three-dimensional passive earth pressures. *Can. Geotech. J.* 42, 1449–1460.
 - ✓ Smart, D.R., Schwass, E., Lakso, A., Morano, L., 2006. Grapevine rooting patterns: a comprehensive analysis and a review. *Am. J. Enol. Vitic.* 57, 89–104.
 - ✓ Smith, J.H.G., 1964. Root spread can be estimated from crown width of Douglas fir, Lodgepole pine, and other British Columbia tree species. *For. Chron.* 40, 456–473.
 - ✓ Sonnenberg, R., Davies, M.C.R., Bransby, M.F., Mickovski, S.B., Bengough, A.G., Hallett, P.D., Hudacsek, P., 2007. Centrifuge modelling of slope reinforcement by vegetation. *Proc 14th ECSMGE Madr.* 3, 1551–1556.
 - ✓ Soubra, A.-H., 2000. Static and seismic passive earth pressure coefficients on rigid retaining structures. *Can. Geotech. J.* 37, 463–478.
 - ✓ Soubra, A.-H., Galvani, D., Regenass, P., 2000. Three-dimensional active earth pressures, in: *European Congress on Computational Methods in Applied Sciences and Engineering ECCOMAS 2000*. Presented at the ECCOMAS 2000, Barcelona.
 - ✓ Soubra, A.-H., Kastner, R., Benmansour, A., 1999. Passive earth pressures in the presence of hydraulic gradients. *Géotechnique* 49, 319–330.
 - ✓ Soubra, A.-H., Macuh, B., 2002. Active and passive earth pressure coefficients by a kinematical approach. *Proc. ICE-Geotech. Eng.* 155, 119–131.
 - ✓ Soubra, A.-H., Regenass, P., 2000. Three-dimensional passive earth pressures by kinematical approach. *J. Geotech. Geoenvironmental Eng.* 126, 969–978.
 - ✓ Southey, J.M., 1992. Root distribution of different grapevine rootstocks on a relatively saline soil. *South Afr. J. Enol. Vitic.* 13, 1–9.
 - ✓ Soyer, J.P., Delas, J., Molot, C., Andral, P., Casteran, P., 1984. Techniques d'entretien du sol en vignoble bordelais. Consequences sur la vigne (production, vigueur, enracinement, nutrition) et sur le sol apres 20 ans d' experimentation. *Prog. Agric. Vitic.* 101, 315–320.
 - ✓ Šraj, M., Brilly, M., Mikoš, M., 2008. Rainfall interception by two deciduous Mediterranean forests of contrasting stature in Slovenia. *Agric. For. Meteorol.* 148, 121–134. doi:10.1016/j.agrformet.2007.09.007
 - ✓ Staelens, J., De Schrijver, A., Verheyen, K., Verhoest, N.E.C., 2008. Rainfall partitioning into throughfall, stemflow, and interception within a single beech (*Fagus sylvatica* L.) canopy: influence of foliation, rain event characteristics, and meteorology. *Hydrol. Process.* 22, 33–45.
 - ✓ Steinacher, R., Medicus, G., Fellin, W., Zangerl, C., 2009. The influence of deforestation on slope (in-)stability. *Austrian J. Earth Sci. Mitteilungen Österr. Geol. Ges.* 102, 90–99.
 - ✓ Stokes, A., Ghani, M.A., Salin, F., Danjon, F., Jeannin, H., Berthier, S., Kokutse, A.D., Frochot, H., 2007. Root morphology and strain distribution during tree failure on mountain slopes, in: *Eco- and Ground Bio-Engineering: The Use of Vegetation to Improve Slope Stability*. Springer, pp. 165–173.
-

References

- ✓ Stokes, A., Norris, J.E., Beek, L., Bogaard, T., Cammeraat, E., Mickovski, S.B., Jenner, A., Iorio, A., Fourcaud, T., 2008. How vegetation reinforces soil on slopes. *Slope Stab. Eros. Control Ecotechnological Solut.* 65–118.
- ✓ Stokes, A., Salin, F., Kokutse, A.D., Berthier, S., Jeannin, H., Mochan, S., Dorren, L.K.A., Kokutse, N., Abd.Ghani, M., Fourcaud, T., 2005. Mechanical resistance of different tree species to rockfall in the French Alps. *Plant Soil* 278, 107–117. doi:10.1007/s11104-005-3899-3
- ✓ Stone, E.L., Kalisz, P.J., 1991. On the maximum extent of tree roots. *For. Ecol. Manag.* 46, 59–102.
- ✓ Stout, B.B., 1956. Studies of the root systems of deciduous trees. *Black Rock For. Bull., Harvard University* 15, 45.
- ✓ Styczen, M.E., Morgan, R.P.C., 1995. *Engineering properties of vegetation.* Taylor & Francis: London, UK.
- ✓ Swanepoel, J.J., Southey, J.M., 1989. The influence of rootstock on the rooting pattern of the grapevine. *South Afr. J. Enol. Vitic.* 10, 23–28.
- ✓ Swanston, D.N., 1970. Mechanics of debris avalanching in shallow till soils of southeast Alaska. *Res. Pap. Pac. Northwest. For. Range Exp. Stn.*
- ✓ Tarazona, T., Santa Regina, I., Calvo, R., 1996. Interception, throughfall and stemflow in two forests of the “Sierra de la Demanda” in the Province of Burgos. *Pirineos* 147–148, 27–40.
- ✓ Tarboton, D.G., 2003. Terrain analysis using digital elevation models in hydrology, in: 23rd ESRI International Users Conference. Citeseer, San Diego, California, USA.
- ✓ Tarolli, P., Tarboton, D.G., 2006. A new method for determination of most likely landslide initiation points and the evaluation of digital terrain model scale in terrain stability mapping. *Hydrol. Earth Syst. Sci. Discuss.* 10, 663–677.
- ✓ Tatarinov, F., Urban, J., Čermák, J., 2008. Application of “clump technique” for root system studies of *Quercus robur* and *Fraxinus excelsior*. *For. Ecol. Manag.* 255, 495–505. doi:10.1016/j.foreco.2007.09.022
- ✓ Taylor, D.W., 1948. Fundamentals of soil mechanics. *Soil Sci.* 66, 161.
- ✓ Teklehaimanot, Z., Jarvis, P.G., Ledger, D.C., 1991. Rainfall interception and boundary layer conductance in relation to tree spacing. *J. Hydrol.* 123, 261–278.
- ✓ Temple, P.H., Rapp, A., 1972. Landslides in the Mgeta area, Western Uluguru Mountains, Tanzania. *Geogr. Ann. Ser. Phys. Geogr.* 54, 157. doi:10.2307/520764
- ✓ Terwilliger, V.J., Waldron, L.J., 1991. Effects of root reinforcement on soil-slip patterns in the Transverse Ranges of southern California. *Geol. Soc. Am. Bull.* 103, 775–785.
- ✓ Terzaghi, K., 1920. Old earth pressure theories and new test results. *Eng. News-Rec.* 85, 632–637.
- ✓ Terzaghi, K., 1941. General wedge theory of earth pressure. *Trans. Am. Soc. Civ. Eng.* 106, 68–80.
- ✓ Terzaghi, K., 1943. *Theoretical soil mechanics.* John Wiley & Sons, New York, NY.
- ✓ Terzaghi, K., Peck, R.B., Mesri, G., 1996. *Soil mechanics in engineering practice.* John Wiley & Sons.

-
- ✓ Thomas, H., Nisbet, T.R., 2007. An assessment of the impact of floodplain woodland on flood flows. *Water Environ. J.* 21, 114–126. doi:10.1111/j.1747-6593.2006.00056.x
 - ✓ Thomas, R.E., Pollen-Bankhead, N., 2010. Modeling root-reinforcement with a fiber-bundle model and Monte Carlo simulation. *Ecol. Eng.* 36, 47–61. doi:10.1016/j.ecoleng.2009.09.008
 - ✓ Tobin, B., Čermák, J., Chiatante, D., Danjon, F., Di Iorio, A., Dupuy, L., Eshel, A., Jourdan, C., Kalliokoski, T., Laiho, R., Nadezhdina, N., Nicoll, B., Pagès, L., Silva, J., Spanos, I., 2007. Towards developmental modelling of tree root systems. *Plant Biosyst. - Int. J. Deal. Asp. Plant Biol.* 141, 481–501. doi:10.1080/11263500701626283
 - ✓ Tockner, K., Ward, J.V., Arcsott, D.B., Edwards, P.J., Kollmann, J., Gurnell, A.M., Petts, G.E., Maiolini, B., 2003. The Tagliamento River: a model ecosystem of European importance. *Aquat. Sci. - Res. Boundaries* 65, 239–253. doi:10.1007/s00027-003-0699-9
 - ✓ Tosi, M., 2007. Root tensile strength relationships and their slope stability implications of three shrub species in the Northern Apennines (Italy). *Geomorphology* 87, 268–283. doi:10.1016/j.geomorph.2006.09.019
 - ✓ Tron, S., Dani, A., Laio, F., Preti, F., Ridolfi, L., 2014. Mean root depth estimation at landslide slopes. *Ecol. Eng.* 69, 118–125. doi:10.1016/j.ecoleng.2014.03.019
 - ✓ Tsukamoto, Y., 1990. Effect of vegetation on debris slide occurrences on steep forested slopes in Japan Islands, in: IAHS-Publ. Presented at the Research Needs and Applications to Reduce Erosion and Sedimentation En Tropical Steeplands (Proceedings of the Fiji Symposium, June 1990), pp. 183–191.
 - ✓ Tubbs, C.H., 1977. Root-crown relations of young sugar maple and yellow birch (No. Research note NC-225), North Central Forest Experiment Station. USDA Forest Service, St. Paul Campus, Minnesota, U.S.A.
 - ✓ Uchida, T., Kosugi, K., Ichirou, Mizuyama, T., 2001. Effects of pipeflow on hydrological process and its relation to landslide: a review of pipeflow studies in forested headwater catchments. *Hydrol. Process.* 15, 2151–2174. doi:10.1002/hyp.281
 - ✓ Ulrich, E., Lelong, N., Lanier, M., Schneider, A., 1995. Interception des pluies en forêt: facteurs déterminants (ONF-Bulletin Technique No. Interprétation des mesures réalisées dans les sous-réseau CATAENAT de RENECOFOR. 30).
 - ✓ Urciuoli, G., Picarelli, L., Leroueil, S., 2007. Local soil failure before general slope failure. *Geotech. Geol. Eng.* 25, 103–122. doi:10.1007/s10706-006-0009-0
 - ✓ Valente, F., David, J.S., Gash, J.H.C., 1997. Modelling interception loss for two sparse eucalypt and pine forests in central Portugal using reformulated Rutter and Gash analytical models. *J. Hydrol.* 190, 141–162.
 - ✓ van Asch, T.W., Buma, J., van Beek, L.P.H., 1999. A view on some hydrological triggering systems in landslides. *Geomorphology* 30, 25–32.
-

References

- ✓ van Asch, T.W., Malet, J.-P., van Beek, L.P., Amitrano, D., 2007. Techniques, issues and advances in numerical modelling of landslide hazard. *Bull. Société Géologique Fr.* 178, 65–88.
- ✓ van Beek, L.P.H., Wint, J., Cammeraat, L.H., Edwards, J.P., 2005. Observation and simulation of root reinforcement on abandoned mediterranean slopes. *Plant Soil* 278, 55–74. doi:10.1007/s11104-005-7247-4
- ✓ van Beek, L.P.H., van Asch, T.W.J., 2004. Regional assessment of the effects of land-use change on landslide hazard by means of physically based modelling. *Natural Hazards* 31, 289–304.
- ✓ Van Den Eeckhaut, M., Marre, A., Poesen, J., 2010. Comparison of two landslide susceptibility assessments in the Champagne–Ardenne region (France). *Geomorphology* 115, 141–155. doi:10.1016/j.geomorph.2009.09.042
- ✓ Van Stan, J.T., Gutmann, E.D., Lewis, E.S., Gay, T.E., 2016. Modeling rainfall interception loss for an epiphyte-laden *Quercus virginiana* forest using reformulated static- and variable-storage Gash analytical models. *J. Hydrometeorol.* 17, 1985–1997. doi:10.1175/JHM-D-16-0046.1
- ✓ van Westen, C.J., Terlien, M.J.T., 1996. An approach towards deterministic landslide hazard analysis in GIS. A case study from Manizales (Colombia). *Earth Surf. Process. Landf.* 21, 853–868.
- ✓ van Westen, C.J., van Asch, T.W.J., Soeters, R., 2006. Landslide hazard and risk zonation—why is it still so difficult? *Bull. Eng. Geol. Environ.* 65, 167–184. doi:10.1007/s10064-005-0023-0
- ✓ Van Zyl, J.L., Van Huyssteen, L., 1980. Comparative studies on wine grapes on different trellising systems: II. Micro-climatic studies, grape composition and wine quality. *South Afr. J. Enol. Vitic.* 1, 15–25.
- ✓ Vannoppen, W., Vanmaercke, M., De Baets, S., Poesen, J., 2015. A review of the mechanical effects of plant roots on concentrated flow erosion rates. *Earth-Science Reviews* 150, 666–678. <https://doi.org/10.1016/j.earscirev.2015.08.011>
- ✓ Varnes, D.J., 1978. Slope movement types and processes. Schuster RL Krizek RJ Eds *Landslides Anal. Control Spec. Rep.* 176 Transp. Res. Board National Academy of Sciences, Washington, DC., pp. 11–33.
- ✓ Vergani, C., Graf, F., 2015. Soil permeability, aggregate stability and root growth: a pot experiment from a soil bioengineering perspective: Soil Permeability, Aggregate Stability, Root Growth. *Ecohydrology* n/a-n/a. doi:10.1002/eco.1686
- ✓ Vergani, C., Chiaradia, E.A., Bischetti, G.B., 2012. Variability in the tensile resistance of roots in Alpine forest tree species. *Ecological Engineering* 46, 43–56. doi:10.1016/j.ecoleng.2012.04.036
- ✓ Vergani, C., Chiaradia, E.A., Bassanelli, C., Bischetti, G.B., 2014a. Root strength and density decay after felling in a Silver Fir-Norway Spruce stand in the Italian Alps. *Plant Soil* 377, 63–81. doi:10.1007/s11104-013-1860-4
- ✓ Vergani, C., Schwarz, M., Cohen, D., Thormann, J.-J., Bischetti, G.B., 2014b. Effects of root tensile force and diameter distribution variability on root reinforcement in the Swiss and Italian Alps. *Canadian Journal of Forest Research* 44, 1426–1440. doi:10.1139/cjfr-2014-0095

-
- ✓ Vergani, C., Schwarz, M., Soldati, M., Corda, A., Giadrossich, F., Chiaradia, E.A., Morando, P., Bassanelli, C., 2016. Root reinforcement dynamics in subalpine spruce forests following timber harvest: a case study in Canton Schwyz, Switzerland. *Catena* 143, 275–288. doi:10.1016/j.catena.2016.03.038
 - ✓ Vergani, C., Giadrossich, F., Schwarz, M., Buckley, P., Conedera, M., Pividori, M., Salbitano, F., Rauch, H.S., Lovreglio, R., 2017a. Root reinforcement dynamics of European coppice woodlands and their effect on shallow landslides: A review. *Earth-Sci. Rev.* doi:10.1016/j.earscirev.2017.02.002
 - ✓ Vergani, C., Werlen, M., Conedera, M., Cohen, D., Schwarz, M., 2017b. Investigation of root reinforcement decay after a forest fire in a Scots pine (*Pinus sylvestris*) protection forest. *For. Ecol. Manag.* 400, 339–352. doi:10.1016/j.foreco.2017.06.005
 - ✓ Vidal, H., 1969. The principle of reinforced earth. *Highw. Res. Rec.*
 - ✓ Viville, D., Biron, P., Granier, A., Dambrine, E., Probst, A., 1993. Interception in a mountainous declining spruce stand in the Strengbach catchment (Vosges, France). *J. Hydrol.* 144, 273–282.
 - ✓ Vorpahl, P., Elsenbeer, H., Märker, M., Schröder, B., 2012. How can statistical models help to determine driving factors of landslides? *Ecol. Model.* 239, 27–39. doi:10.1016/j.ecolmodel.2011.12.007
 - ✓ Vrecl-Kojc, H., Škrabl, S., 2007. Determination of passive earth pressure using three-dimensional failure mechanism. *Acta Geotech. Slov.* 4, 11–23.
 - ✓ Waisel, Y., Eshel, A., Kafkafi, U., 1991. *Plant roots: the hidden half.* Marcel Dekker, Inc.
 - ✓ Waldron, L.J., 1977. The shear resistance of root-permeated homogeneous and stratified soil. *Soil Sci. Soc. Am. J.* 41, 843–849.
 - ✓ Waldron, L.J., Dakessian, S., 1981. Soil reinforcement by roots: calculation of increased soil shear resistance from root properties. *Soil Sci.* 132, 427–435.
 - ✓ Waldron, L.J., Dakessian, S., Nemson, J.A., 1983. Shear resistance enhancement of 1.22-meter diameter soil cross sections by pine and alfalfa roots. *Soil Sci. Soc. Am. J.* 47, 9–14.
 - ✓ Wallerstein, N., Thorne, C.R., Doyle, M.W., 1997. Spatial distribution and impact of large woody debris in northern Mississippi. Presented at the Proceedings of the conference on management of landscapes disturbed by channel incision. University of Mississippi, Oxford, MS, pp. 145–150.
 - ✓ Wang, W.L., Yen, B.C., 1974. Soil arching in slopes. *J. Geotech. Eng.* 100.
 - ✓ Warburton, J., Milledge, D.G., Johnson, R., 2008. Assessment of shallow landslide activity following the January 2005 storm, Northern Cumbria. *Cumberl. Geol. Soc. Proc.* 7, 263–283.
 - ✓ Weiss, G., 1999. Protective forests in Alpine countries: From commons to the welfare state, in: *Proceeding of the 10th Biennial Conference of the American Society for Environmental History (ASEH).* Tucson, Arizona U.S.A.
 - ✓ Whited, T.L., 2005. *Northern Europe: an environmental history.* Abc-clio.
-

References

- ✓ Wilford, D.J., Sakals, M.E., Innes, J.L., Sidle, R.C., 2005. Fans with forests: contemporary hydrogeomorphic processes on fans with forests in west central British Columbia, Canada. *Geol. Soc. Lond. Spec. Publ.* 251, 25–40. doi:10.1144/GSL.SP.2005.251.01.03
- ✓ Williams, L.E., Smith, R.J., 1991. The effect of rootstock on the partitioning of dry weight, nitrogen and potassium, and root distribution of Cabernet Sauvignon grapevines. *Am. J. Enol. Vitic.* 42, 118–122.
- ✓ Wilson, P., Elgamal, A., 2010. Passive earth pressure force-displacement relationships, in: *Proceedings of the 5th International Conference on Recent Advances in Geotechnical Earthquake Engineering and Soil Dynamics*. San Diego, California, USA, pp. 1–11.
- ✓ Wilson, P.R., 2009. Large scale passive force-displacement and dynamic earth pressure experiments and simulations (PhD dissertation). University of California, San Diego, California, USA.
- ✓ Winkler, R.D., Spittlehouse, D.L., Golding, D.L., 2005. Measured differences in snow accumulation and melt among clearcut, juvenile, and mature forests in southern British Columbia. *Hydrol. Process.* 19, 51–62. doi:10.1002/hyp.5757
- ✓ Wohl, E., 2014. A legacy of absence: wood removal in US rivers. *Prog. Phys. Geogr.* 38, 637–663. doi:10.1177/0309133314548091
- ✓ Wohl, E., 2017. Bridging the gaps: an overview of wood across time and space in diverse rivers. *Geomorphology* 279, 3–26. doi:10.1016/j.geomorph.2016.04.014
- ✓ Wohl, E., Bledsoe, B.P., Fausch, K.D., Kramer, N., Bestgen, K.R., Gooseff, M.N., 2016. Management of large wood in streams: an overview and proposed framework for hazard evaluation. *JAWRA J. Am. Water Resour. Assoc.* 52, 315–335. doi:10.1111/1752-1688.12388
- ✓ Wohl, E., Cenderelli, D.A., Dwire, K.A., Ryan-Burkett, S.E., Young, M.K., Fausch, K.D., 2010. Large in-stream wood studies: a call for common metrics. *Earth Surf. Process. Landf.* n/a-n/a. doi:10.1002/esp.1966
- ✓ Wohl, E., Scott, D.N., 2016. Wood and sediment storage and dynamics in river corridors: Wood and Sediment Dynamics in River Corridors. *Earth Surf. Process. Landf.* 1–19. doi:10.1002/esp.3909
- ✓ Wu, T.H., 1984. Soil movements on permafrost slopes near Fairbanks, Alaska. *Can. Geotech. J.* 21, 699–709.
- ✓ Wu, T.H., 1995. Slope stabilization. *Slope Stab. Eros. Control Bioeng. Approach* 233, 221–264.
- ✓ Wu, T.H., Bettadapura, D.P., Beal, P.E., 1988. A statistical model of root geometry. *For. Sci.* 34, 980–997.
- ✓ Wu, T.H., McKinnell III, W.P., Swanston, D.N., 1979. Strength of tree roots and landslides on Prince of Wales Island, Alaska. *Can. Geotech. J.* 16, 19–33.
- ✓ Wu, T.H., McOmber, R.M., Erb, R.T., Beal, P.E., 1988. Study of soil-root interaction. *J. Geotech. Eng.* 114, 1351–1375.

-
- ✓ Wu, T.H., Watson, A., 1998. In situ shear tests of soil blocks with roots. *Can. Geotech. J.* 35, 579–590.
 - ✓ Wu, W., Sidle, R.C., 1995. A distributed slope stability model for steep forested basins. *Water Resour. Res.* 31, 2097–2110.
 - ✓ Yang, Y., Chen, L., Li, N., Zhang, Q., 2016. Effect of root moisture content and diameter on root tensile properties. *PLoS ONE* 11, e0151791. doi:10.1371/journal.pone.0151791
 - ✓ Yesilnacar, E., Topal, T., 2005. Landslide susceptibility mapping: A comparison of logistic regression and neural networks methods in a medium scale study, Hendek region (Turkey). *Eng. Geol.* 79, 251–266. doi:10.1016/j.enggeo.2005.02.002
 - ✓ Yildiz, A., Askarinejad, A., Graf, F., Rickli, C., Springman, S.M., 2015. Effects of roots and mycorrhizal fungi on the stability of slopes, in: *Proceedings of the XVI ECSMGE Geotechnical Engineering for Infrastructure and Development*. Presented at the Geotechnical Engineering for Infrastructure and Development, ICE Publishing, London, pp. 1693–1698. doi:10.1680/ecsmge.60678
 - ✓ Yilmaz, I., 2009. Landslide susceptibility mapping using frequency ratio, logistic regression, artificial neural networks and their comparison: A case study from Kat landslides (Tokat—Turkey). *Comput. Geosci.* 35, 1125–1138. doi:10.1016/j.cageo.2008.08.007
 - ✓ Zhang, C.-B., Chen, L.-H., Jiang, J., 2014. Why fine tree roots are stronger than thicker roots: The role of cellulose and lignin in relation to slope stability. *Geomorphology* 206, 196–202. doi:10.1016/j.geomorph.2013.09.024
 - ✓ Zhang, C.-B., Chen, L.-H., Liu, Y.-P., Ji, X.-D., Liu, X.-P., 2010. Triaxial compression test of soil–root composites to evaluate influence of roots on soil shear strength. *Ecol. Eng.* 36, 19–26. doi:10.1016/j.ecoleng.2009.09.005
 - ✓ Zhang, M., Javadi, A., Min, X., 2006. Triaxial tests of sand reinforced with 3D inclusions. *Geotext. Geomembr.* 24, 201–209. doi:10.1016/j.geotextmem.2006.03.004
 - ✓ Zhou, G., Esaki, T., Mitani, Y., Xie, M., Mori, J., 2003. Spatial probabilistic modeling of slope failure using an integrated GIS Monte Carlo simulation approach. *Eng. Geol.* 68, 373–386.
 - ✓ Zhou, Y., Watts, D., Li, Y., Cheng, X., 1998. A case study of effect of lateral roots of *Pinus yunnanensis* on shallow soil reinforcement. *For. Ecol. Manag.* 103, 107–120.
 - ✓ Zhu, D.-Y., Qian, Q., 2000. Determination of passive earth pressure coefficients by the method of triangular slices. *Can. Geotech. J.* 37, 485–491.
 - ✓ Ziemer, R.R., 1981. Roots and the stability of forested slopes, in: In: Timothy R. H. Davies and Andrew J. Pearce (Eds). *Proceedings of the International Symposium on Erosion and Sediment Transport in Pacific Rim Steeplands*. Presented at the Erosion and Sediment Transport in Pacific Rim Steeplands., Int. Assn. Hydrol. Sci. Pub., Christchurch, New Zealand, pp. 343–361.
 - ✓ Ziemer, R.R., Swanston, D.N., 1977. Root strength changes after logging in southeast Alaska. Dept. of Agriculture, Forest Service, Pacific Northwest Forest and Range Experiment Station.
-

References

- ✓ Zimmermann, M., 1990. Debris flows 1987 in Switzerland: geomorphological and meteorological aspects, in: Proceedings of the 2nd Hydrology in Mountainous Region. Presented at the Artificial Reservoirs; Water and Slopes, IAHS Publ. 194, Lausanne, Switzerland, pp. 387–393.
- ✓ Zimmermann, U., 2008. Cofanetto bosco di protezione (Gruppo bosco di protezione Svizzera L'allestimento del cofanetto è stato sostenuto nei contenuti e finanziariamente dal UFAM). Centro per la selvicoltura di montagna, Bildungszentrum Wald, CH-7304 Maienfeld, Maienfeld, Switzerland.
- ✓ Zizioli, D., Meisina, C., Valentino, R., Montrasio, L., 2013. Comparison between different approaches to modeling shallow landslide susceptibility: a case history in Oltrepo Pavese, Northern Italy. *Nat. Hazards Earth Syst. Sci.* 13, 559–573. doi:10.5194/nhess-13-559-2013

LIST OF PUBLICATIONS

This PhD dissertation is an original monograph that includes parts of published or submitted peer-reviewed papers, selected from my publication list. A list of such manuscripts follows:

- ❖ **Cislaghi, A.**, Chiaradia, E.A., Bischetti, G.B., 2017. Including root reinforcement variability in a probabilistic 3D stability model. *Earth Surface Processes and Landforms* 42, 1789–1806. doi:10.1002/esp.4127. (Chapter 2)
- ❖ **Cislaghi, A.**, Vergani, C., Chiaradia, E.A., Bischetti, G.B., 2017. Presented at the International Conference Soil Bioengineering Methods for Slopes at BOKU in October 2016. (Chapter 3)
- ❖ **Cislaghi, A.**, Rlgon, E., Lenzi, M.A., Bischetti, G.B., 2017. A probabilistic multidimensional approach to quantify large wood recruitment from hillslopes in mountainous-forested catchments. Accepted to *Geomorphology*. (Chapter 4)
- ❖ **Cislaghi, A.**, Bordoni, M., Meisina, C., Bischetti, G.B., 2017. Soil reinforcement provided by the root system of grapevines: quantification and spatial variability. *Ecological Engineering* 109, 169-185. doi:10.1016/j.ecoleng.2017.04.034. (Chapter 5)
- ❖ **Cislaghi, A.**, Cohen, D., Gasser, E., Bischetti, G.B., Schwarz, M., 2017. Field measurements of passive earth forces in steep shallow landslide-prone areas. Submitted to *Journal of Geophysical Research: Earth Surface*. (Chapter 6)

